SCRAP TIRE - DERIVED GEOMATERIALS IN RETAINING WALL APPLICATIONS

A Thesis Submitted

in Partial Fulfillment of the Requirements

for the Degree of

DOCTOR OF PHILOSOPHY

by

SODOM BALI REDDY

DEPARTMENT OF CIVIL ENGINEERING
INDIAN INSTITUTE OF TECHNOLOGY GUWAHATI
GUWAHATI

OCTOBER 2017

CERTIFICATE

This is to certify that the thesis entitled "**Scrap tire-derived geomaterials in retaining wall applications"** submitted by **Sodom Bali Reddy** (Roll No.11610421), to the Indian Institute of Technology Guwahati, for the award of degree of Doctor of Philosophy in Civil Engineering is a record of bonafide research work carried out by him under my supervision and guidance. The thesis work, in my opinion, has reached the requisite standard fulfilling the requirement for the degree of Doctor of Philosophy.

The results contained in this thesis have not been submitted in part or full to any other University or Institute for award of any degree or diploma.

Dr. A. Murali Krishna
Associate Professor
Department of Civil Engineering
Indian Institute of Technology Guwahati
Guwahati-781039, India

STATEMENT

I do hereby declare that the matter embodied in this thesis is the result of investigations carried out by me in the Department of Civil Engineering, Indian Institute of Technology Guwahati, Guwahati, Assam, and India.

In keeping with the general practice of reporting scientific observations, due acknowledgements have been made wherever the work described is based on findings of other investigators.

Sodom Bali Reddy

Guwahati
Date: 30 October 2017

DEDICATION

I DEDICATE MY DISSERTATION WORK TO MY BROTHER LATE. SODUM RAMI REDDY, MY FAMILY AND ALL MY GURUS.

ACKNOWLEDGEMENTS

I owe sincere gratitude to many people for having the pleasure of submitting the Thesis.

I have great pleasure in expressing my deep sense of gratitude to my thesis supervisor and research guide, ***Dr. A. Murali Krishna*** *for his inspiring guidance and constant encouragement throughout the course of my research work. I am grateful to him for sparing his valuable time and effort at all stages of the work. I am very much obliged to him for all the help, affection and kind suggestions, which helped me to complete the work successfully.*

I am thankful to Prof. Subashisa Dutta, Head of Civil Engineering Department and Prof. Arup Kumar Sarma, Prof. Sajal K. Deb, former Heads' of Civil Engineering, IIT Guwahati, for their support and permission to pursue this research programme. My thanks are due to the Civil Engineering office staff for their constant help.

I am indebted to Doctoral Committee members Dr. Sreedeep, Dr. Arindam Dey and Dr. Kanagaraj for sparing their valuable time in reviewing my work and valuable suggestions. I would also like to thank the faculty members of Geotechnical Engineering of Civil Engineering Department for their suggestions and support during my PhD work. I owe great thanks to the staff of Civil Engineering, particularly Mr. Hariram Upadhyay, Mr. Hazarika and Mr. Deb Nath for their kind helps in conducting the experiments and data collection.

My sincere thanks to Technical Officers of Civil Engineering Department, particularly Dr. Arun Ch. Borsaikia, for his kind help in conducting the shaking table tests.

I am extremely grateful to my parents for their encouragement and moral support throughout my education life, without which I could not have seen the light of the day.

The most important factors to acknowledge are the greatest support and love I received from my brother.

I would also like to thank my friends Arup Deka, Pradeep Dammala, Arup Bhattacharjee, Shiv Shankar, Chiranjib Prasad Sarma, Doordarshi Chatarjee, Sudheer, Srikanth and many others for their companionship, support and encouragement.

Finally, I thank the Almighty for providing strength with blessings in every step taken by me.

Sodom Bali Reddy

ABSTRACT

Earth retaining structures such as retaining walls, bridge abutments, bulkheads, braced excavations and mechanically stabilized walls are often subjected to different loading conditions. Among various parameters that need to be considered in the design of retaining structures, lateral earth pressures and horizontal displacements resulting from the supported backfill are the most predominant. These are the influencing parameters on the performance of the structure under variety of loading conditions. The development and implementation of methods, for the reduction of earth pressures and wall displacements, reduce the structural capacity requirements and lead to the overall construction economy. With the efforts of reducing the lateral earth pressures and wall displacements of the earth retaining structures, light weight/compressible novel materials came into practice that are effectively serve the purpose. These materials include expanded polystyrene (EPS) geofoam, waste plastic, fly-ash, pure shredded tire, and sand – tire chip mixtures, etc. Other hand, scrap tires are undesired urban waste and are increasing every year. Scrap tire stockpiles can pose health hazard and fire hazard, thus alternative approaches to utilize large amounts of scrap tires has received attention of engineering community. Reuse of scrap tires prevents wastes that require disposal in landfills and also preserve the natural resources towards attaining sustainability. Use of scrap tire-derived materials as alternative materials in civil engineering applications, especially in geotechnical applications, has been practiced in several occasions.

Aim of the present research work is to investigate the beneficial effects of the use of scrap tire derived geomaterials in retaining wall applications. Sand and tire chips were chosed for preparing sand – tire chips (STC) mixtures. Index and mechanical properties of different STC mixtures (0–100%) were determined through laboratory

investigations and optimum mixing ratio of STC was evaluated. A series of physical retaining wall models of 600 mm height were tested under static and dynamic conditions to investigate the model behavior using different STC mixtures as lightweight fill material and tire chips as a compressible inclusion. The effects of STC mixtures, compressible inclusions layer thickness, surcharge pressures, base excitations (frequency and acceleration) and earthquake excitations on the performance of the retaining walls were studied. Results were analyzed to understand the effect of each of the considered parameters on the horizontal wall displacements, lateral earth pressures and acceleration amplifications at different elevations of the wall. Numerical model was developed to simulate the static and shaking table tests on wall models, using a computer program FLAC (Fast Lagrangian Analysis of Continua) and used for parametric studies. Further, two retaining wall systems were designed using STC0 and STC30 mixtures and financial benefits were evaluated.

The addition of tire chips to sand (up to approximately 30–50%) resulted in significantly increased shear strength. The optimum mixing ratio of sand and tire chips, which show better compressibility characteristics (due to lesser void ratio) and high load-carrying behaviour (due to high shear strength), is in the range of 30–40% by weight. The model studies with STC mixtures as lightweight backfill material indicated significant improvement in wall behaviour in terms of displacements and lateral earth pressures and accelerations. Maximum reduction in displacement is in the order of 65%, for optimum STC mixture (STC30), under both static and dynamic loading condition. By using STC30 material dynamic induced pressures were reduced by, up to 80%. Tire chips as compressible inclusion, behind the wall showed remarkable advantage in reducing displacements (upto 25% reduction) and lateral earth pressures (up to 60 % reduction), under static loading. The corresponding reductions in dynamic case were,

up to 75% and 80%, respectively. The developed numerical model, for retaining wall with different STC mixtures, is able to simulate the behaviour of laboratory models and showed the maximum reductions in displacement and pressures for STC30 backfill. With the assumed rates of TC, sand, and other materials, using STC30 mixture backfill showed an average saving of 20% to 30% in the total estimated cost of construction.

Overall, the present research work concludes that the STD geomaterial possess the beneficial engineering properties which indicate the promising potential for the use in Geoengineering applications. STC mixtures prove to be a cost effective lightweight fill material and reduce the demand for traditional materials with the replacement by recycled scrapped tire chips. Thus, use of STD material in geotechnical applications will create a sustainable future.

TABLE OF CONTENTS

LIST OF FIGURES

LIST OF TABLES

NOTATIONS AND ABBREVIATIONS

NOTATIONS

English symbols

a	Acceleration
B	Total length of backfill
b	Length of STC30 mixture zone
c	Cohesion
C_c	Coefficient of curvature
C_u	Uniformity coefficient
f	Frequency
$FS_{overturing}$	Factors of safety of overturning
$FS_{sliding}$	Factors of safety of sliding
G	Shear modulus
G_{max}	Initial shear modulus
H	Height of wall
t	Compressible inclusion thickness of tire chips
G_S	Specific gravity value of sand
G_{TC}	Specific gravity value of tire chips
G_{STC}	Specific gravity value of STC mixtures
W_S	Weights of sand
W_{TC}	Weights of tire chips contents
W_{STC}	Weights of STC mixture

Greek symbols

ρ	Density of soil/sand
ϕ	Angle of internal friction
γ_{dmin}	Minimum unit weight
γ_{dmax}	Maximum unit weight
δ	Interface friction angle

ABBREVIATIONS

AASHTO	American Association of State Highway and Transportation Officials
ASTM	American Standard for Testing Materials
BT	Baled Tires
CE	Civil Engineering
EQ	Earthquake
FDM	Finite Difference Method
FEM	Finite Element Method
FF	Fundamental frequency
FHWA	Federal Highway Administration
FLAC	Fast Lagrangian Analysis of Continua
GR	Ground Rubber
IS	Indian Standard
PGA	Peak ground acceleration
TDF	Tire Derived Fuel

Chapter 1. INTRODUCTION

1.1 BACKGROUND

Earth retaining structures such as retaining walls, bridge abutments, bulkheads, braced excavation and mechanically stabilized walls play a very important role in public life. These civil engineering structures are being used in many infrastructural, urban development projects (Fig. 1.1) and are often being subjected to different loading conditions. Among various parameters that need to be considered in the design of retaining structures, lateral earth pressures and horizontal displacements resulting from the supported backfill are the most predominant and the same are the influencing parameters on the performance of the structure under variety of loading conditions. The development and implementation of methods for the reduction of the earth pressures and displacements will result in increased safety and reduced construction cost of such structures. With the efforts of reducing the lateral earth pressures and wall displacements of the earth retaining structures, many lightweight/compressible novel materials came into practice that effectively serve for the purpose. These materials include expanded polystyrene (EPS) geofoam (Bathurst et al. 2007; Ertugrul and Trandafir, 2011), waste plastic (Graettinger et al. 2005), fly ash (Kumar and Mandal, 2017), pure shredded tire (Cecich et al. 1996), and sand – tire chip mixtures (Hazarika and Yasuhara, 2007; Prezzi et al. 2011), etc.

On the other hand, different industrial waste products (waste tires, plastic bottles, fly ash, cement kiln dust, stone dust, and rice-husk-ash, etc.) are being generated each year and their amount is increasing day by day due to raising world population and urbanization. Efficient disposal of these waste materials is a big challenge for the waste

management/Environment problem. Among them, disposal of waste tires (not biodegradable material) has become a big problem worldwide. It was reported that the annual rate of scrap tire generation is 200–300 million in the United States (Salgado and Prezzi, 2004 and Ahn and Cheng, 2014), 104 million in Japan (Hazarika et al., 2010 and 2012), 112 million in India (Rao and Dutta, 2006), and 20 million in Korea (Kim and Kang, 2013). The disposal of scrap tires in landfills has imposed dreadful threats on the ecosystem, including the danger of fire accidents. Stockpiles of scrap tires caused huge and adverse impacts on the environment. Considering the abundant availability of scraped tires in the developed countries and associated disposal problems, recycling of tires for different applications were being practiced.

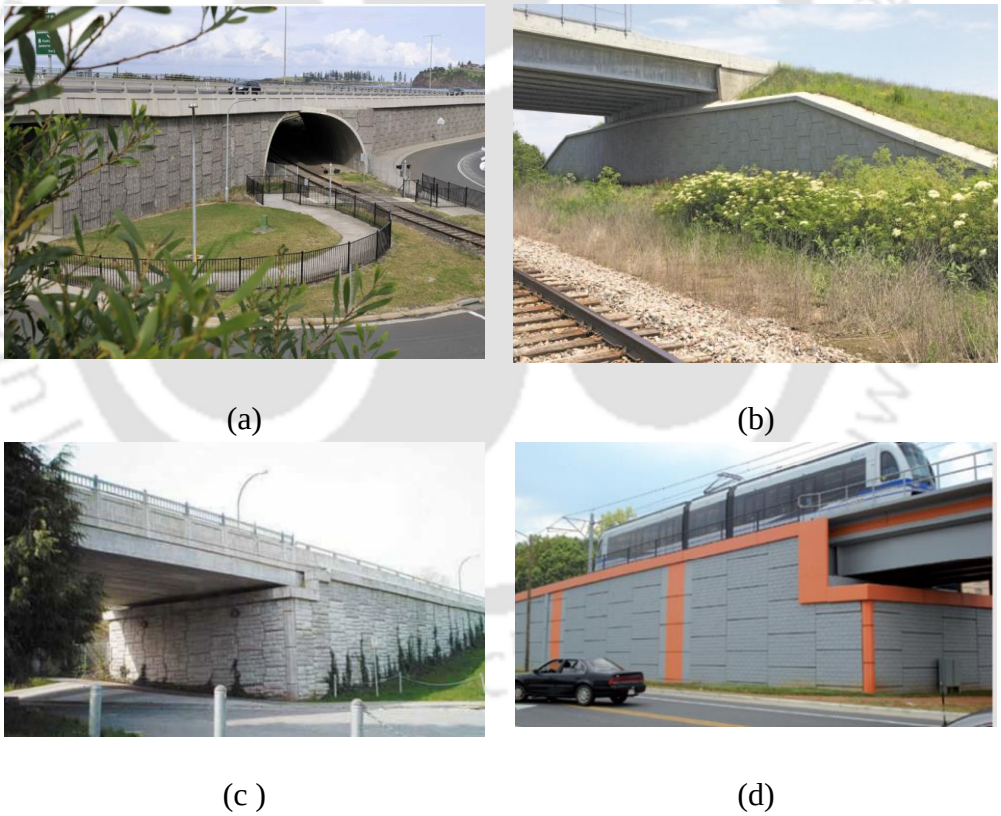

(a) (b)

(c) (d)

Fig. 1.1 Applications of earth retaining systems (Vivas and Calatrava, 2016)

Use of scrap tire-derived materials in civil engineering applications serves in creating a sustainable future. Use of tire-derived materials as alternative materials in civil engineering applications, especially in geotechnical applications, has been

practiced in several occasions. In some situations, use of tire-derived materials may provide greater economy than those materials traditionally used. American Society for Testing And Materials (ASTM) D6270 (2012) recommends using the terms based on the particle sizes: granulated rubber (maximum size of 12 mm), tire chips (between 12 and 50 mm) and tire shred (between 50 and 305 mm) as depicted in Fig. 1.2

Fig. 1.2 Scrap tire-derived geomaterials (modified after Hazarika and Yasuhara, 2015)

Several researchers (Bressette, 1984; Ahmed, 1993; Humphrey and Sandford, 1993; Benda,1995; Cosgrove, 1995; Gebhardt, 1997; Yang, 2002; Ghazavi, 2004; Prezzi et al. 2011 and Sheikh et al. 2014) have evaluated the engineering properties of the scrap tire chips and sand tire chip mixtures by conducting permeability, compressibility, large direct shear tests, and tri-axial tests on the samples. Investigations

have also been carried out by various researchers to explore the usage of scrap tire-derived geomaterials in geotechnical applications like: recycled tire chips as a fill material in road/ embankment construction (Eldin and Senouci, 1993; Bosscher et al. 1997; Salgado et al. 2003; Vinot and Baleshwar, 2013). Lightweight fill/ compressible inclusion material in retaining wall backfill under different loading conditions (Humphrey and Manion 1992; Cecich et al. 1996; Humphrey 1996; Tweedie et al. 1998a,b and c; Humphrey and Tweedie, 2002; Hazarika et al., 2004; Tandon et al. 2007; Hazarika et al., 2008a; Prezzi et al. 2011; Xiao, 2012; Ravichandran and Huggins, 2014); and waste tire shreds as a leachate collection layer (Bhalla et al. 2010; Mondal and Warith 2008; and Warith et al. 2004) etc.

Aim of the present research work is to investigate the beneficial effects due to the use of scrap tire-derived geomaterials, in the form of tire chips, in retaining wall applications. From the earlier researches, it is noticed that any lightweight and compressible material can be used in retaining wall applications in two forms: a) STC as a lightweight backfill material (Fig. 1.3a); and b) Tire chips as a compressible inclusion behind the wall (Fig. 1.3b).

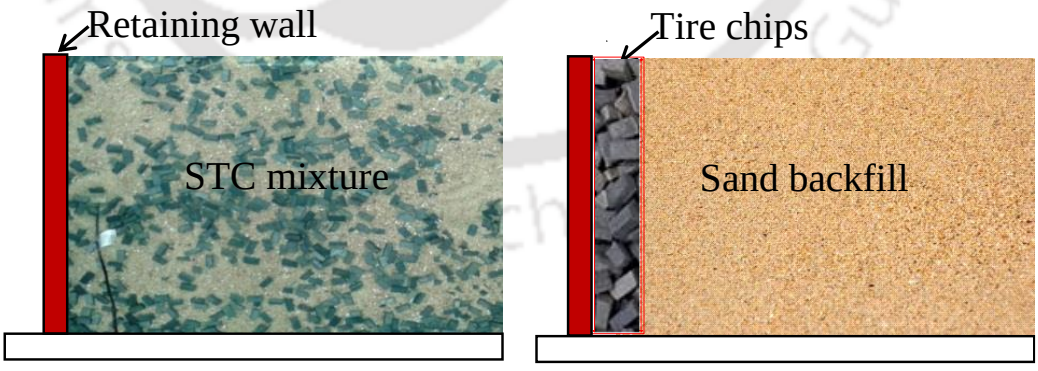

Fig. 1.3 Application of tire chips: a) Sand –tire chips (STC) mixtures as a lightweight fill; b) Tire chips as compressible inclusion

1.2 BROAD OBJECTIVE OF THE PRESENT STUDY

The broad objective of the present research is to increase the confidence of the geo-engineering field for the use of large amount of scrap tire-derived geomaterials in retaining wall applications.

This research work has the goals of ascertaining the engineering properties of sand – tire chips (STC) mixtures; and to study the behavior of retaining wall models for considering sand –tire chips (STC) mixtures as a lightweight fill material and tire chips as a compressible inclusion.

1.3 ORGANIZATION OF THESIS

This thesis is organized into eight chapters.

Chapter 1 presented the introduction to the problem, objective of the research work and organization of the thesis. In **Chapter 2**, literature relevant to the present research work, are briefly presented and discussed. Literature was reviewed in two parts: a) scrap tire derived geomaterials properties of tire chips and its mixtures; and b) scrap tire- derived geomaterials in geoengineering applications. The chapter concludes with critical appraisal of the literature and detailed scope of the work.

Chapter 3 presented the materials used and methods adopted in this investigation. The index and engineering properties of the materials used in the investigation (sand, tire-chips and their mixtures) are presented. Methodology adopted in construction of small scale retaining model walls and a brief description of experimentation procedures is presented.

Physical model tests conducted in this research work are discussed in chapters 4 and 5. **Chapter 4** deals with the static and shaking table tests performed on retaining wall models with STC mixtures as lightweight backfill materials. The parameters

studied include the effect of backfill type, effect of surcharge pressure, effect of dynamic excitation parameters (acceleration and frequency) on model wall behavior in terms of wall displacements and pressures. **Chapter 5** deals with the static and shaking table tests performed on retaining wall models with tire chips as compressible inclusions. The parameters studied include the effect of tire chip compressible inclusion and other parameters.

Chapter 6 presents numerical simulations of the static and dynamic physical model tests conducted on retaining wall models with different STC mixtures. Methodology followed in simulating different materials and their properties are discussed. Validation of the numerical model and its sensitivity are presented. Full-scale model wall with different backfill materials along with the various parametric studies are presented and discussed.

An attempt has been made to evaluate the economic benefits of retaining wall systems with the use of sand tire mixture, which is presented in **Chapter 7.** The study considers geotechnical and structural design of retaining walls backfilled with different backfill materials. Different height of retaining walls are considered for comparison purpose and finally cost analysis is presented.

Chapter 8 summarizes the research work and presents the conclusions drawn from the study. The limitations of the study and future scope of work are also outlined in the chapter.

Chapter 2. LITERATURE REVIEW

2.1 INTRODUCTION

The broad objective of the present study is to investigate the use of scrap tire-derived (STD) geomaterials for retaining wall applications through physical and numerical model studies. This chapter presents the literature reviewed as per the broad objective of the study. The literature review is presented in two parts: a) About scraps tires, generation, problems and the properties of scrap tires derived geomaterials and its mixtures with sand/soil; b) Geoengineering applications with the use of scrap tire delivered materials. The chapter concluded with critical appraisal of the literature followed by the scope of the study.

2.2 SCRAP TIRE-DERIVED GEOMATERIALS AND THEIR MIXTURES

Disposal of scraped tires has become a major concern in worldwide. It is reported that in a year, 200–300 million tires in United States (Salgado and Prezzi, 2004; Ahn and Cheng, 2014; RMA, 2016), 104 million of scrap tires in Japan (Hazarika et al., 2008a and 2010), 112 million tires in India (Rao and Dutta, 2006) and 20 million tires in Korea (Kim and Kang, 2013) are being discarded. Scrap tire stockpiles can pose health hazard and fire hazard, thus alternative approaches to utilize large amounts of scrap tires has received attention of engineering community. Reuse of scrap tires prevents wastes that require disposal in landfills and preserve the natural resources towards attaining sustainability.

Scrap tires have been used in various applications (after RMA, 2016) as shown in Table 2.1. The largest volume of waste tires has been used as tire-derived fuel (TDF)

in cement kilns, power plants, and paper mills for higher energy. TDF mainly produces the auxiliary fuel, pyrolysis oil, flammable gas, and char. In general, pyrolysis process can be expensive and can cause air pollution problems (Tsai 2015).

Table 2.1 Utilization of waste tires (after RMA, 2016)

Year	Thousands of Tons in various fields								
	TDF	GR	CE	Reclamation Projects	Exported	Punched/ Stamped	Agricultural	BT	Electric Arc Furnace
2005	2144.6	552.5	639.9	0	111.9	100.51	47.6	0	18.9
2007	2484.3	789.1	561.5	132.58	102.0	1.85	7.1	0	27.1
2009	2084.7	1354.2	284.9	130	102.1	1.9	7.1	27.76	27.1
2011	1427.0	1093.5	294.9	54.29	302.5	1.9	7.1	1.92	65.5
2013	2120.2	975	172	49.17	245.8	1.9	7.1	30	65.6
2015	1922.6	1020.7	274.9	52.54	102.1	41.2	7.1	9.19	26

Compared to other applications, civil engineering applications hold great promise to consume large quantities of scrap tires. Next to TDF, scraped tires are largely used in civil engineering field in the form of tire-derived materials. Instead of whole tires, scrap tires are shredded and used alone or used after mixing with soil. The particle size and size distribution of shredded tires can differ; these materials are called scrap tire-derived (STD) geomaterials. ASTM D6270 (2012) recommends using the terms based on the particle sizes: granulated rubber (maximum size of 12 mm), tire chips (between 12 and 50 mm) and tire shred (between 50 and 305 mm). Scrap tires can be used in geotechnical engineering applications in lieu of soils as lightweight fill material, insulation layer material, and drainage material. Prior to field application, it is critical to characterize the engineering properties and evaluate the performance based on laboratory model tests and field pilot studies. Several investigators have studied engineering properties of STD materials. The following sections summarize the properties of scrap tire-derived geomaterials and its mixtures, which are being used in geotechnical applications.

2.2.1 Properties of scrap tire-derived geomaterials

STD geomaterials have been used in various geoengineering applications due to various beneficial properties in the form of tire crumbs, tire chips and tire shreds and their mixtures with soil. Several investigators have studied index and engineering properties of STD geomaterials. The range of specific gravity values for scrap tire chips was reported to be 1.02–1.24 (Ahmed, 1993; Humphrey et al. 1993) which makes the STD materials lighter. They possess high hydraulic conductivity, but it decreases with increase in overburden stress (Zimmerman, 1997; Reddy and Saichek, 1998; Reddy et al. 2010), hence provide better drainage characteristics. Humphrey et al. (1993) investigated the properties of tire-derived aggregate (TDA) in a large size shear box. It was observed that smaller size shreds, with an equal dimensional shape, have higher shear strength than larger size shreds. Further, it was found from the compressibility tests (Fig. 2.1), that TDA is highly compressible in the first cycle of loading, although, it decreased in subsequent cycles of loading and unloading.

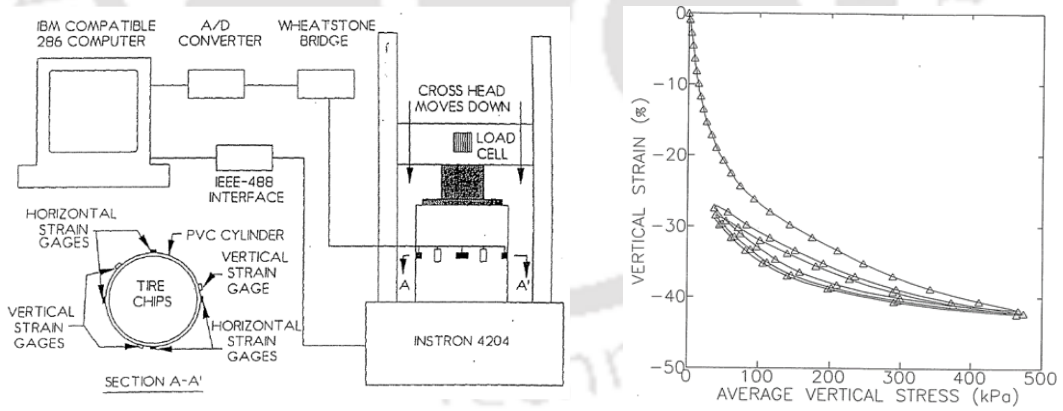

(a) (b)

Fig. 2.1 Compressibility tests on TDA and the responses: (a) compressibility tests, (b) response of compressible test (after Humphrey et al. 1993)

Table 2.2 shows various unit weights of different types of compacted tire shreds. As shown in the table, the unit weight of compacted tire shred ranges from 2.4 kN/m^3 to 7.0 kN/m^3. These values are approximately half of those of typical soils.

Table 2.3 shows the hydraulic conductivity of different types of tire-derived geomaterials.

Table 2.2 Dry unit weight of tire-derived geomaterials

Reference	Tire-derived material size, cm	Dry unit weight, kN/m^3	Compaction type
Humphrey et al., 1992, Humphrey and Sandford, 1993	0.2-7.6	6.13	60% Standard
	0.2-5.1	6.29	60% Standard
	0.2-2.5	2.4	60% Standard
Ahmed, 1993	1.3-2.5	4.90	ASTM D 4253
	1.3-5.1	6.07	50% Standard
	2.3	6.26	Standard
	1.27-5.1	6.56	Modified
	1.3-2.5	6.71	Modified
Tweedie et al., 1998	3.8	6.96	Full scale field test
	7.6	6.78	Full scale field test
Hazarika et al. 2008	2.0	6.75	Compaction
Reddy et al. 2016	2.0	6.45	Compaction

Table 2.3 Hydraulic conductivity of different types of tire-derived geomaterials

Reference	Tire-derived material size, cm	Hydraulic Conductivity (cm/s)	Void ratio, e
Humphrey et al., 1992, Humphrey and Sandford, 1993	1-5.1	7.7	0.925
	0 1-5.1	2.1	0.488
	1.9-7.6	15.4	1.114
	1.9-7.6	4.8	0.583
	1-3.8	6.9	0.833
	1-3.8	1.5	0.414
Lawrence et. al., 1998	1.3-3.8	7.6	0.693
	1.3-3.8	1.5	0.328
Reddy and Saichek, 1998	1.25 -14	0.65	-

The shear strength of scrap tire-derived (STD) geomaterials were determined using triaxial shear and direct shear box has been reported by Bressette (1984), Ahmed (1993), Humphrey et al. (1993), Benda (1995), Cosgrove (1995), Gebhardt (1997), Wu et al. (1997) and Zornberg et al. (2004a). Shear strength properties of different types of scrap tire-derived geomaterials are summarized and presented in Table 2.4. Friction angle values in the range of 6–38° and cohesion values up to maximum 82 kPa were reported. Pando and Garcia (2011) summarized the shear strengths of TDA of various sizes obtained by previous researchers. It was reported that the TDA (maximum size of 4.5 mm) has effective cohesion of 0–14 kPa, and effective friction angle of 14.9–19.2°, when subjected to 25 to 100 kPa confining pressures.

Table 2.4 Shear strength of different types of tire-derived geomaterials

Reference	Tire-derived material size, cm	c (kN/m^2)	φ (°)	Remarks
Humphrey et al. 1993	<3.8	8.6	25	Normal stress : 19.2-71.8 (kN/m^2)
	<5.1	4.3-7.7	21-26	
	<7.6	11.5	19	
Bernal et al. 1996	5.1	0	17-35	17° at 5% strain 35° at 20% strain
Masad et al. 1996	0.46	70.0	6	10% strain
		71.0	11	20% strain
		82	15	30% strain
Xiao et al. 2015	0.05 - 10	8.87	38	-

From the literature reviewed on the properties of STD geomaterials the following unique characteristics are summarized which lead to their use in geoengineering applications.

- Low compacted dry density and thermal conductivity
- High compressibility, enough to absorb vibrations
- Moisture absorption – they are relatively impervious to absorption
- High hydraulic conductivity

2.2.2 Properties of STD geomaterial mixtures

In order to improve the mechanical properties of STD geomaterials, it can be mixed with soil, mostly sand. Several investigators have studied the mechanical properties of STD geomaterials mixed with sand (Edil and Bosscher, 1994; Masad et al. 1996; Tatlisoz and Benson, 1998; Bergado et al., 2005; Ghazavi and Sakhi, 2005; Cetin et al. 2006; Rao and Dutta 2006; Lee et al., 2010; Sheikh et al. 2013; Mashiri et al. 2013; Mashiri et al. 2015; Vinod et al. 2015; Anvari et al. 2017).

Ahmed (1993) presented the first comprehensive study of the properties of sand mixed with tire chips using triaxial apparatus. The confining pressure and gravimetric proportions of the tire chips mainly controlled the shear strength behavior of STC mixtures. The shear strength was increased with increase in the tire chips content in the mixture, up to a maximum improvement occurred when the voids between the tire chips were completely filled with sand. The maximum improvement occurred for the mixture with gravimetric proportion of 30% of tire chips. It was also reported that the compaction effort had almost no effect on the shear strength and on load-deformation response of the sand-tire chips mixtures.

Edil and Bosscher (1994) characterized tire shred – soil mixtures with varying tire shred contents using large-scale direct shear tests and concluded that tire shred inclusions improved the shear strength of tire shred – sand mixtures, especially for low and intermediate confining pressures. Tatlisoz et al. (1998) conducted large-scale direct shear tests with tire shreds, sand, sandy silt, sand-tire shreds and sandy silt-tire shreds mixtures. It was found that the shear strength of the sand-tire shreds mixtures increases with increasing tire shreds content up to 30% by volume. It was noted that the friction angle of the sandy silt-tire shreds mixtures was independent of tire shreds content. The increase in shear strength of the sandy silt-tire shreds mixtures was primarily due to an

increase in apparent cohesion. Similar experiments were performed by Foose et al. (1996) and the results obtained were almost identical. The shear strength of tire shreds-Ottawa sand mixtures was determined by Masad et al. (1996) using triaxial tests by varying sizes and concentration of shreds in the composite. They concluded that the mixtures were suitable fill materials for the construction of highway embankments over soft compressible soils. The shear strength characteristics were improved from 36º to 40º and 11.77 to 26.48 kPa in terms of friction angle and cohesion, respectively. Lee et al. (1999) performed tri-axial tests using pure tire shreds and tire shred – sand mixtures with varying different confining pressures. Lee et al. (1999 and 2010) performed triaxial tests using pure tire shreds and tire shred – sand mixtures to investigate the effect of varying confining pressures on shear strength.

The investigations on compaction of clay and clayey soil mixed with tire shreds were performed by Cetin et al. (2006) and their results are shown in Fig. 2.2. It is clear from the Proctor curves that the maximum densities are higher for clayey soil alone and decreases as the percentage of tire shreds increases both for fine and for coarse tire shreds soil mixtures. Oikonomou and Mavridou (2008) performed similar tests on sand-tire shred mixture and they reported that dry density decreases as the percentage of rubber increases regardless of the rubber size. It shows that, tire shreds or tire shred soil mixture potential for lightweight fill material (Cetin et al. 2006; Oikonomou and Mavridou 2008).

Ghazavi and Sakhi (2005) studied the effect of size of waste tire shreds on shear strength parameters of sand reinforced with shredded waste tires. It has been found that shred content, shred width, shred aspect ratio for a given width, compaction, and normal stress are influencing factors on shear strength of the mixtures. Cetin et al. (2006) performed tests on tire shreds-clayey soil mixture using small-scale direct shear box.

The study was carried out at different tire shred content and sizes. They found that the best mixtures, which gave high value of shear strength, are those with 20% coarse tire shreds (2–4.75 mm) and 30% fine tire shreds (< 0.425 mm). As shown in Figure Fig. 2.3 (a & b), cohesion increases as the tire shreds content increases up to 40%, while the angle of internal friction decreases and vice versa beyond 40% tire shred content.

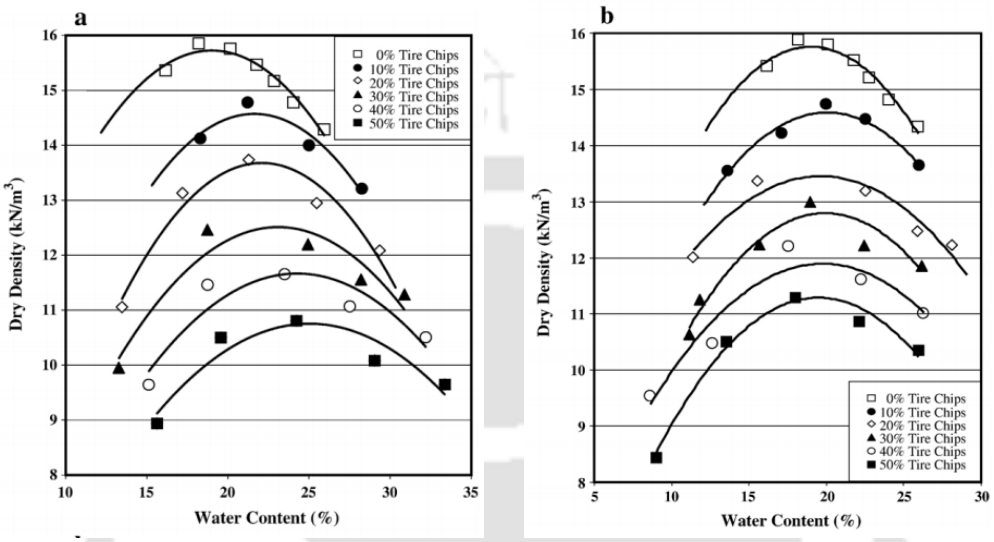

Fig. 2.2 Compaction curves: (a) Fine tire chips, (b) Coarse tire chips (after Cetin et al. 2006)

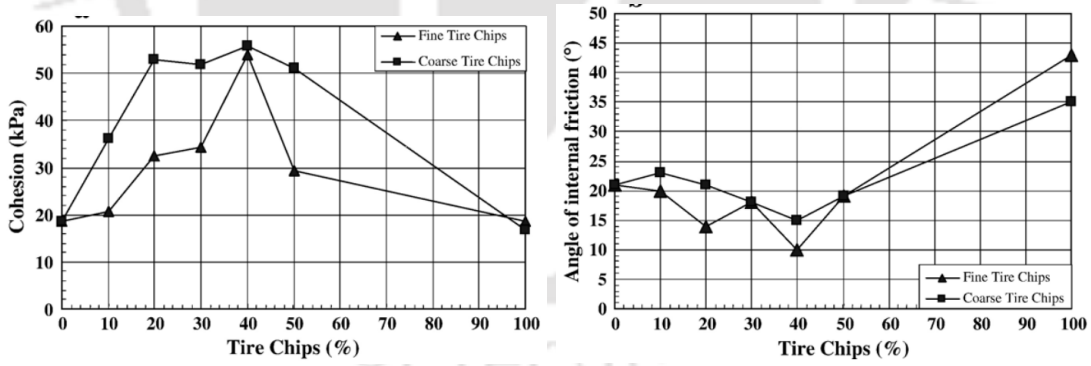

Fig. 2.3 Cohesion and friction angle versus percentage tire shreds (after Cetin et al. 2006)

Rao and Dutta (2006) conducted compressibility and triaxial compression tests by varying chip size and chip content under different confining pressures. The specimens were prepared at particular sand matrix unit weight (i.e. 14.89 kN/m^3). It revealed that tire chip–sand admixtures up to 20% chip content behave like gravel–sand

mixtures. In addition, the compressibility becomes excessive for a chip content of more than 20%. Kim and Santamarina (2008) investigated behavior mixture of small sand particles and large soft rubber particles through experimental and numerically. They discussed about porosity of the different sand –scrap tire-derived geomaterial mixtures were presented in Fig. 2.4. The minimum porosity was observed where V_{rubber} (volume of rubber) equal to 0.6. The sand skeleton controls the behavior for $V_{rubber} < 0.3$, while the rubber skeleton prevails at $V_{rubber} > 0.6$. Similar type of experiments were conducted by Prasad and Raju (2009) using granular types of soils.

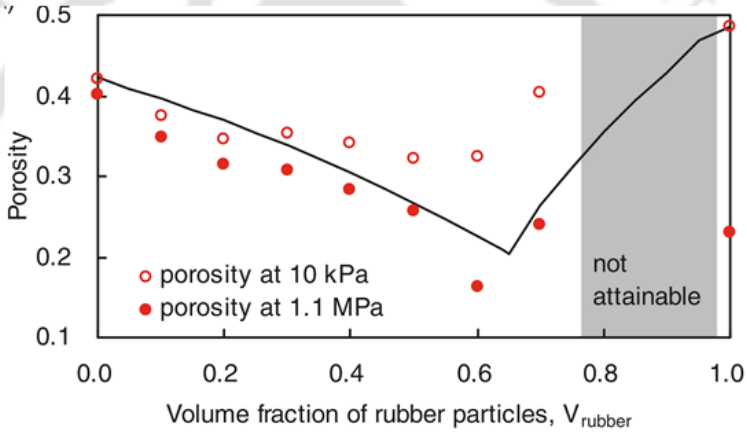

Fig. 2.4 Porosity of sand – rubber particles (after Kim and Santamarina, 2008)

Balachowski and Gotteland (2007) performed consolidated drained tri-axial compression tests, measured the shear strength behavior of tire shred - sand mixtures. The displacement rate was controlled to 0.4 mm/min and the confining pressures used varied from 100 kPa to 300 kPa. The results obtained showed that 30% tire shred content by dry mass is an optimum for the maximum shear strength of the composite. This value was also reported by (Singh and Vinot 2011) who measured the shear strength of tire shred sand mixtures using large-scale direct shear box by varying the concentration of tire shreds in the mixture from 10% to 50% with an interval of 10% and compacting the test specimen in the shear box to achieve nearly the maximum dry density. Singh and Vinot (2011) and Vinot and Singh (2013) conducted direct shear

strength tests on the same mixtures with variation of the shred size and confirmed the same results. Srivastava et al. (2014) and Srivastava and Gupta (2014) investigated the application of shredded tire waste in expansive black cotton soils to reduce the volume change potential and enhance shear strength of the black cotton soil. Reddy et al. (2016), Balunaini et al. (2009, 2014a) and Mashiri et al. (2015) were also discussed about the characterization of sand- tire chips (STC) mixtures. Fig. 2.5 shows the void ratio of different ratio of sand tire chips (different size of tire chips) mixtures. Shear strength properties of tire chips mixed with sand/soil are summarized from various literatures and values are presented in Fig. 2.6 and Table 2.5.

From the figure, it is observed that the void ratio is decreased with increasing tire chips contents up to 30 to 40% after that it is increased. Fig. 2.5 indicates that 30 to 40 % tire chips is optimum mixture upto, which the void ratio is decreased with increasing tire chips contents after that the void ratio increased. At this optimum mixture, most of the voids between the tires chips are filled with sand particles. Maximum shear strength occurs approximately at minimum void ratio that is with closer packing. Larger air voids may cause settlement problems due to compaction under loads. It is observed from the Fig. 2.6 and Table 2.5, that internal friction angle is high at 30% tire chips compared to other mixtures. Shear strength (friction angle) and deformability (void ratio) properties for different mixtures indicated that optimum percentage of tire chips in mixture would lie in the range of 28–30 %.

Few studies (Feng et al. 2000; Anbazhagan et al. 2011; Kaneko et al. 2013a,b; Mashiri et al. 2013, 2016, 2017) have been examined the cyclic behavior of sand tire mixture. Feng et al. (2000) reported the results of torsional resonant columns at different confining pressures to sand – tire mixtures where the tire crumbs were between 1.68 mm to 4.75 mm in size and had a specific gravity of 1.1. Different volumetric

proportions of tire crumbs were mixed with sand and test were carried out at four different levels of confining pressures. The results were normalized with the maximum

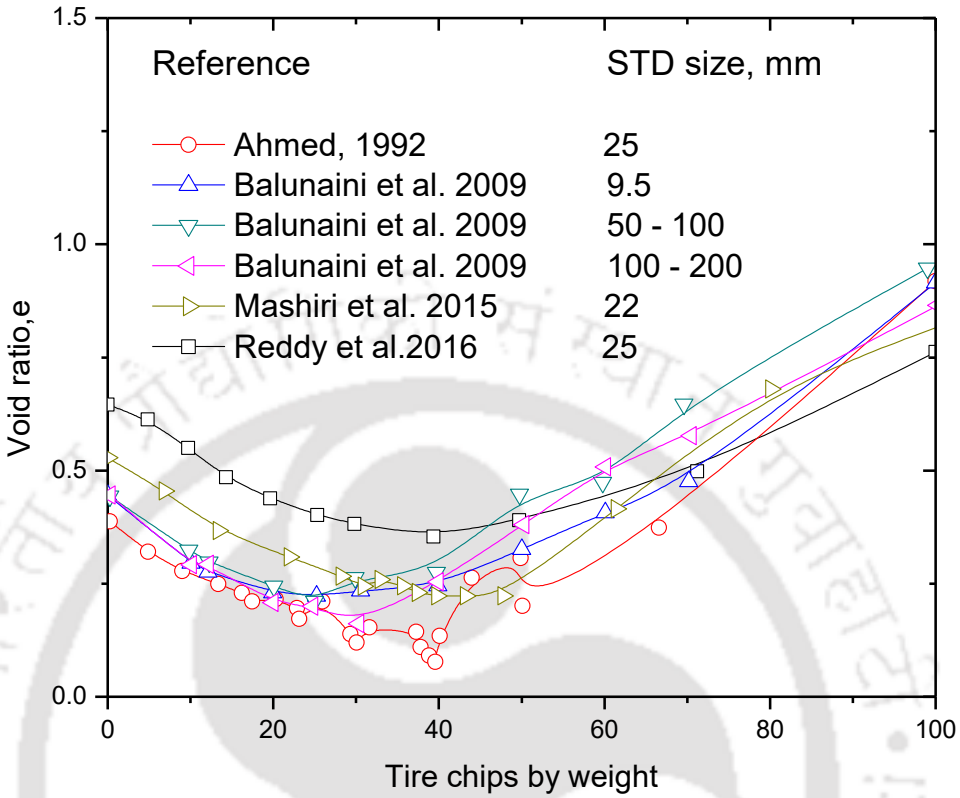

Fig. 2.5 Void ratio of different sand tire chips mixtures

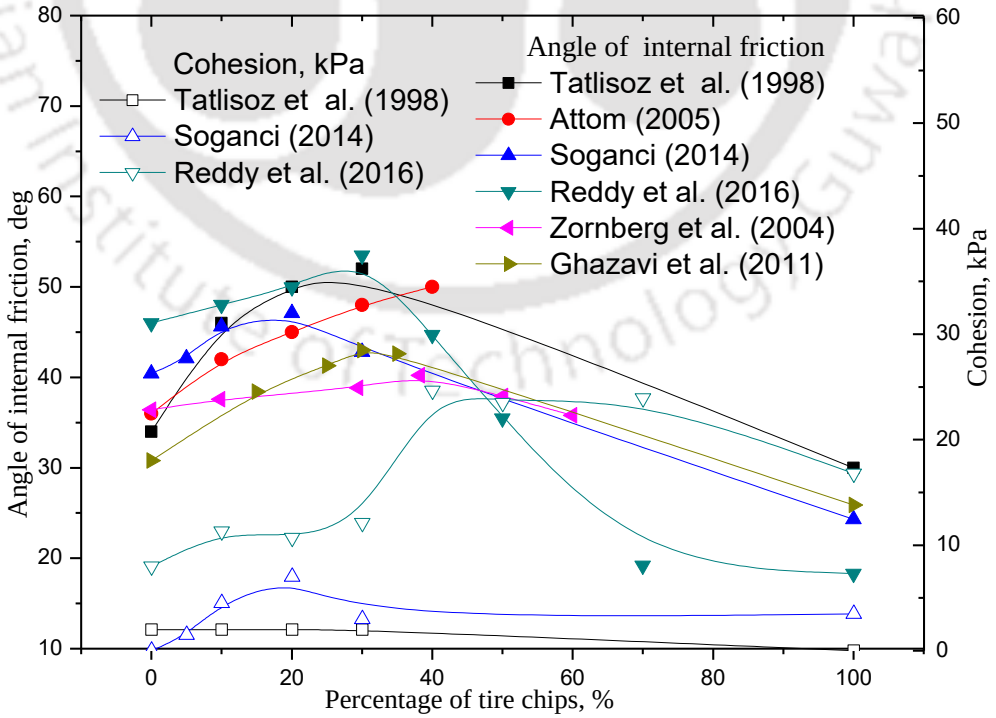

Fig. 2.6 Shear strength properties of sand tire chip mixtures

Table 2.5 Shear strength of tire-derived geomaterials mixing with sand

Reference	Material	Shear Strength Parameters
Tatlisoz et al. (1998)	100 % sand	c =2 kPa ; φ = 34°
	100 % tire chips	c = 0 kPa ; φ = 30º
	90 %sand + 10% tire chips	c = 2 kPa ; φ = 46º
	80% sand + 20% tire chips	c =2 kPa ; φ = 50º
	70% sand + 30% tire chips	c =2 kPa ; φ = 52º
	100 % sandy silt	c =21 kPa ; φ =30º
	90% sandy silt + 10% tire chips	c =8 kPa ; φ = 53º
	80% sandy silt + 20% tire chips	c = 38 kPa ; φ = 54º
	70% sandy silt + 30% tire chips	c = 39 kPa ; φ = 53º
Edinçliler et al. (2004)	100% Sand	c= 6.9 kPa; φ = 33°
	100 Tire Buffings	c= 3.1 kPa; φ = 22°
	95% Sand+5% Tire Buffings	c=10.4kPa; φ = 28.2°
	90% Sand+10% Tire Buffings	c= 8.7 kPa; φ = 29°
Attom (2006)	100% Sand C	φ = 36°
	10% Shredded tire +%90 Sand C	φ = 42°
	20% Shredded tire + %80 Sand C	φ = 45°
	30% Shredded tire + % 70 Sand C	φ = 48°
	40% Shredded tire + %60 Sand C	φ = 50°
Soganci (2015)	100% sand	c = 0 kPa; ϕ = 40.4°
	100% tire crumb	c = 3.5 kPa; ϕ = 24.3°
	95% sand + 5% tire crumb	c = 1.5 kPa; ϕ = 42.1°
	90% sand + 10% tire crumb	c = 4.5 kPa; ϕ = 45.6°
	80% sand + 20% tire crumb	c = 7 kPa; ϕ = 47.1°
	70% sand + 30% tire crumb	c = 3 kPa; ϕ = 42.8°

shear modulus and minimum damping ratio. The shear modulus of sand tire crumb mixtures was strongly influenced by the volumetric proportion of tire crumb in the mixture. The damping ratio of pure tire crumb increased slightly with the confining pressure, which is the opposite to the behavior of soils. Anbazhagan et al. (2011) reported on the use of tire crumbs mixing with soil for developing low-cost damping materials. Kaneko et al. 2013 studied the dynamic properties of sand tire chips mixtures.

They found that higher damping ratio at 15% of tire chips by mass. Mashiri et al. (2016) presented the liquefaction potential and dynamic properties of sand-tire chip mixtures. They observed that the damping behavior of sand-scrap tire mixtures is not affected by the type of scrap tire and the specimen preparation. Further, they found that the damping ratio is slightly higher for sand-scrap tire mixtures with higher content of scrap tires than mixtures with a lower content of scrap tires.

The optimum sand-tire chips mixture has low void ratio and high shear strength properties. Due to the low void ratio and high shear strength of tire shreds together with their widespread availability, they have been used as lightweight fill for geotechnical applications such as backfill behind retaining wall, bridge abutments, and embankments.

STC mixtures are advantageous for use in geotechnical applications because of their low density and high durability, shear strength and thermal insulation; in many cases, they are also cheaper compared with other fill materials. The use of tire rubber as a lightweight geomaterial for embankments or as backfill against retaining walls is very promising and should be promoted. Thus, large volumes of waste tires can be consumed.

2.3 STD GEOMATERIALS AND ITS MIXTURES FOR GEOENGINEERING APPLICATIONS

Construction of Earth retaining structures requires large volumes of backfill material; in general, cohesion less sand can be preferred. Due to unavailable of natural resources and saving natural resources, people looking for use of waste materials. Proper utilization of waste and by-product materials can solve the problem of disposal and sometimes it creates sustainability.

2.3.1 Retaining Walls

STD geomaterial mixtures are lightweight and high shear strength materials so they produce low horizontal pressure on the backside of the retaining walls. Moreover, they are free draining materials (Reddy et al. 2010), thus providing effective drainage and do not allow build-up of any excess pore water pressures behind the wall. Cecich et al. (1996) conducted numerous laboratory experiments on tire chips in order to determine their index properties and shear strength parameters and then designed retaining walls with different heights. Factors of safety for sliding and overturning (Cecich et al. 1996) were tabulated in Table 2.6. From the table, they found that higher factors of safeties against sliding and overturning as compared to sand backfill.

Table 2.6 Comparison of factors of safety for retaining walls (after Cecich et al. 1996)

Height of wall (ft)	Sliding factor of safety		Overturning factor of safety	
	Sand backfill	Shredded tire backfill	Sand backfill	Shredded tire backfill
10	4.15	>20	2.10	>20
20	1.68	10.37	1.84	2.12
30	1.54	3.35	1.65	2.14

Tweedie et al., (1998a, b and c) constructed the largest test retaining wall models of height 4.88 m and used concrete blocks to apply surcharge of 36 kPa. Granular soil and tire shreds were considered as backfill materials. A cross section through the facility is shown in Fig. 2.7. Lateral pressures were measured at-rest and active conditions. It was reported that, horizontal pressures from tire shreds was about 45% less in at-rest condition and 35% less in active condition than for granular soil. Humphrey et al., (1998) constucted an abutment of 300-m long (Fig. 2.8), using STD geomaterials for a Bridge in Topsham. Four types of instruments were installed to monitor lateral earth pressure against the abutment wall, settlements, and heating. It was reported that the tire shred fill compressed about 370 mm during the placement of the overlying soil

cover. Tire sherds used as lightweight fill to improve the slope stability for two highway projects constructed on weak marine clay.

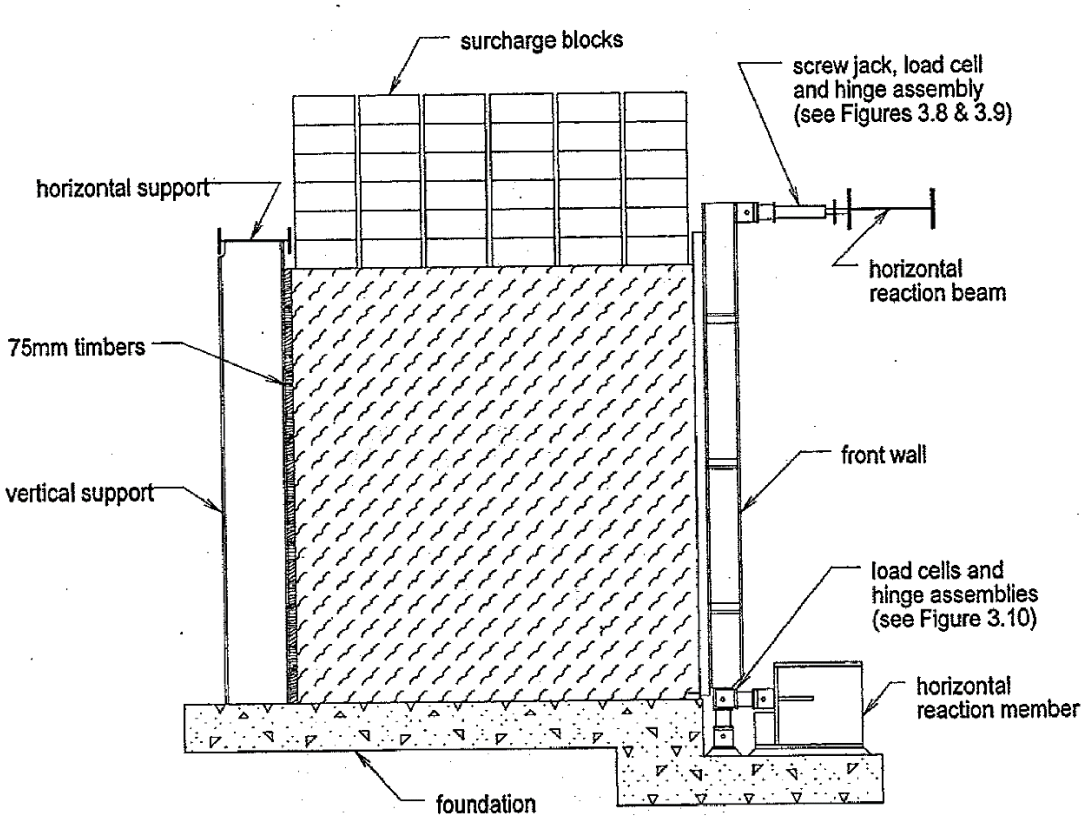

Fig. 2.7 Cross section through University of Maine retaining wall test facility (after Tweedie, et al., I998c)

Huggins and Ravichandran (2011) and Ravichandran and Huggins (2014) performed a numerical study on the seismic behaviour of cantilever retaining walls backfilled with sand and pure waste tire chips using a finite element software (PLAXIS 2D). Fig. 2.9 shows the PLAXIS model with mesh. Soil was modelled as Mohr-Coulomb elastic plastic material available in PLAXIS and the wall is modelled as elastic plate material with plain strain conditions. They observed that the not much effect of the size of the tire chips on the shear force at the base of the wall but there was almost 33% decrease in the shear force with the introduction of tire chips. Further, found that 50% reduction in bending moment at the base of the wall.

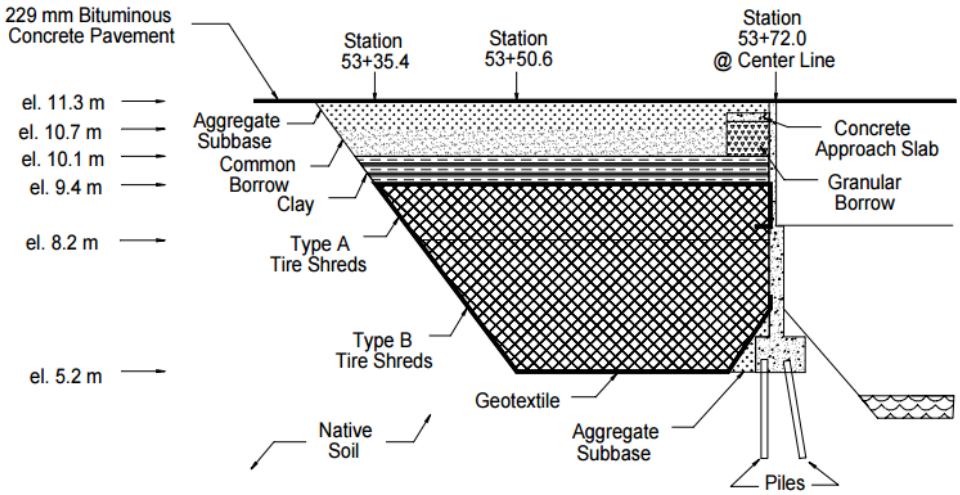

Fig. 2.8 Abutment of the 300 m long Merrymeeting Bridge (after Humphrey et al. 1998)

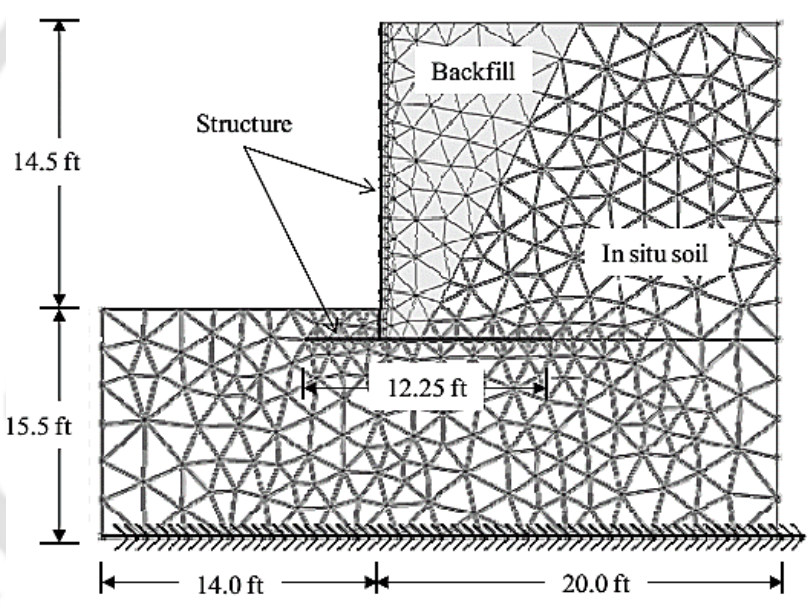

Fig. 2.9 PLAXIS model mesh used in the study (after Huggins and Ravichandran 2011)

Xiao et al. (2012) studied seismic responses of geosynthetically reinforced walls with two types of backfills using shake table tests. The backfills are tire-derived aggregates (TDA) and poorly graded sand, respectively. A section of reduced-scale geogrid reinforced wall (1.6 m high, 1.5 m deep, and 1.5 m long) was built in a box that was anchored on a shaking table (Fig. 2.10). The segmental MSE wall was instrumented

with accelerometers, linear variable differential transformers, linear potentiometers, and dynamic soil stress gauges to record the accelerations, wall vertical deformations, horizontal deflections of the wall face, and transient effective stresses during the shaking, respectively.

Table 2.7 and Table 2.8 present the maximum lateral displacements and maximum accelerations of the four layers of the MSE walls with TDA and sand backfills, respectively. The study revealed that, 29 % reduction in top displacements and 24% reduction in backfill accelerations.

Fig. 2.10 Shake table test of seismic responses of MSE walls (after Xiao et al. 2012)

Table 2.7 Maximum lateral displacements of the MSE walls with TDA and sand backfills (after Xiao et al. 2012)

Locations of displacements	TDA backfill, relative to table movement, cm	Sand backfill, relative to table movement, cm	TDA backfill, relative to underlying layer, cm	Sand backfill, relative to underlying layer, cm
Layer 4 (top)	29.5	41.5	9.7	12.5
Layer 3	23	34.6	5.0	8.0
Layer 2	20.6	34.6	5.0	9.0
Layer 1 (bottom)	15.7	25.2	15.7	25.2

Table 2.8 Maximum accelerations measured in the TDA and Sand backfills (after Xiao et al. 2012)

Locations of displacements	TDA backfill, g	Sand backfill, g
Layer 4 (top)	1.6	2.1
Layer 3	1.6	2.7
Layer 2	2.1	3.9
Layer 1 (bottom)	2.5	5.2

Lazizi (2014) performed numerical analyses of cantilever retaining wall models backfilled with sand alone and waste tire reinforced sand under static and seismic loadings. It has been observed that there was not much change in the horizontal and vertical displacements of the wall with the inclusion of tire chips as a backfill under static loading conditions. But under seismic excitation, the higher value of Von Mises stress for the case of retaining wall supporting waste tire reinforced sand is 3.46 times lower compared to the case of retaining wall supporting sand.

Ravichandran et al. (2014) numerically modelled a cantilever earth retaining wall using PLAXIS 2D as shown in Fig. 2.11. The backfill materials were with only sand and only tire chips considered under seismic loading conditions. The backfill material was modelled as Hardened soil (HS) model. They observed that a 43% reduction in the wall tip displacement after applying El-Centro earthquake acceleration at the base.

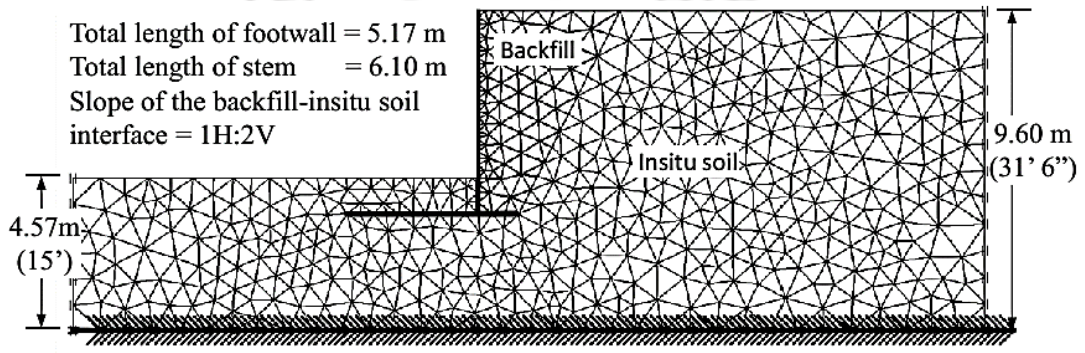

Fig. 2.11 Sample finite element mesh and the wall configuration (after Ravinchandran and Huggins 2014)

Wall displacement histories, for sand and tire chips backfills were compared in the Fig. 2.12. Sand backfill had undergone a tip displacement of 21.6 mm while that of tire chips was 12.3 mm. It was reported that the reduction in displacements was due to the absorption of acceleration by the tire chips.

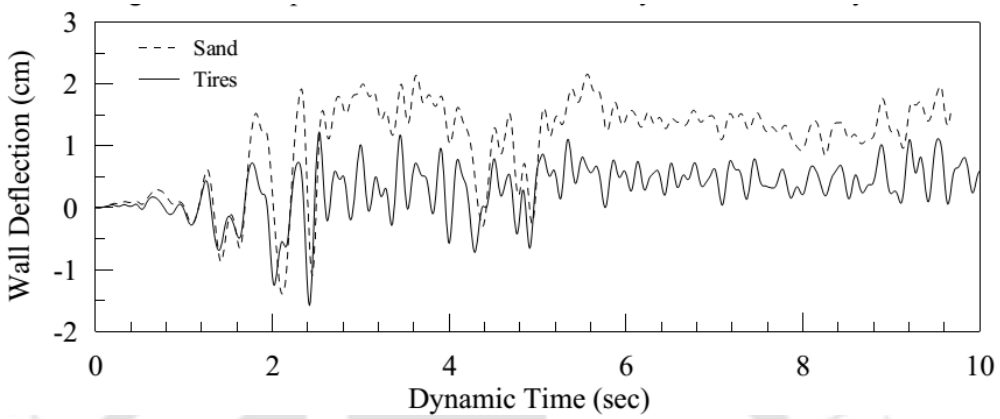

Fig. 2.12 Comparison of wall tip displacement for sand and tire chips (after Ravichandran and Huggins 2014)

Ahn and Cheng (2014) studied the dynamic performance of retaining wall with two backfills (TDA and sand) under simulated earthquakes based on a full-scale shaking table test (Fig. 2.13). It was found that amount of wall sliding increased but the dynamic pressure on the wall exerted by the TDA backfill substantially decreased. Further, they found that top soil layer experienced larger lateral displacements and generated greater dynamic pressure on the wall. In case of TDA, the top soil layer shall be strengthened with additional reinforcement such as geogrid to reduce movement.

Hazarika et al. (2008b) investigated the influence of sand and sand mixed with tire chips as backfill material of retaining as represented in Fig. 2.14. It was concluded from the study that, by using sand mixed with tire chips prevent any liquefaction related damages. Since liquefaction tends to increase the earth pressure against the wall, prevention of liquefaction could reduce the incremental dynamic earth pressure (Fig. 2.15) on soil structures.

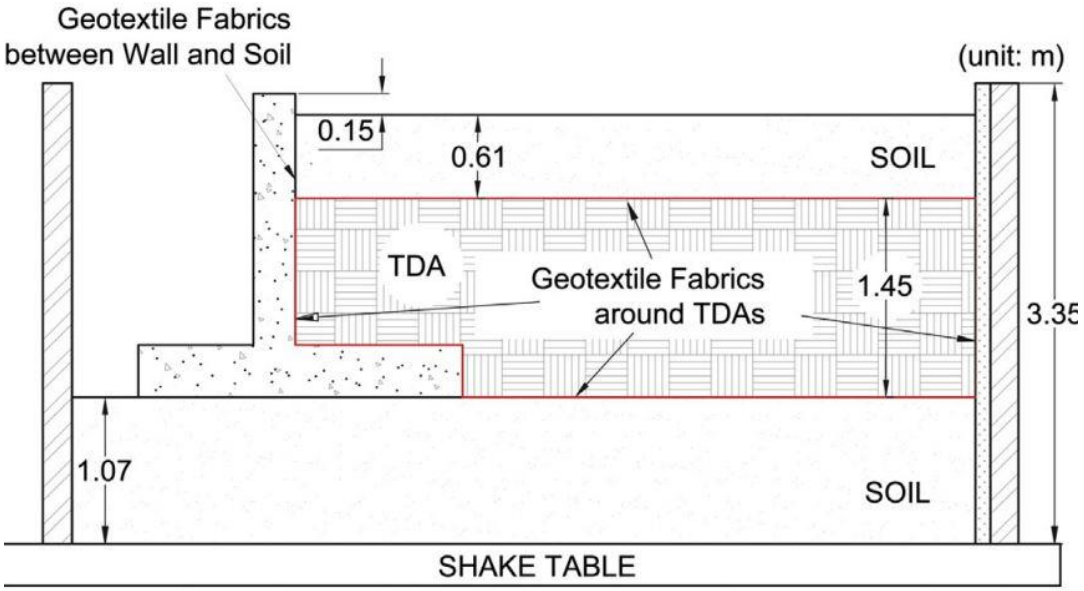

Fig. 2.13 Schematic diagram of full-scale retaining wall (after Ahn and Cheng, 2014)

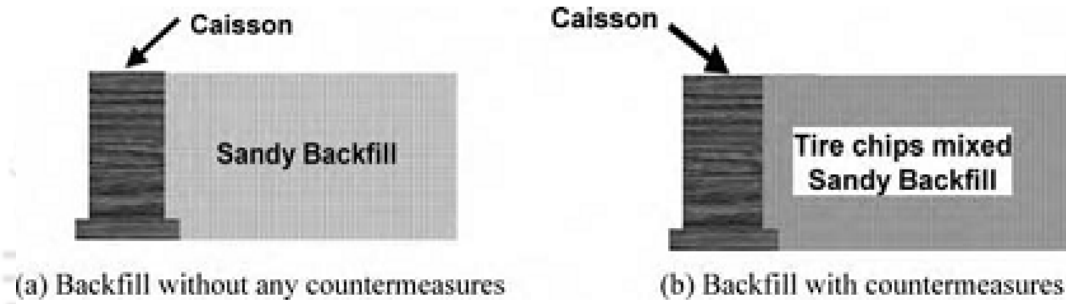

Fig. 2.14 Test conditions adopted (after Hazarika et al., 2008b)

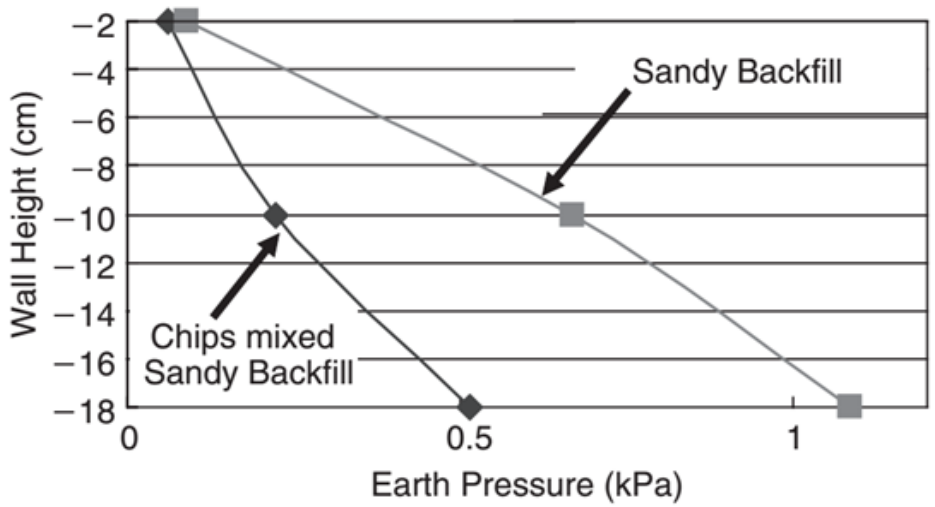

Fig. 2.15 Incremental seismic earth pressure (after Hazarika et al., 2008b)

Compressible Inclusion Just Behind Retaining Wall

Most of retaining walls and bridge abutments are designed to move very slightly outward to allow fully active conditions developed within the backfill, thereby reducing the horizontal pressure on the wall as compared to at-rest condition (Horvath, 1997; Hazarika and Okuzono, 2004; Hazarika et al. 2006, Hazarika, 2008a and Reddy and Krishna, 2013). However, sometimes the retaining walls or abutment walls may not move away from the backfill, thus leading to relatively high "at-rest" horizontal pressures. A cheaper and best alternative method would be to use STD geomaterials immediately behind the wall to allow creating active conditions within the backfill even if the wall does not move. STD geomaterials have high compressible behavior (Rao and Dutta, 2006) to allow the soil backfill to develop active state, reducing lateral earth pressures.

Humphrey et al., (1997) constructed rigid frame structure with 1.00 m wide vertical strip of tire shreds used as backfill as shown in Fig. 2.16. Pressure cells, soil strain meters, slope indicators, and temperature sensors were installed to monitor lateral earth pressures on the wall, as well as the temperature and movement within the tire shred zone. They observed that, the pressure for tire shred backfill is less than half of the pressure with soil backfill.

Field tests were performed by Hazarika et al. (2004) using a 1.5 m high rigid retaining wall against which the variation of static at rest pressure was measured. The setup of the field test is shown in Fig. 2.17. Fig. 2.18 shows the results of the tests (earth pressure distribution) for two conditions; conventional retaining wall and retaining wall with compressible buffer (thickness = 30 cm). It can be seen from the figure that the earth pressure is greatly reduced by using tire chips as compressible inclusion.

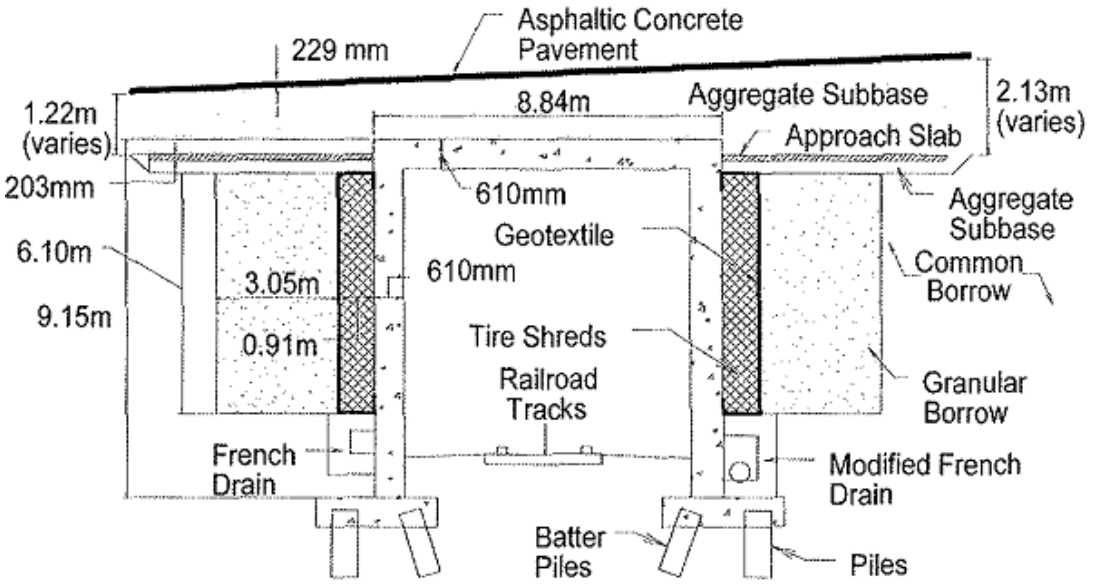

Fig. 2.16 Rigid frame structure with three-foot wide vertical strip of tire shreds (after Humphrey et al. 1997)

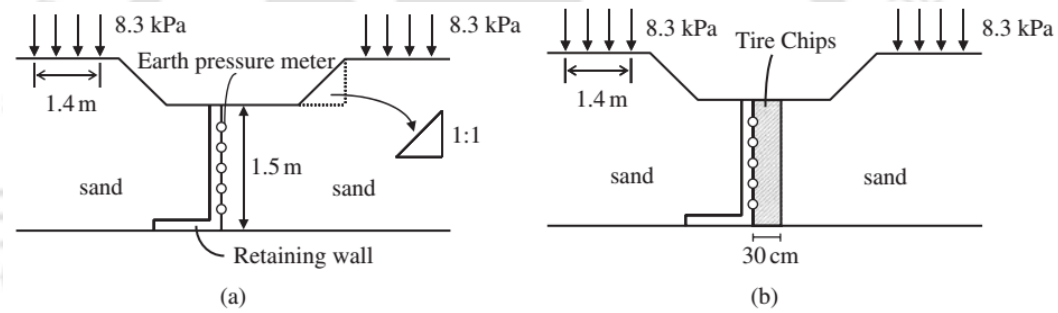

Fig. 2.17 Field-tests: (a) Sand alone, (b) Tire chips as compressible inclusion (after Hazarika et al. 2004)

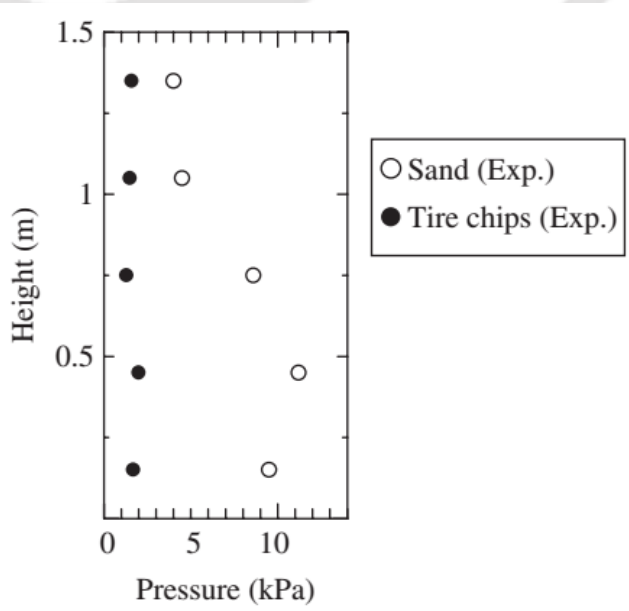

Fig. 2.18 Reduction of earth pressure (after Hazarika et al. 2004)

Kaneda et al. (2008) performed numerical investigation on retaining wall by using compressible inclusion (tire chips) behind of wall (Fig. 2.19). Results obtained from the numerical models were validated with the field experimental. It was observed that, lateral earth pressure was decreased by using compressible inclusion behind of wall as shown in Fig. 2.20.

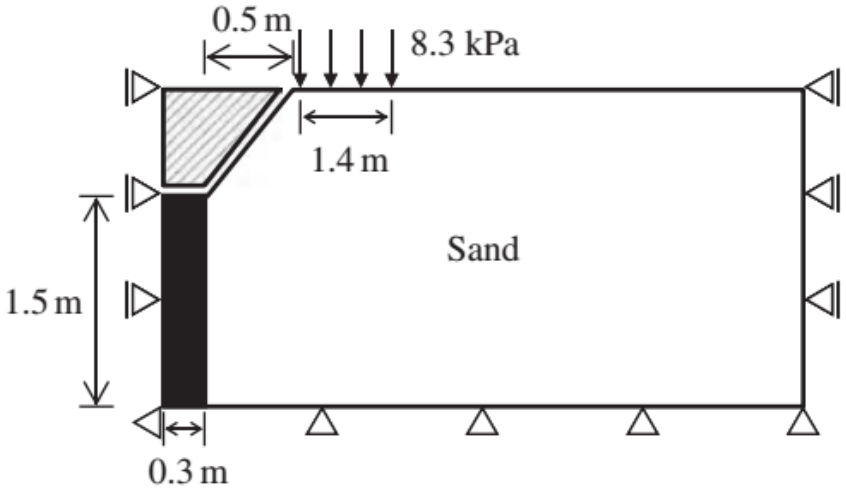

Fig. 2.19 Numerical model of rigid retaining wall (after Kaneda et al. 2008)

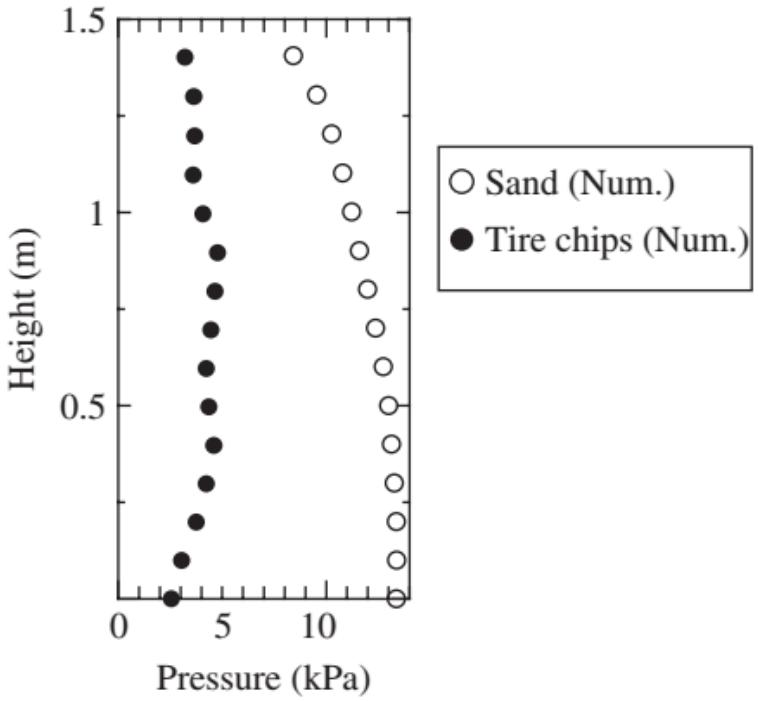

Fig. 2.20 Reduction of earth pressure (after Kaneda et al. 2008)

Large –scale underwater shaking table tests on gravity type model caisson with tire chips studied by Hazarika et al. (2008a). The model caisson made 700 mm height and compressible thickness layer was considered as 300 mm using tire chips (average size of tire chips 20 mm). Cross section of caisson model shown in Fig. 2.21. The seismic performance of earthquake resistant techniques was evaluated by subjecting the soil-structure system into three different earthquake loadings and measured the respective responses. The results in terms of total seismic thrust and caisson top displacements were presented in Fig. 2.22. The results demonstrated that the seismic load against the caisson quay wall was reduced using the cushion. In addition, the presence of the protective tire chips cushion significantly reduced the earthquake-induced residual displacement of the caisson quay wall. Nakhaee and Marandi (2011) investigated dynamic performance of retaining walls using granulated rubber-soil mixture FLAC model considered in the study. They used different rubber percentages (0%, 10% and 14%). It was concluded from the study that, increase in rubber percentage causes less displacement in the wall at the end of the earthquakes. Maximum horizontal pressure applied to the wall was decreased with an increase in rubber percentage.

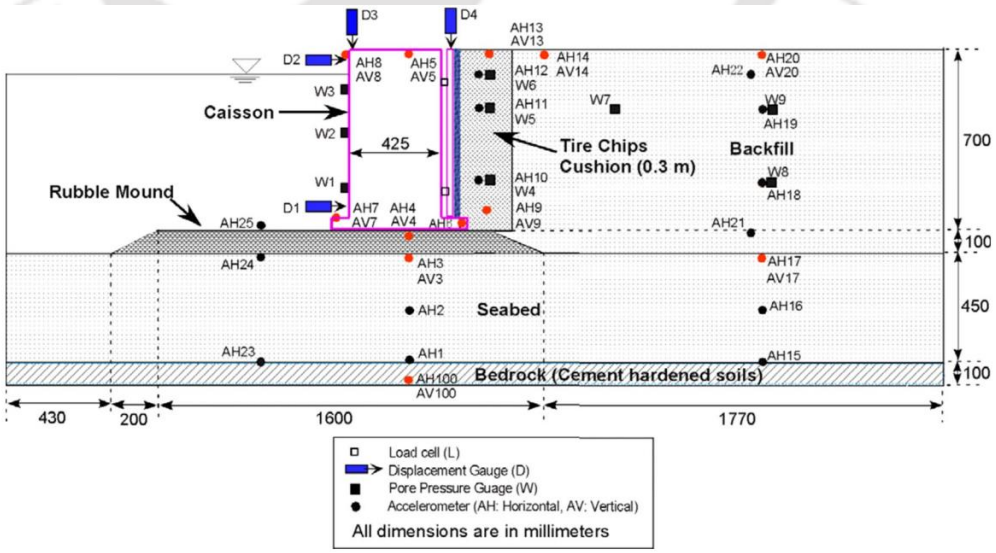

Fig. 2.21 Cross section of test caisson model (after Hazarika et al., 2008a)

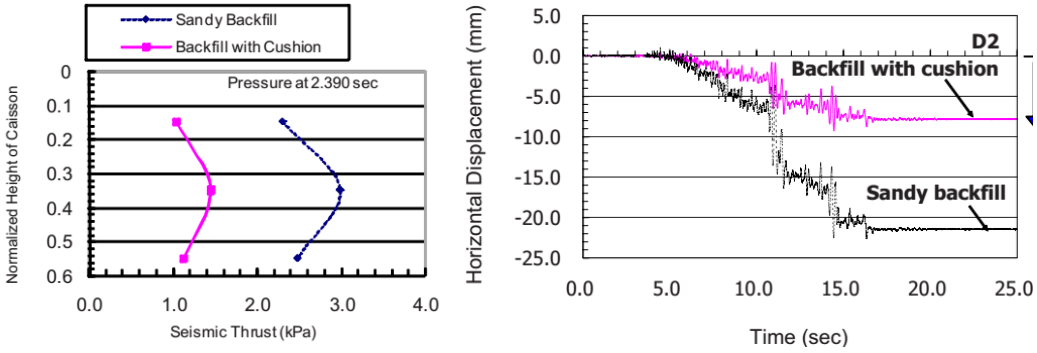

(a) (b)

Fig. 2.22 Effect of cushion on caisson: (a) total seismic thrust, (b) top (at 5 cm from the caisson top. (after Hazarika et al., 2008a)

2.3.2 Highways/Embankments

Construction of highways/embankments requires large volumes of construction materials; therefore, the use of waste materials has been of great interest. Properties of waste tires such as durability, strength, resiliency, and high frictional resistance are favorable for use in highway embankments. The mixture of STD geomaterials with soil/sand for embankment construction may not only provide alternative means of reusing tires to address economic and environmental concerns, but also help to solve geotechnical problems associated with low shear strength (Zornberg et al. 2004a). Tire shreds have been used as lightweight fill material in many embankments and retaining structures in various U.S. states and outside the U.S.A (Bosscher et al. 1997; Humphrey 1996; Humphrey et al. 1998, Dickson et al. 2001; Salgado et al. 2003; Salgado and Prezzi, 2004; Zornberg et al. 2004b, Yoon et al. 2005 and 2006). These studies show that the use of tire shred-soil mixtures have lower compressibility and higher shear strength and thus perform better than only tire shreds. Embankments constructed with soil-tire chip mixtures can potentially have steeper slopes because the backfill has higher shear strength and lower unit weight. Steeper side slopes decrease the volume of material needed. In addition, because of using lightweight material, settlement of underlying soil will be reduced (Tatlisoz et al. 1998).

Salgado et al. (2003), Salgado and Prezzi (2004) and Yoon et al. (2005-2006) constructed the tire/soil embankment. The subgrade was prepared and a 150 mm thick layer of compacted aggregate base was placed and compacted. A layer of geotextile was laid on the compacted aggregate base as shown in Fig. 2.23. The geotextile was laid transversely with an overlap between rolls of 600 mm. The transverse splices of the geotextile were pinned with hog ring clips. A 300mm thick lift of premixed tire shred and soil mixture was placed on the filter fabric. Each layer of tire shred and soil fill was uniformly placed across the full width of the roadway cross section. As shown in Fig. 2.23, the tire and soil embankment was covered with 0.9 m of cohesive encasement material. The encasement material was placed and compacted at the same time the tire and soil lift was placed. They observed that, maximum settlement was approximately 12 mm and the settlement stabilized after 200 days of traffic. Maximum lateral movement was observed about 5 mm. Samples of groundwater were analyzed for metals which apply to a secondary drinking water standard and standard of maximum contaminant level for drinking water according to Indiana Department of Environmental Management (IDEM). Except for manganese, all levels were well below the standard limits. No evidence of internal heat generation was detected. This confirmed that the use of tire shred and soil mix is a proper way to prevent self-heating of the tire shreds. Observations showed no signs of slope stability problems, cracking on the road or erosion.

Shahin et al. (2011) studied slope stability analysis using bauxite residue sand tire mixtures with variation of embankment heights with slope angle of 30˚ using 2D plain strain conditions (Fig. 2.25). Tire grains (4 mm) range varied from 10% to 40% by weight. It was observed that in all cases (Fig. 2.26), the factor of safety decreases with the increase of embankment height, as expected and all embankment heights,

significant improvement in slope stability occurs with increasing tire grain content (especially at 30%).

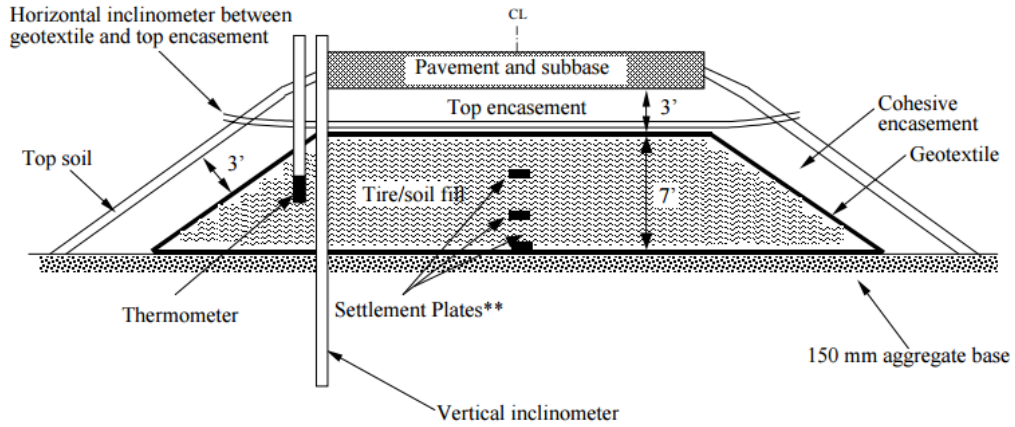

Fig. 2.23 Schematic diagram of tire shred and soil embankment (after Salgado et al., 2003)

Fig. 2.24 Sand - tire chip mixture (75/25) (after Yoon et al. 2006)

In an investigation of an embankment constructed in Lakeville in the USA, the levels of all metals in the groundwater were below the standard limits prescribed for secondary drinking water. In addition to this, tire chips have high sorption capacity for

volatile organic chemicals, which means that tires can be used to eliminate chemicals from contaminated water (Park et al., 1996). Tire shred–sand mixtures were found to be effective in inhibiting exothermic reactions since the tire shreds are entirely covered with the sand (Yoon et al., 2006).

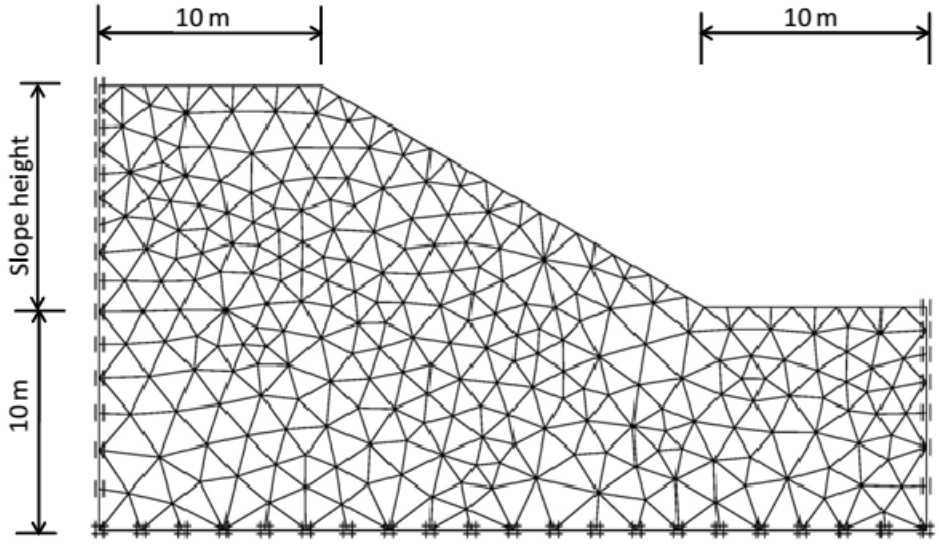

Fig. 2.25 Finite element mesh used in PLAXIS for the stability analysis of 10 m height embankment with slope angle of 30˚. (after Shahin et al., 2011)

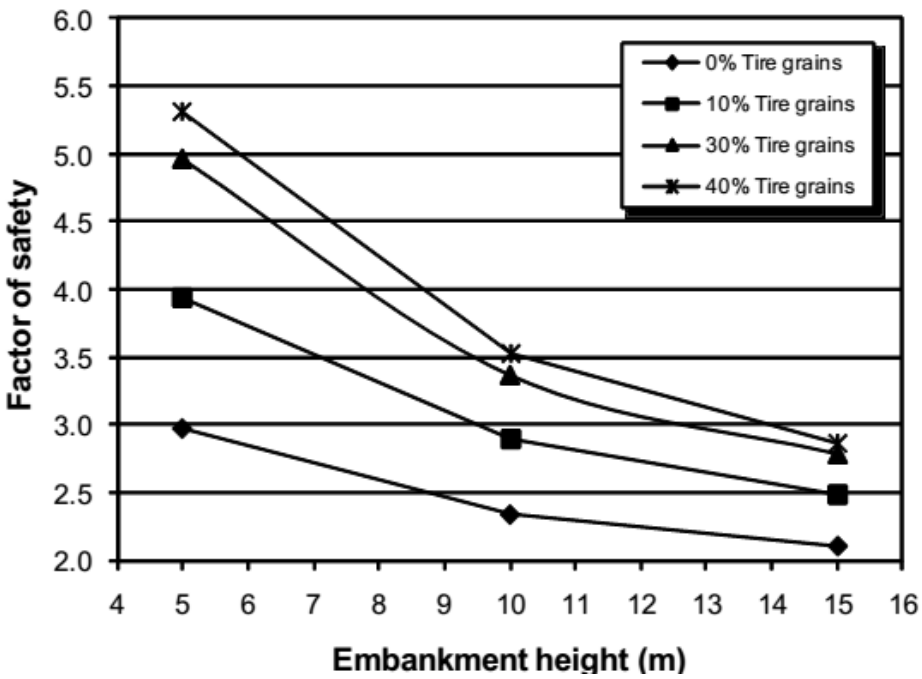

Fig. 2.26 Effect of tire grains contents on factor of safety with embankment height (after Shahin et al., 2011)

2.3.3 Foundations

Various laboratory studies were conducted to assess the improvement of the bearing capacity of soil reinforced with tire shreds. The results of sand mixed randomly with shredded tire obtained by Hataf and Rahimi (2005) showed that the bearing capacity ratio (ratio of bearing capacity of improved to unimproved soil) increases as tire shreds content and aspect ratio increase. However, the bearing capacity was the maximum pressure applied on the sample beyond which the failure occurred. As shown in Table 2.9, the optimum tire shreds content after which the bearing capacity ratio starts to decrease was found to be 40% and the optimum aspect ratio for the maximum bearing capacity ratio was 4.

Alqaissi (2012) studied influence of tire chips on the behavior of strip footing on sandy soil by performing a series of laboratory model tests. The test setup used was shown in Fig. 2.27 (280 mm length, 250 mm width and 250mm depth container). The model strip footing was made of steel plate with dimensions of 30× 30×270 mm was adopted. Testing was conducted on sand beds with tire chips inclusions of 10%, 20% and 30%. As shown in Fig. 2.28, settlement of strip footing on sand-tire chips mixture was about 22% lesser than that in the case of pure sand, and the ultimate bearing capacity of the mixture noticeably increased up to two times with inclusion of 20% tire chips.

Table 2.9 Bearing capacity ratio of tire shred sand mixture (after Hataf and Rahimi, 2005)

Tire shreds content %	Size of shreds, cm						
	2×4	2×6	2×8	2×10	3×6	3×9	3×12
10	1.17	1.46	1.46	1.56	1.56	1.73	1.83
20	1.6	2.03	2.0	1.97	1.9	2.13	2.2
30	2.15	2.73	2.8	2.84	2.69	2.8	3.0
40	-	3.2	3.4	-	-	-	3.9
50	-	2.95	3.3	-	-	-	3.9

Fig. 2.27 Model container for typical foundation (after Alqaissi 2012)

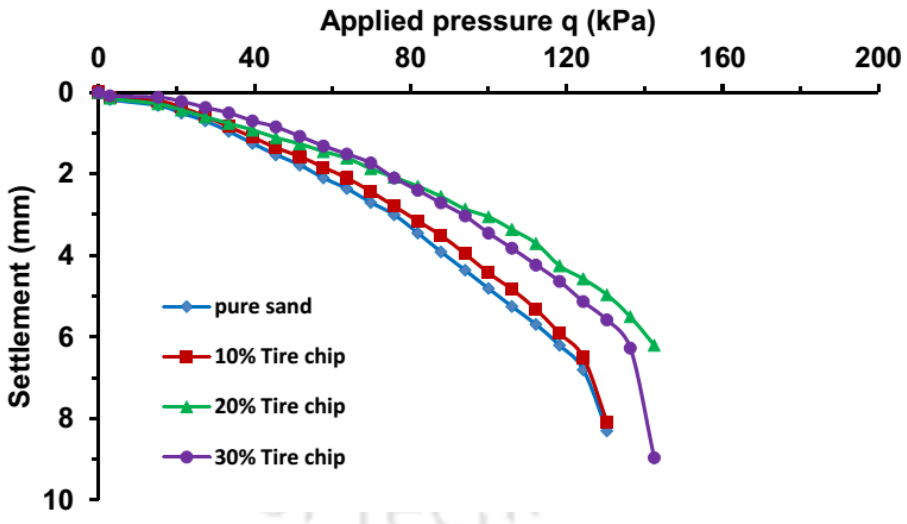

Fig. 2.28 Effect of tire chip contents on settlement. (after Alqaissi 2012)

Bandyopadhyay et al. (2015) studied the performance of sand and shredded rubber tire mixture as a natural base isolator for earthquake protection. The building foundation was modeled by a 200 mm by 200 mm and 40 mm thick rigid plexi-glass block. The whole setup (Figure 14) was mounted on a shake table and subjected to

sinusoidal motions with varying amplitude and frequency. They observed that the net bearing capacity increased significantly for 30% and 50% shredded tire mixture due to increase in cohesion. The net bearing capacity values reported were 173 kPa, 120 kPa, 1037 kPa and 1235 kPa for sand, 20%, 30%, 50 % tire chips by weight, respectively

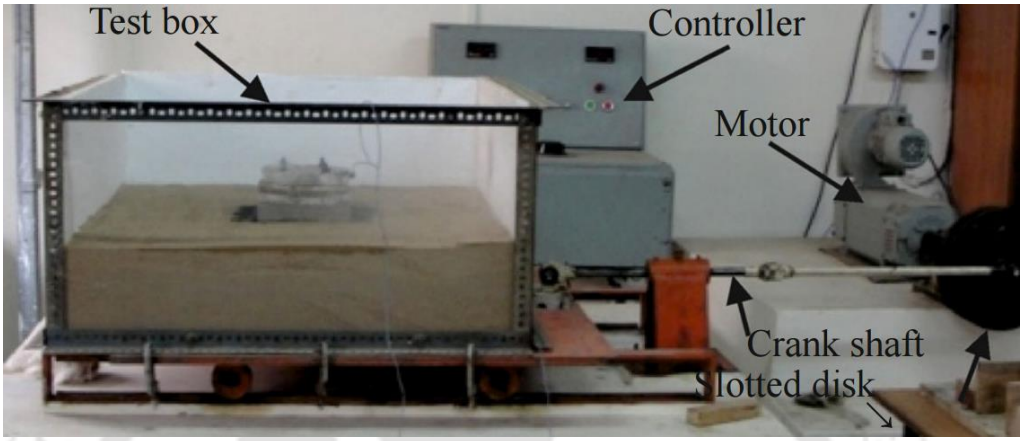

Fig. 2.29 Model setup adopted for foundation tests (after Bandyopadhyay et al. 2015)

Tsang (2008) proposed a promising seismic isolation method particularly suitable for developing countries, which makes use of rubber–soil mixtures (Fig. 2.30). A series of numerical simulations and parametric studies have been done to demonstrate the effectiveness and the robustness of the method. Fig. 2.31 (a) and (b) shows the Fourier amplitude spectra (FAS) of the horizontal and vertical ground accelerations, respectively. Fig. 2.31 (c) and (d) shows the corresponding normalized horizontal and vertical ground acceleration time histories of the two scenarios. They concluded that, seismic isolation with rubber–soil mixtures could reduce the horizontal and vertical ground accelerations by 60–70% and 80–90%, respectively.

2.3.4 Drainage Layer in Embankment, Landfill Cover and Liner Systems

Tire chips, tire shreds, and rough shreds have potential to be used as drainage material in lieu of granular material in landfill cover and liner systems. Extensive laboratory and field studies were conducted by (Reddy and Saichek, 1998 a and b) and

(Reddy et al. 2002 and Reddy et al. 2008) to evaluate this application. Tire shreds were evaluated for hydraulic conductivity as a function of normal stress. Tire shred drainage layer in final cover is subjected to low vertical stress, so there is no concern with reduction of hydraulic conductivity. However, vertical stress due to overlying waste would be a concern if used as a drainage material in bottom liner system. It was shown that even under high normal stress conditions, tire shreds maintain high hydraulic conductivity to serve as an effective drainage layer.

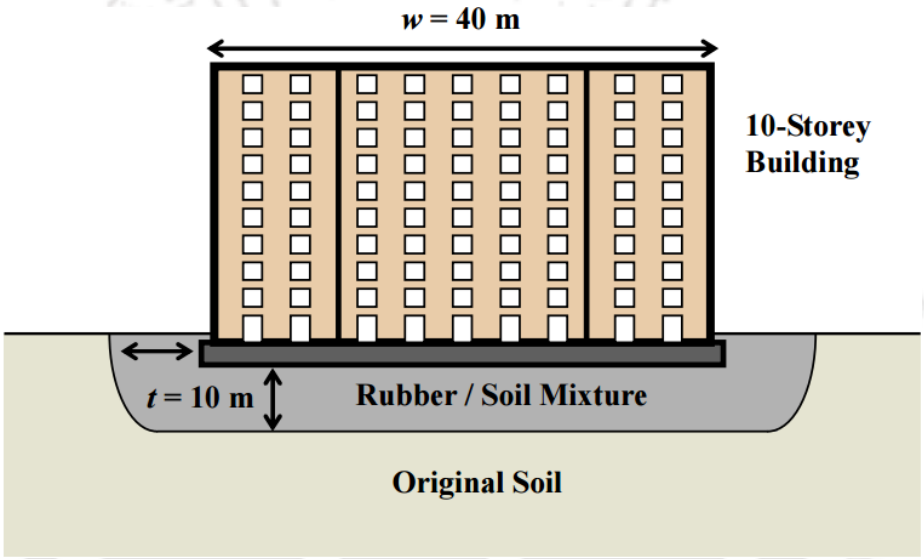

Fig. 2.30 Schematic drawing of the seismic isolation method using a layer of rubber–soil mixture (after Tsang, 2008)

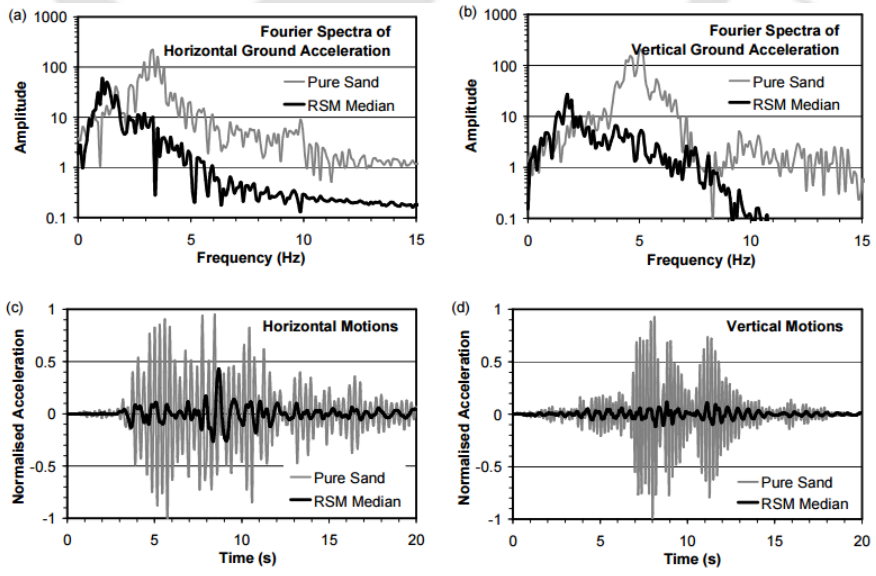

Fig. 2.31 The Fourier amplitude spectra different acceleration time histories (after Tsang, 2008)

Model clogging and transmissivity tests also demonstrated that the tire shredded drainage layers possess excellent properties to serve as effective drainage media. Hazarika et al. (2010) examined the use of tire shreds as a drainage layer in embankment. They have used 240-ton scrap tire shreds were used in the construction of the drainage layers in embankment. Tire shreds could contain steel wires; hence, any potential damage to underlying geomembrane in cover or liner system is a major concern. This issue was investigated through field test plots as well as large-scale laboratory model tests (Reddy and Saichek, 1998a) and found that a geotextile cushion is necessary to be placed between the geomembrane and tire shreds to protect the geomembrane. Reddy et al. (2008) used tire shreds as drainage material in final cover at a landfill, monitored its performance, and found that it performed excellent.

2.4 CRITICAL APPRAISAL OF LITERATURE

Use of scrap tire- derived (STD) geomaterials in geoengineering applications has received growing interest to prevent creation of wastes and conserve natural resources towards achieving sustainability. The studies on STD geomaterial properties like specific gravity, hydraulic conductivity, compressibility, shear strength parameters and STD geomaterial mixture properties indicated the merits of STD geomaterials and their mixtures in geoengineering applications.

Several researchers have studied on the use of scrap tire-derived (STD) geomaterials and their mixtures as alternative fill material for static and seismic loading conditions. For ex. Humphrey and Manion 1992; Cecich et al. 1994; Tweedie et al. 1998(a, b and c); Salgado et al., 2002; Salgado et al., 2003; Zornberg et al. 2004b; Yoon et al., 2006; Hazarika et al. 2007, Tandon et al. 2007; Tsang et al. 2012; Xiao, 2012; Ravichandran and Huggins, 2014. Tire chips, tire shreds, and rough shreds have been used as drainage material in lieu of granular material in landfill cover and liner systems

(Reddy and Saichek, 1998; Reddy et al., 2002; Reddy et al., 2008). The studies indicate that performance of retaining walls could be improved by the use of lightweight backfill materials or compressible materials behind the wall. Few studies on STD geomaterials showed that STD geomaterials could be adopted for both the above solutions.

Considering the importance of the public infrastructure facilities, like retaining walls and their volume, a comprehensive study to show the benefits of the use of STD geomaterials in retaining wall applications is essential. Model studies on the performance of retaining walls using STD geomaterials and their mixtures are limited in the literature.

2.5 OBJECTIVES AND SCOPE OF THE WORK

Aim of the present research work is to investigate the beneficial effects of the use of scrap tire-derived geomaterials, in the form of tire chips, in retaining wall applications. This is divided into two major objectives:

a. Application of Sand –Tire Chips (STC) mixtures as a light weight fill material
b. Application of tire chips as a compressible inclusion

To achieve the above objectives, through physical and numerical simulations, the following scope is formalized.

- Evaluation of index and engineering properties of materials (sand, tire chips and STC mixtures).
- Physical model (static and seismic) tests to study the behaviour of retaining wall using different Sand – Tire Chips (STC) mixtures as light weight backfill material.
- Physical model (static and seismic) tests to study the behaviour of retaining wall with tire chips as compressible inclusions.

- Development of numerical models for retaining wall models to perform parametric numerical simulations with the different STC mixtures properties.
- To evaluate the financial benefits by design and cost analysis of retaining walls using STD geomaterials

2.6 SUMMARY

This chapter presented review of the published studies related to properties of scrap tire-derived geomaterials and its mixtures. Further, studies on laboratory model tests, numerical simulations and field studies presented and discussed briefly in order to provide critical insight into various behavioral aspects these structures. Critical appraisal of the literature review and scope of the present study were presented.

Chapter 3. MATERIALS AND METHODS

3.1 INTRODUCTION

Present study involves the laboratory experiments on retaining wall models, with different types of backfill materials, under static and seismic conditions. Sand and tire chips were used to prepare different sand –tire chips (STC) mixtures of different proportions. Sand and different STC mixtures were used as backfill materials, while, tire chips were used as compressible inclusion just behind the retaining wall. This chapter presents the details of materials used in experiments and their properties. The details of the method adopted for building the model wall, shaking table facility, instrumentations and testing procedure under static and seismic cases are also described.

3.2 MATERIALS

3.2.1 Sand

Locally available cohesionless sand has been used for the study. The particle size characteristics of the sand were determined as per IS: 2720 (part 4) -1985, which showed a coefficient of uniformity (C_u) and Coefficient of Curvature (C_c) as 1.82 and 1.02, respectively. The particle size distribution curve of the sand is shown in Fig. 3.1. The maximum unit weight (γ_{dmax}) (as per IS: 2720 (Part 14) - 1983) and minimum unit weight (γ_{dmin}) of the sand were determined as 16.00 kN/m^3, and 13.6 kN/m^3, respectively. The sand is classified as 'poorly graded' with letter symbol 'SP' as per, Unified Soil Classification System. The shear strength parameters of sand, at unit weight of 15.57 kN/m^3, corresponding to 85% relative density, were determined by conducting large size direct shear tests. Direct shear tests using a shear box of 300 ×

300 × 300 mm were carried out at three normal stresses of 25, 75, and 125 kPa. The shearing rate was kept at 1.25 mm/min for all the tests. The shear stress-shear strain responses obtained from direct shear tests are presented in Fig. 3.2. The peak friction angle (ϕ) obtained from direct shear test is 48°. Properties of the sand are shown in the Table 3.1.

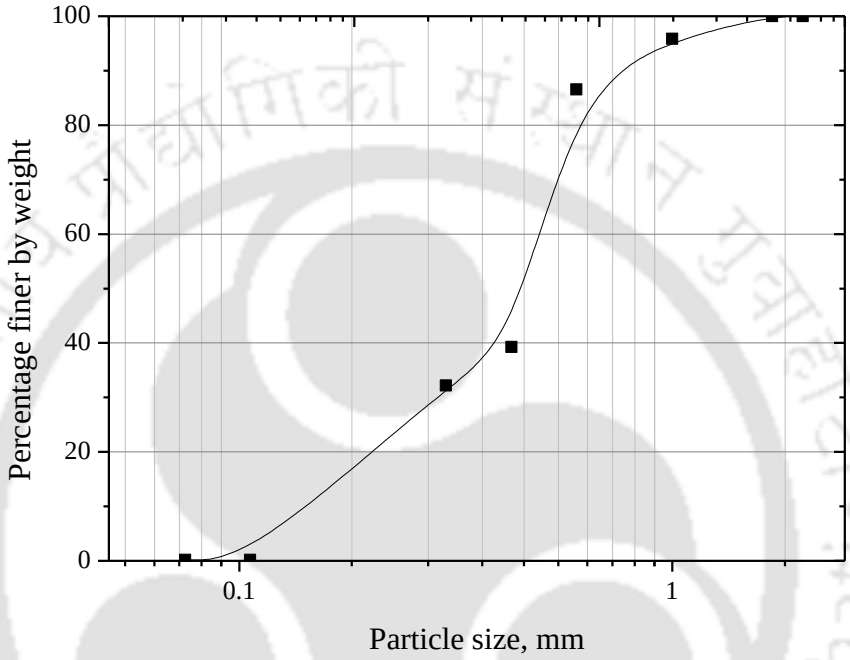

Fig. 3.1 Grain size distribution of the sand

Table 3.1 Properties of sand

Properties	**Value**
Specific gravity of sand (G_S)	2.62
Maximum void ratio(e_{max})	0.94
Minimum void ratio (e_{min})	0.64
Maximum dry unit weight (kN/m^3)	16.0
Minimum dry unit weight (kN/m^3)	13.6
Angle of internal friction	48°

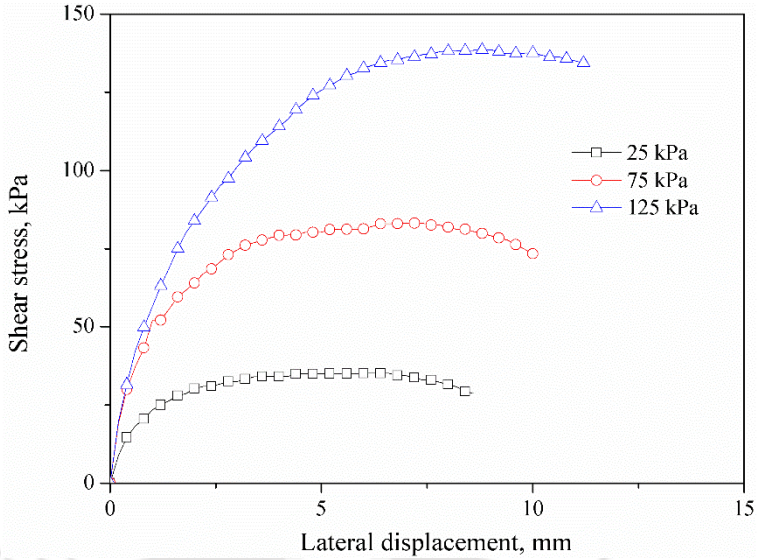

Fig. 3.2 Shear stress vs. Lateral displacment of sand

3.2.2 Tire chips

Scrap tire-derived (STD) geomaterials in the form of tire chips (TC) are adopted for the study. The scrap tire chips of, approximately, 20 mm long with 10×10 mm square cross section, cut from scrap tires, and were used. The pictorial view of tire chips is shown in Fig. 3.3. Specific gravity (G_{TC}) value of tire chips is determined using a large size pycnometer (1,000 mL) as per IS: 2720 (part 3) -1980. The other index properties, such as unit weights, maximum and minimum void ratios of tire chips were determined and are reported in Table 3.2. The compacted dry unit weight of the tire chips was found to be 6.45 kN/m^3.

Fig. 3.3 Picture of tire chips

Table 3.2 Index properties of tire chips

Properties	Value
Specific gravity of tire chips (G_{TC})	1.08
Maximum void ratio(e_{max})	0.97
Minimum void ratio (e_{min})	0.65
Compacted unit weight (kN/m^3)	6.45
Minimum unit weight (kN/m^3)	5.39

3.2.3 Sand -Tire chips (STC) mixtures

Sand-Tire chips (STC) mixtures were prepared manually by adding tire chips (TC) to sand in selected proportions by weight. Percentages of TC considered in the different mixtures were 10%, 20%, 30%, 40%, 50%, and 70%, which are represented as STC10, STC20, STC30, STC40, STC50 and STC70, respectively (Table 3.3). STC0 mixture represents 0% tire chips, i.e., pure sand. The calculated amounts of sand and TC were placed together, and mixed thoroughly to form a uniform STC mixture as shown in Fig. 3.4. The grain size distribution curves of STC mixtures were evaluated and shown in Fig. 3.5

Table 3.3 Backfill STC mixtures

Backfill material	% Sand	% Tire chips (by weight)
STC0	100	0
STC10	90	10
STC20	80	20
STC30	70	30
STC40	60	40
STC50	50	50

STC mixture weight ratios are converted to volume ratios (Eq. 3.1) using the weights of sand (W_s) and tire chips (W_{TC}) contents in each mixture along with specific gravity values of sand (G_S) and tire chips (G_{TC}) of the individual materials. The volume ratios (%V_{TC}) are presented in Table 3.4 and shown in graphical form in Fig. 3.6.

$$\%V_{TC} = \frac{\frac{W_{TC}}{G_{TC}}}{\frac{W_S}{G_S} + \frac{W_{TC}}{G_{TC}}} \times 100 \qquad \text{(Eq. 3.1)}$$

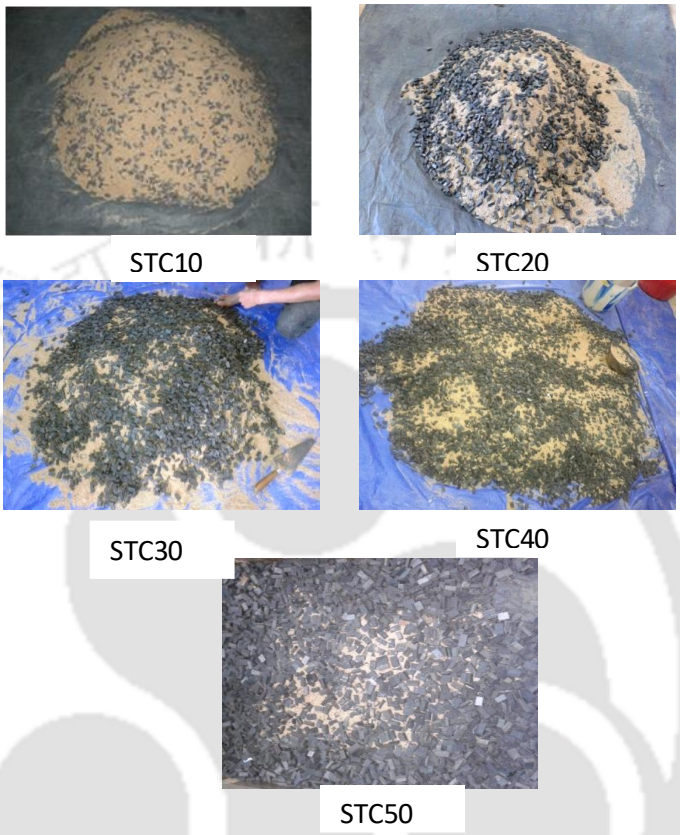

Fig. 3.4 Different STC mixtures

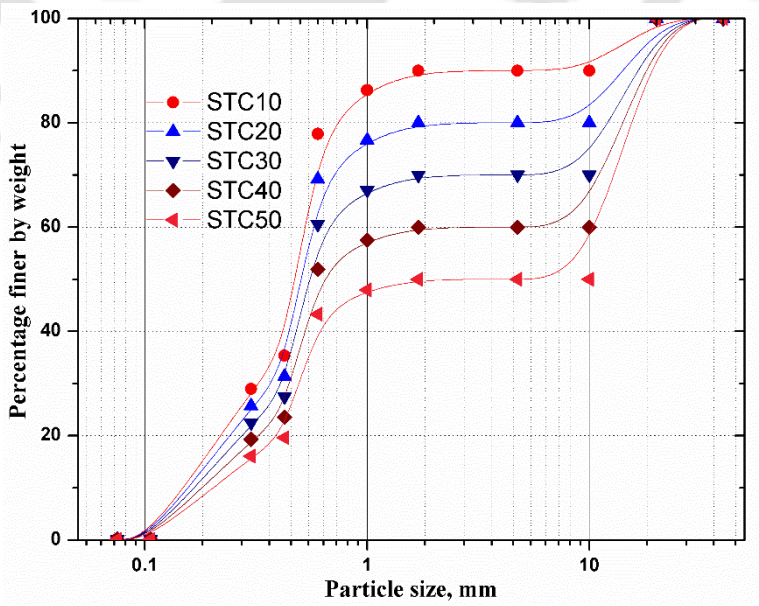

Fig. 3.5 Grain size distribution curves of the STC mixtures

The laboratory-tests have been performed to determine (1) dry unit weight (2) specific gravity, and (3) shear strength properties of STC mixtures at different gravimetric ratios. For each test, sufficient amount of STC mixture was collected from the mass mixture (target) prepared and used for the test specimens. After completing each test, the corresponding weights of sand and TC used in the test specimens were measured to evaluate the achieved percentage of TC in the test specimen (Eq.3.2). The percentage mixture ratio of tire chips (*%TC*) was also calculated by the dry weight of the tire chips (W_{TC}) relative to that of the total mixture material (W_{TC} + W_S), where W_S is the weight of sand, as per the Eq. 3.2.

$$\%TC = \frac{W_{TC}}{W_{TC} + W_S} \times 100 \quad \text{(Eq. 3.2)}$$

The targeted ($\%W_{TCtargeted}$) and achieved ($\%W_{TCachieved}$) weight percentage of tire chips evaluated from different test specimens are shown in the Table 3.4. The achieved percentages are within ±1% variation from that of the targeted %.

Table 3.4 Target and achieved (%) of tire chips in the mixture

STC Mixture	$\%W_{TCtargeted}$	$\%W_{TCachieved}$	$\%V_{TC}$
STC10	10	9.72	20.71
STC20	20	19.60	37.16
STC30	30	29.35	50.56
STC40	40	39.30	61.11
STC50	50	49.60	70.49
STC70	70	71.17	85.69
TC	100	100	100

Specific Gravity

Specific gravity (G_{STC}) values of STC mixtures were measured using large size pycnometer (1000 ml). Average specific gravity values of each STC mixture is calculated from three values obtained for different samples and are presented in Fig. 3.7. The specific gravity values for STC mixtures are also calculated (Eq.3.3) using

specific gravity values of sand (G_S), tire chips (G_{STC}) alone and the corresponding weights used in the mixtures. Fig. 3.7 shows the measured and calculated specific gravity values of the different STC mixtures, which are well matched. Hence, it can be stated that for any targeted STC mixture, the specific gravity value can be calculated ($G_{STC(cal)}$) using the specific gravity values of sand and TC alone, along with the proposed weights (*S* and *TC*) for that mixture.

$$G_{STC(Cal)} = \frac{W_{STC}}{\frac{W_S}{G_S} + \frac{W_{TC}}{G_{TC}}} \quad \text{(Eq. 3.3)}$$

Unit weight

The dry unit weights of the mixtures were determined by using a cylindrical mould typically used for relative density tests. The dimensions of the mould were 28 cm in diameter and 24 cm in height. For finding maximum unit weight, the mold was filled in three layers with the mix, each layer compacted by 56 blows using the modified Proctor compaction hammer that weighs 4.53 kg. The compacted dry unit weights of each mixture was determined. In each proportion, the target mixture proportions achieved was calculated by measuring the weights of sand and TC, as previously explained. For STC mixtures beyond 40%, compaction problems existed due to higher tire-chip content by volume than the sand, which require special attentive compaction for obtaining uniform compacted samples.

The dry unit weight values of all the STC mixtures are presented in Fig. 3.8 . It is observed that, the dry unit weight values are decreased linearly with increasing the percentage of tire chips content in the STC mixture, which was due to the lower specific gravity value of the scrap tire chips than that of the sand. Fig. 3.8 also presents the reduction in dry unit values with reference to the sand unit weight. It can be observed that, by using 30% tire chips, about 20% reduction in dry unit weight was achieved.

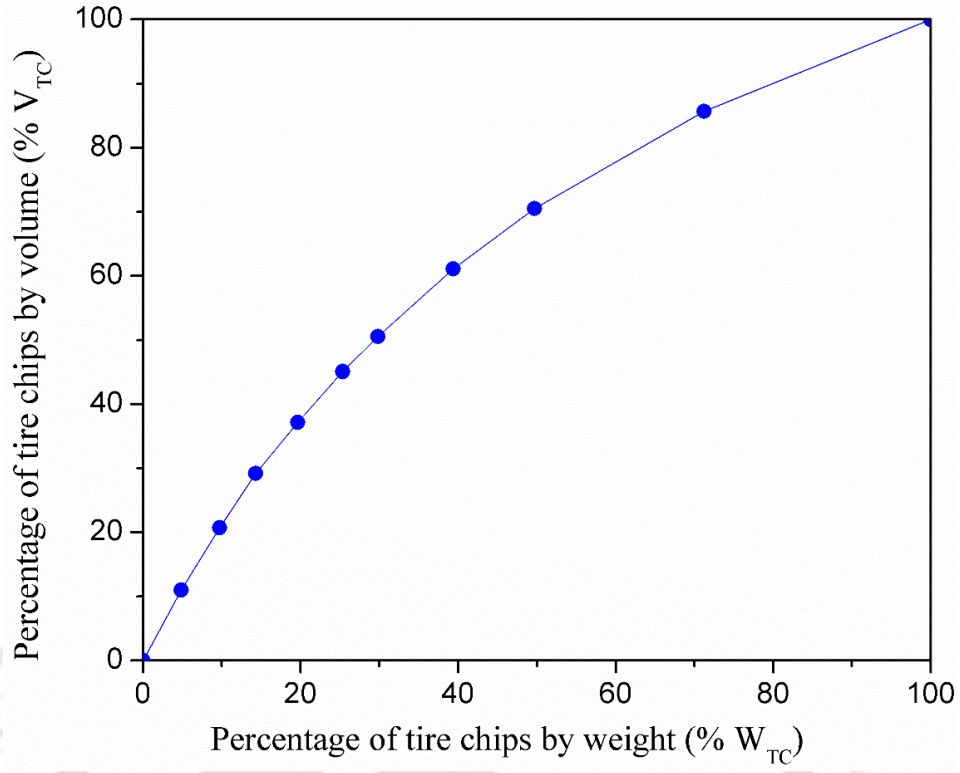

Fig. 3.6 Relationship between weight ratios and volume ratios of tires chips

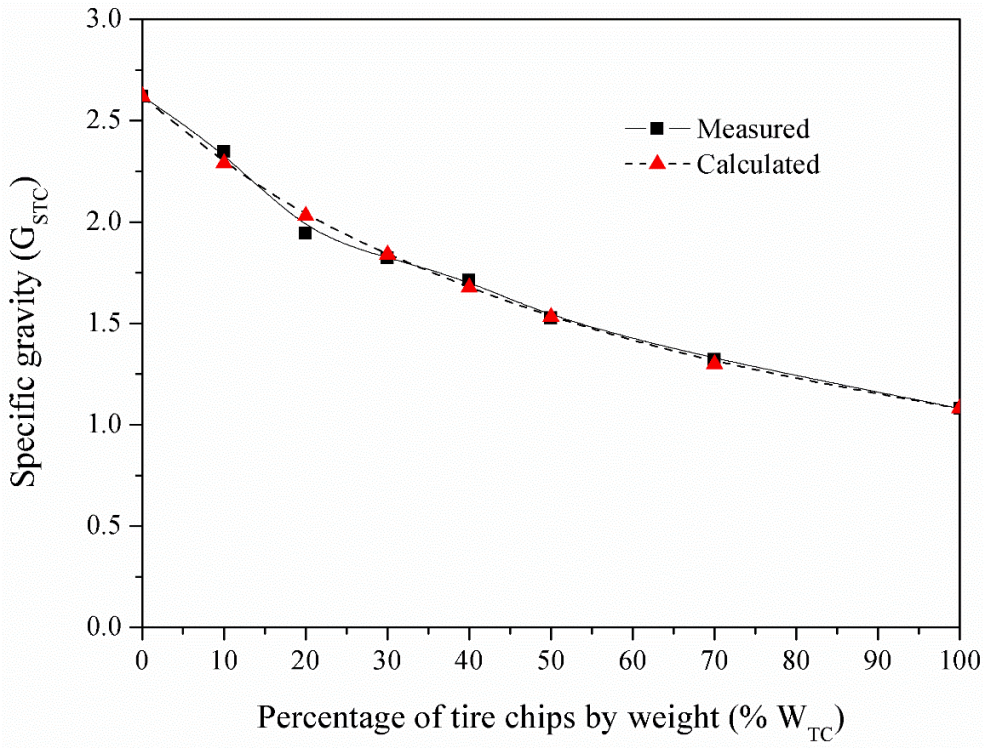

Fig. 3.7 Specific gravity values of sand- tire chip mixtures

Void Ratio

Using dry unit weights and specific gravity values of STC mixtures in the compacted and loose states, the void ratios (e_{STC}) of the mixtures were calculated (Eqs. 3.4 and 3.5), which are plotted in Fig. 3.9. In Fig. 3.9, the void ratios at the compacted and loose states of the mixtures followed a decreasing trend up to 40% tire-chip content and then an increasing trend beyond 40%. This trend may be explained as the following. When sand and tire chips were mixed, the sand particles fill the voids between the tire chips, and the minimum–maximum void ratio of the mixture decreased. This would continue until all the voids between the tires chips are completely filled with sand particles. When all voids between the tire chips filled with sand particles, any further addition of tire chips would increase both the overall volume of the mixture and consequently its minimum – maximum void ratio. A similar trends was also reported by Ahmed (1993),Lade et al. (1998), Balunaini et al. (2009, 2014a), and Mashiri et al. (2015).

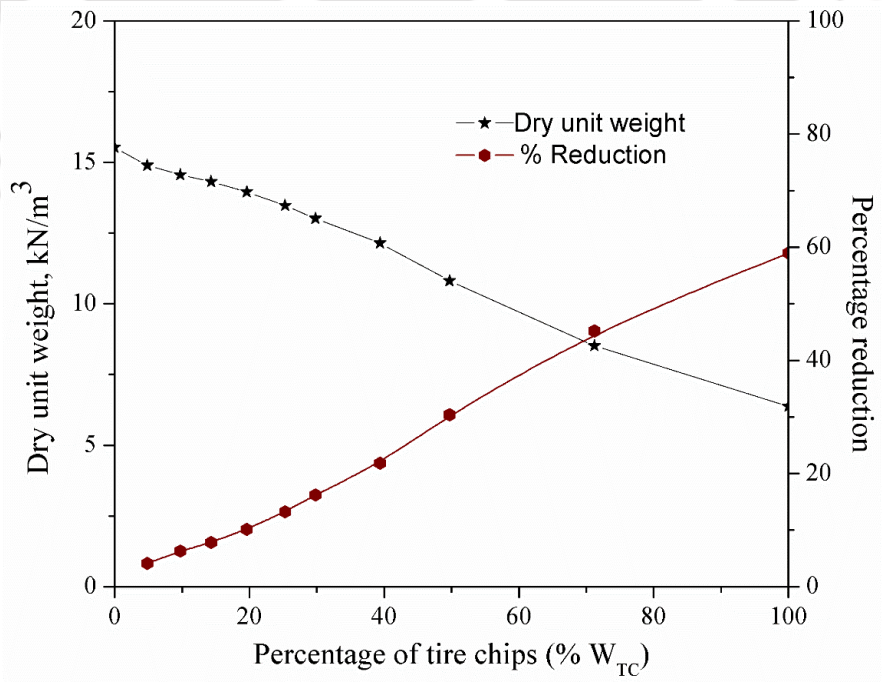

Fig. 3.8 Dry unit weights of sand- tire chip mixtures

$$e_{STC} = \frac{V_{voids}}{V_{solids}} \qquad \text{Eq. 3.4}$$

$$e_{STC} = \frac{V_m - \left(\frac{W_S}{G_S} + \frac{W_{TC}}{G_{TC}}\right)}{\frac{W_S}{G_S} + \frac{W_{TC}}{G_{TC}}} \qquad \text{Eq. 3.5}$$

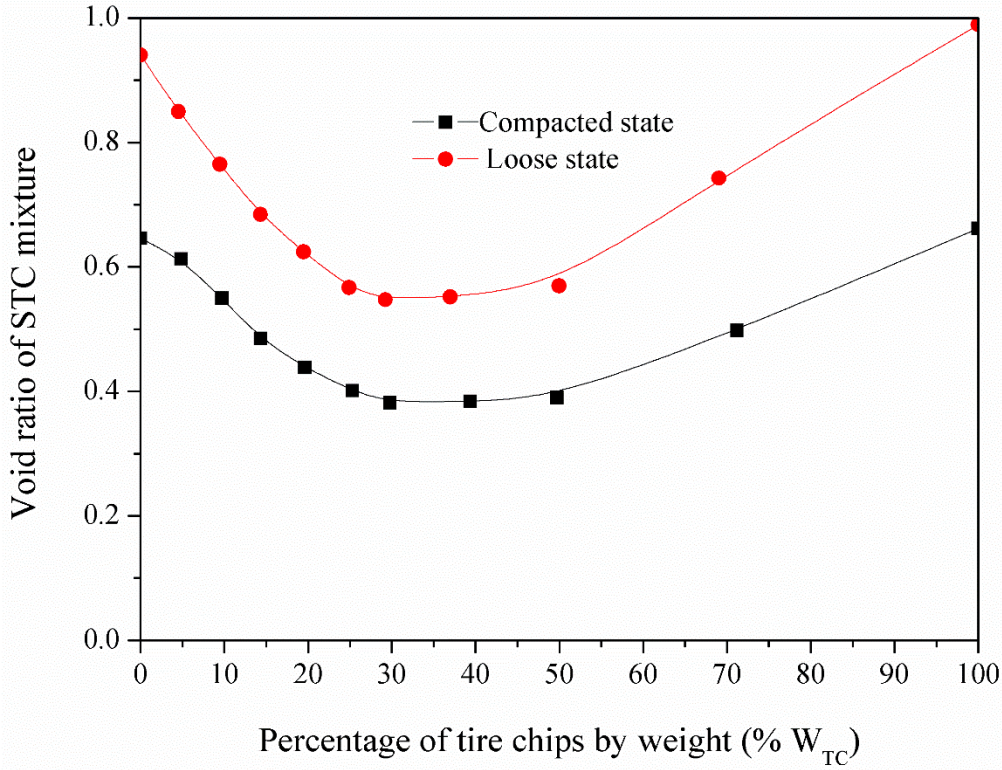

Fig. 3.9 Total void ratios of STC mixtures

Large direct shear tests

A large direct shear test setup (Fig. 3.10), having shear box of 30 × 30 × 30 cm (Fig. 3.11), has been used to determine the shear strength properties of STC mixtures. The tire chip contents, ranging from 10%, 20%, 30%, 40%, 50%, and 70%, by total weight of STC mixture were considered. For preparing the specimens, amount of STC mixture of each proportion was determined using compacted unit weight values, obtained from unit weight tests, and the volume of the shear box. Required quantity of STC mixture was prepared by mixing the sand and tire chips manually to maintain the uniform mixture. The mixed material was steadily poured into the shear box in three

layers. Each layer was compacted using a rectangular wooden plate and imparting uniform compacting energy that was adopted in the unit weight tests. A similar compaction procedure was adopted by Ghazavi (2004) to make compacted STC mixture samples. Large direct shear tests were carried at three normal stresses of 25, 75, and 125 kPa. The shearing rate was kept at 1.25 mm/min for all the tests. Shearing force and shear displacements were measured during testing. For calculating the shear stresses on the specimen, area corrections were applied.

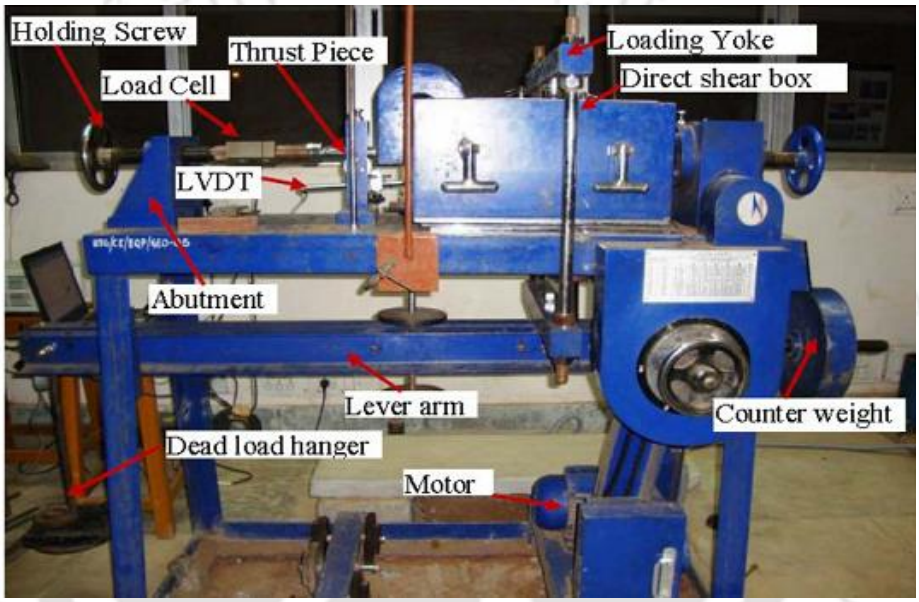

Fig. 3.10 Large size direct shear test setup

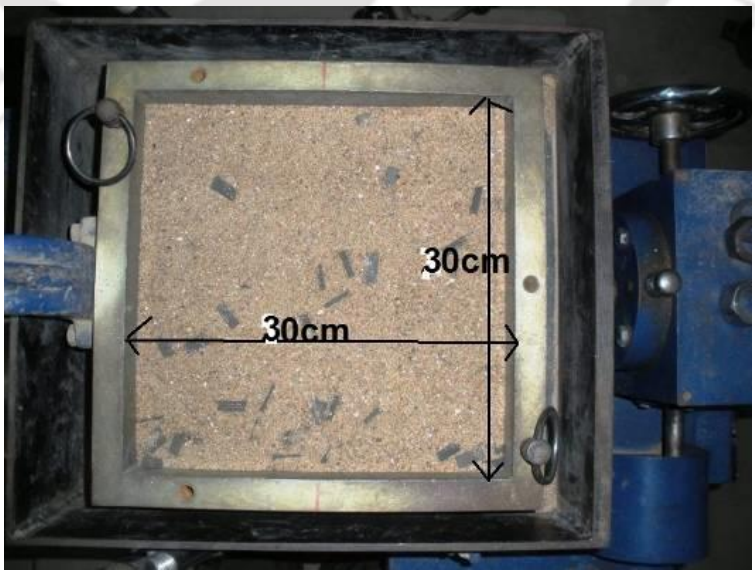

Fig. 3.11 Shear box with sand- tire chip mixture.

Fig. 3.12 shows the results obtained at a normal stress of 125 kPa in terms of shear stress variation with shear strain for different STC mixture samples. It is observed from the figure that the peak shear stress values are increased with increase in TC content up to 30%. Thereafter, increase of tire chips content in the STC mixture reduced peak shear stress. The increased shear strength behavior (up to STC30) is attributed to the reinforcement effect of tire chips in the STC matrix, which was also reported by Zornberg et al. (2004a). Further, referring to Fig. 3.6, it can be noticed that TC content of 30% by weight is equivalent to 50% by volume. Beyond this mixture proportion, it appears that the tire chips content behavior dominated the whole shear response, gradually reaching the shear response of pure tire chips. It is also seen that STC 70% and pure tire chips showed similar shear stress response. Further, it can be observed that initial stiffness of the mixtures is decreased with increase in TC content. It is evident that the amount of tire chips has significant influence on the shear behavior of the mixtures. However, the strain corresponding to peak shear stress increases with the increase in the percentage of tire chips as compared to sand alone, which indicates that the behavior changing from brittle to ductile with the addition of tire chips. This ductile behavior facilitates the use of STC mixtures in resilient structures. For example, Tsang et al. (2012) reported the application of STC mixtures in geotechnical seismic isolation of structures.

Fig. 3.13 shows the shear envelopes (shear stress versus normal stress) of STC mixture specimens. TC up to 50%, the peak shear stresses and for the remaining (70% and pure TC), shear stresses at a strain of 10% were considered for shear envelopes. For different normal stresses, shear resistances of STC mixtures are higher than that of pure sand, but the increasing trend maintains up to 30% of TC, beyond which the shear resistance decreased.

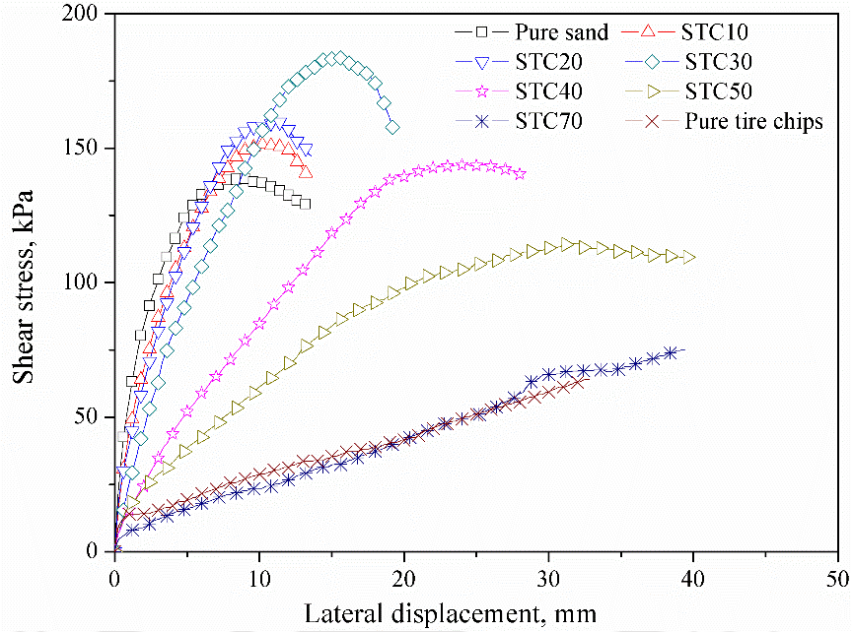

Fig. 3.12 Shear stress vs. Lateral displacement of STC mixtures at 125kPa normal stress

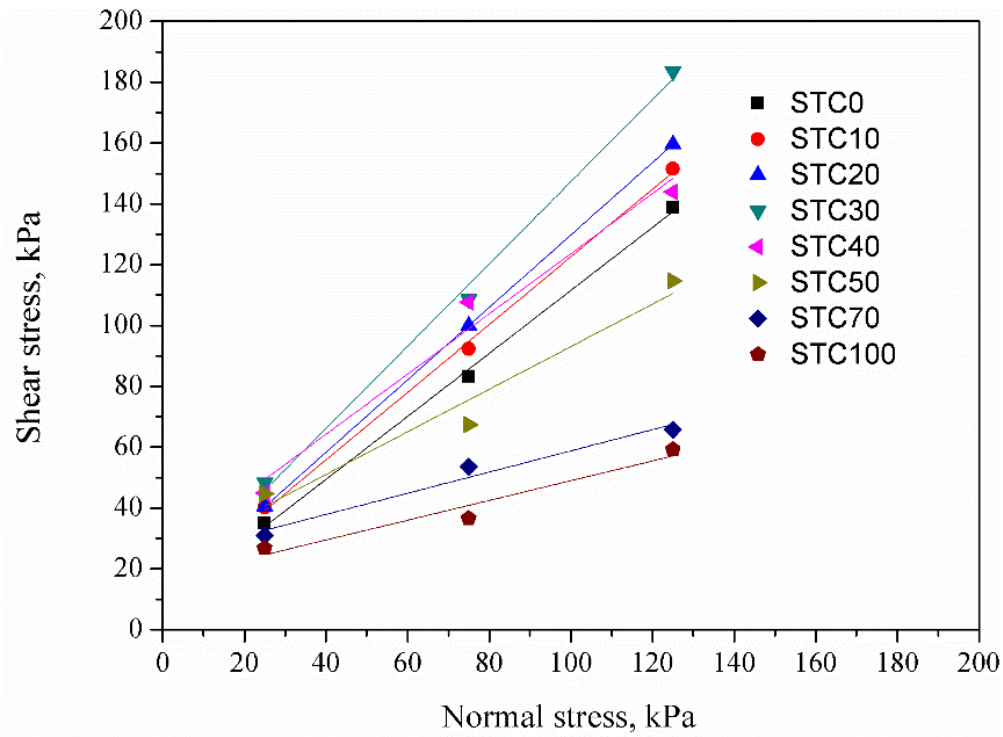

Fig. 3.13 Shear envelopes for STC mixtures

Based on the shear envelopes of different STC mixtures, shear strength parameters are determined and presented in Fig. 3.14. Here the shear strength parameters were determined in two ways: one considering cohesionless material giving only ϕ (angle of internal friction), and the other as c -ϕ material (c = apparent cohesion).

It is observed that by adding of TC, up to 30% by weight, internal friction angle values are increased in both the cases. The apparent cohesion was increased up to 40%TC. Range of ϕ values obtained for different mixtures is about 20º to 55º and the c values range is 8-25 kPa. Ahmed (1993), Foose et al. (1996), and Ghazavi et al. (2011) have also reported similar range of shear strength parameters for different sand- STD materials in various sizes.

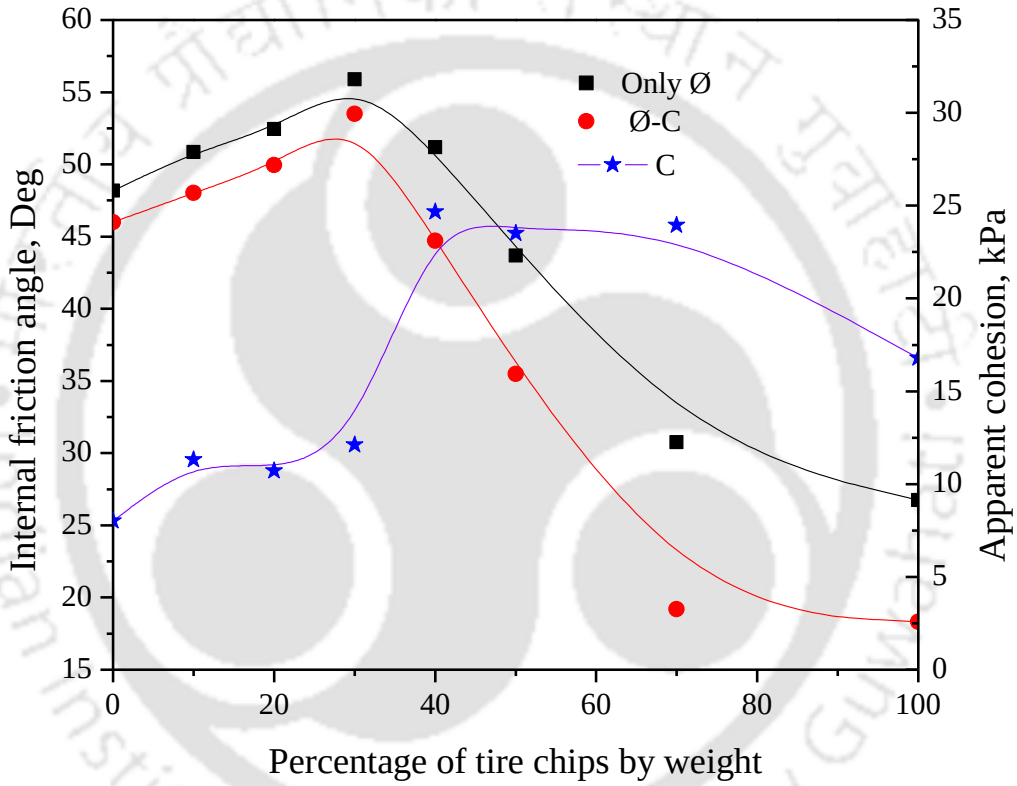

Fig. 3.14 Variation of friction angle for different proportion of STC mix

Further, it can be seen from the figure that apparent cohesion value was jumped from about 10 kPa to 25 kPa in between the STC 30 and STC 40 mixtures. Pure tire chips predominantly exhibit significant apparent cohesion behavior in the order of 15 kPa to 35 kPa (Ahmed 1996 and Yang et al. 2002). As the volume of tire chips increase from 50 to 60 % with an increase in tire chip content from 30 to 40 % (by weight), tire chips behaviour dominates the STC mixture behaviour beyond 30 % STC. This may be

the reason of the sudden jumping of apparent cohesion value at 40% tire chips. Banzibaganye (2014) also reported similar results.

3.2.4 Optimum STC Mixture and Discussion

Given the wide range of possible mixture proportions, it is to be determined the optimum-mixing ratio, which results in better compressibility characteristics and high load-carrying behaviour. To find the optimum STC mixture ratio, variations of dry unit weight, internal friction angle, and void ratio values with percentage tire chips were plotted together, as shown in Fig. 3.15. Internal friction angle value is high where the void ratio is less.

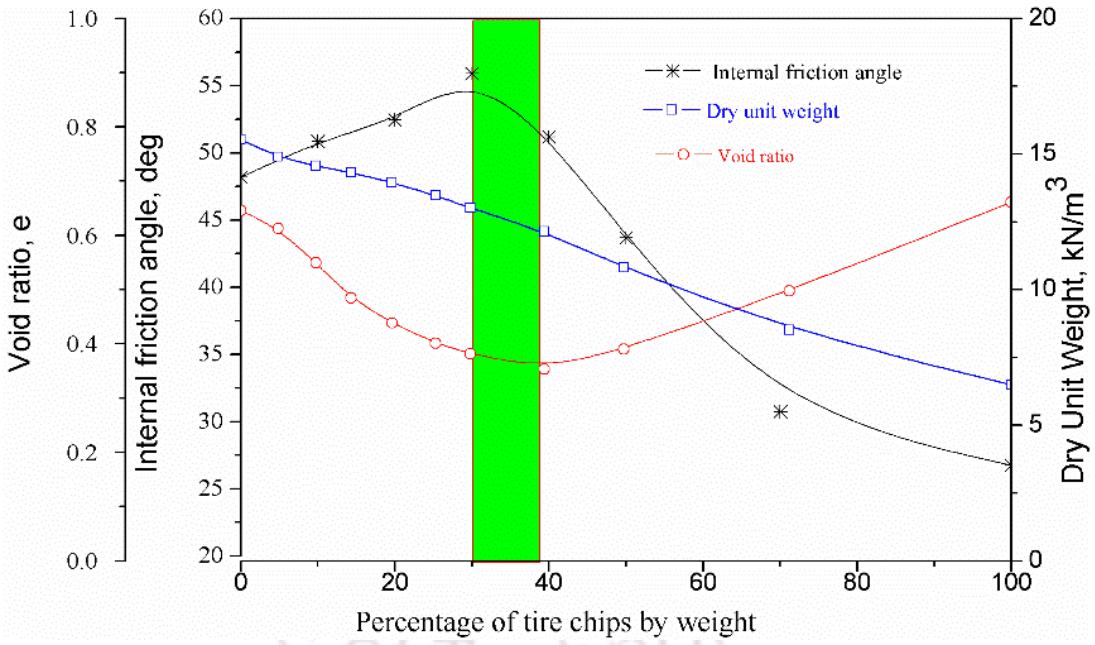

Fig. 3.15 Total Typical plot of internal friction angle, dry unit weight, and void ratio

Fig. 3.15 shows that at about 30–40% mixture proportion, the material depicted lesser void ratio and higher strength value (friction angle). Thus, it can be stated that STC mixture with 30-40% tire chips (by weight) is the optimum mixture, which can be adopted for geotechnical engineering applications. The similar range was reported by Zornberg et al. (2004) and Tanchaisawat et al. (2010) for different types of sand-tire

chips. This is equivalent to the volume ratio of 50–60%, which can reduce the demand for a huge volume of sand material in any geotechnical application. Further, it can also be noticed (Fig. 3.15) that at the optimum mixing ratio of the STC mixture, the dry unit weight was reduced by nearly 20%. The optimum mixing ratio of the STC mixture effectively works as lightweight material for geo-engineering applications, like retaining wall backfill, embankments, and foundations. The use of scrap tires in geoengineering applications solves the problem of disposal to some extent and promotes recycling tires, which minimizes the requirement of other construction materials providing economic benefits. Thus, as per the definition of sustainability (ASCE 2011), the use of recycled tire is a sustainable approach for a better future. However, it may not be economically beneficial if recycled tire chips are expensive in some areas where the availability of scraped tires is scarce and the recycling process is not common.

3.3 SHAKING TABLE FACILITY AND INSTRUMENTATION

3.3.1 Shaking table facility

For seismic design, it is essential to study the behavior of different models under different seismic excitations with different accelerations and frequencies. In the present study, seismic excitations were simulated using a 'uni-axial shaking-table' with a loading platform of 2.5 × 2.5 m size (Fig. 3.16) and payload of 5 ton. The shaking table is equipped with servo-hydraulic actuator to excite test models within a displacement range of ± 250 mm.

The shaking table can create indefinite oscillations under controlled conditions, within the limitations imposed by payload, hydraulic power pack and actuator performance. The hydraulic actuator is fully computer controlled with the capability to apply simple harmonic sinusoidal excitations or actual recorded (or scaled) earthquake

motions within the performance limits of the hydraulic actuator. This shaking table can produce maximum acceleration up to ±2g at an operational frequency range of 0.1 to 10 Hz.

Fig. 3.16 Shaking table at IITGuwahati

3.3.2 Instrumentations

Various instrumentations were employed to observe the behavior of retaining wall model structures under the static and seismic testing on shaking table. They include Pressure sensors, Inductive Displacement Transducers, and Accelerometers. All these instruments are of analog voltage output type and generate continuous data to the application software and MGCplus data acquisition system (Fig. 3.17a), during testing.

Earth pressure sensors

Earth pressure sensors were used to obtain the earth pressures behind the retaining walls in static and seismic case. Four pressure sensors of strain-gauge type with 50 kPa capacity and 0.01 kPa sensitivity were used. These sensors are circular in shape and have a diameter of 50 mm. The pressure sensor with end connector is shown

in Fig. 3.17b. The calibration of these sensors was done, by putting standard dead weights on top of the sensor and reading the voltage output through data acquisition system. By changing the dead weights, different voltage values were obtained for different weights. Using the obtained data, the calibration coefficients were calculated.

Displacement Transducers

Three linear variable differential transformers (LVDTs) (Fig. 3.17c) were used to record horizontal movements of the wall. The sensing range of these transducers is 0 to 50 mm. The LVDTs are sensitive to measure the displacements in the order of 0.01mm. The LVDTs works with a power supply of 10 V. LVDTs are connected to MGCplus data acquisition system and further connected to computer to record the displacements.

Accelerometers

Accelerometers (ADXL 335) that were developed by Bhattacharya et al. (2012) were used in the study. The ADXL 335 is a small, thin, 3-axis accelerometer requiring very low power with signal conditioned voltage outputs. It measures acceleration with a full-scale range of ± 3g. The accelerometers are sensitive to measure the accelerations in the order of 0.001g. The MEMS accelerometer (Fig. 3.17d) works with a power supply within the range of 1.8–3.6 V with a very low current of 350 mA. However, a constant voltage power supply of 3 V is adopted as recommended by Bhattacharya et al. (2012).

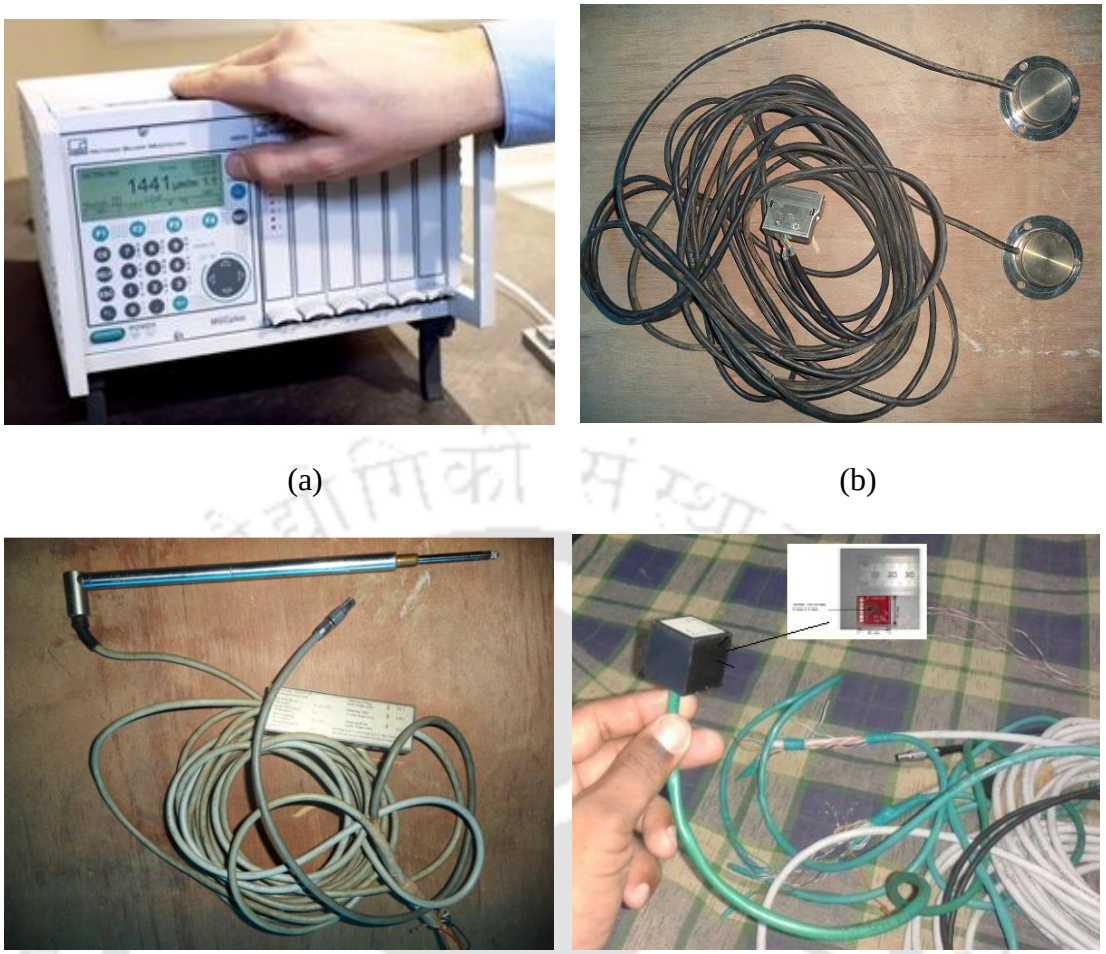

(a) (b)

(c) (d)

Fig. 3.17 Instrumentations; (a) MGCplus data acquisition system, (b) Pressure sensors with end connector, (c) Linear variable differential transformers (LVDTs), (d) Accelerometer with end connector

3.4 MODEL CONSTRUCTION AND TESTING PROCEDURE

Retaining wall models were constructed with two different configurations. One using different STC mixtures as lightweight materials and the other using tire chips as compressible inclusions A control case model wall was considered with sand backfill (represented by STC0) for comparing the model behavior under both the configurations. The unit weight of sand was maintained at 15.57 kN/m^3 in all the wall models. The following sections provide details of model constructions and testing procedures under static and seismic conditions.

3.4.1 Retaining wall models backfilled with lightweight materials

Retaining wall models of 600 mm height were constructed in a model container of 1200 mm × 600 mm in plan and 1000 mm height. The model container was made of Perspex sheets of 10 mm thickness and braced by a steel frame, made of steel angle sections, that also facilitates for easy lifting and handling. The wall of 600 mm high and 580 mm length was made with eight hollow rectangular (2 mm thick) steel sections, each of 580 mm length, 25 mm wide and 75 mm height cross section, which were joined using steel rods of 12 mm diameter. These steel rods were further connected to a bottom plywood base forming a rigid connection. Backfill area of 800 mm × 580 mm in plan was adopted that was filled up to full height of the wall (600 mm) using sand or other STC mixtures in different model tests.

In case of retaining walls backfilled with lightweight materials, STC mixtures STC10, STC20, STC30, STC40 and STC50, representing 10%, 20%, 30%, 40%, and 50% proportion of tire chips by weight, respectively, were used as backfill material. After providing temporary support to the wall facing, backfilling was done in stage wise by free falling technique (placing the calculated amount of backfill material based on layer thickness and target density) and compacting manually to achieve the target density. After complete filling of the backfill material up to full height of the wall (600 mm), a solid wooden platform has been placed on the surface of backfill to facilitate the surcharge application using concrete cubes (Fig. 3.18). Typical model wall with container after construction completed is shown in Fig. 3.19.

To monitor the horizontal displacements of the wall, linear variable differential transformers (LVDTs), L1, L2 and L3 were positioned on the front face of the wall at 125, 380, and 580 mm elevations from the base of the wall, respectively. Four pressure sensors, P1, P2, P3 and P4 were placed inside the wall, in contact with the wall facing

at 37, 187, 337, and 487 mm elevations to measure horizontal soil pressures against the facing. After complete backfilling, the temporary external support of wall was removed, and different surcharge pressures are applied in the form of concrete cubes to investigate the model wall behavior under static loading conditions. Similar configuration model walls, after complete construction, were placed on the 1-g shaking table for dynamic testing with different sinusoidal and earthquake motions. During dynamic testing, accelerometers (A1, A2 and A3) were used to record accelerations at different elevations within the backfill (as shown in Fig. 3.20), in addition to LVDTs and pressure sensors.

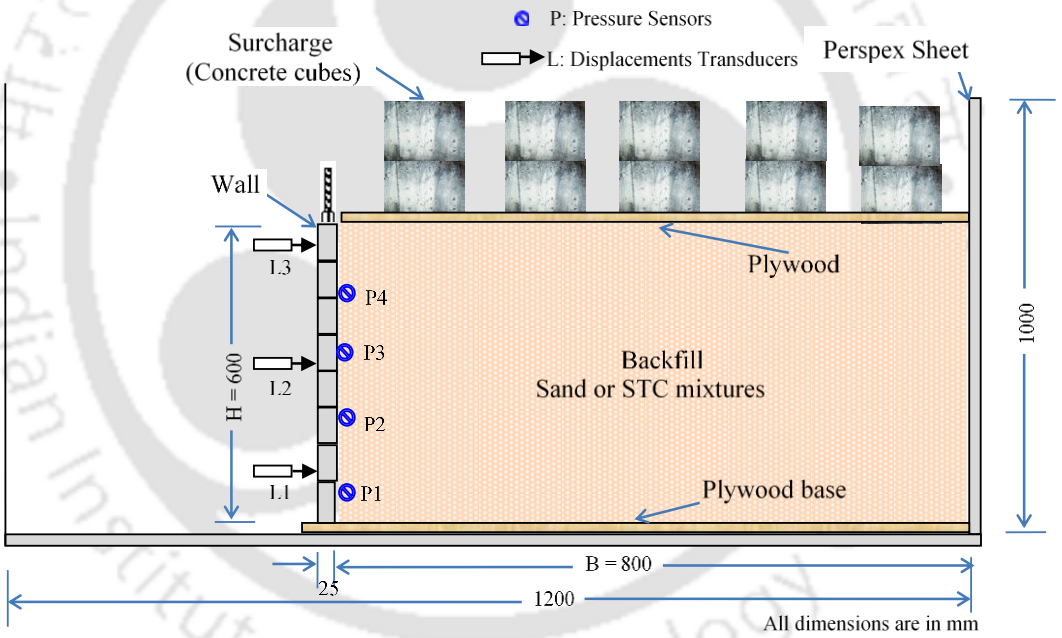

Fig. 3.18 Schematic diagram of retaining wall model for static tests

3.4.2 Retaining wall models with compressible inclusions

In case of model walls with compressible inclusions, different thickness layers of tire chips (average size of 20 mm) were placed vertically behind retaining wall. The compressible inclusion was prepared by filling tire chips inside a bag made from plastic product. This bag was used to wrap the tire chips so that they do not mix with the backfill soil. Further, this bag also prevents the movement of sand particles into tire

chips and clogging which may affect the compressibility of tire chips. Such confinement also makes the backfilling easier. The average dry unit weight of the tire chips achieved after filling and tamping was 6.43 kN/m^3. Similar procedures for testing, under static and dynamic loading for earlier configuration, were followed. Schematic diagram of model wall with compressible inclusion (*t*) is shown in Fig. 3.21. A photograph of the model wall container fixed on the shaking table is shown in Fig. 3.22.

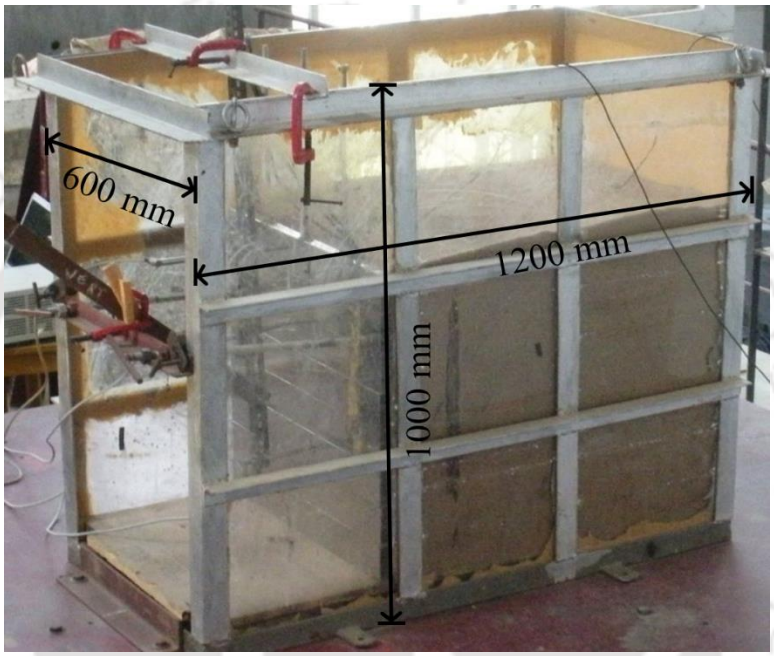

Fig. 3.19 Typical model wall with container

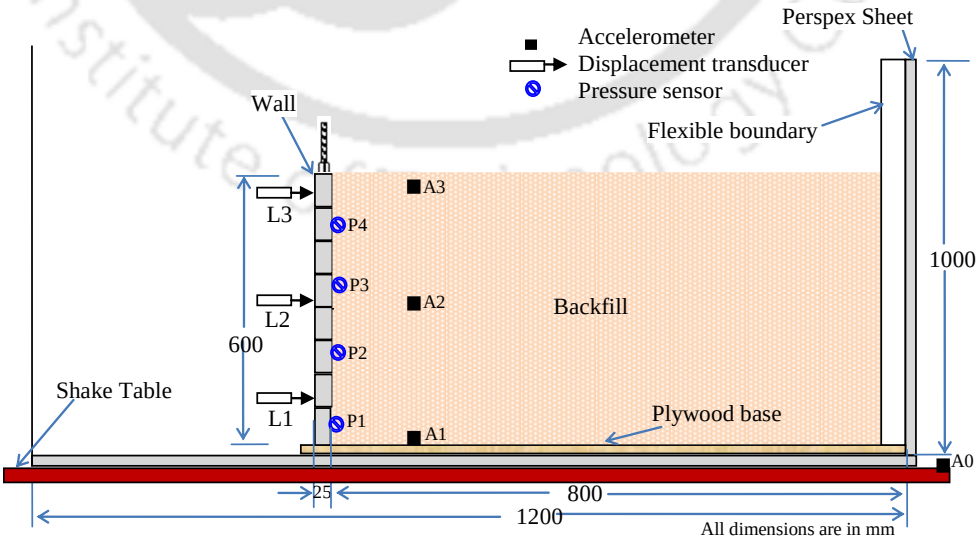

Fig. 3.20 Schematic diagram of retaining wall model for dynamic tests

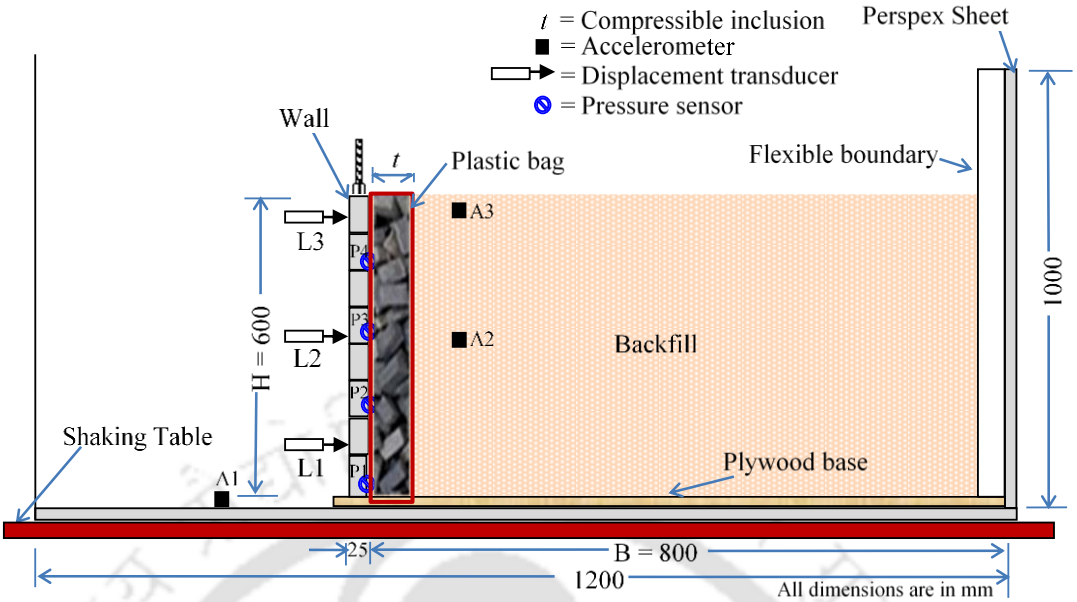

Fig. 3.21 Schematic diagram of retaining wall model with compressible inclusion on shaking table

Fig. 3.22 Model wall with container on shaking table

3.5 SUMMARY

This Chapter described the properties of different materials (sand, tire chips and STC mixtures) used in the model tests. By observing the variation of void ratio and shear-strength values of various mixtures, the optimum mixing ratio of sand and tire chips is in the range of 30–40% by weight. This is equivalent to the volume ratio of 50–60%, which can reduce the demand for huge volume of sand material in any geotechnical application. This optimum mixture will provide better compressibility characteristics (due to lesser void ratio) and high load-carrying behaviour (due to high shear strength). Further, the STC mixture, at the optimum content, results in lightweight material due to 20% lesser unit weight in comparison to sand alone. Various instrumentations, shaking table facility and methods adopted for the construction of retaining wall models were discussed in detail along with the testing procedure.

Chapter 4. RETAINING WALL MODELS BACKFILLED WITH STC MIXTURES

4.1 INTRODUCTION

In this chapter, static and dynamic tests conducted on retaining wall models backfilled with lightweight materials (different STC mixtures) are discussed. Scrap tire chips (Section 3.2.2) mixed with sand were used as the lightweight materials in these tests. Testing program has been devised to study the effects of different parameters on the performance of the wall models. The parameters studied include the backfill type, surcharge pressure, dynamic excitation parameters (acceleration and frequency), and different earthquake excitations. The results were discussed in terms of horizontal wall displacement, lateral earth pressures, and acceleration amplifications.

4.2 TESTING PROGRAMME

In static case, six model tests (T1–T6) were conducted on retaining wall models with pure sand (STC0, control case) and different STC mixtures (STC10, STC20, STC30, STC40 and STC50) as backfill with different surcharge pressures. The STC mixtures were prepared by mixing tire chips in sand with different proportions by weight. Static loading up to 10 kPa, in the form of concrete cubes (Fig. 3.18) was applied to each model wall in multiples of 1 kPa. Table 4.1 shows the details of model test parameters.

In dynamic case, the retaining wall models have been tested with different sinusoidal excitations and random earthquake excitations using 1-*g* shaking table (Fig. 3.16). The details about the test conditions for sinusoidal excitations are shown in Table 4.2. The table shows various test codes, which were represented in the form of

backfill_acceleration_frequency. Sinusoidal excitations with peak acceleration values of 0.1*g*, 0.2*g* and 0.3*g* at 3 and 5 Hz frequency have been adopted. Each sinusoidal excitation was applied for 20 cycles. These idealized sinusoidal excitation studies, only give relative behavioral aspects of the model structures. However, during the real earthquake excitation, model behavior will be significantly affected by various ground excitation parameters (the frequency content, intensity).

Table 4.1 Test parameters for static tests on model walls with STC mixtures

Test Code.	**STC mixture**	**Unit weight, kN/m^3**	**% TC (by weight)**	**%Sand**	**Surcharge, kPa**
T1	STC0	15.57	0	100	0 - 10
T1-R1	STC0	15.59	0	100	
T1-R2	STC0	15.55	0	100	
T2	STC10	14.61	10	90	
T3	STC20	14.11	20	80	
T4	STC30	13.17	30	70	
T5	STC40	12.28	40	60	
T6	STC50	10.41	50	50	

Note: R1 –Repeated one time, R2- Repeated second time

Retaining wall models were also tested with different (STC mixtures) backfill materials by applying four real earthquake excitations with different frequency contents with different magnitudes. Ground motions (Center for Engineering Strong Motion Data) recorded during 2014 South Napa (SN), 2011 Sikkim (SK), 2011 New Zealand (NZ), and 2011 Tohoku (TH) earthquakes, having moment magnitude values ranging from 6.0 to 9.0, were selected for the study. The selected records cover a wide range from medium intensity earthquakes (Sikkim, 2011) to stronger intensity earthquakes (Tohoku, 2011). Fig. 4.1 shows actual acceleration time histories and FFT of earthquake ground motions. It can be seen from the figure that these different ground motions are with different peak ground acceleration (PGA) levels, durations and frequency contents. This shows the importance of consideration of real earthquake

ground motions, which may be different with different frequency content and their magnitudes.

Table 4.2 Details about test conditions using sinusoidal excitations

Test code	**Backfill**	**Acceleration (*a*), g**	**Frequency (*f*), Hz**
STC0_0.1_3	Sand (STC0)	0.1	3
STC10_0.1_3	STC10		
STC20_0.1_3	STC20		
STC30_0.1_3	STC30		
STC40_0.1_3	STC40		
STC50_0.1_3	STC50		
STC0_0.2_3	Sand (STC0)	0.2	3
STC10_0.2_3	STC10		
STC20_0.2_3	STC20		
STC30_0.2_3	STC30		
STC40_0.2_3	STC40		
STC50_0.2_3	STC50		
STC0_0.3_3	Sand (STC0)	0.3	3
STC10_0.3_3	STC10		
STC20_0.3_3	STC20		
STC30_0.3_3	STC30		
STC40_0.3_3	STC40		
STC50_0.3_3	STC50		
STC0_0.3_5	Sand (STC0)	0.3	5
STC10_0.3_5	STC10		
STC20_0.3_5	STC20		
STC30_0.3_5	STC30		
STC40_0.3_5	STC40		
STC50_0.3_5	STC50		

Details about all the four earthquake ground motion records are listed in Table 4.3. From the table it can be seen that PGA values are in the range of about 0.12 g to 2.68 g. The FFT results of each record indicate predominant frequencies of 2.17, 6.24, 2.25 and 6.05 Hz for SN, SK, NZ and TH earthquakes, respectively. Frequencies of 2 to 3 Hz are representative of typical predominant frequencies of medium to high frequency earthquakes (Bathurst and Hatami 1998) and fall within the expected earthquake parameters (AASHTO 2002). However, the selected earthquake records in

this study are fall in the range of 2 to 6 Hz. Details about test conditions for earthquake excitations are shown in Table 4.4.

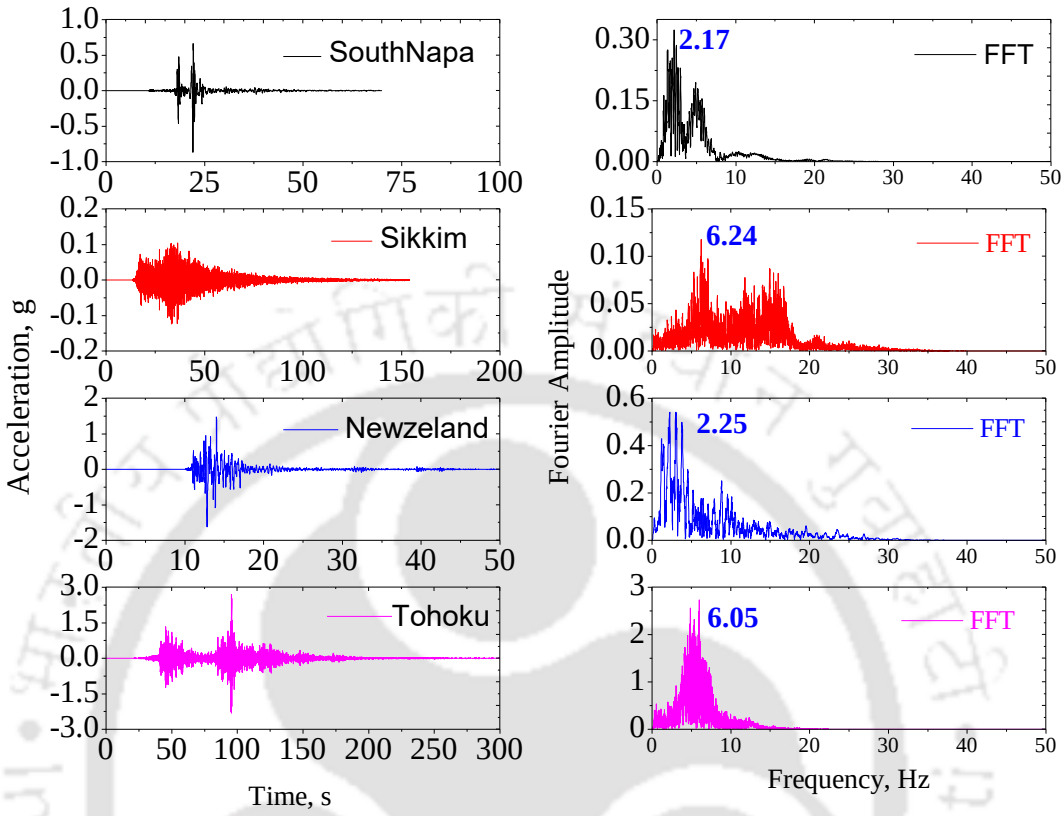

Fig. 4.1 Original earthquake excitations and their FFT analysis

Table 4.3 Ground motion parameters of actual earthquake records

SI. No	Properties	Earthquake excitations			
		South Napa (SN)	**Sikkim (SK)**	**New Zealand (NZ)**	**Tohoku (TK)**
1	Magnitude (M_w)	6.0	6.9	6.4	9.0
2	Original PGA, g	0.85	0.123	1.61	2.68
3	Scaled PGA, g	0.17	0.123	0.161	0.268
4	Predominant frequency (f), Hz	2.17	6.24	2.25	6.05
5	Duration, sec	70	160	50	300
6	Earthquake database	CESMD	CESMD	CESMD	CESMD
7	Year	2014	2011	2011	2011

The staged shaking procedure has been adopted for seismic testing. For each model wall, the order of shaking events started with smaller intensity records and

followed by the larger ones as shown in the Table 4.5. Each sinusoidal shaking stage lasted for 20 cycles, and random earthquake excitation lasted as per its duration. Approximately, 5 minutes gap was given in between the shaking stages for making other stage settings.

Table 4.4 Details about test conditions using irregular excitations

Test code	**Backfill**	**Irregular excitations**
STC0_SN EQ	Sand (STC0)	South Napa
STC0_SK EQ		Sikkim
STC0_NZ EQ		New Zealand
STC0_TK EQ		Tohoku
STC10_SN EQ	STC10	South Napa
STC10_SK EQ		Sikkim
STC10_NZ EQ		New Zealand
STC10_TK EQ		Tohoku
STC20_SN EQ	STC20	South Napa
STC20_SK EQ		Sikkim
STC20_NZ EQ		New Zealand
STC20_TK EQ		Tohoku
STC30_NZ EQ	STC30	South Napa
STC30_TK EQ		Sikkim
STC30_SN EQ		New eland
STC30_SK EQ		Tohoku
STC40_NZ EQ	STC40	South Napa
STC40_TK EQ		Sikkim
STC40_SN EQ		New Zealand
STC40_SK EQ		Tohoku
STC50_NZ EQ	STC50	South Napa
STC50_TK EQ		Sikkim
STC50_SN EQ		New Zealand
STC50_SK EQ		Tohoku

Table 4.5 Order of shaking of the model walls

S.No	Excitations	PGA, *g*	Frequency / Predominant Frequency, Hz	Cycles/Duration
1	Sinusoidal	0.1	3	20 cycles
2		0.2	3	20 cycles
3		0.3	3	20 cycles
4		0.1	5	20 cycles
5		0.3	5	20 cycles
6	SN EQ	0.17	2.17	70 s
7	SK EQ	0.123	6.24	160 s
8	NZ EQ	0.161	2.25	50 s
9	TK EQ	0.268	6.05	300 s

The model walls have been instrumented with accelerometers, earth pressure sensors, displacement transducers at different elevations to monitor the retaining wall model response as discussed in the previous chapter. Results are discussed in terms of displacements, incremental earth pressures, amplification factors at different elevations.

4.3 STATIC RESPONSE OF RETAINING WALL MODELS

The wall models were built with pure sand (control case) and various STC mixtures (10%, 20%, 30%, 40%, and 50%) as backfill materials (Table 4.1). The retaining wall model response with different backfill materials was monitored at before (at rest condition) and after the removal of temporary support; and with different surcharge pressures. The results obtained are discussed in terms of horizontal displacements and lateral earth pressures in the following sections.

4.3.1 Horizontal displacements

Horizontal wall displacements along the height of the wall were monitored using three LVDTs positioned as shown in Fig. 3.18. The horizontal wall displacements were measured after the support removal (without surcharge loading) and the variations of the same along the height of wall for all the model tests are shown in Fig. 4.2. Test

T1 was repeated to verify the repeatability of the model test results. For STC0 backfill tests (T1), the horizontal displacements for the repeated tests are reasonably matched to each other, confirming the repeatability of the tests. Maximum wall displacement is observed to be about 1.75 mm in this case (Test T1). It can be seen from the figure that for model walls with STC mixtures, the displacements were lesser compared to model wall with sand (STC0). Among different tests, Test T4 with STC30 backfill showed lowest wall top displacement of 0.65 mm. Percentage reduction of wall top displacements with STC mixtures is calculated with reference to top displacement of control case. Variations of the top displacement and its percentage reduction with percentage tire chips are shown in Fig. 4.3. It is revealed that top displacements were reduced by 30 –65 % in comparison to control case (pure sand).

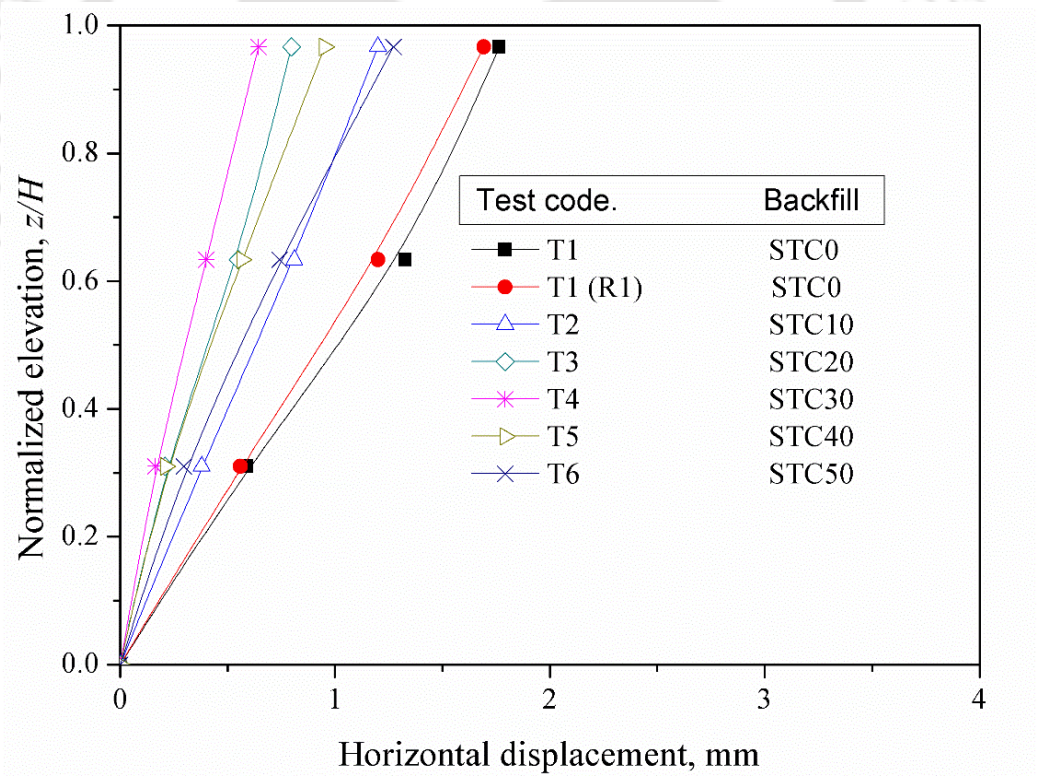

Fig. 4.2 Displacement profiles of wall models after support removal

The surcharge pressures, (up to 10 kPa in multiples of 1 kPa, using concrete cubes) have been applied on the backfill surface of all the model walls for observing

the wall displacements and lateral earth pressures variations. Fig. 4.4 and Fig. 4.5 presents the displacements of wall models along the height for different surcharge pressures for control case (pure sand) and STC30, respectively. It is observed that, displacements along the height of wall are increased by increasing the surcharge pressures, as excepted. Maximum displacements at the top of the wall at 10 kPa surcharge are noted as 6 mm and 2.4 mm for STC0 and STC30 backfill walls, respectively. The top displacements of wall at different surcharge loading conditions in different tests with different STC mixtures are presented in Fig. 4.6. It is seen from the figure that the top displacements are increased with increasing surcharge pressures in all STC mixtures. The figure also depicts the fact that at all surcharge loading conditions the lowest displacements are shown for STC30 mixture and the highest for the STC0 backfill. Displacements in the range of 3.5 mm - 6 mm for STC0 are recorded for surcharge variation from 1 to 10 kPa. The corresponding displacements variations for STC30 are in the range of 0.5 mm - 1.1 mm.

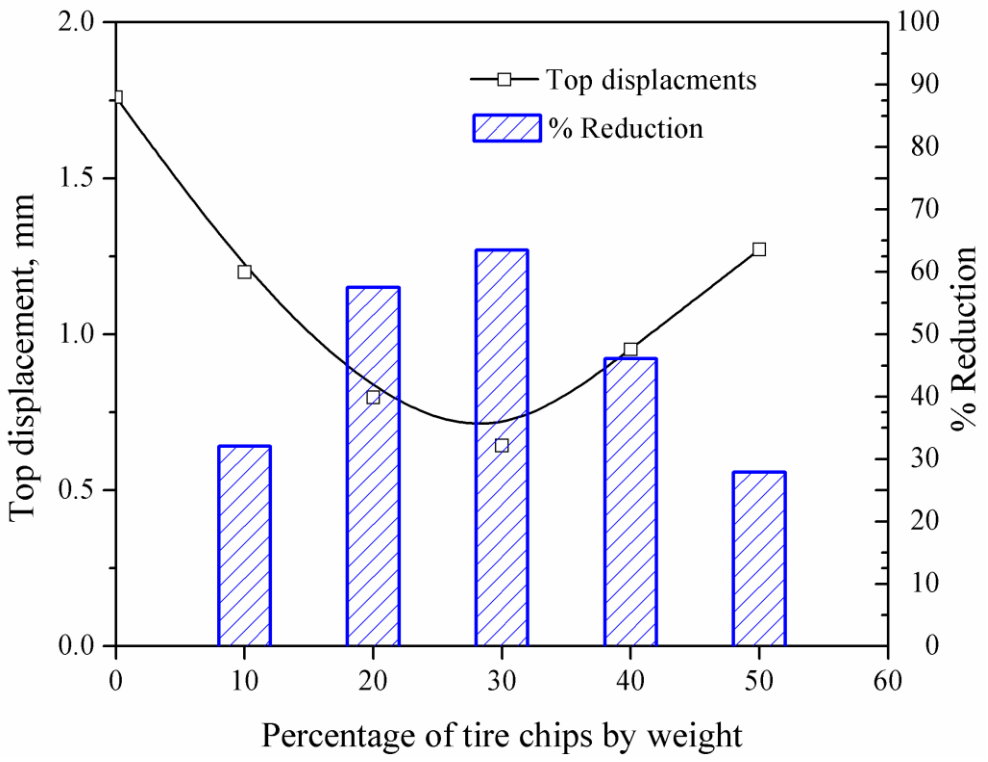

Fig. 4.3 Top displacements and percentage reduction

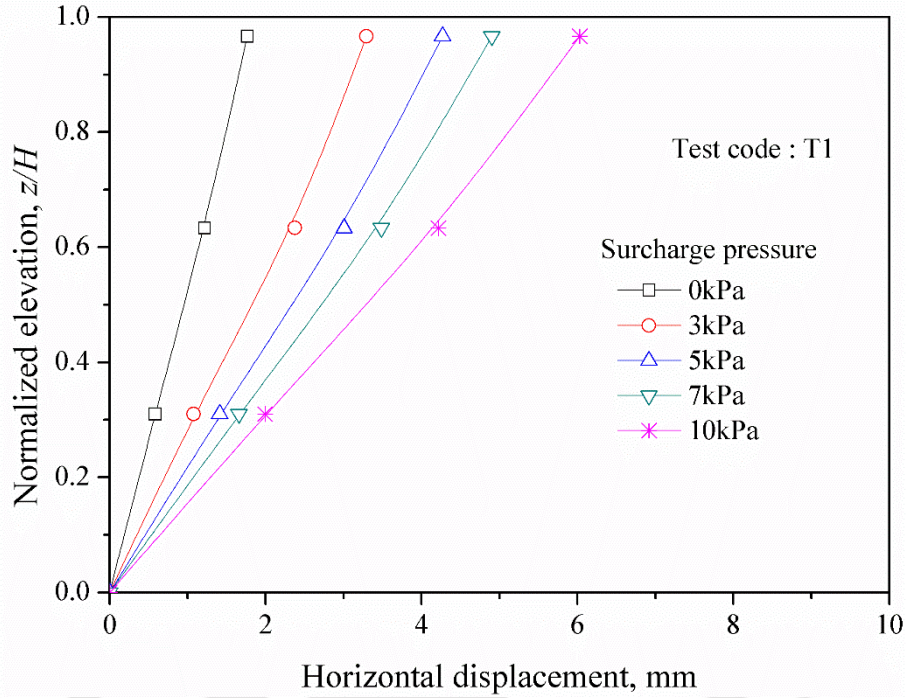

Fig. 4.4 Horizontal displacement profile for STC0 (sand alone) with different surcharge pressures

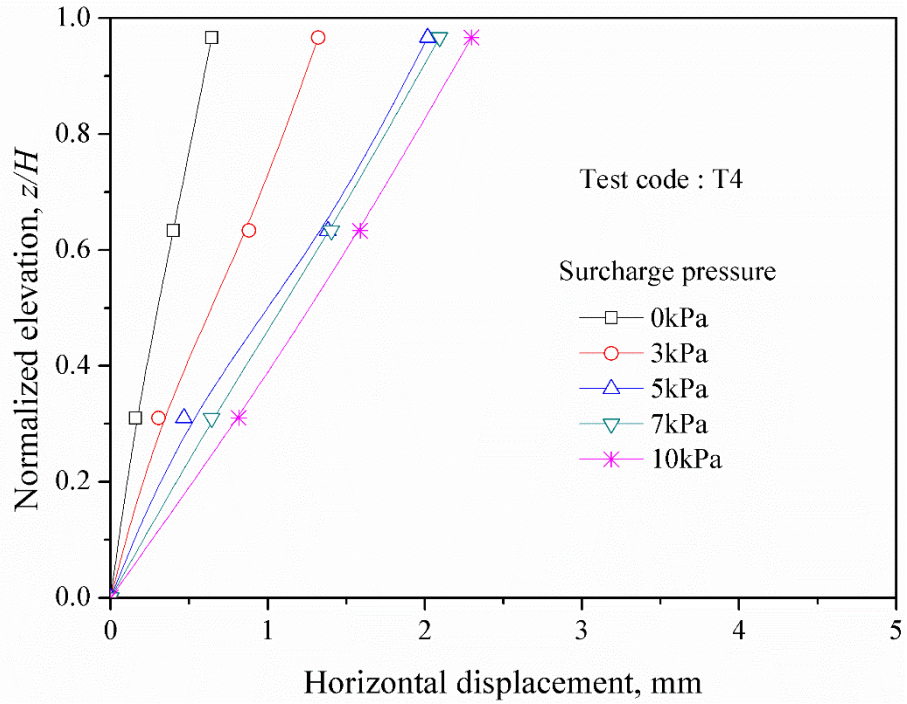

Fig. 4.5 Horizontal displacement profile for STC30 with different surcharge pressures

Fig. 4.7 presents the variation of top displacements at 10kPa surcharge and percentage reduction with tire chip content (%TC) for model wall with different STC mixtures. Wall top displacements of 6.0, 4.4, 2.8, 2.3, 3.42, and 4.3 mm are seen from

the figure, for 0, 10, 20, 30, 40 and 50 % of tire chips, respectively. The top displacement displacements are decreased by increasing tire chips content up to 30%. Beyond the STC30, further addition of TC resulted in increasing maximum lateral displacements. Referring to the Fig. 4.3 and Fig. 4.7, it can be stated that wall displacements are reduced significantly (up to about 60 %) by addition of TC up to 30 % by weight. The reason behind this displacement reduction is that, when tire chips content is increasing in the place of sand the unit weight was decreased (Fig. 3.8) due to the fact that TC has less specific gravity as compared to sand and a lower void ratio can be seen at STC30 (Fig. 3.9). Further, it can also be observed from Fig. 3.15, that addition of tire chips (up to 30 %) in sand increased the shear strength properties (angle of internal friction values).

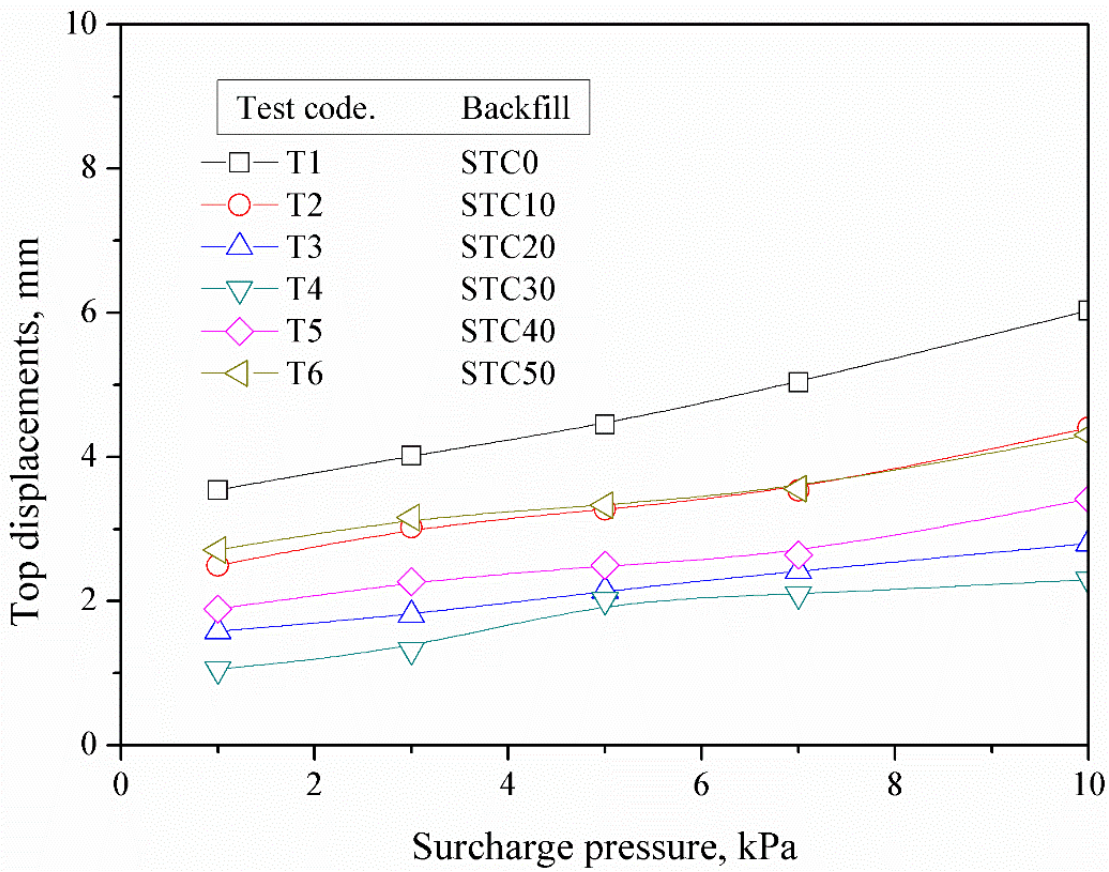

Fig. 4.6 Maximum (top) displacements with different STC mixtures under different surcharge pressures

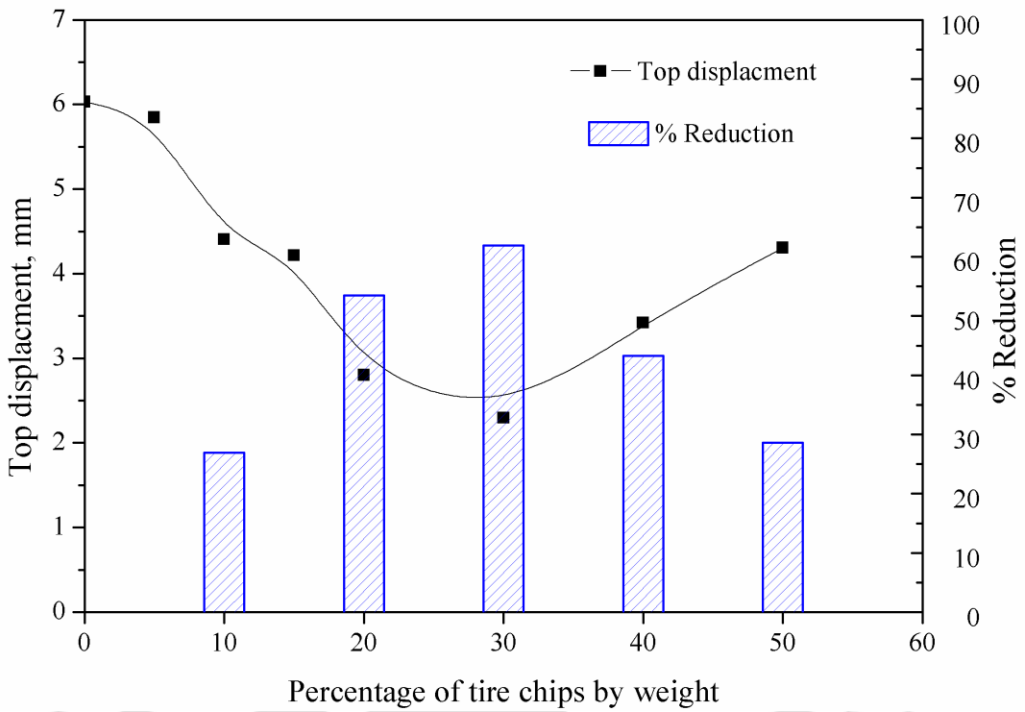

Fig. 4.7 Top displacements and its percentage reduction with different STC mixtures under 10 kPa

4.3.2 Lateral earth pressures on wall models

Lateral earth pressures were monitored at two conditions (at rest and after support removal) using four earth pressures sensors at different elevations on the retaining wall models. Fig. 4.8 shows the earth pressure responses under both the conditions for all the wall models with different STC mixtures. Fig. 4.8(a) shows the lateral earth pressures along the height of wall for 'at rest condition' while, Fig. 4.8(b) for 'after support removal condition'. The figures indicate that lateral pressures fall in the range of 0–2 kPa under both the conditions. Though there is no consistent trend in relative variations of pressures for different wall models, it can be observed that the pressures after support removal condition are low compared to the at rest condition. Further, it can also be seen that the lateral earth pressures were affected by the STC mixtures, resulting in lowest earth pressures for STC30 model (Test T4). Based on maximum values of lateral earth pressures at at-rest and active conditions, percentage reductions were calculated and shown in Fig. 4.9. The percentage reduction of earth

pressure was increased by increasing TC up to 30%. By using STC30, it can be seen that about 50–60 % reduction in earth pressures.

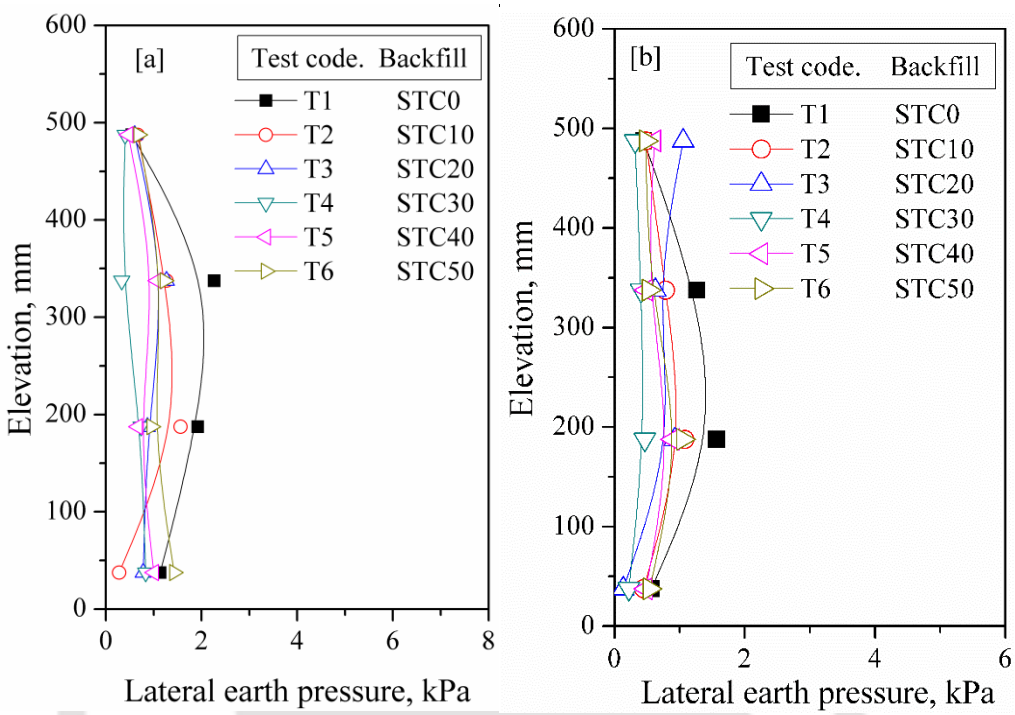

Fig. 4.8 Lateral earth pressure profiles; (a) at rest condtion, (b) after support removal

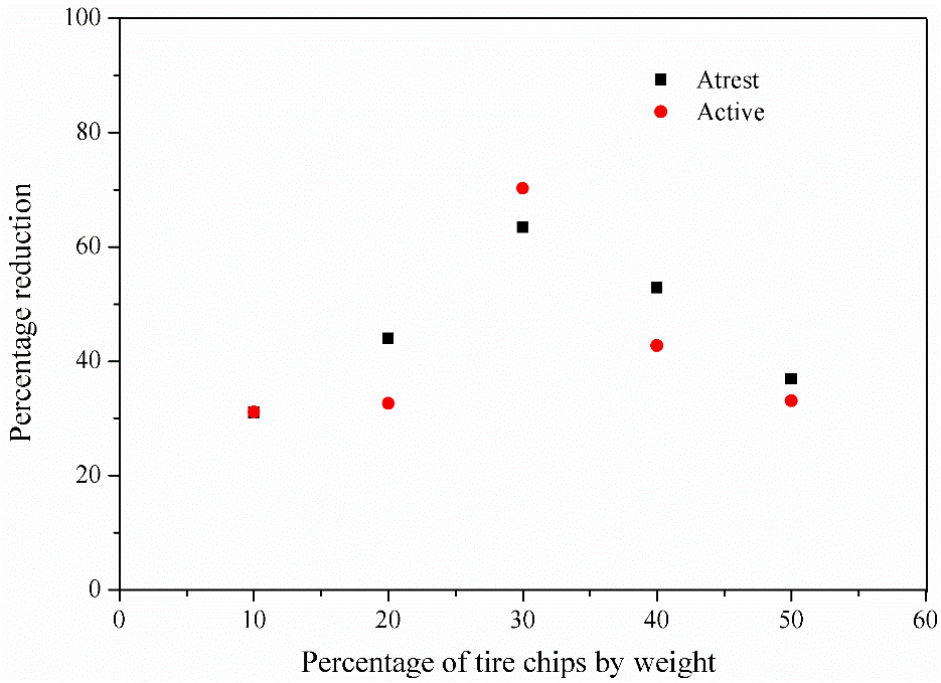

Fig. 4.9 Percentage reduction of maximum earth pressures with %TC

Fig. 4.10 presents the maximum lateral earth pressures on model wall with different surcharge pressures for different STC mixtures. It is seen from the figure that

the maximum earth pressures are increased with increasing surcharge pressures in all model walls. The figure also depicts the fact that at all surcharge loading conditions the lowest pressures is shown for STC30 mixtures and highest for the control case with STC0 backfill. Lateral earth pressures in the range of 2.0 - 5.0 kPa for STC0 are recorded for surcharge variation from 1 to 10 kPa. The corresponding earth pressures variations for STC30 are in the range of 1.5 - 3.0 kPa. Fig. 4.11 presents the variation of maximum lateral earth pressures on the wall at 10 kPa surcharge for different STC mixtures (%TC) and percentage reduction. Maximum lateral earth pressures of 4.8, 3.4, 3.1, 2.7, 3.07, and 3.6 kPa are seen from the figure, for 0, 10, 20, 30, 40 and 50 % of tire chips, respectively. The maximum lateral earth pressures are decreased by increasing tire chips content up to STC30. Beyond this %TC further addition of TC resulted in increasing maximum lateral earth pressures. The percentage reduction of maximum lateral earth pressure is about 50 % for STC30 model wall.

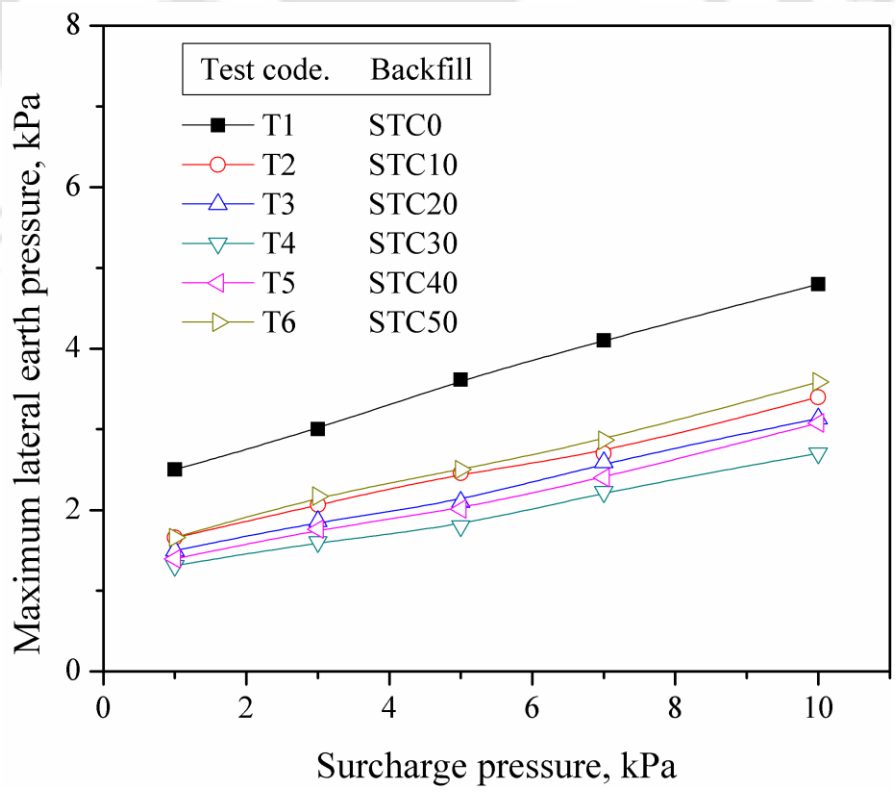

Fig. 4.10 Maximum lateral earth pressures with different surcharge pressures

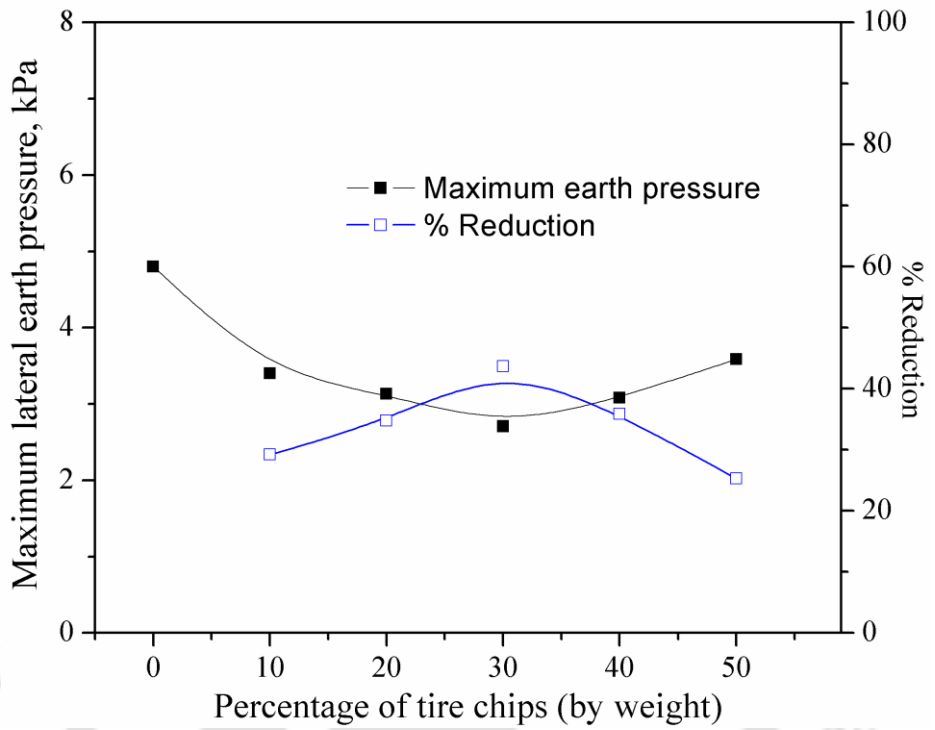

Fig. 4.11 Maximum lateral earth pressures at 10 kPa surcharge pressure

4.3.3 Comparison of experimetnal and theoretical results

Measured earth pressures are compared with theoretical earth pressure evaluations. Pressures before the support removal were compared with the pressure at at-rest condition (Eq. 4.1) and pressures after support removal are compared with active earth pressure condition (Eq. 4.2). It may be noted that, in fact, the pressures after support removal will be in between these two values.

$$p_o = (1 - \sin\phi)\gamma z \qquad \text{(Eq. 4.1)}$$

$$p_a = \frac{(1-\sin\phi)}{(1+\sin\phi)}\gamma z \qquad \text{(Eq. 4.2)}$$

Where p_o is the earth pressure at at-rest condition at a depth z from the top of wall; p_a is the earth pressure at active condition at a depth z from the top of wall; γ and ϕ are the dry unit weight and angle of internal friction of backfill material under consideration.

Fig. 4.12 and Fig. 4.13 show the comparison of theoretical and measured earth pressures with different STC mixtures in both conditions. Measured earth pressures are

reasonably matching with theoretical maximum earth pressures in all STC mixtures as shown inFig. 4.12 and Fig. 4.13.

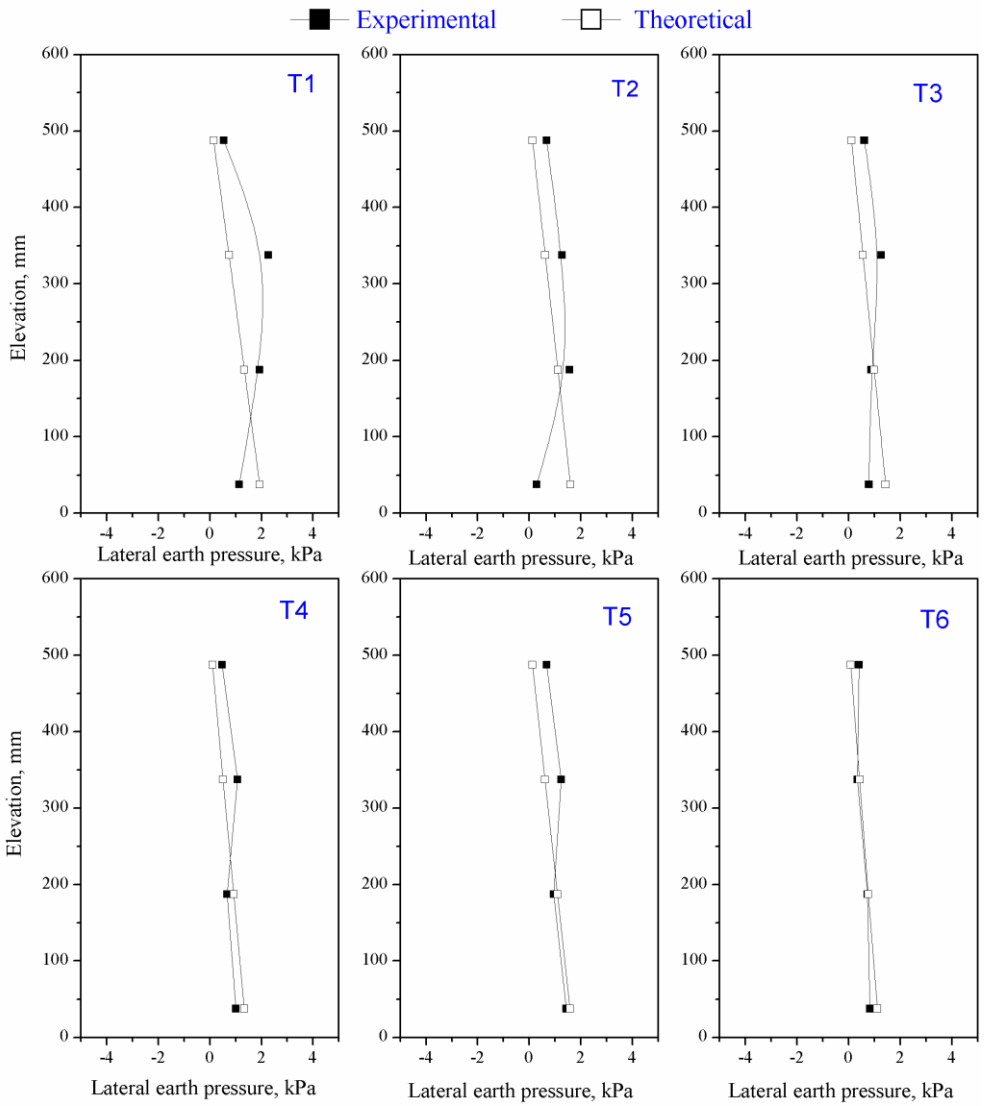

Fig. 4.12 Comaprsion of lateral earth perssurres at atrest condtion

The experimental results indicate that the horizontal displacements and lateral earth pressures are reduced by a range of 50–60 % while using STC30 mixture. Referring to Chapter-3, higher shear strength properties (friction angle) and lower deformation properties (void ratio) can be seen at STC30. Moreover, the tire chips are being lighter, and depicting higher shear properties (in the element tests), contributed to the observed response. Though the unit weight of the STC mixture beyond STC30 is

reducing, the reduced shear strength behaviour and increased deformation, behaviour (void ratio) resulted to the detrimental effect of addition of tire chips. The study shows the beneficial effect of mixing the tire chips in cohesion less backfill (sand) up to about 30 % by weight.

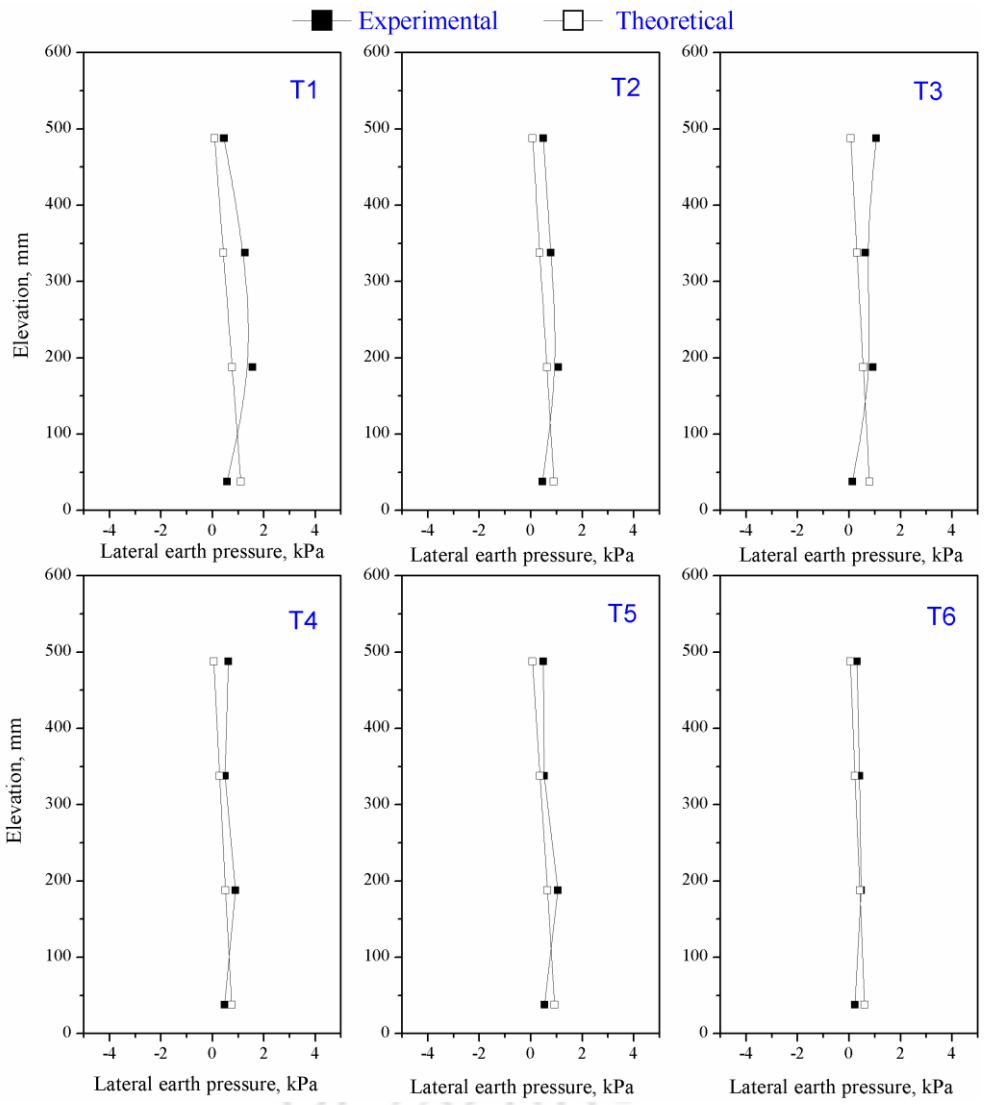

Fig. 4.13 Comaprsion of lateral earth perssurres at after surpport removal

4.4 WALL MODELS SUBJECTED TO SINUSOIDAL EXCITATIONS

1-*g* shaking table tests performed on small-scale retaining wall models backfilled with sand (control case) and different STC mixtures are discussed here. Retaining wall

models were tested with different sinusoidal excitations to measure the model wall response in terms of lateral incremental earth pressures, lateral displacements of wall, and accelerations. Testing procedure as described in section 4.2 was adopted. Each model retaining wall was instrumented with LVDTs, accelerometers and pressure sensors at different locations as shown in Fig. 3.20. The following sections discuss the dynamic response of the model walls in terms of horizontal displacements, incremental lateral earth pressures, and acceleration amplifications.

4.4.1 Response of model wall backfilled with sand

Table 4.6 shows different model tests carried out on model walls backfilled with sand (STC0) under varying shaking conditions. Each model wall was subjected to 20 cycles of corresponding sinusoidal shaking. The displacements measured by L1, L2 and L3 at the elevations of 125, 380 and 580 mm from the base, respectively.

Table 4.6 Details of different sinusoidal excitation tests on model wall with sand backfill

Test code	Backfill	Acceleration (*a*), *g*	Frequency (*f*), Hz
STC0_0.1_3	STC0 (sand alone)	0.1	3
STC0_0.1_5		0.1	5
STC0_0.2_3		0.2	3
STC0_0.3_3		0.3	3
STC0_0.3_5		0.3	5

Fig. 4.14 shows the typical variations of displacements with number of cycles at different elevations for the test STC0_0.1_3. The figure depicts increasing trend of displacements with increasing number of cycles and greater displacements at higher elevations. The maximum displacements recorded during shaking were about 0.61, 0.38,

and 0.12 mm at elevations of 580, 380 and 125 mm, respectively. Fig. 4.15 shows the typical variation of accelerations with number of cycles, at different elevations, for the test STC0_0.1_3. It can be seen that the accelerations were amplified at higher elevations. Which these maximum accelerations at location A2 and A3 were found to be about 1.16 and 1.32, of that at A1 location, respectively.

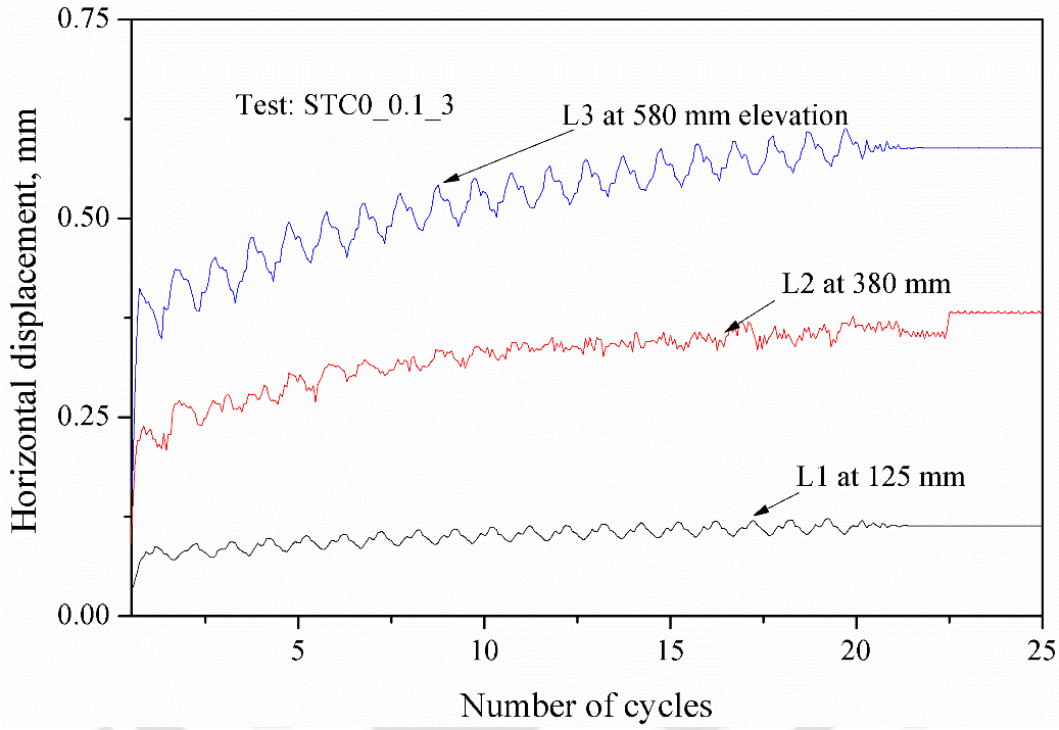

Fig. 4.14 Typical displacement histories at different elevations for the test STC0_0.1_3

Fig. 4.16 shows the typical variation of the lateral dynamic incremental earth pressures with number of cycles for the test STC0_0.1_3. Incremental earth pressure is the measured increment due to cyclic loading. From the figure, it is observed that the incremental pressures were varying with depth and increasing with loading cycles. The maximum dynamic incremental earth pressures recorded for shaking were about 0.379 kPa, 0.151 kPa, 0.115 kPa and 0.036 kPa at elevations of 37, 187, 337 and 487 mm, respectively.

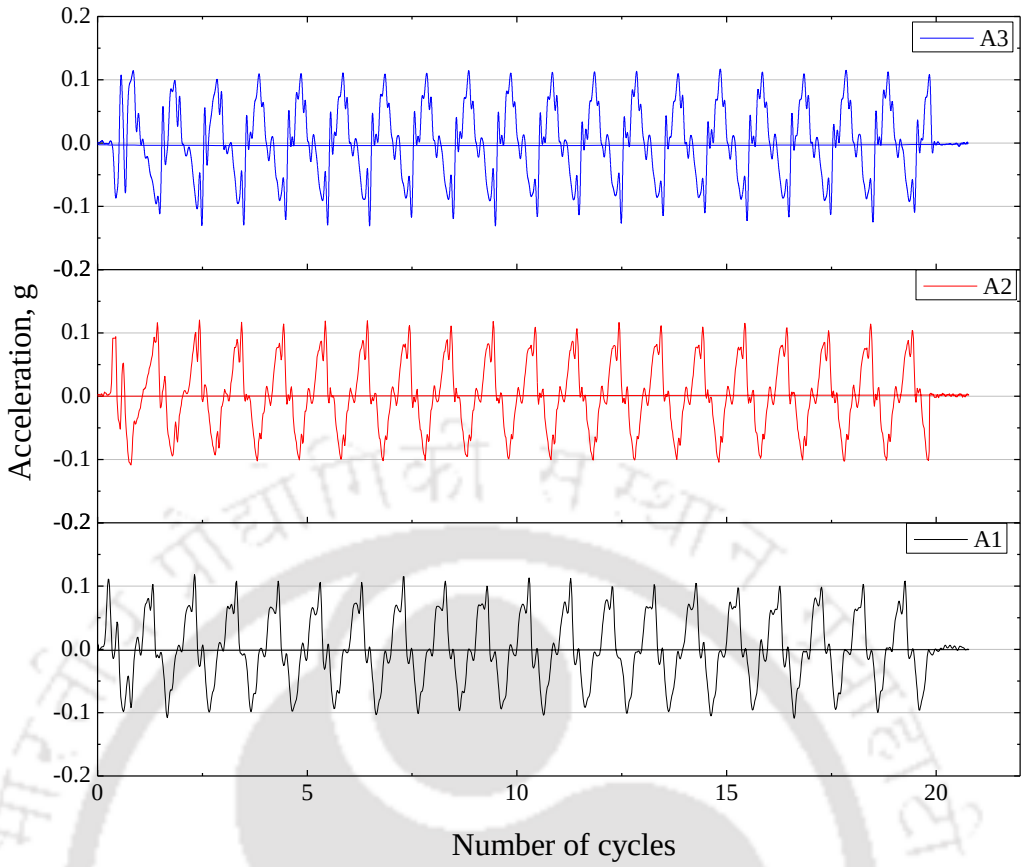

Fig. 4.15 Typical variation of acceleration with time for the test STC0_0.1_3

To observe the horizontal displacements and lateral incremental earth pressures along height of the wall for different shaking levels, displaced profiles and lateral earth pressure profiles of different wall models were presented. To evaluate the acceleration response at different elevations of retaining model walls, acceleration amplification factors were used to represent the accelerations. These acceleration amplification factors were evaluated by using the maximum acceleration in the acceleration history for each accelerometer device. Acceleration amplification factor is the ratio of maximum acceleration value in the backfill material to the corresponding base maximum acceleration value. Similar type of procedure adopted by Lin et al. (2017).

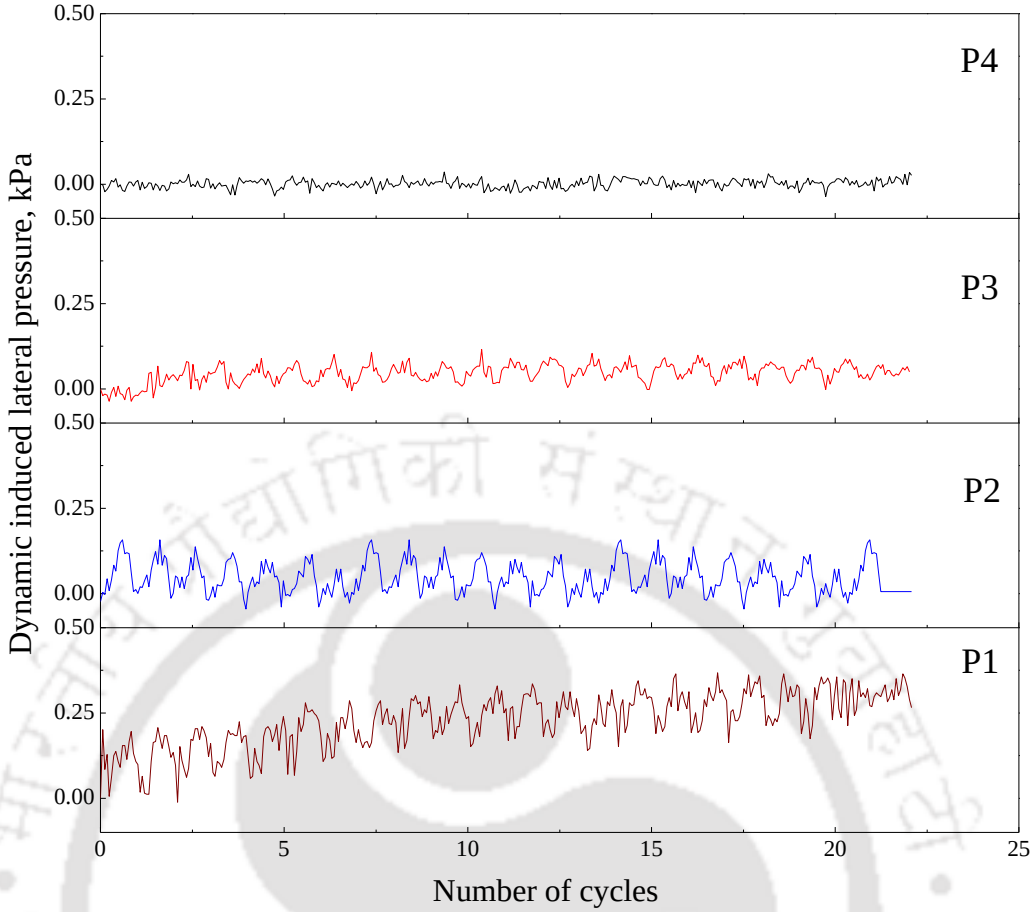

Fig. 4.16 Variation of incremental earth pressures with time for test STC0_0.1_3

Effect of base acceleration

Fig. 4.17(a) shows the displacement profiles, at the end of 20 cycles of dynamic excitation at different acceleration levels (at f = 3 Hz), revealing the influence of base acceleration on the horizontal displacement response of wall. It is observed, from the figure, that the displacements are significantly increased with the increasing base acceleration of input excitation. The maximum displacements were observed at higher elevations. The maximum displacement of 0.61 mm is observed for 0.1g (STC0_0.1_3) base acceleration and the corresponding values for 0.2g (STC0_0.2_3) and 0.3g (STC0_0.3_3) base accelerations are 3.22 mm and 4.32 mm, respectively.

Incremental lateral earth pressures are observed during the dynamic excitation along the height of the wall in different tests. Fig. 4.17(b) shows the measured

incremental lateral earth pressures along the height of the wall for STC0_0.1_3, STC0_0.2_3 and STC_0.3_3 tests. It is observed, from the Fig. 4.17(b), that incremental lateral earth pressures are depicting the increasing trend with increase in base acceleration. Maximum earth pressures are observed at bottom of the wall. However, slight inconsistent trend is noted at P2 and P3 locations which are attributed to the pressure sensors' capacity (50 kPa) in contrast to the measured range of pressure values (0-2 kPa). Fig. 4.17(c) shows the acceleration amplification factor profiles. As seen the figure, acceleration amplifications are higher at top of the backfill and found to be increased with increasing base acceleration. These results are in agreement with results of the model wall tests by El-Emam and Bathurst 2007, Zarnani 2011, where the acceleration amplification increased with increasing base acceleration.

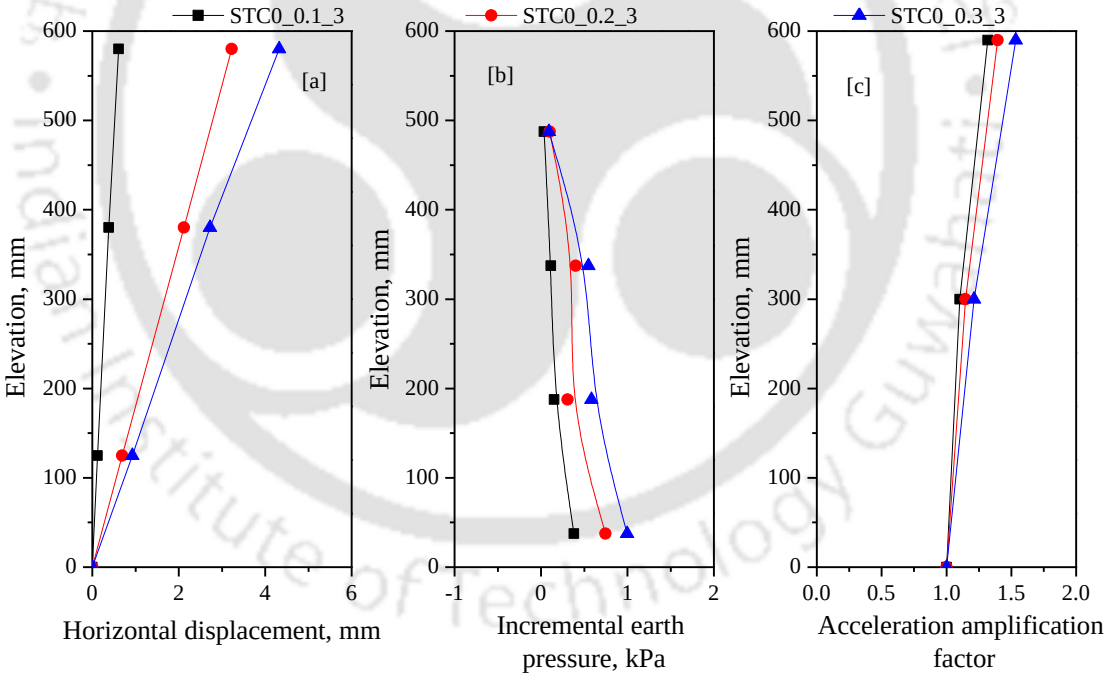

Fig. 4.17 Effect of base acceleration on model response; (a) Normalized displacement profile. (b) Incremental earth pressure profile. (c) Acceleration amplification factor profile

4.4.2 Response of model wall backfilled with different STC mixtures

Different STC mixtures (STC10, STC20, STC30, STC40, and STC50) and pure sand (STC0) were considered as backfill materials to study the effect/influence of

different STC mixtures on dynamic response of the retaining wall models. After completing the model construction, each model wall was subjected excitations as presented in Table 4.2 and results are compared with control case (pure sand). In the sinusoidal shaking table tests, excitations of three accelerations (0.1*g*, 0.2*g* and 0.3*g*) at frequency of 3Hz and 5Hz were adopted.

Fig. 4.18 shows displacement profiles for wall model tests with different backfills subjected to 0.1*g* acceleration (*a*) at 3 Hz frequency (*f*). It is observed, from the figure, that the displacements are significantly affected with the type of backfill material. The maximum top displacement of 0.61 mm is observed for the test STC0_0.1_3 with STC0 backfill and it reduced to 0.27 mm for the test STC30_0.1_3 with STC 30 backfill.

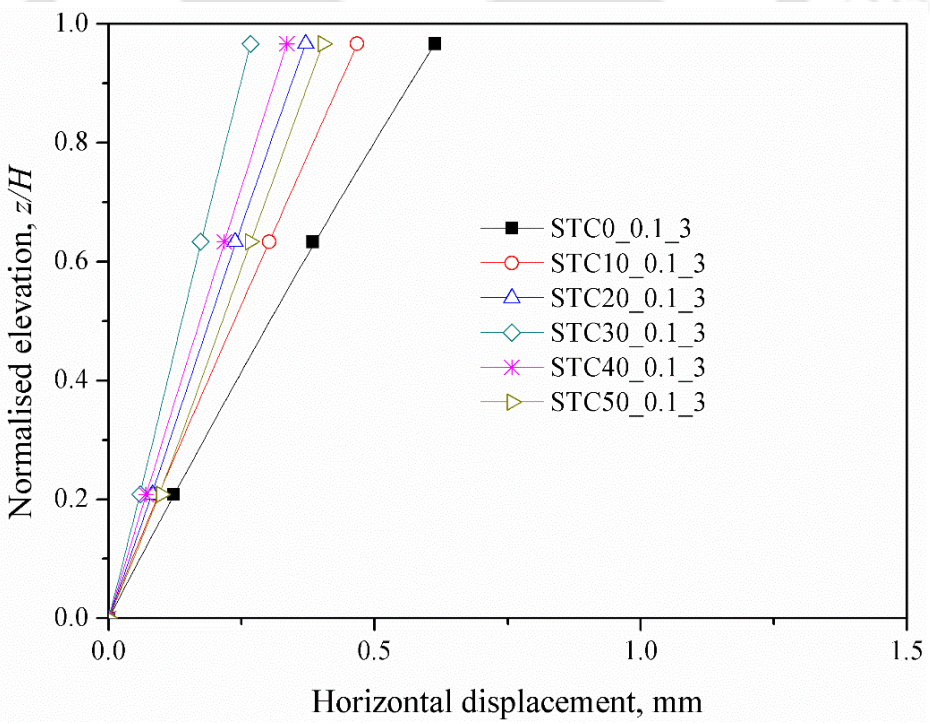

Fig. 4.18 Effect of STC mixtures on displacement profile for 0.1*g*_3Hz

Further, effect of STC mixtures on maximum displacements and reduction are shown in Fig. 4.19, which depicts about 20% to 55% reduction by using tire chips in

the backfill. Maximum reduction in displacement, about 55%, is seen for the wall model with 30 % of tire chips (STC30_0.1_3) compared to the reference test (STC0_0.1_3) with sand backfill.

Fig. 4.20 shows the incremental earth pressures along the height of wall with different backfill materials (different STC mixtures) for a base excitation of 0.1g at frequency of 3 Hz. As seen from the figure, the lateral earth pressures are reduced with increase in tire chips contents up to 30% by weight in STC mixture. Incremental earth pressures have been found to follow nonlinear trend for STC0, STC10, STC20, and STC40.

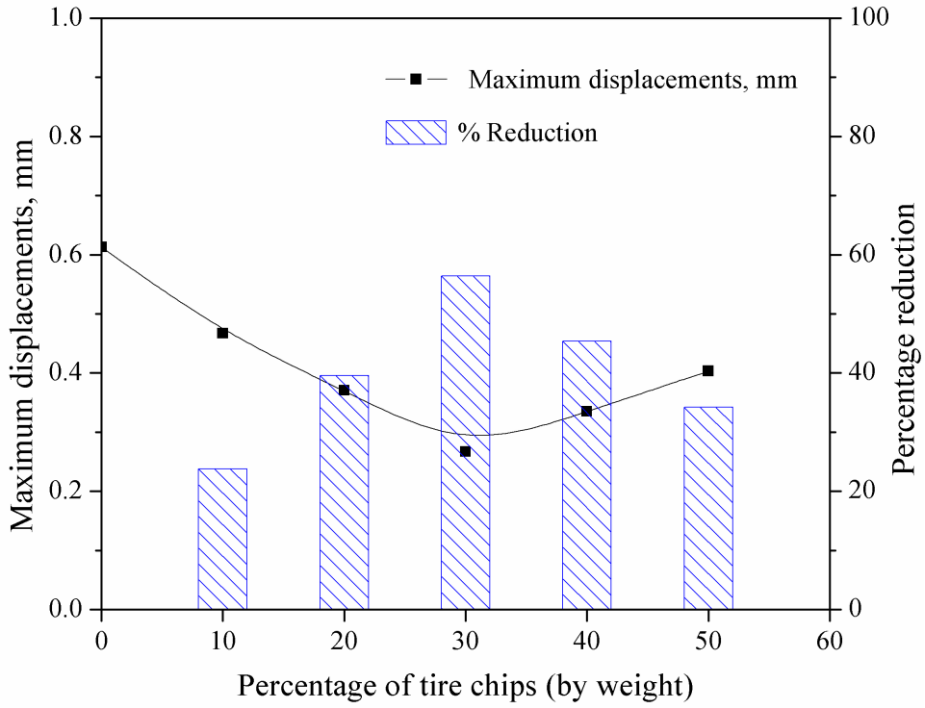

Fig. 4.19 Maximum displacement and percentage reduction at dynamic excitation of 0.1*g*_3Hz

It is important to note that the incremental lateral earth pressures are almost identical along the height of wall, where backfill materials were STC30 and STC40 mixtures. Further, the variation of maximum earth pressure with different STC mixtures (%TC) and its percentage reduction are shown in Fig. 4.21. The maximum incremental lateral earth pressures were found to be decreased with increasing tire chips contents

up to 30% by weight. The percentage reduction in incremental earth pressures is found around 80% for STC30. Referring to the reduction of lateral earth pressures and wall displacements using STC mixtures and considering design considerations, it can be stated that, sectional dimensions of retaining wall as well as cost of project can be reduced.

Acceleration responses of retaining wall models with different STC mixtures are presented in terms of acceleration amplification factors. Fig. 4.22 shows the effect of STC mixtures on acceleration amplification of the backfill. From the figure, it is observed that maximum acceleration amplification is at the top of the wall in all STC mixtures. Further, it is observed that, acceleration amplification at top of the wall is decreased with increasing STC mixtures, with values of 1.32, 1.19, and 1.25 for STC0, STC30, and STC50, respectively. Maximum amplification was observed for sand (STC0_0.1_3) and lower amplification was observed for 30% of tire chips (STC30_0.1_3). When tire chips were mixed with sand, attenuation of the acceleration is observed. This may be because tire chips are lighter resulting in lower inertial effect.

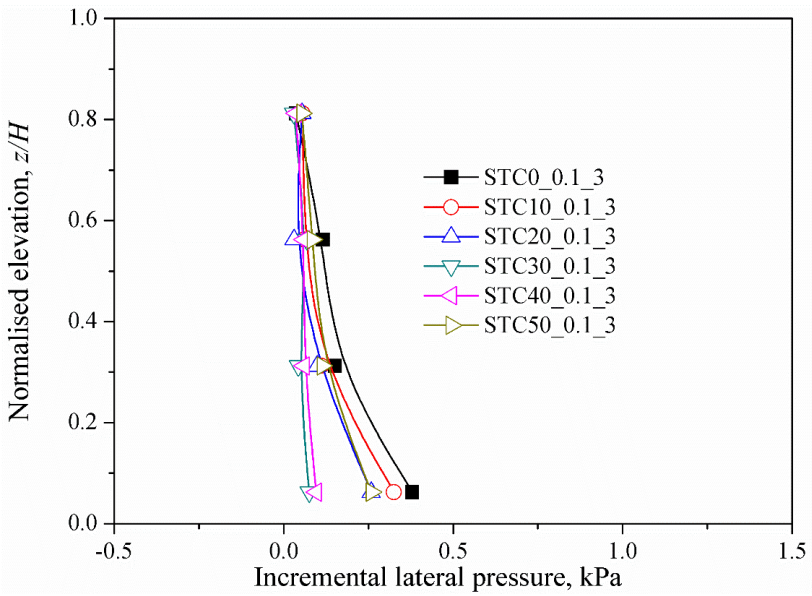

Fig. 4.20 Effect of STC mixtures on lateral earth pressure profile at dynamic excitation of 0.1*g*_3Hz

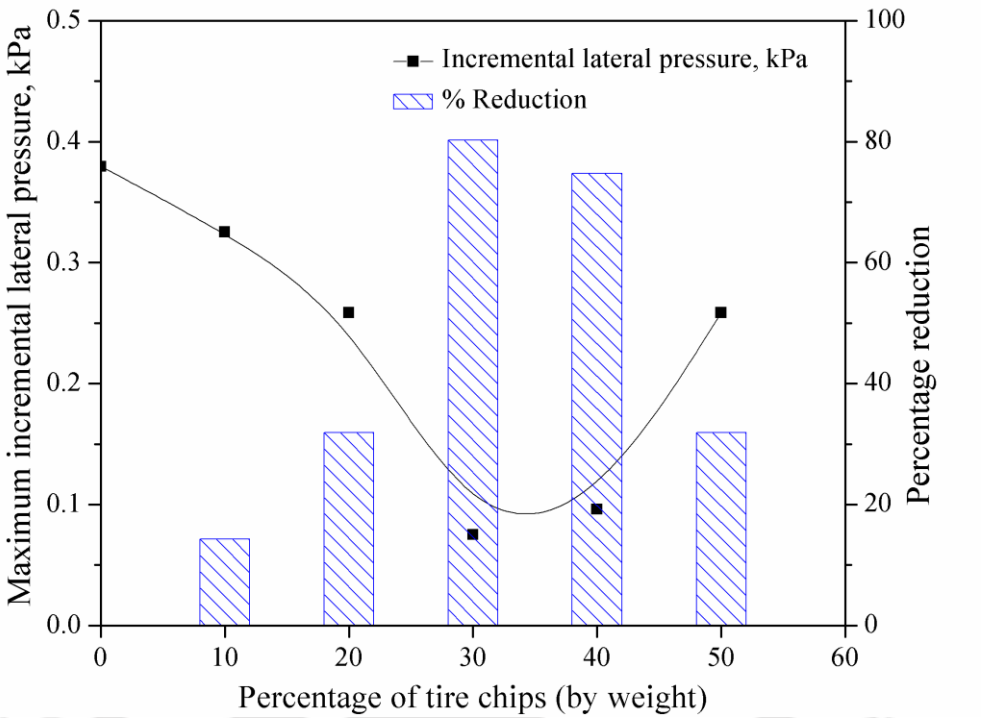

Fig. 4.21 Maximum lateral earth pressure and percentage reduction at dynamic excitation of 0.1*g*_3Hz

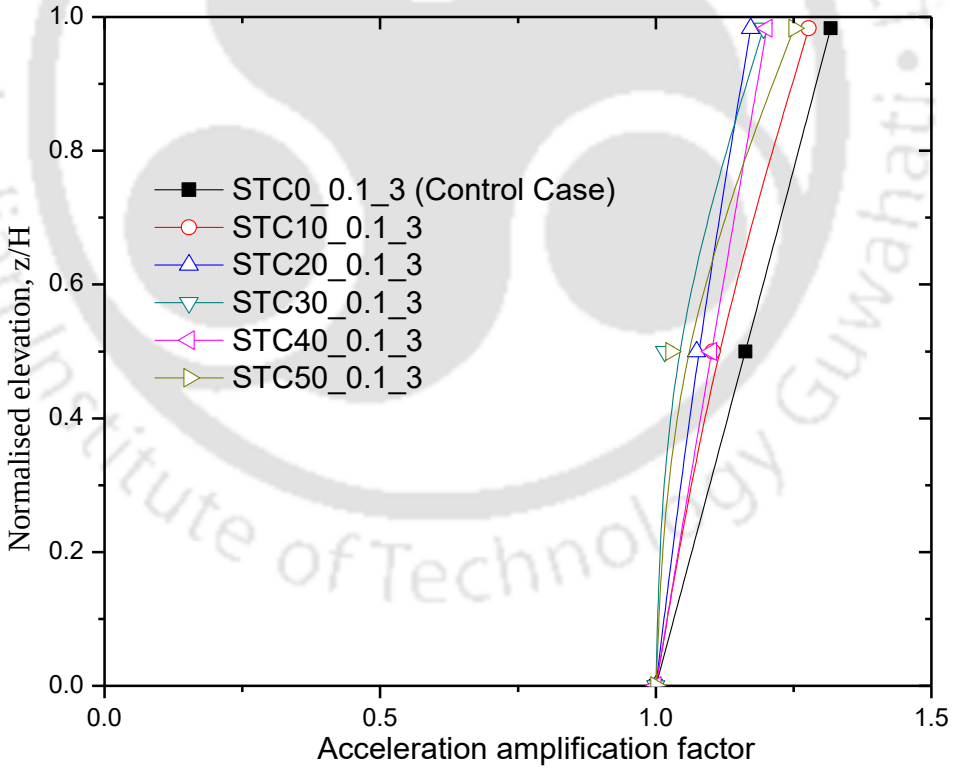

Fig. 4.22 Effect of STC mixtures on acceleration amplification at dynamic excitation of 0.1*g*_3Hz

Fig. 4.23 shows the wall model response with different STC mixture backfills for 0.2*g* acceleration and 3Hz frequency of base excitation. Fig. 4.23(a) shows the normalized displacement profile for different tests. The horizontal displacements (δ_h) appear normalized by the wall height (H). The maximum normalized displacement of 0.54% is observed for STC0_0.2_3 test and the corresponding values for STC10_0.2_3, STC20_0.2_3, STC30_0.2_3, STC40_0.2_3 and STC50_0.2_3 tests are 0.41%, 0.31%, 0.21%, 0.29% and 0.37%, respectively. Fig. 4.23 (b) shows the incremental lateral earth pressure profiles observed for tests. The incremental lateral earth pressures ($\sigma_{h\_incremental}$) appear normalized by the vertical pressure (γH). The maximum normalized earth pressure of 0.080 is observed for STC0_0.2_3 test; and the corresponding values for STC10_0.2_3, STC20_0.2_3, STC30_0.2_3, STC40_0.2_3, and STC50_0.2_3 tests are 0.065, 0.055, 0.014, 0.026, and 0.045, respectively. Fig. 4.23(c) presents the acceleration amplification factors along the height of model wall with different STC mixtures. From the Fig. 4.23(c), it is observed that acceleration amplification factor is less for STC30_0.2_3 compared to the control test (STC0_0.2_3).

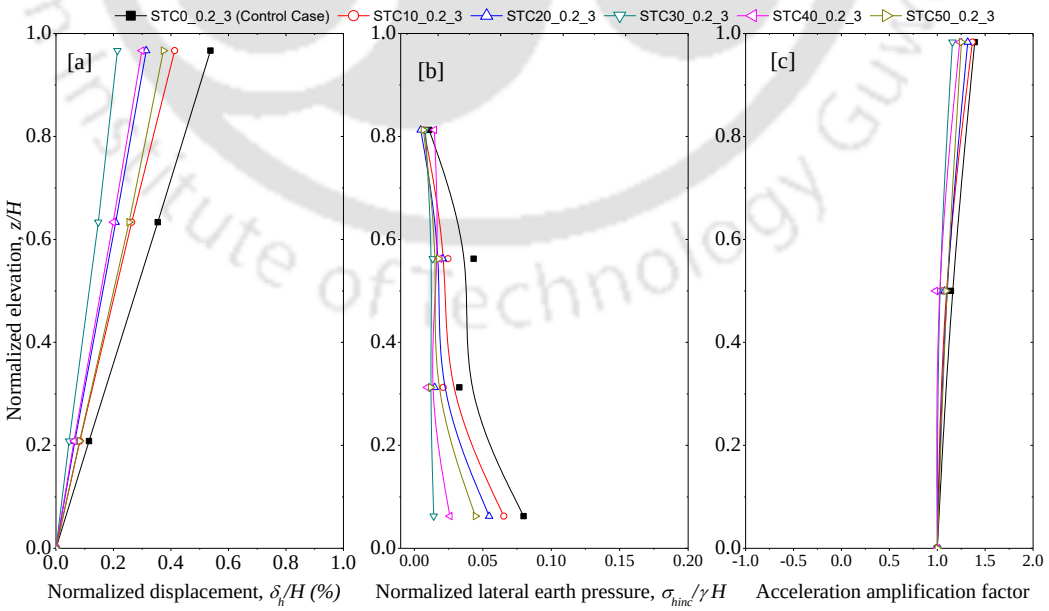

Fig. 4.23 Model wall response at 0.2*g*_3Hz: a) normalized displacements profile; b) Normalized earth pressures profile and c) Acceleration amplification factors

Higher base acceleration (a = 0.3g) was applied on model wall at frequency (f) of 3Hz and 5Hz for different STC mixture backfill walls. Fig. 4.24 shows the effect of different STC mixture backfills on model response in terms of normalized displacement profile (a=0.3g and f=3 Hz). Variations of the top displacement and its percentage reduction with reference to the control case (STC0_0.3_3 Test) with percentage tire chips are shown in Fig. 4.25. From the Fig. 4.19 and Fig. 4.25, 55% to 65% reduction in top displacement is observed as compared to control cases.

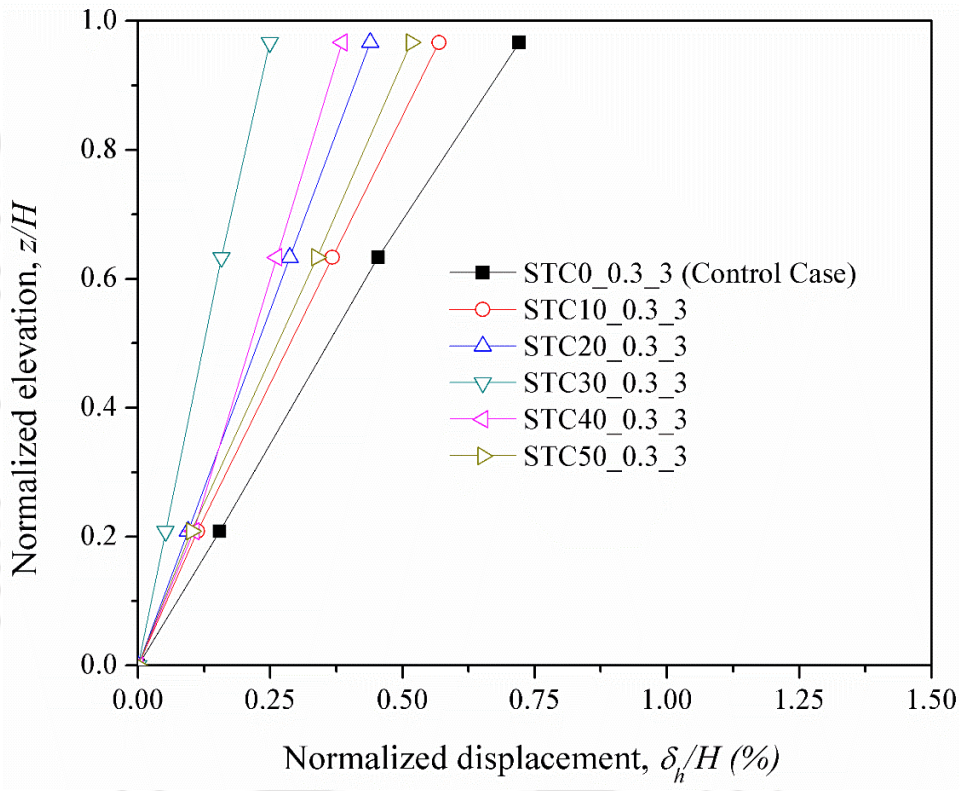

Fig. 4.24 Effect of backfill material on normalized horizontal displacement profile for 0.3g_3Hz

Fig. 4.26 shows the acceleration amplification profile for different tests at an acceleration (a) of 0.3g at frequency (f) of 3 Hz. Maximum acceleration amplifications were observed at the top of the wall in all the tests. Further, it is observed that acceleration amplifications decreased with increasing STC mixtures up to STC30.

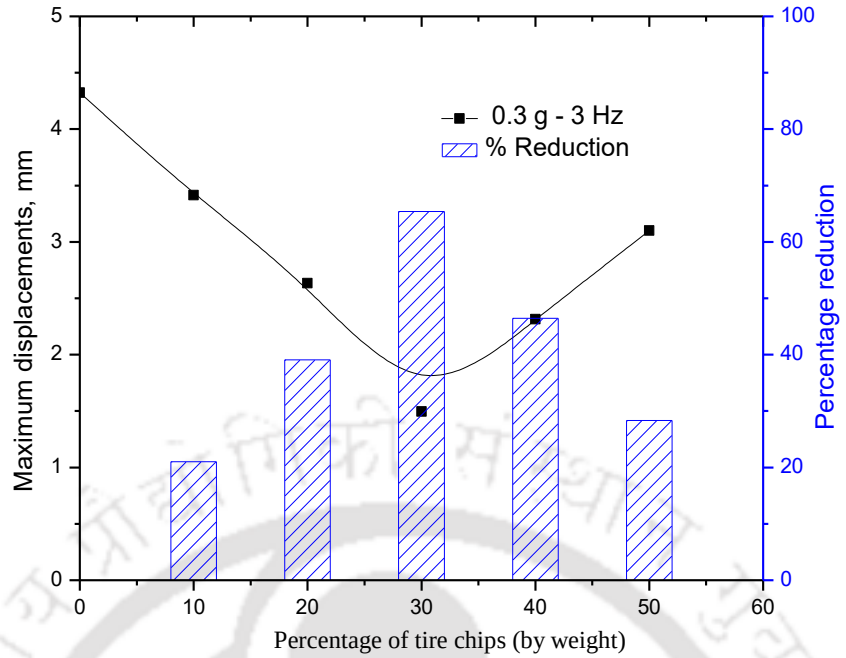

Fig. 4.25 Effect of STC mixtures on maximum displacement values and % reduction for 0.3*g*_3Hz

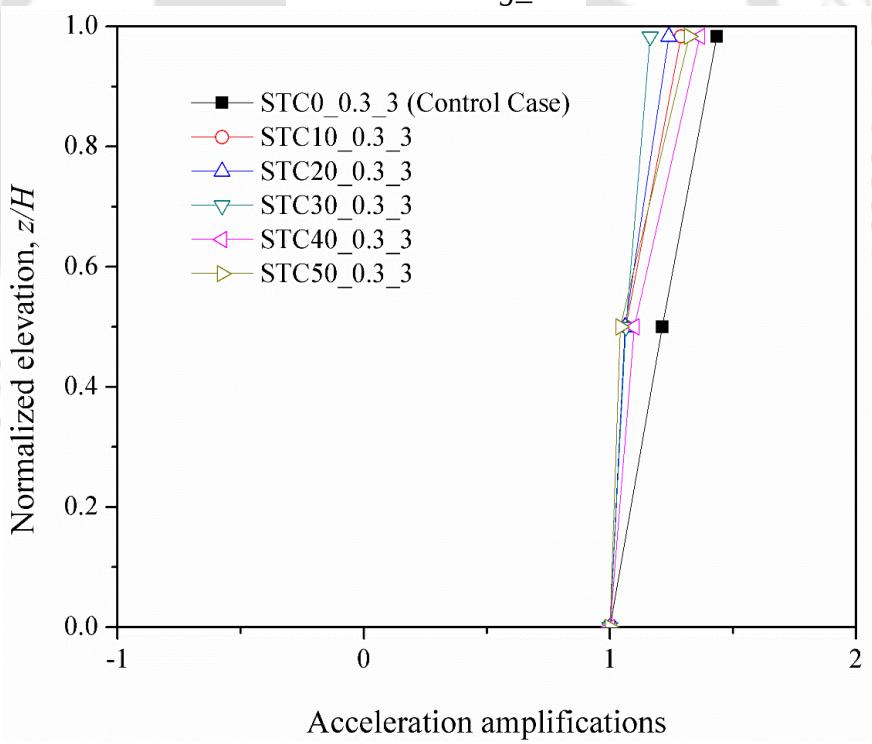

Fig. 4.26 Effect of STC mixtures on acceleration amplifications for 0.3*g* _3Hz

Fig. 4.27 shows the normalized increment earth pressures ($\sigma_{hinc}/\gamma H$) profile at base excitation of 0.3*g*_3Hz. Though there is nonlinear trend in relative variations of

pressures for different wall models, it can be observed that the pressures are higher at bottom. Further, it can be seen that the STC mixtures significantly affected the earth pressures, giving lowest earth pressure for STC30_0.3_3 and STC40_0.3_3 wall models.

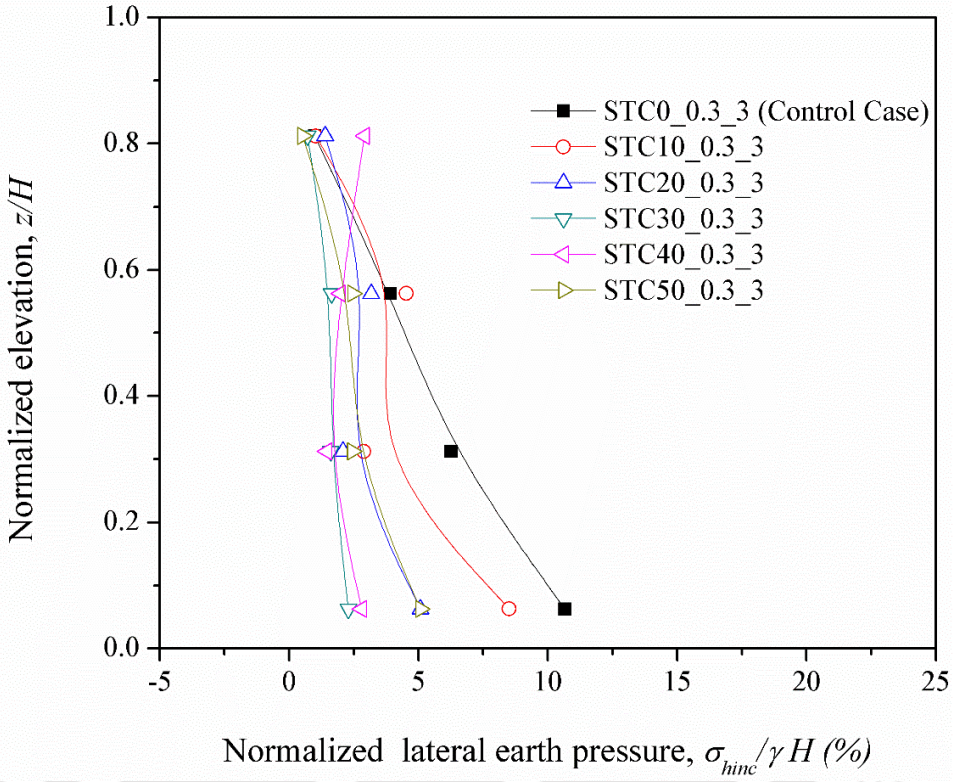

Fig. 4.27 STC mixtures on normalized pressures for 0.3*g*_3Hz

Maximum (top) displacements measured at different accelerations of base excitation with different STC mixtures are reported in Table 4.7. From the table, it is concluded that the maximum displacements were reduced by 55% to 65% for STC30 mixture backfill. Further, model tests were conducted on different STC mixtures backfills for 0.3*g* acceleration at frequency of 5Hz of base excitation and results are presented in terms of normalized displacements, normalized incremental earth pressures and acceleration amplification factors in Fig. 4.28. Table 4.8 presents the comparison of maximum displacement for 0.3*g* acceleration at 3 Hz and 5 Hz frequencies of base excitation for different STC mixtures and percentage reduction of

displacement. Incremental earth pressures and acceleration amplification factor profiles response for 0.3*g* _5Hz was found to be similar to that for 0.3*g*_3Hz base excitation.

Table 4.7 Maximum displacements and percentage reduction with different base acceleration

Mixture Proportions	Maximum displacements			% Reduction		
	0.1*g*	0.2*g*	0.3*g*	0.1*g*	0.2*g*	0.3*g*
STC0 (Control test)	0.61	3.22	4.32	-	-	-
STC10	0.47	2.48	3.41	23.76	22.98	21.06
STC20	0.37	1.88	2.63	39.53	41.61	39.12
STC30	0.27	1.28	1.49	56.43	60.25	65.51
STC40	0.33	1.79	2.31	45.36	44.41	46.53
STC50	0.40	2.24	3.09	34.21	30.43	28.47

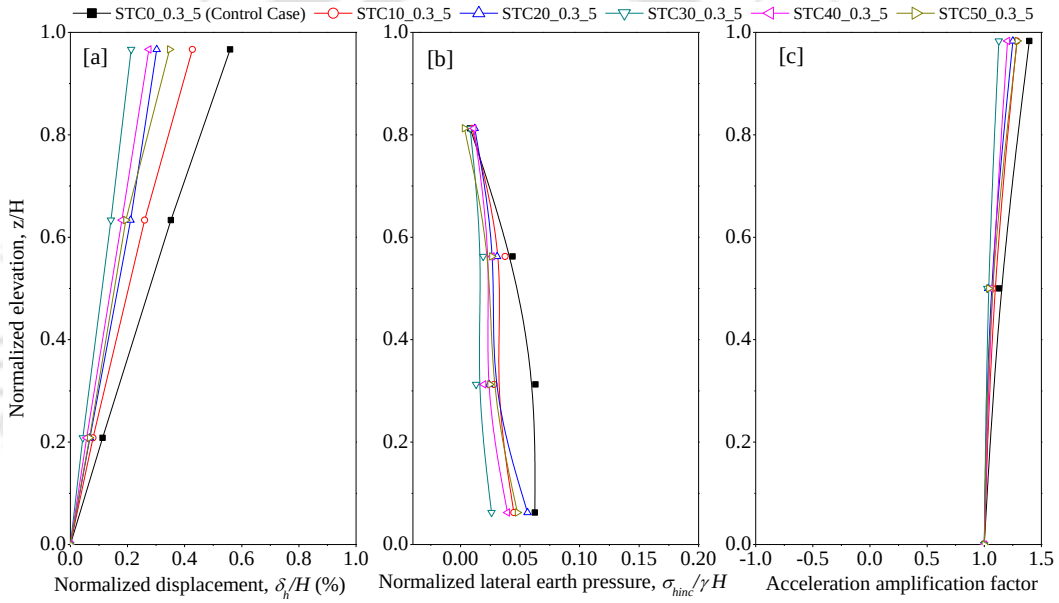

Fig. 4.28 Effect of STC mixtures on model response at 0.3g_5Hz: a) Displacements profile; b) Incremental earth pressures profile and c) Acceleration amplification factors profile

The following analysis attempts to explain the behavior/mechanisms causing the difference in performance of different STC mixtures backfills of retaining wall models. From the Fig. 4.19, Fig. 4.24, Fig. 4.28a, Table 4.7 and Table 4.8, it is concluded that maximum displacements are reduced in the range of 60% to 65% when STC30 mixture backfill is used in place of STC0 (only sand backfill). From the Fig. 4.21, Fig. 4.23b, Fig. 4.27, Fig. 4.28b, it is revealed that incremental lateral earth

pressures are significantly reduced with STC mixtures. The STC30 mixture material shows more reduction of earth pressures as compared to other STC mixtures. From the Fig. 4.22, Fig. 4.23c, Fig. 4.26, Fig. 4.28c, it is revealed that attenuation of acceleration amplification factor when tire chips mixed sand as backfill material. Attenuation of acceleration and displacements of model wall shows the higher damping/seismic isolation behavior when using STC mixtures.

Table 4.8 Maximum displacements and percentage reduction

Mixture Proportions	Maximum displacements		% Reduction	
	0.3g			
	3Hz	5Hz	3Hz	5Hz
STC0 (Control test)	4.32	3.35	-	-
STC10	3.41	2.56	21.06	23.58
STC20	2.63	1.81	39.12	45.97
STC30	1.49	1.28	65.51	61.79
STC40	2.31	1.65	46.53	50.75
STC50	3.09	2.08	28.47	37.91

Therefore, the lightweight of tire chips and high shear strength properties of STC mixture contributed to the observed model responses. Based on all the tests results it is concluded that tire chips mixing with sand as a STC mixture, more beneficial effect in dynamic condition can be achieved. The reduction of horizontal displacement of wall, incremental lateral earth pressure, and acceleration amplification implies lesser dimensions of retaining wall. This optimization of dimensions of the retaining wall leads to sustainability as compared to conventional backfill material.

4.5 MODEL WALLS SUBJECTED TO EARTHQUAKE EXCITATIONS

In this section, series of model tests using the real earthquake (EQ) excitations were discussed. The selected records cover a wide range from medium intensity earthquakes (Sikkim, 2011) to stronger intensity earthquakes (Tohoku, 2011). The

details about testing program and sequence of excitations applied are shown in Table 4.4 and Table 4.5, respectively.

4.5.1 Response of model wall backfilled with sand

In this section tests results were discussed only for retaining wall model backfilled with sand (control case) subjected four earthquake excitations. Fig. 4.29 shows the displacement variations with time at different LVDT locations for SK and NZ earthquakes. From the figure, it is observed that the maximum displacement is found at L3 location and the corresponding values are about 1.375 mm and 0.875 mm. Fig. 4.30 shows the incremental earth pressure variations with time (for SK and NZ earthquakes) at different elevations. From the figures, it is observed that the maximum incremental pressure is measured at P3 location and the corresponding value is about 0.87 kPa. Fig. 4.31 shows the accelerations variations with time at different revelations for SK and NZ earthquakes. From the figure, it is observed that the accelerations are more at the surface.

Further, the results of wall models, in the form of variations of horizontal displacement, acceleration amplification factors and incremental pressures along height of the wall for different dynamic excitations are presented in Fig. 4.32. Table 4.9 shows the maximum values of the observations for different earthquake excitations. Maximum horizontal displacements at the top of wall are ranged within 0.72 mm for SN EQ and 2.43 mm for TK EQ. The maximum horizontal displacements are 1.37 mm and 0.787 mm observed respectively for SK and NZ earthquakes. The acceleration amplification factors for SN, SK, NZ and TK earthquakes are 1.70, 1.82, 1.80 and 2.02, respectively. The reason for getting the similar displacement response for SN and NZ earthquake can be justified with its predominant frequency, which is 2.17 and 2.25 for SN and NZ EQs.

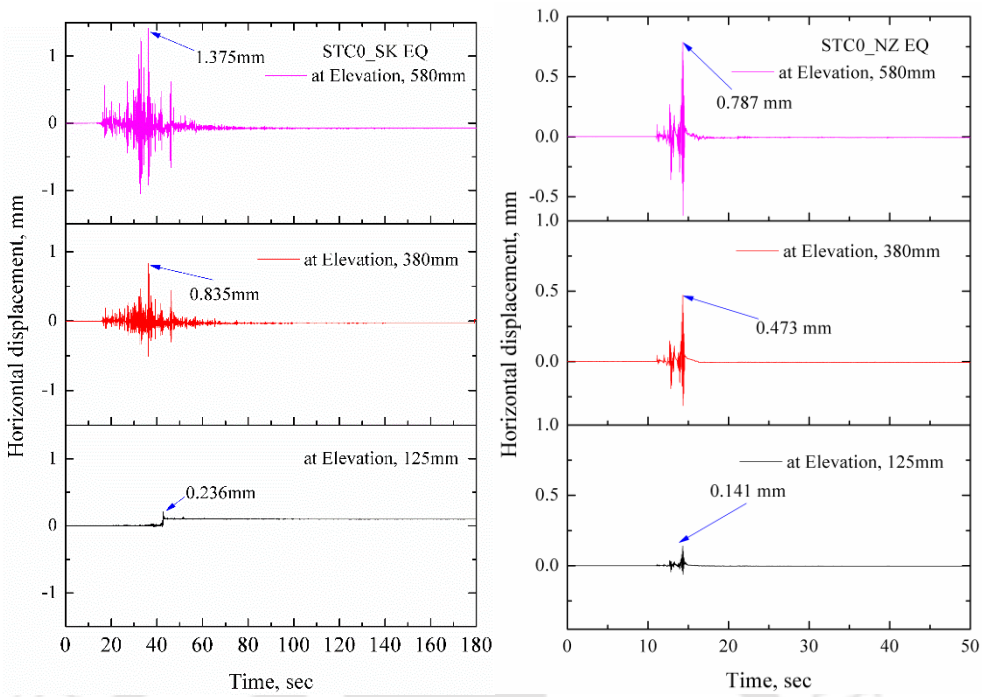

(a) (b)

Fig. 4.29 Displacements histories at different elevations for STC0 model: a) Sikkim (SK) earthquake and New Zealand (NZ) earthquake

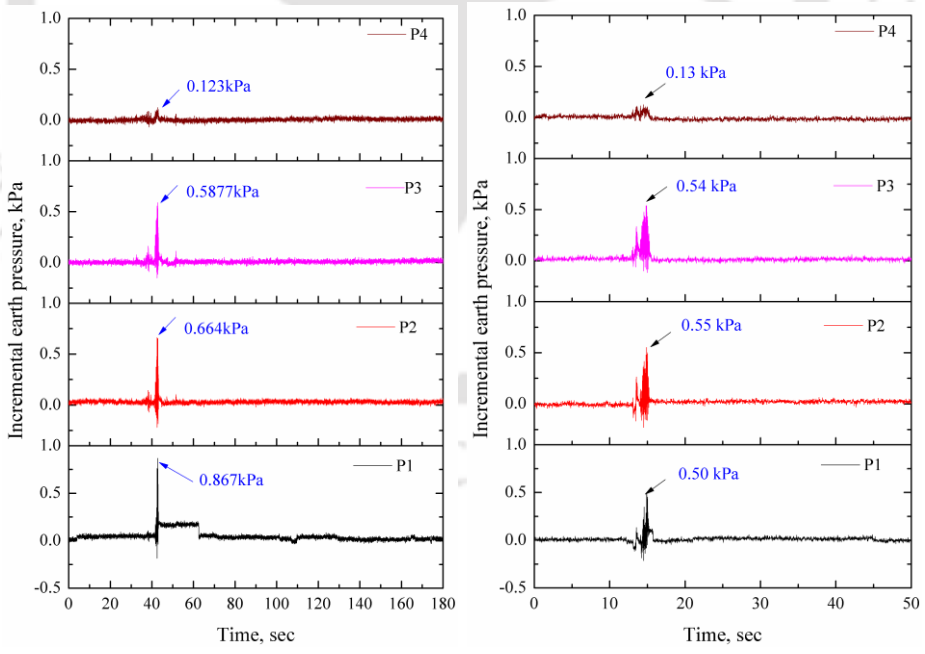

(a) (b)

Fig. 4.30 Incremental earth pressures histories at different elevations for STC0 model: a) Sikkim (SK) earthquake and b) New Zealand (NZ) earthquake

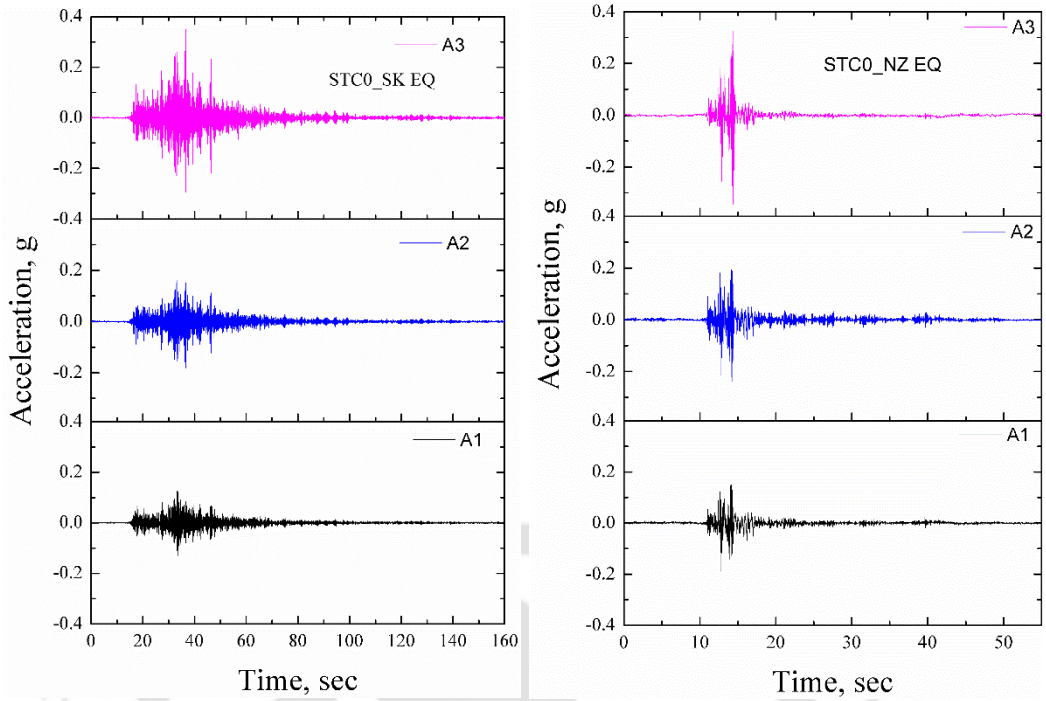

(a) (b)

Fig. 4.31 Accelerations histories at different elevations for STC0 model: a) Sikkim (SK) earthquake and b) New Zealand (NZ) earthquake

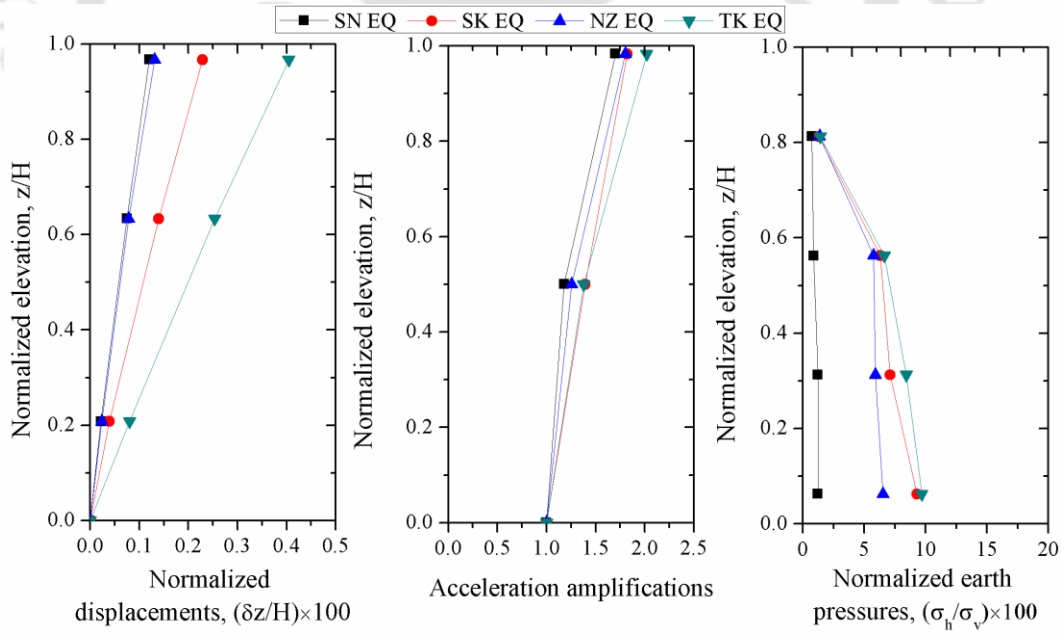

(a) (b) (c)

Fig. 4.32 Model wall response subjected to different scaled earthquake excitations; a) horizontal displacements; b) acceleration amplification factors and c) incremental lateral earth pressures

Table 4.9 Responses of model wall with different earthquake excitations

Earthquakes	Responses	
	Max. Horizontal displacement, mm	Max. amplification factor
SN EQ	0.723	1.70
SK EQ	1.375	1.82
NZ EQ	0.787	1.80
TK EQ	2.428	2.02

4.5.2 Response of model wall backfilled with different STC mixtures

Displacements response

The displacement responses for model walls with different STC mixtures and STC0 backfills subjected different earthquake excitations are compared and discussed. Wall displacement histories at top for different models with STC mixtures subjected to SK EQ excitation are shown in Fig. 4.33. Further, the compassion of displacements for backfill with and without tire chips at top, middle and bottom locations of model for SN EQ excitation are shown in Fig. 4.34, Fig. 4.35, and Fig. 4.36. From the figures, it concluded that maximum displacements at top (L3) location are 0.723 mm for control test (STC0) and 0.539, 0.285, 0.556 mm for STC 10, STC 30 and STC 50 backfills, respectively. The percentage reduction is calculated for all STC mixtures with reference to STC0 model wall. At STC30 mixture, the percentage reduction is maximum of about 60 %.

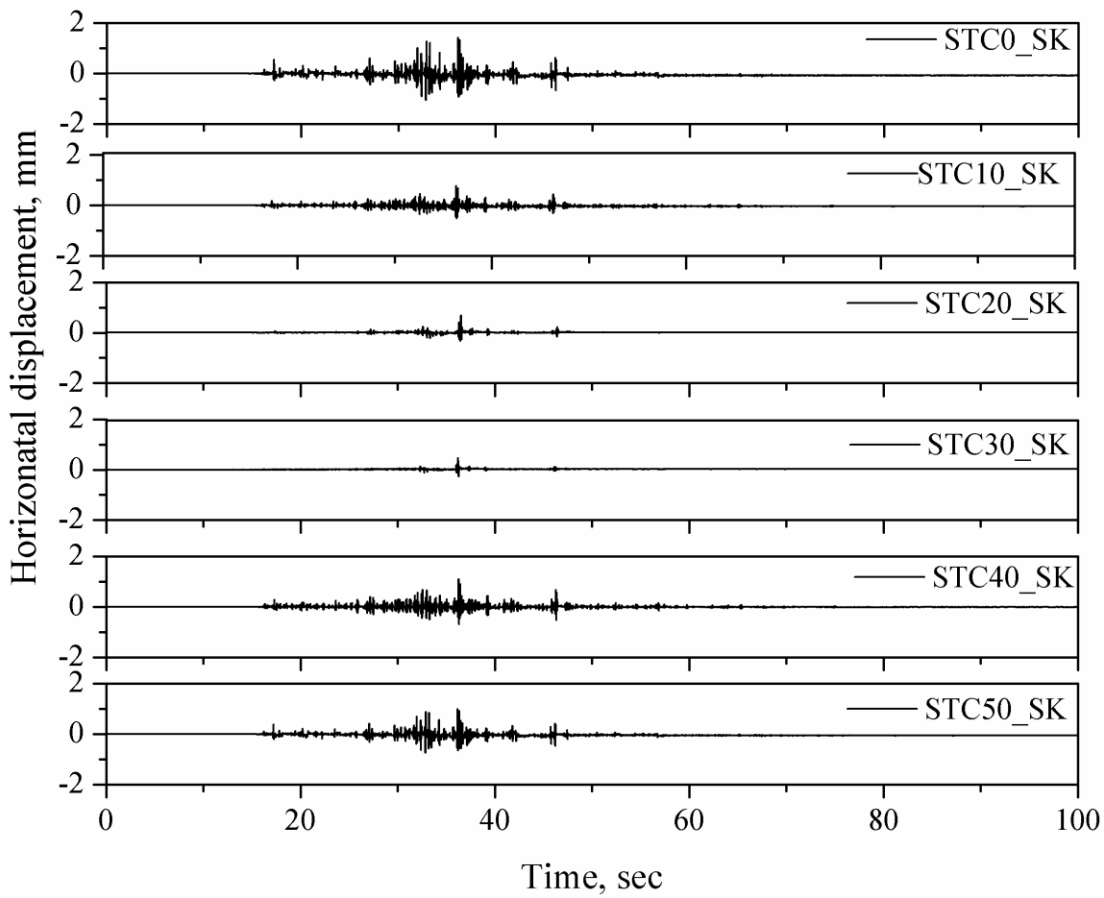

Fig. 4.33 Top displacement histories of wall models with different STC mixtures for SK EQ

Displacement profiles (after the excitation) of the model walls with different STC mixtures for TK EQ excitation are shown in Fig. 4.37. From the figure, maximum displacements are 2.43 mm for control test (STC0) and 1.90, 1.66, 0.94, 1.40, 1.93 mm for STC 10, STC 20, STC30, STC40 and STC 50 mixtures, respectively. The percentage reduction was calculated for all STC mixtures models and shown in Fig. 4.38. At STC30 mixture, the percentage reduction is about 60 % was found.

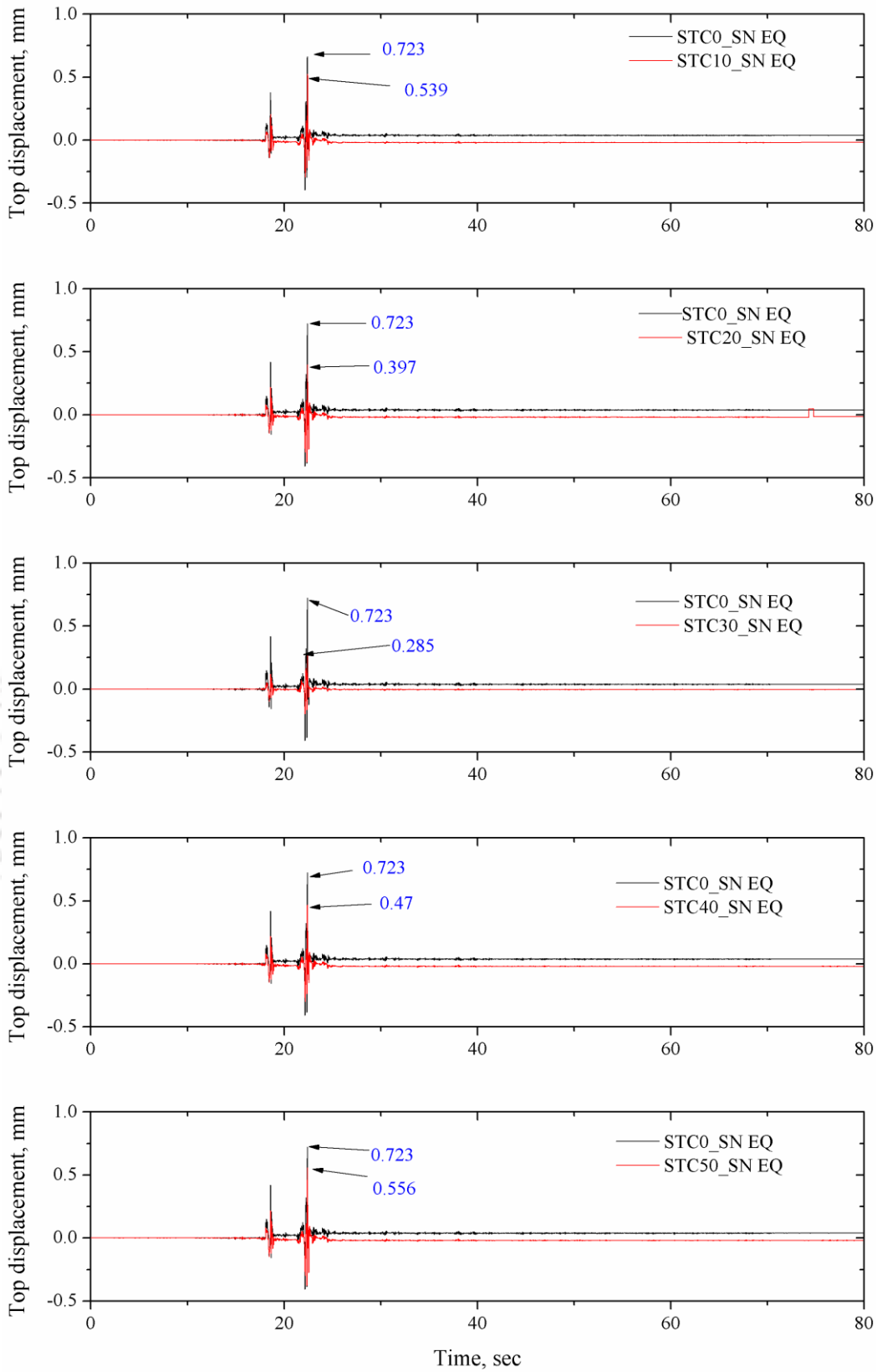

Fig. 4.34 Displacement responses at top of model walls with STC mixtures for SN EQ excitation

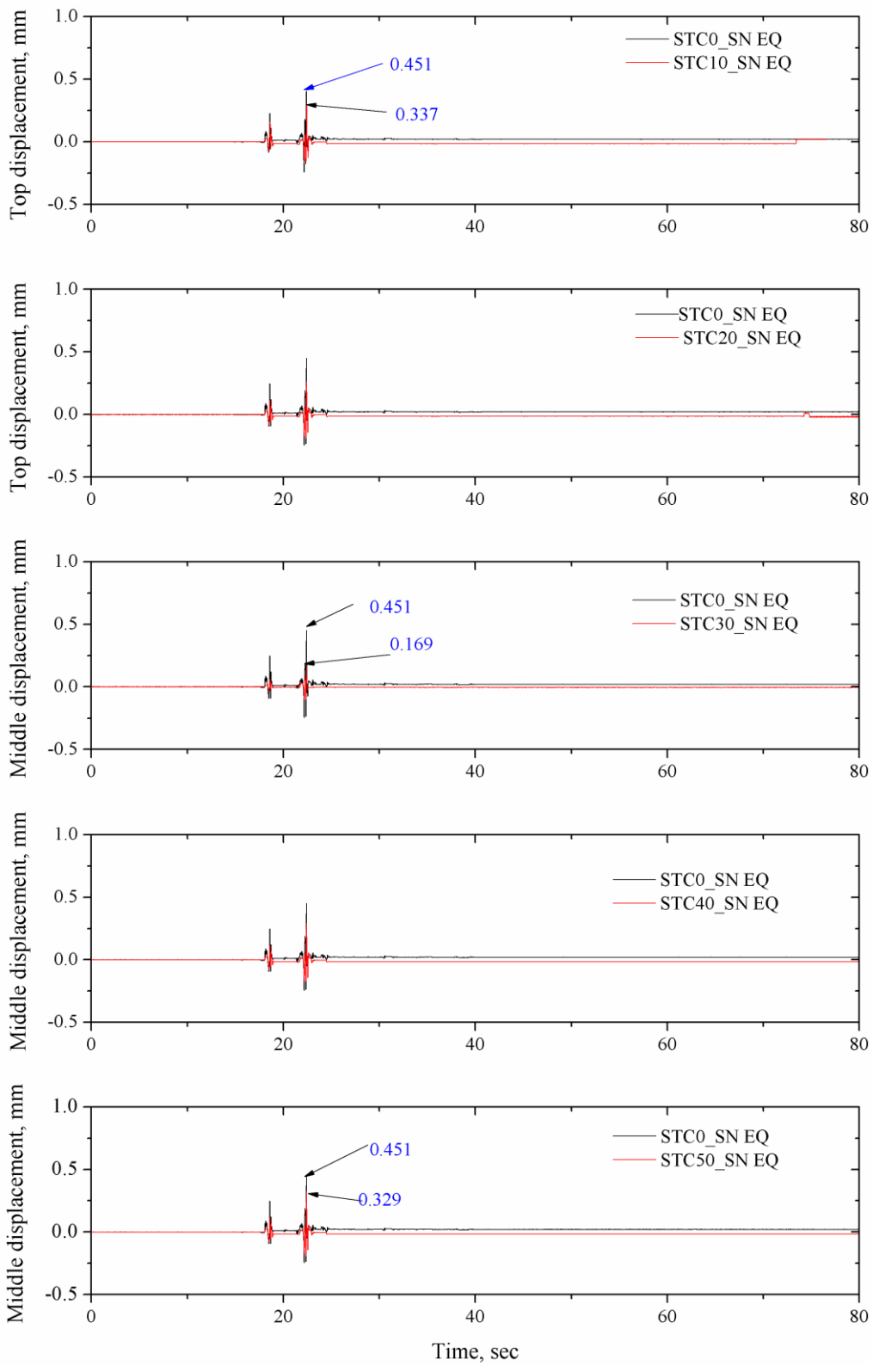

Fig. 4.35 Displacement responses at middle of the model walls with STC mixtures for SN EQ excitation

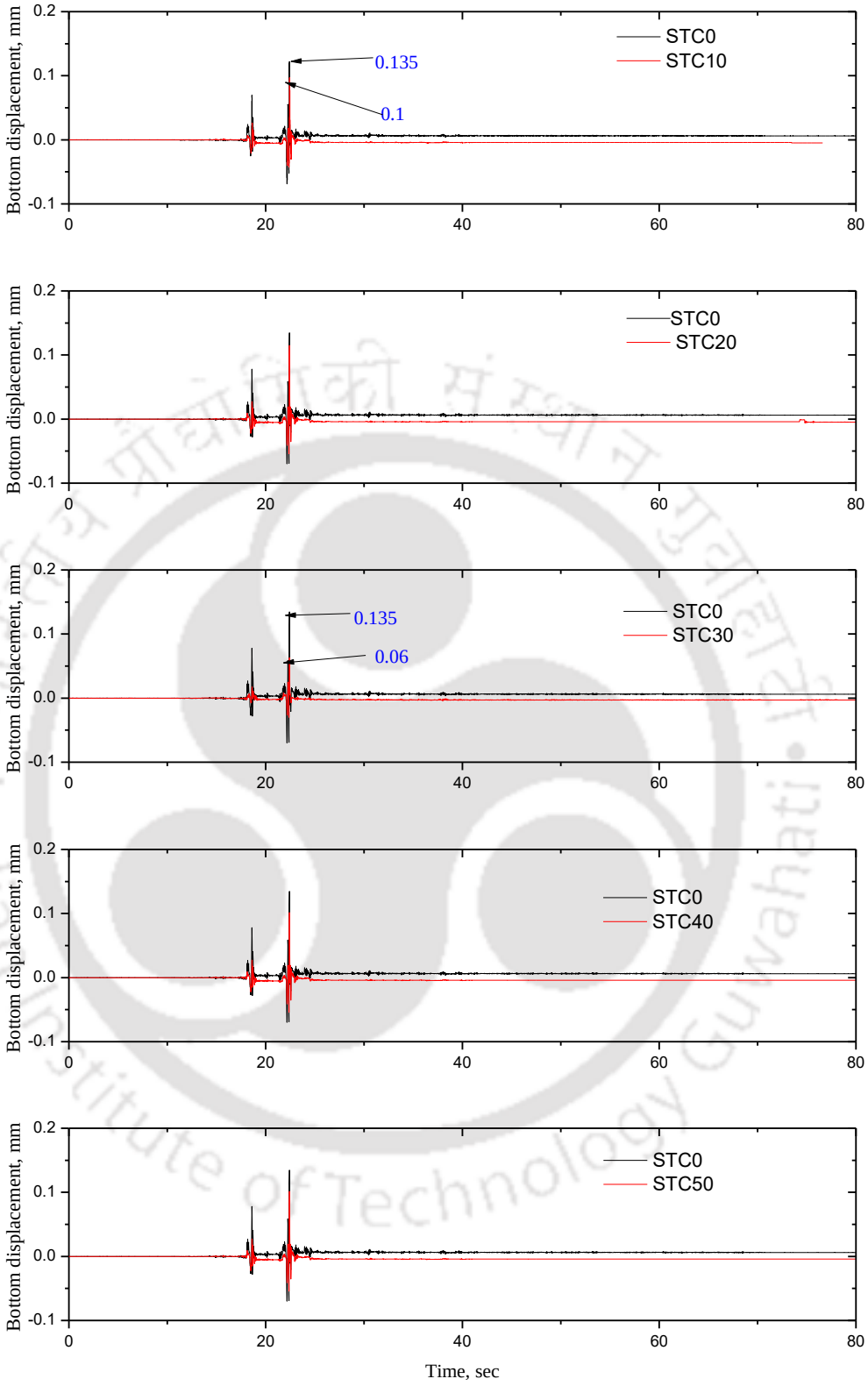

Fig. 4.36 Displacement responses at bottom of the model walls with STC mixtures for SN EQ excitations

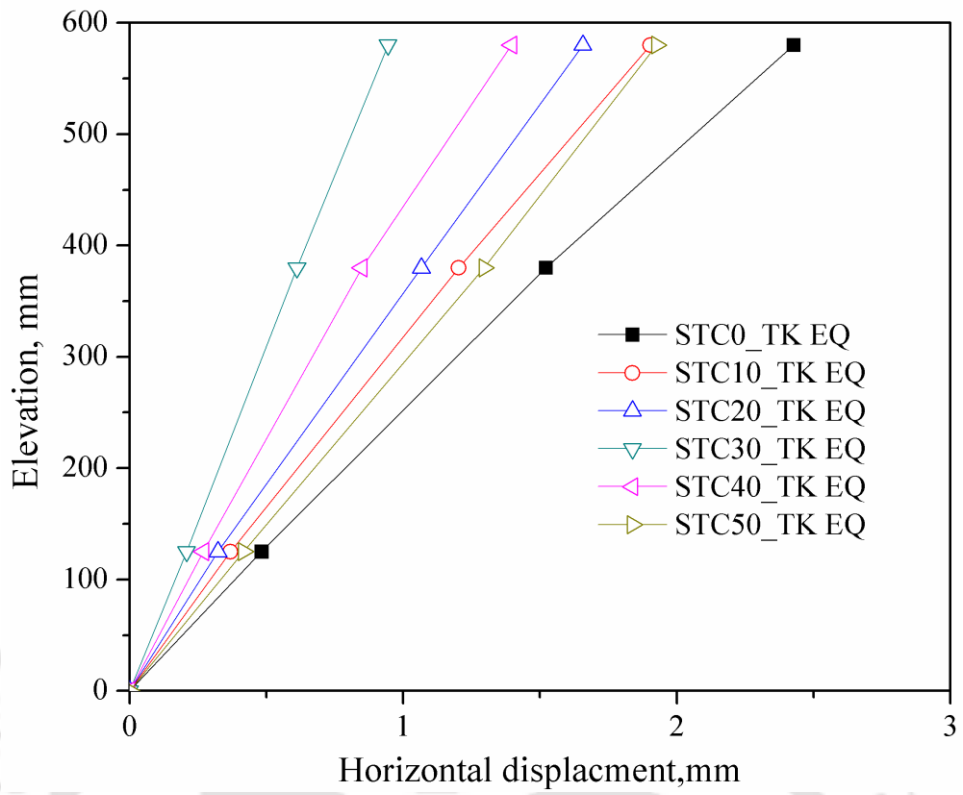

Fig. 4.37 Displacement profiles of TK EQ excitation of different STC mixtures

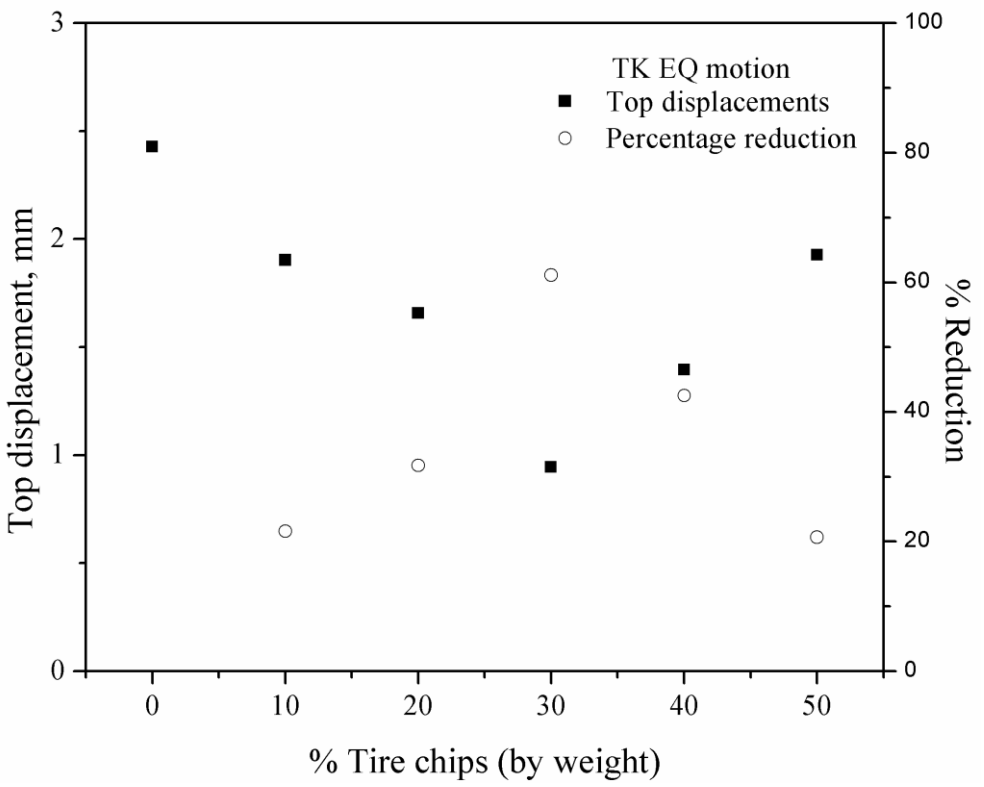

Fig. 4.38 Comparison of maximum displacement and its percentage reduction with STC mixtures for TK EQ excitation

Incremental lateral earth pressures

The histories of incremental lateral pressures, at 337 mm and 37 mm, from base during SK EQ excitation with different STC mixtures are shown in Fig. 4.39. The maximum incremental lateral pressures are 0.59 kPa for STC0, 0.09 kPa for STC30 and 0.11 kPa for STC50. At 37 mm elevation, maximum incremental lateral pressure is 0.87 kPa for STC0 and the minimum pressure is 0.13 kPa for STC30. Further, incremental earth pressure along the height of wall after the NZ EQ excitation, for different model walls are shown in Fig. 4.40.

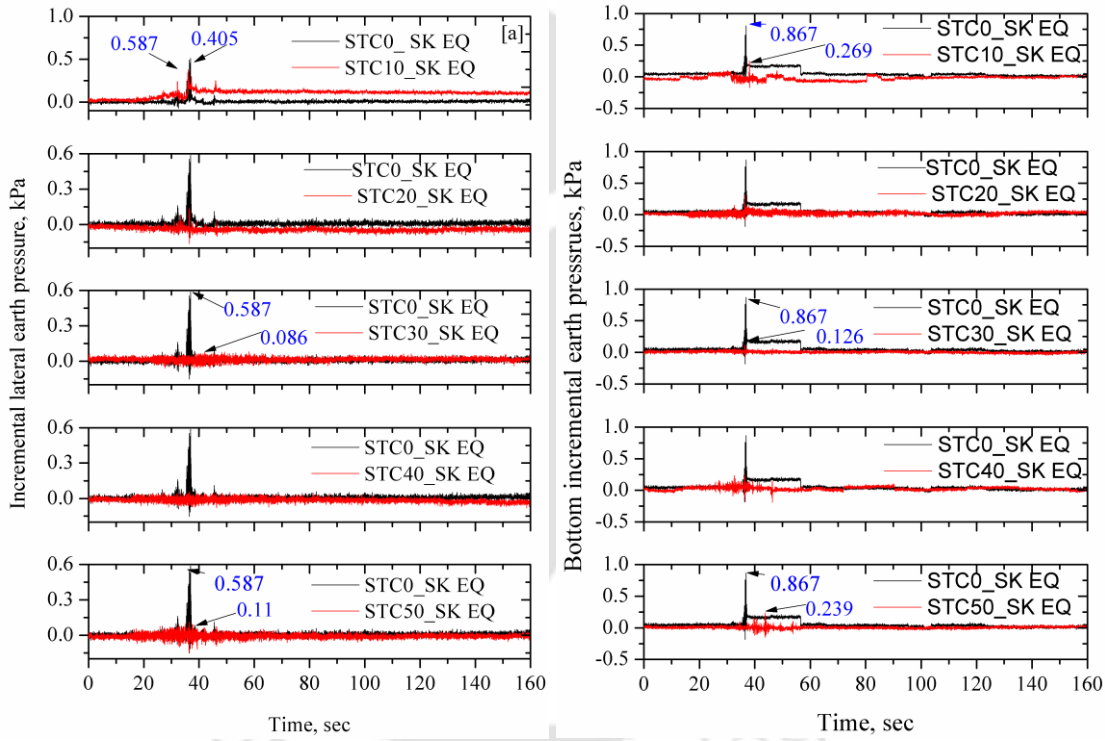

(a) at elevation of 337 mm (b) at elevation of 37 mm

Fig. 4.39 Dynamic incremental lateral earth pressure with time subjected to SK EQ excitation

Lateral earth pressures showed decreased trend when tire chips were present in the sand backfill. The maximum incremental earth pressures are noted at the bottom for different STC mixtures and its % reduction is shown in Fig. 4.41 for NZ EQ excitation.

From the figure, it was found that using STC30 mixtures, earth pressure was reduced by nearly 75 % when compared to control test (STC0 backfill).

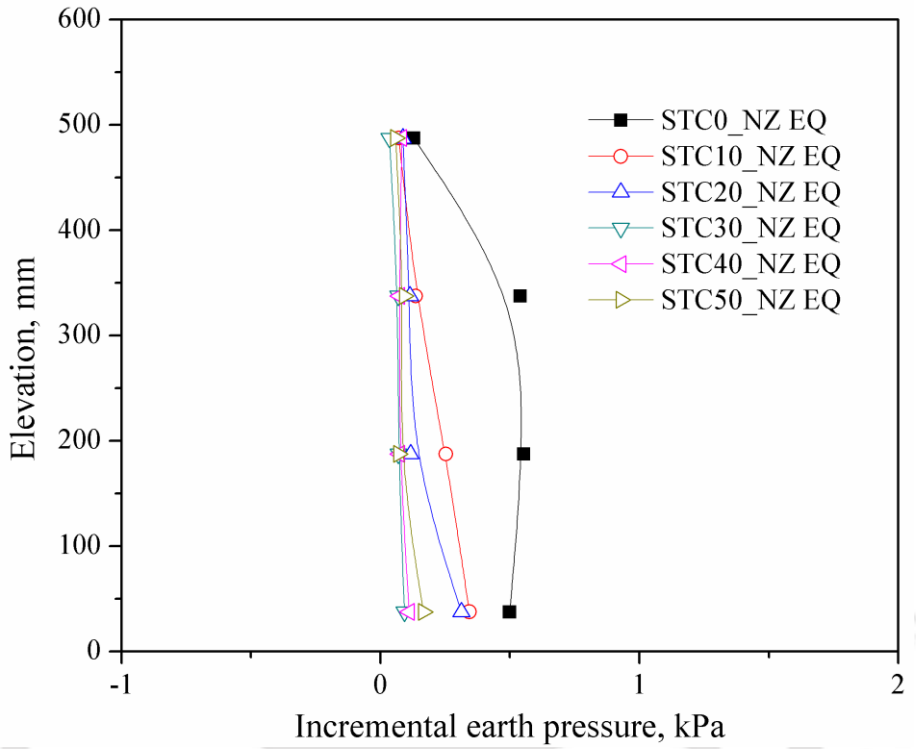

Fig. 4.40 Incremental lateral earth pressures with different backfill materials subjected NZ EQ excitation

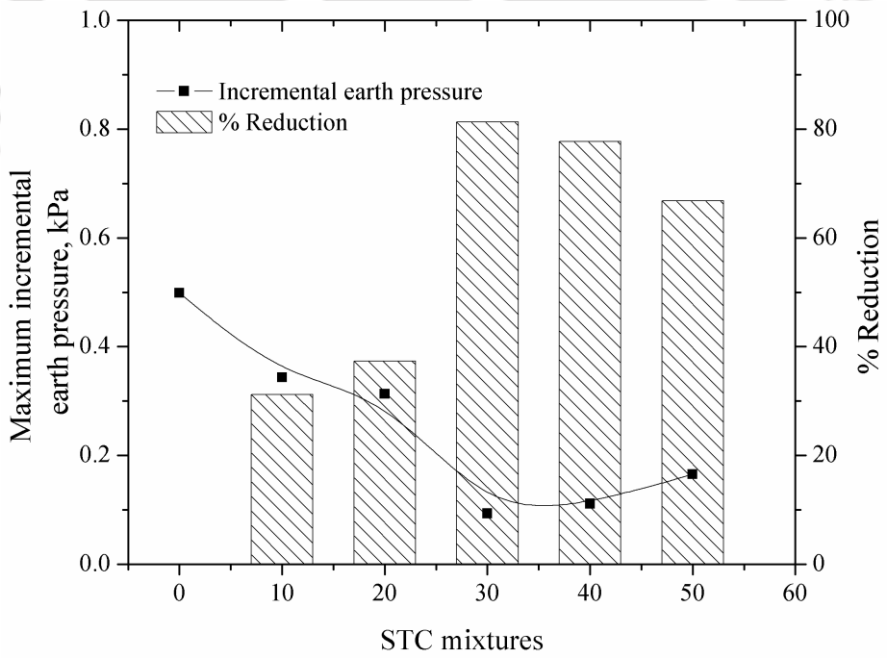

Fig. 4.41 Incremental lateral earth pressures and its percentage reduction at bottom for NZ EQ excitation

Acceleration amplification factor

Fig. 4.42 presents the acceleration amplification factors of the model walls backfilled with different STC mixtures that were subjected to South Napa (SN) earthquake excitation. The figure provides the comparison of amplification factor profiles along the height of the wall with same configuration but constructed to different STC mixture backfills and subjected to similar base excitation (SN EQ). From the figure, it is observed that the accelerations are amplified more at the top of the wall in almost all the cases. Further, accelerations are less amplified when using STC mixture in place of pure sand.

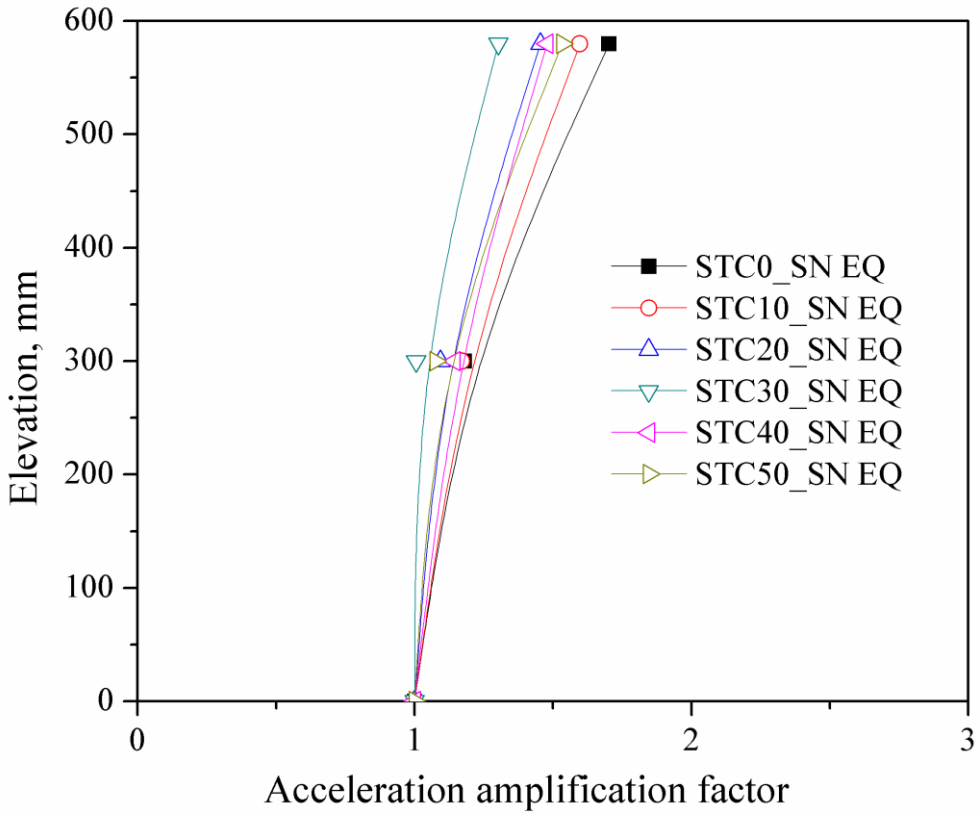

Fig. 4.42 Effect of STC mixtures on acceleration amplification of model wall subjected to SN EQ excitation

Fig. 4.43 to Fig. 4.46 show the variation of horizontal displacements, incremental earth pressures, and acceleration amplification factors along the height of

the wall for the SN, SK, NZ, and TK Earthquake excitations for all the STC mixture models. As seen from the figures, a significant reduction of earth pressures and displacements were observed in all earthquake excitations with increase in tire chips contents by weight. Further, maximum displacements with different STC mixtures and its % reductions are reported in Table 4.10. From the table, it is concluded that the displacements are reduced by 68%. Maximum reductions of displacements were observed at STC30 mixture in all earthquake excitations. At STC30 mixture ratio, shear strength properties were increased and specific gravity is less as compare to pure sand. Another important point was observed is that at STC30 mixture, the void ratio is less as compared to pure sand. Where tire chips are mixed with sand, there is a decrease in acceleration amplification factor is clearly observed.

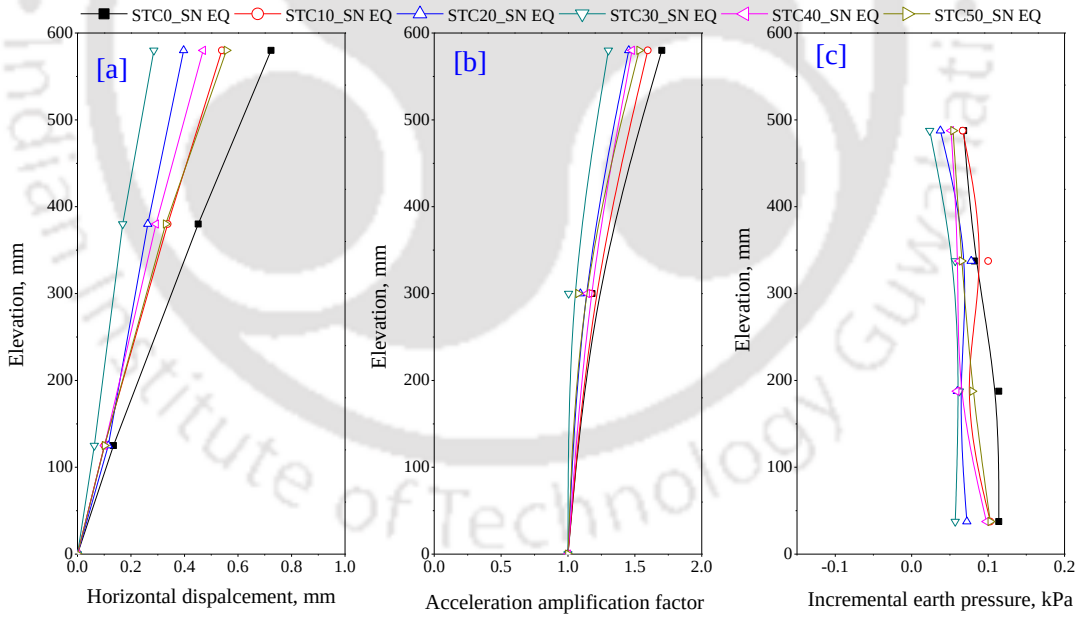

Fig. 4.43 Response of model wall using STC mixtures for SN Earthquake excitation: a) Displacement profile; b) Acceleration amplification and c) Incremental earth pressures

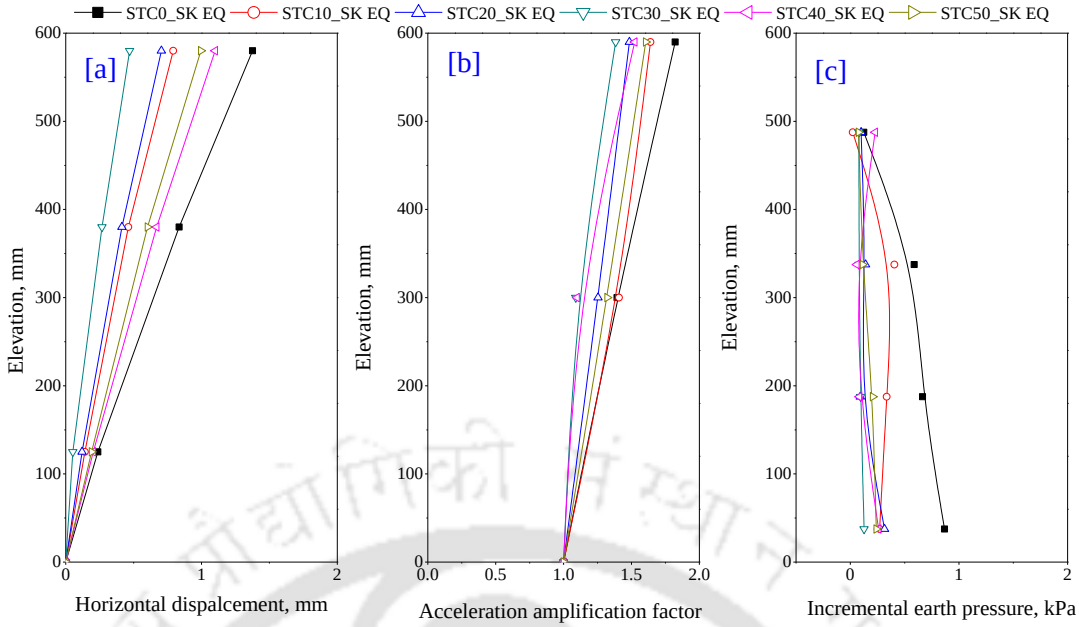

Fig. 4.44 Response of model wall using STC mixtures for SK Earthquake excitation: a) Displacement profile; b) Acceleration amplification and c) Incremental earth pressures

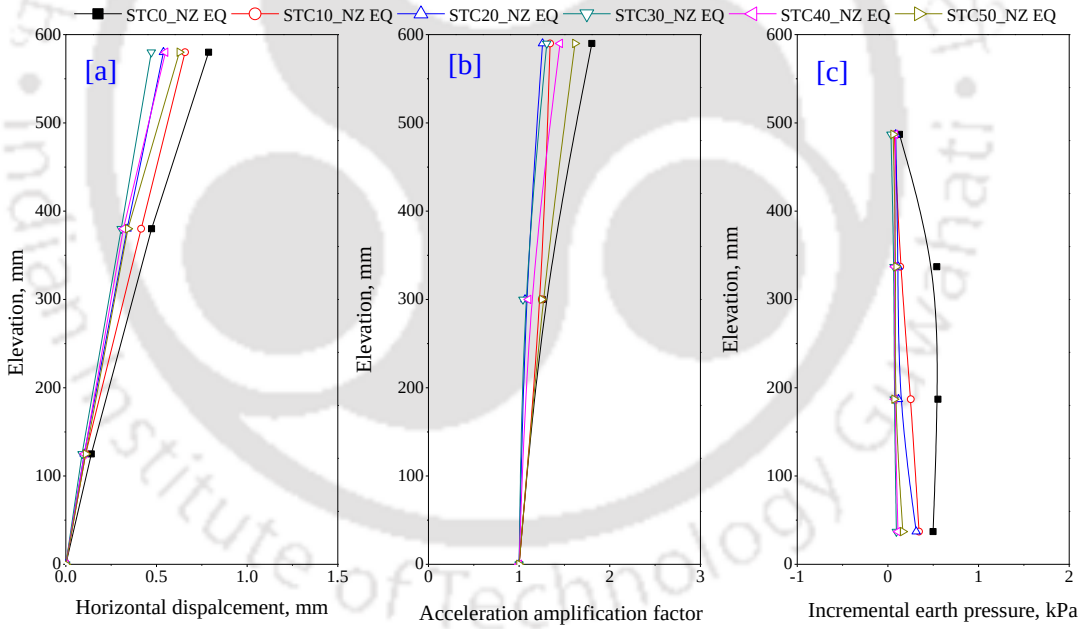

Fig. 4.45 Response of model wall using STC mixtures for NZ Earthquake excitation: a) Displacement profile; b) Acceleration amplification and c) Incremental earth pressures

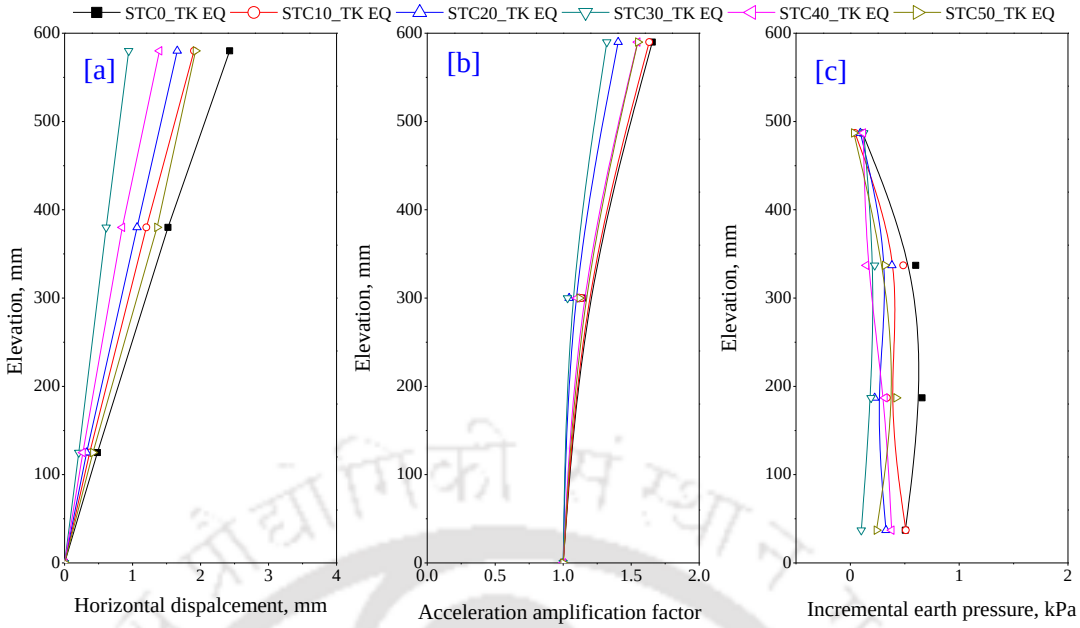

Fig. 4.46 Response of model wall using STC mixtures for TK Earthquake excitation: a) Displacement profile; b) Acceleration amplification and c) Incremental earth pressures

Table 4.10 Maximum displacements and percentage reduction with different earthquake excitations

Mixture Proportions	Maximum displacements				% Reduction			
	SN	NZ	SK	TK	SN	NZ	SK	TK
STC0	0.72	0.79	1.37	2.43	-	-	-	-
STC10	0.54	0.66	0.79	1.90	25.38	19.69	42.45	21.60
STC20	0.397	0.54	0.70	1.65	45.13	46.29	48.82	31.75
STC30	0.286	0.47	0.47	0.94	60.52	68.08	65.77	61.11
STC40	0.47	0.55	1.10	1.39	35.05	43.64	20.04	42.51
STC50	0.55	0.63	0.99	1.93	23.02	25.35	27.69	20.65

4.6 SUMMARY

Retaining wall models were tested under static and dynamic loading conditions. From the different series of model tests presented herein, the flowing conclusions are drawn.

- Displacements and lateral earth pressures are decreasing with increasing STC mixture up to 30%.

- Experimental lateral earth pressures reasonably matching with analytic solution results under static loading conditions.
- Displacements and incremental lateral earth pressures are low for STC mixtures backfilled walls compared to the control case with sand alone.
- The acceleration amplifications were decreased with the increasing of STC mixtures up to STC30 mixture.
- Using STC30 mixture, displacements were reduced by up to 65%.
- Dynamic excitation induced pressures were reduced by up to 80% compared with the control test (STC0) model wall.

Based on all the above observations, shredded tire chips mixed with sand can be effective backfill material for retaining wall structures for seismic prone regions.

Chapter 5. RETAINING WALL MODELS WITH TIRE CHIPS INCLUSIONS

5.1 INTRODUCTION

In this chapter, physical model tests conducted on retaining wall with compressible inclusions are discussed. Recycled tire chips (Section 3.2.2) were used as the compressible inclusion material in these tests. Testing program has been devised to study the effects of different parameters on the static and dynamic performance of the wall models. The parameters studied include the thickness of compressible inclusion (t), surcharge pressure, dynamic excitation parameters (acceleration and frequency), and different scaled earthquake excitations. The following sections discuss the effect of each of these parameters on the static and seismic response of the wall models in terms of horizontal face displacements, lateral earth pressures, and acceleration amplifications to bring out the effectiveness of tire chips as compressible inclusions.

5.2 TESTING PROGRAMME

In static case, three model tests (TC0–TC180) were conducted on retaining wall models with pure sand (control case) and two compressible inclusion thickness (90 mm and 180 mm) as shown in Table 5.1. Static loading was applied up to 10 kPa, as discussed in Chapter 3. In seismic case, the retaining wall models have been tested with different sinusoidal excitations and irregular earthquake excitations using 1-g shaking table. The details about the test conditions for sinusoidal excitations are shown in Table 5.2. Retaining wall models were also tested by applying four irregular earthquake excitations with different frequency contents with different magnitudes. More details

about the irregular earthquake excitations were discussed in Chapter 4. The details about the test conditions using irregular earthquake excitations are shown in Table 5.3.

Table 5.1 Test parameters for static case

Test code	**Compressible inclusion thickness (*t*), mm**	***t/H***	**Surcharge, kPa**
TC0	0	0	0 to 10 kPa
TC90	90	0.15	
TC180	180	0.3	

Table 5.2 Details about test conditions using sinusoidal excitations

Test code	**Compressible inclusion thickness (*t*) (mm)**	***t/H***	**Acceleration (*a*) *g***	**Frequency (*f*) Hz**
TC0_0.1_3	0	0	0.1	3
TC90_0.1_3	90	0.15		
TC180_0.1_3	180	0.3		
TC0_0.2_3	0	0	0.2	3
TC90_0.2_3	90	0.15		
TC180_0.2_3	180	0.3		
TC0_0.3_3	0	0	0.3	3
TC90_0.3_3	90	0.15		
TC180_0.3_3	180	0.3		
TC30_0.3_5	0	0	0.3	5
TC90_0.3_5	90	0.15		
TC180_0.3_5	180	0.3		

The model walls have been instrumented with earth pressure sensors, displacement transducers and accelerometers, at different elevations to monitor the retaining wall model response as discussed in the Chapter 3. Results are discussed in terms of displacements, incremental earth pressures, amplification factors at different elevations.

Table 5.3 Details about test conditions using irregular earthquake excitations

Test code	Compressible inclusion thickness (t) (mm)	*t/H*	Earthquake excitation
TC0_SN EQ	0	0	South Napa
TC0_SK EQ			Sikkim
TC0_NZ EQ			New Zealand
TC0_TK EQ			Tohoku
TC90_SN EQ	90	0.15	South Napa
TC90_SK EQ			Sikkim
TC90_NZ EQ			New Zealand
TC90_TK EQ			Tohoku
TC180_SN EQ	180	0.30	South Napa
TC180_SK EQ			Sikkim
TC180_NZ EQ			New Zealand
TC180_TK EQ			Tohoku

5.3 STATIC RESPONSE OF RETAINING WALL MODELS

5.3.1 Wall horizontal displacements

The retaining wall model was built with pure sand (control case) and with compressible inclusion of two t/H ratios (0.15 and 0.30). Horizontal wall displacements along the height of the wall were monitored using three LVDTs positioned as shown in Fig. 3.21. The horizontal wall displacements measured after the support removal (without surcharge loading) are shown in Fig. 5.1, which depict the variation of horizontal displacements along the height of wall for all the model tests. Maximum wall displacement is observed to be about 1.75 mm in TC0 test. Among different tests, test TC90 and TC180 showed top displacement as 1.55 mm and 1.43 mm. Percentage reduction of displacements is calculated by using top displacements. Variations of the top displacement and its percentage reduction with reference to the control case with t/H ratios are shown in Fig. 5.2. It is revealed that about 20% reductions in top displacements as compared to control case (pure sand).

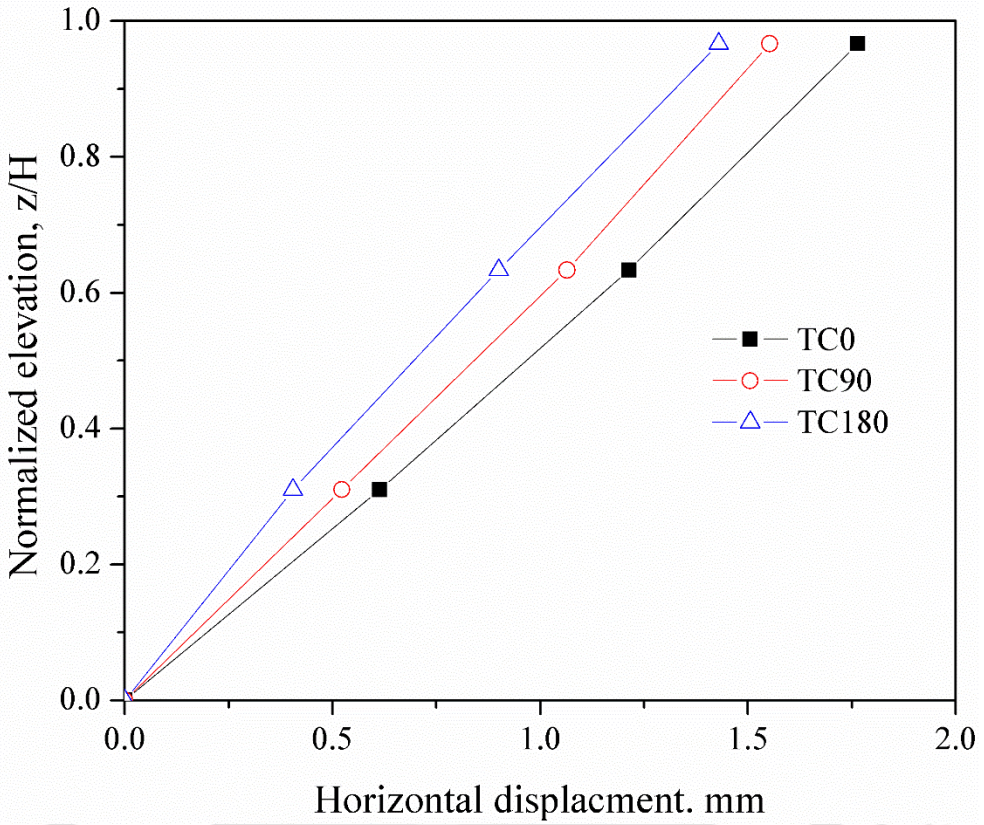

Fig. 5.1 Horizontal displacement of model wall with compressible inclusion thickness

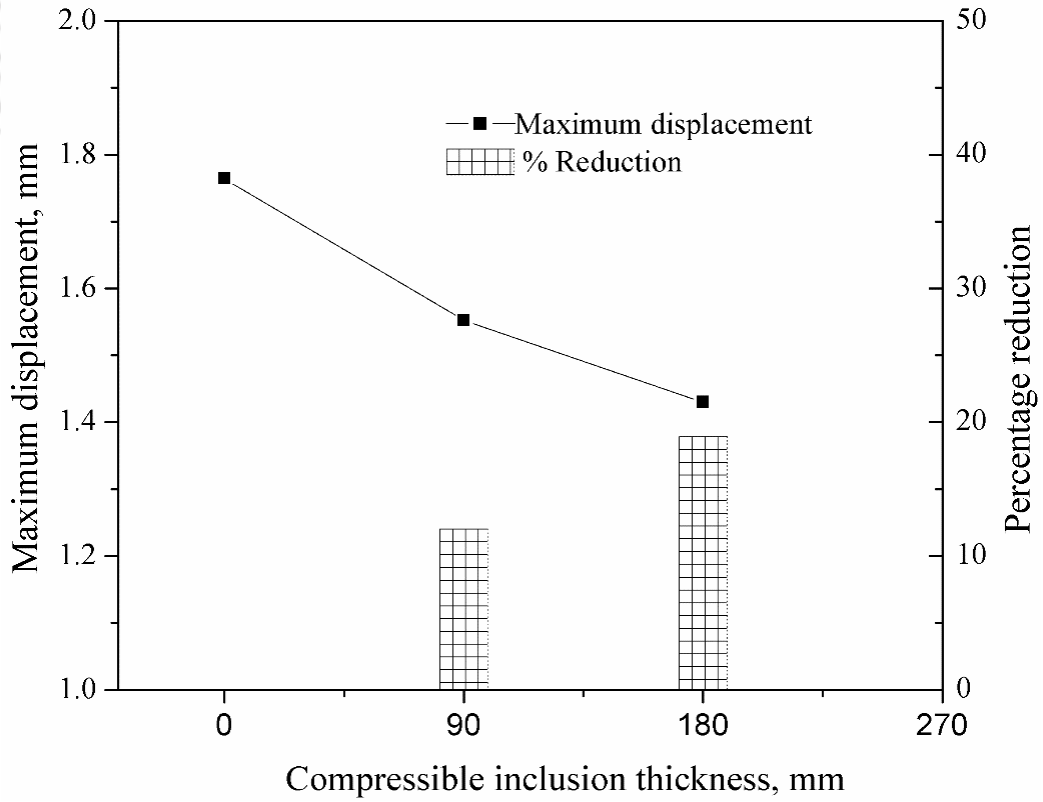

Fig. 5.2 Top displacements and its percentage reduction with compressible inclusion

Fig. 5.3 presents the displacement responses of model walls along the height under 10 kPa surcharge pressure. Maximum displacements at the top of the walls at 10 kPa surcharge are noted as 6 mm, 5.3 mm and 4.9 mm for t/H=0, t/H=0.15, t/H=0.30, respectively. The top displacements of wall at different surcharge loading conditions in different tests with different t/H ratios are presented in Fig. 5.4. It is seen from the figure that the top displacements are increased with increasing surcharge pressures in all tests. The figure also depicts the fact that at all surcharge loading conditions the lowest displacements are shown for t/H =0.3 and highest for the control case with t/H=0 backfill. Displacements in the range of 3.5–6 mm for t/H=0 are recorded for surcharge variation from 1 to 10 kPa. Fig. 5.5 presents the variation of wall top displacement under 10kPa surcharge with different t/H ratios and percentage reduction. The percentage reduction in settlement is about 25 % for t/H=0.3. Referring to Fig. 5.1 to Fig. 5.5, it can be stated that wall displacements are reduced up to 25 % by using tire chips as compressible inclusion just behind the retaining wall.

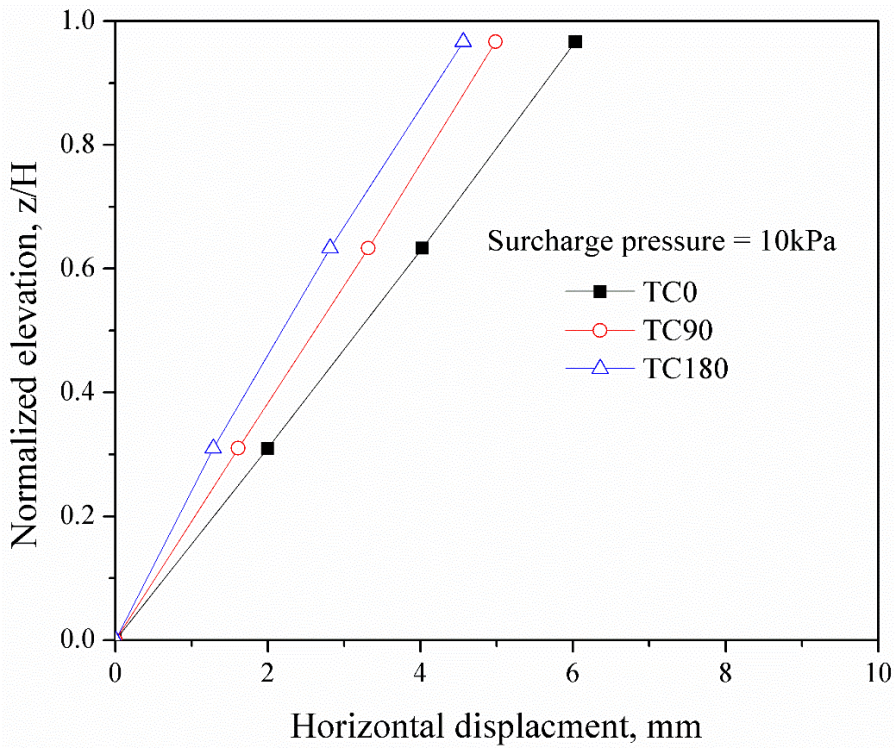

Fig. 5.3 Horizontal displacement of model wall with compressible inclusion thickness

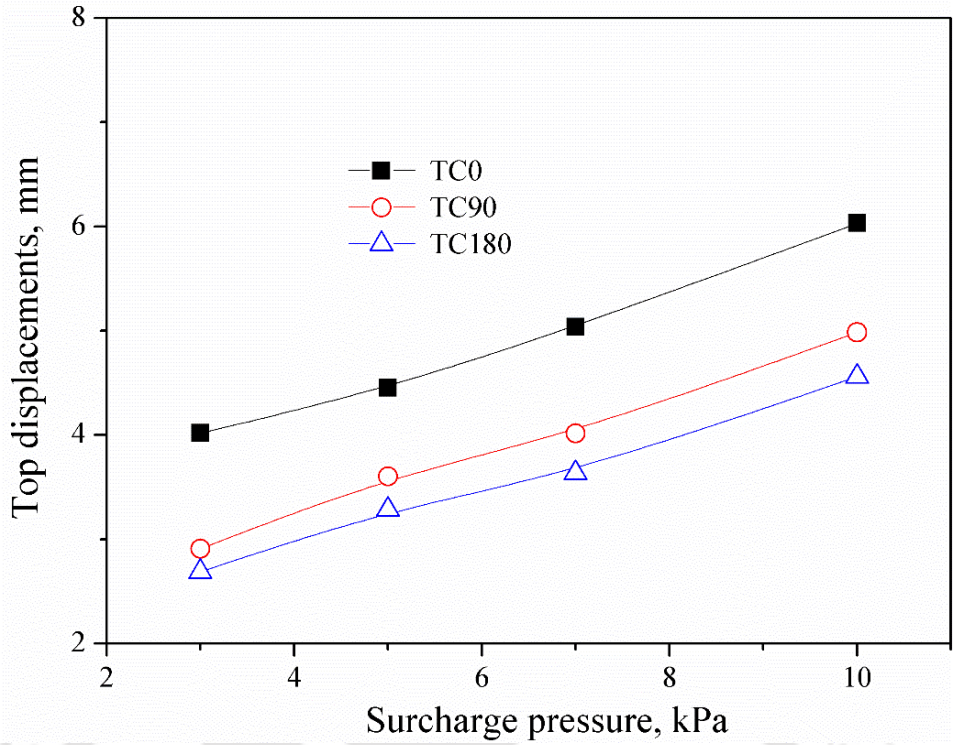

Fig. 5.4 Effect of surcharge pressure on top displacements of model wall with different compressible inclusion thickness (*t*)

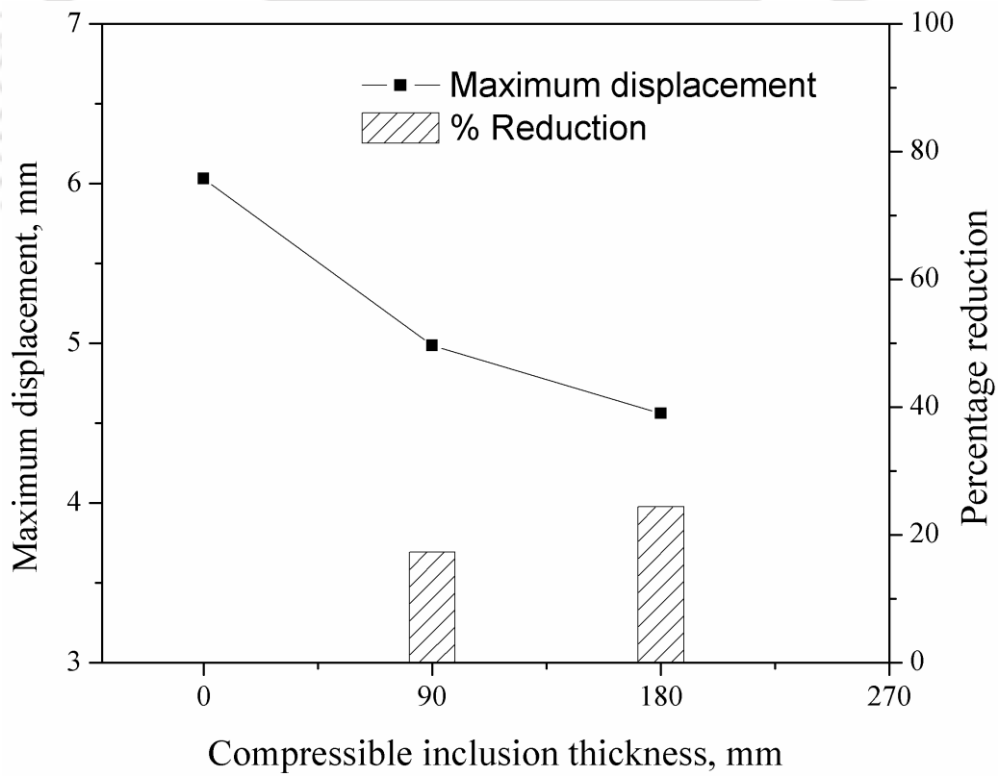

Fig. 5.5 Top displacements of model wall and its percentage reduction under 10 kPa with different thickness (*t*/*H*)

5.3.2 Lateral earth pressure on wall models

Lateral earth pressures were monitored after support removal using four-earth pressure sensors were placed at different elevations on the retaining wall. Fig. 5.6 shows the lateral earth pressure responses for all the model walls with different *t*/*H* ratios. The figures indicate that lateral pressures fall in the range of 0 – 2 kPa. Though there is no consistent trend in relative variations of pressures for different model walls, it can be observed that the pressures after support removal condition are low. Further it can also be seen that the earth pressures were affected by the *t*/*H* ratio giving lowest earth pressure for *t*/*H*=0.3 model wall (TC180). Percentage of reduction is calculated using measured lateral earth pressures at elevation of 187 mm from base for all the three tests. Percentage reduction with reference to the control case and with tire chips inclusions are presented in Fig. 5.7. It is revealed that 60% reduction in earth pressure as compared to control case (TC0).

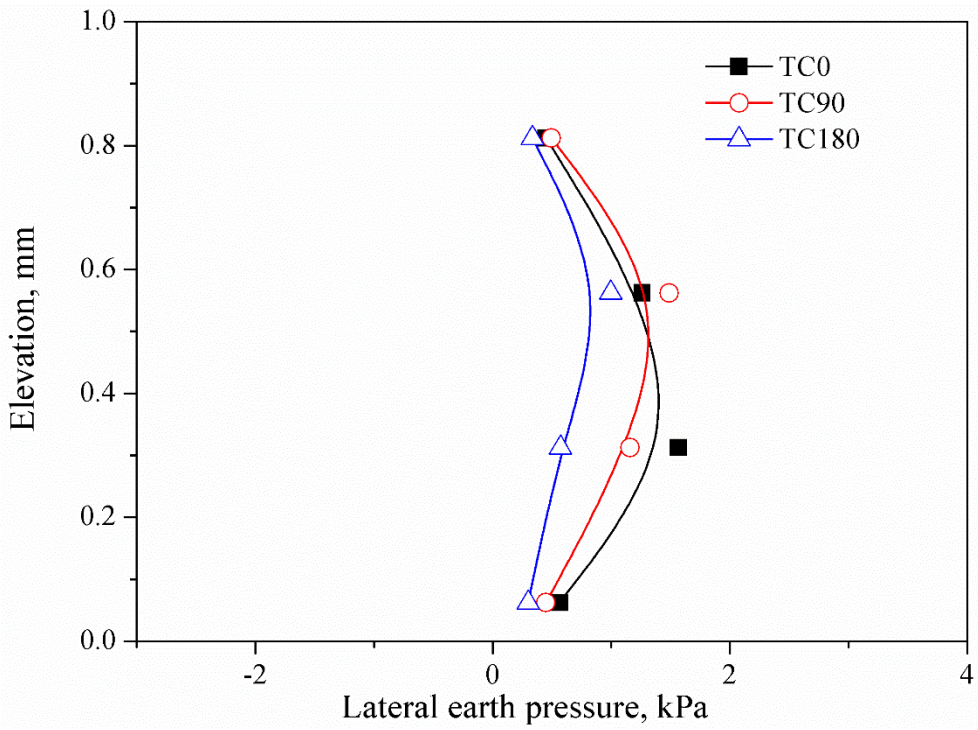

Fig. 5.6 Lateral earth pressure profile with different compressible inclusions

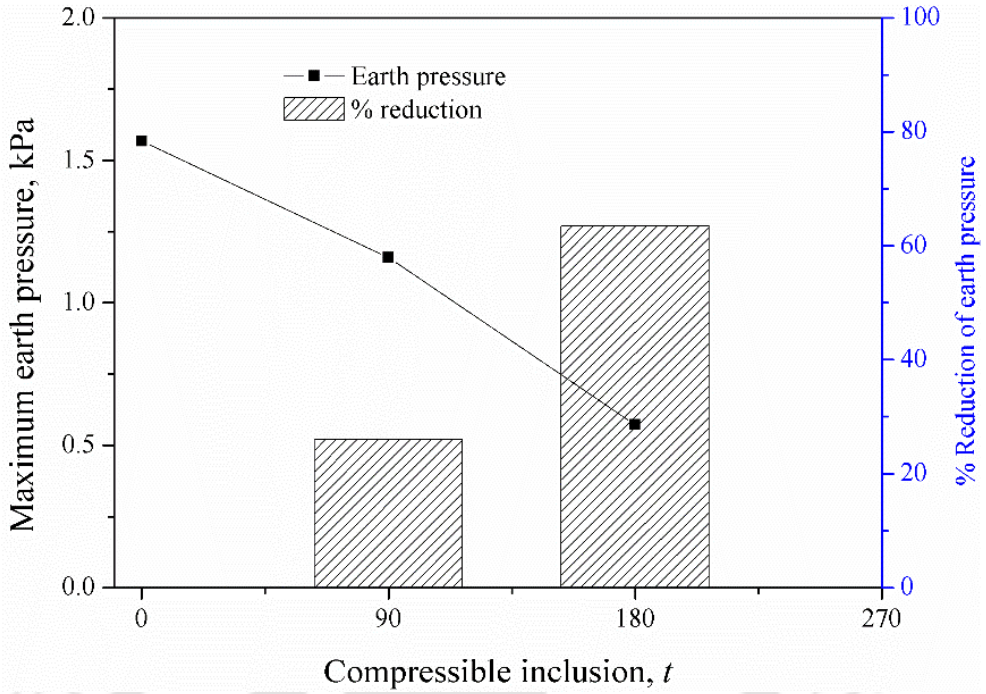

Fig. 5.7 Percentage reduction of lateral earth pressure

Fig. 5.8 (a and b) presents the lateral earth pressures of model walls along the height with different surcharge pressures for t/H=0.15, and t/H=0.3. It is observed that, lateral earth pressures are higher for both the model walls for higher surcharge pressures. Fig. 5.8 (c) shows the comparison of lateral earth pressures along height of the wall model with different t/H ratios, under 10 kPa. The maximum earth pressures on wall at different surcharge pressures in different tests (different t/H) and its percentage reduction are presented in Fig. 5.9. The figure depicts the fact that at all surcharge loading conditions, the lowest earth pressures are shown for t/H =0.3 and highest for the control case with t/H=0 backfill. Lateral earth pressures, in the range of 3.5–6 kPa for t/H=0, are recorded for surcharge variation from 1 to 10 kPa. The corresponding earth pressures variations for t/H=0.15 are in the range of 0.5–1.1 kPa. The percentage reduction in earth pressure is about 60 % for t/H=0.3. Referring to the Fig. 5.6 to Fig. 5.9, it can be stated that wall displacements are reduced significantly (up to about 60 %) by vertically inclusion of tire chips just behind the soil retaining wall models.

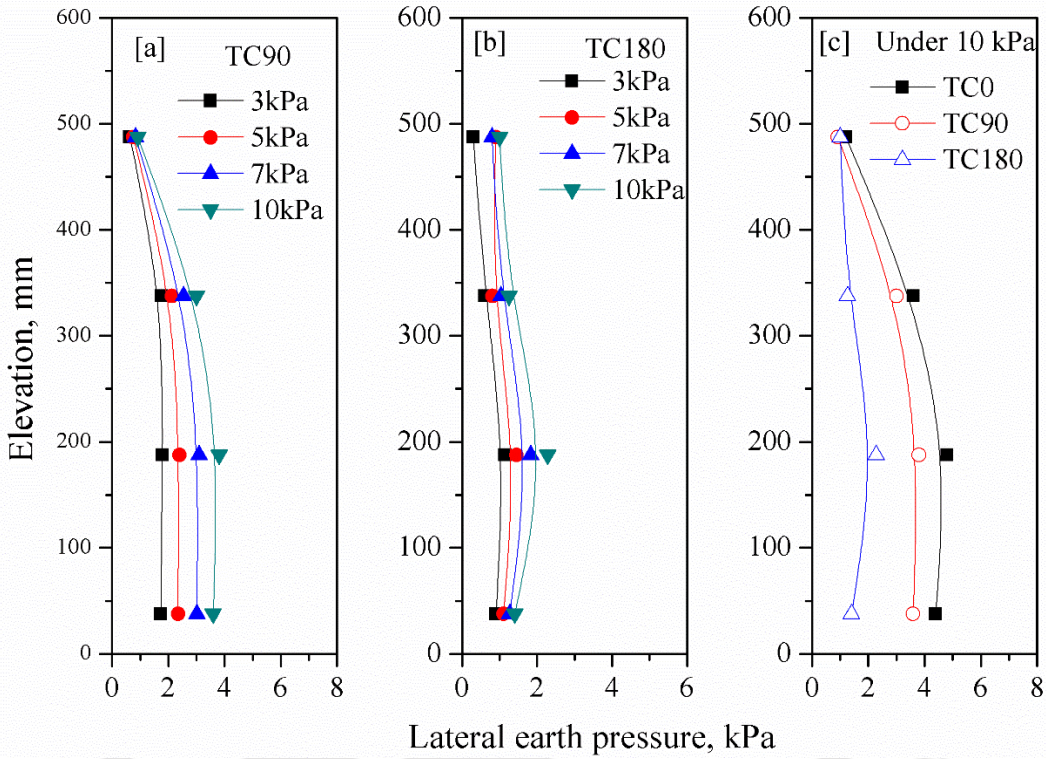

Fig. 5.8 Effect of compressible inclusion on lateral earth pressures

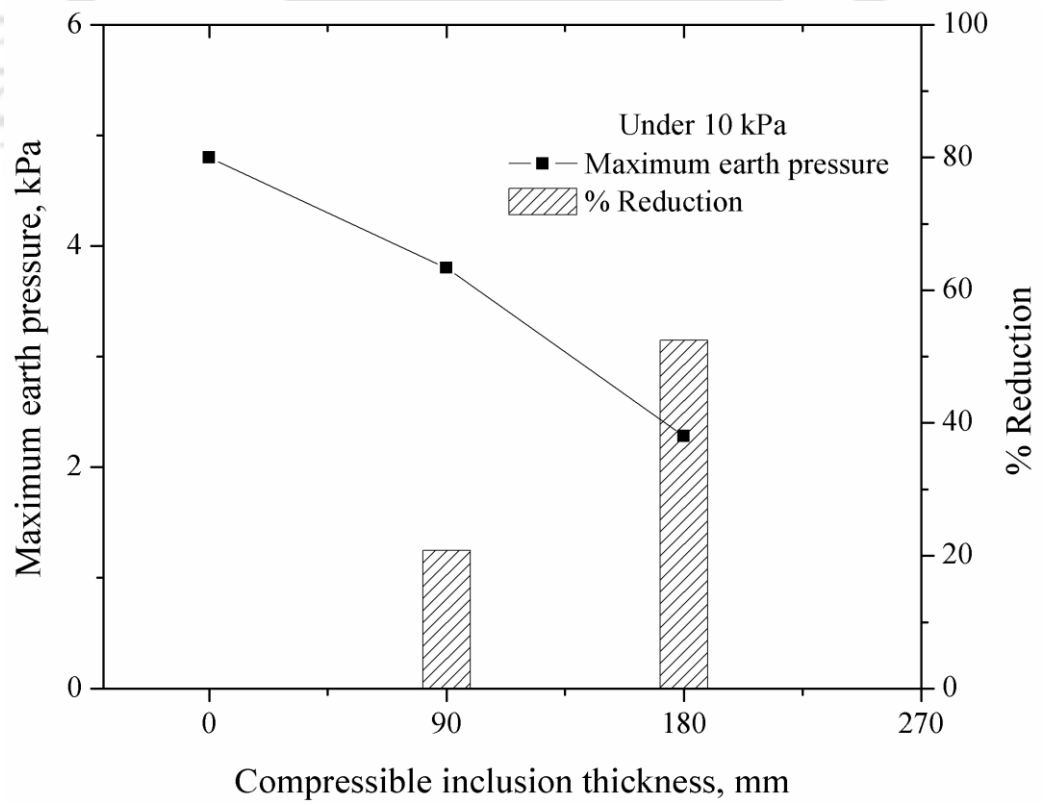

Fig. 5.9 Effect of surcharge pressure on lateral earth pressures

5.4 MODEL WALL RESPONSE SUBJECTED TO SINUSOIDAL EXCITATIONS

The effect of compressible inclusions on dynamic response of model wall is examined by applying different input base excitations. Variations of horizontal displacements at different elevations of the wall with increasing number of dynamic loading cycles are shown in Fig. 5.10, for the test TC90_0.3_3. The figure shows the nonlinearly increasing trend of displacements with increase in number of cycles. Further, higher displacements at higher elevations are observed. Wall displacements of 2.53, 1.58, and 0.46 mm are seen from the figure, at 580, 380, and 125 mm elevations, respectively.

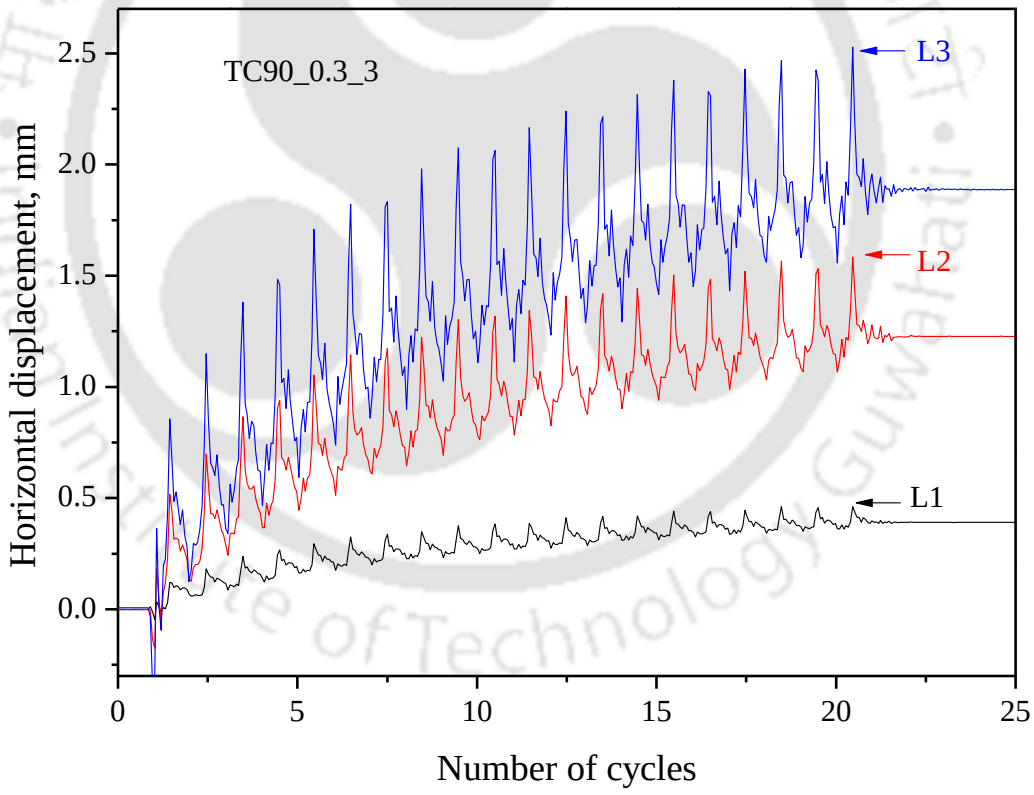

Fig. 5.10 Typical displacement histories at different elevations for the test TC90_0.3_3

Typical accelerations with number of cycles, at different elevations for the model test TC90_0.3_3, is shown in Fig. 5.11. It is observed that the accelerations were amplified at top elevations. Acceleration amplification factors at location A2 and A3 were found to be 1.49 and 1.86, respectively.

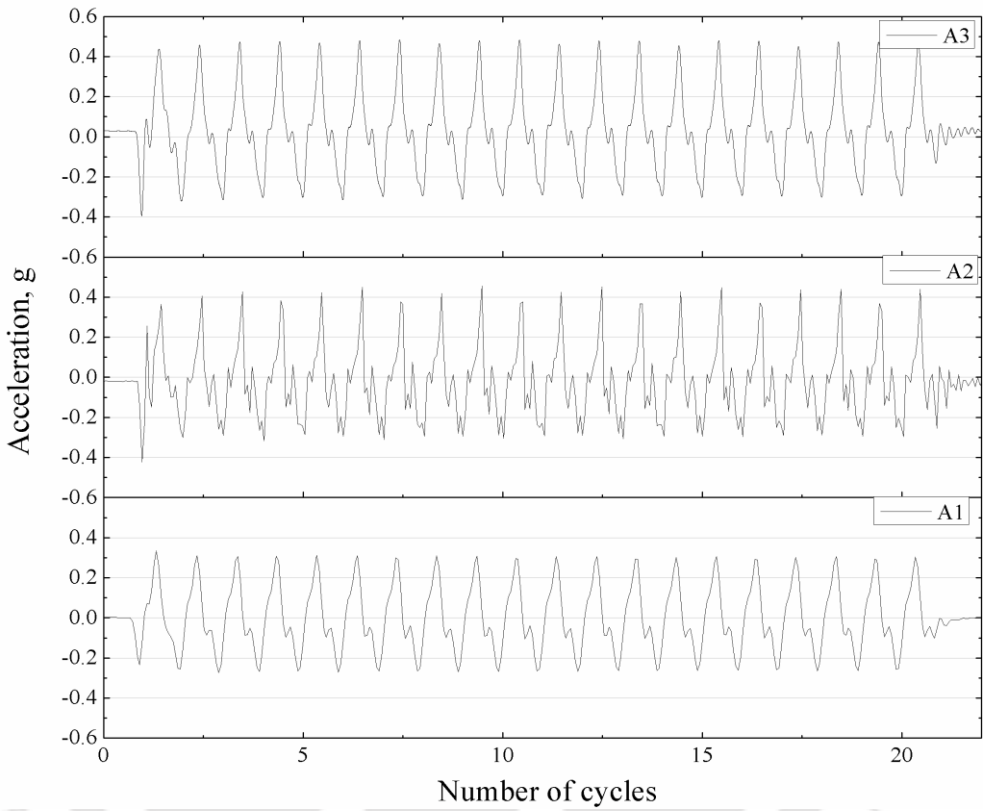

Fig. 5.11 Typical acceleration histories at different elevations for the test TC90_0.3_3

Variation of incremental lateral earth pressures at different elevations of the wall with increasing number of dynamic loading cycles is shown in Fig. 5.12, for the test TC90_0.3_3. The figure shows the increasing trend of lateral earth pressures with increase in the number of cycles. Further, higher lateral earth pressures are observed at the bottom of the model wall. Dynamic incremental earth pressures of 0.38 kPa, 0.42 kPa, 0.41 kPa and 0.08 kPa are seen from the figure, at 487.5, 337.5, 187.5 and 37.5 mm elevations, respectively.

Model wall responses with different compressible inclusion thickness are compared with that of the controlled case model wall at identical excitation levels. Fig. 5.13 shows the effect of compressible inclusion on model wall displacements along the height of wall (a = 0.1g and f = 3 Hz). It is observed, from the figure, that the displacements significantly decrease with the increasing compressible inclusion thickness. The maximum displacement of 0·61 mm for the test TC0_0·1_3 is reduced to 0·324 and 0·195 mm, for the tests TC90_0·1_3 and TC180_0·1_0·3, respectively. When recycled tire chips were used to partially replace the soil backfill, due to the lightweight and compressible nature of the tire chips, the soil thrust on the wall was reduced and thereby the wall displacements were reduced. This absorbance characteristic may also be treated as additional damping.

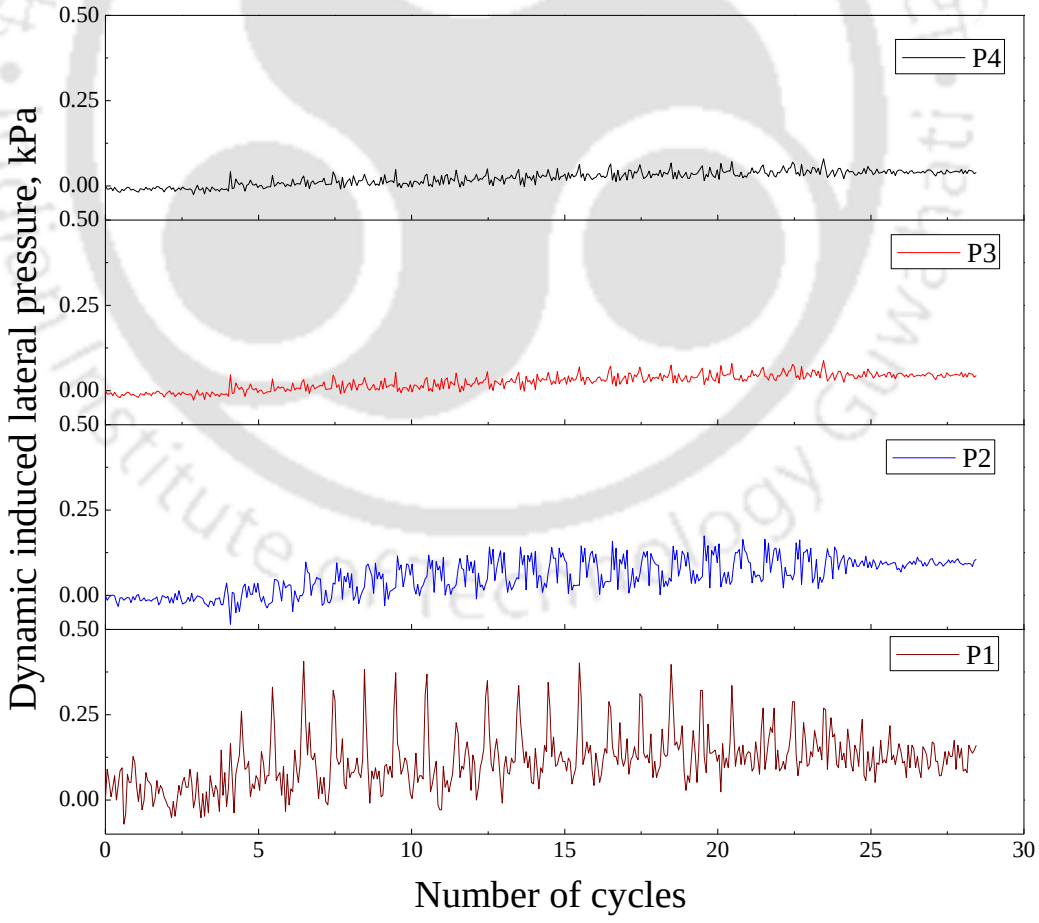

Fig. 5.12 Typical incremental earth pressure histories for the test TC90_0.3_3

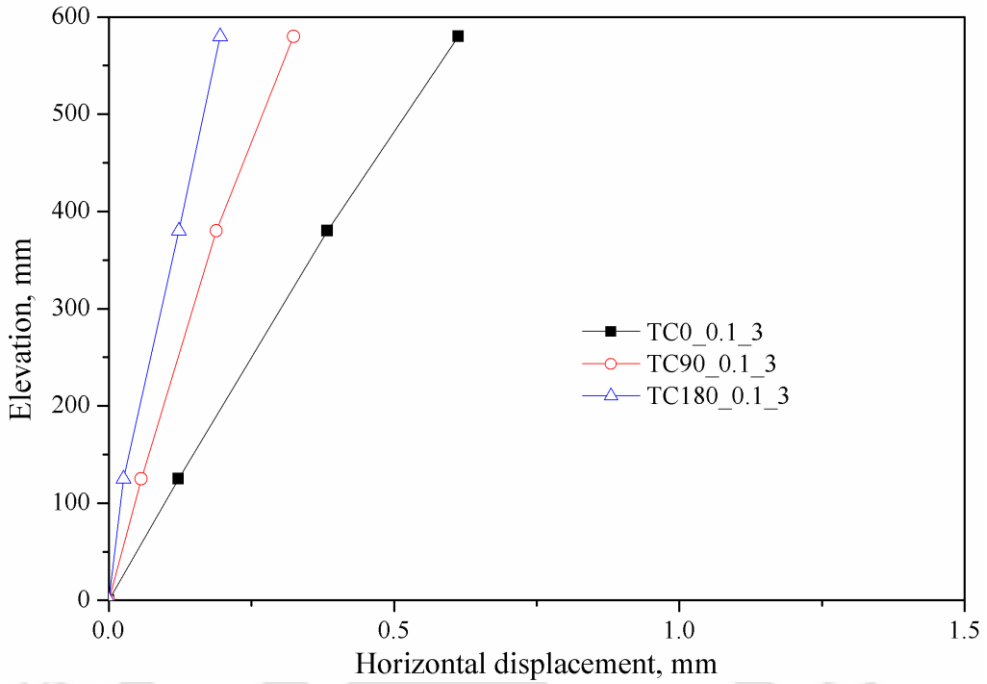

Fig. 5.13 Effect of compressible inclusion on wall displacement for 0.1g_3Hz

Fig. 5.14 shows the measured incremental lateral earth pressures along the height of the wall for TC0_0.1_3, TC90_0.1_3 and TC180_0.1_3 tests (a = 0.1g and f = 3 Hz). It is observed, from the figure, that incremental lateral earth pressures depict a decreasing trend with an increase in compressible inclusion thickness. Maximum earth pressures are observed for the TC0_0·1_3 test and lower earth pressures are observed for the TC180_0·1_3 test. The bottom incremental earth pressure 0·38 kPa is observed for the test TC0_0·1_3 and the corresponding values for the tests TC90_0·1_3 and TC180_0·1_0·3 are 0·21 kPa and 0·1 kPa, respectively. Fig. 5.15 shows the acceleration amplification for different tests which indicates that the acceleration amplification factors are increased on increasing the tire chips compressible inclusion thickness. With the inclusion of compressible tire chips just behind the wall, the sand backfill will tend to move more under cyclic loading, which will result in higher accelerations in the backfill for model wall with thicker compressible inclusions. This type of behavior has been reported by Hazarika et al. (2006)

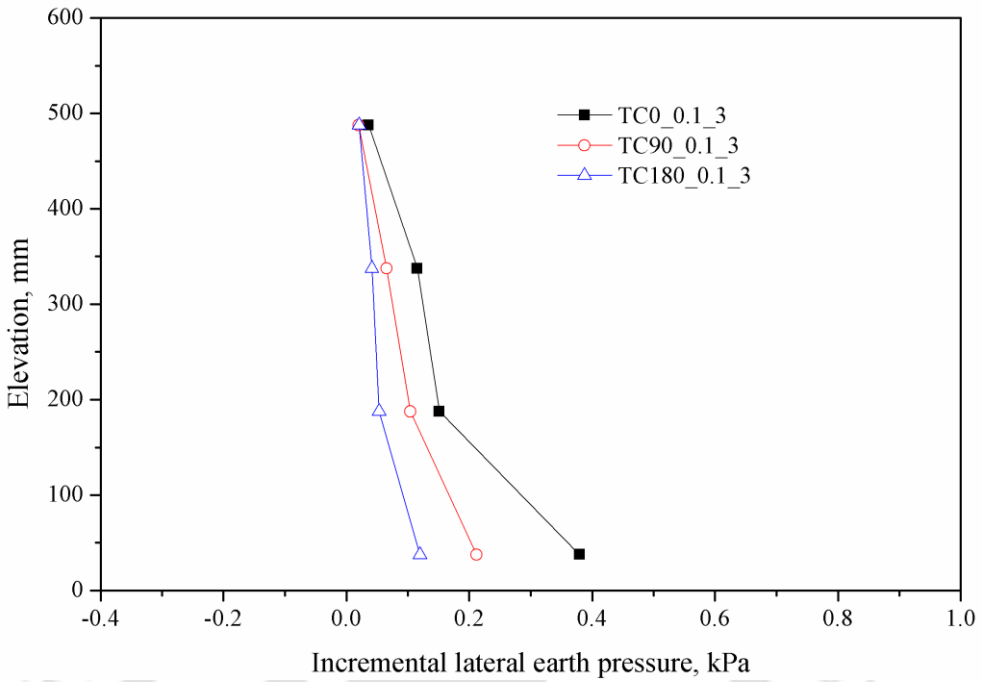

Fig. 5.14 Effect of compressible inclusion on incremental earth pressures for 0.1g_3Hz

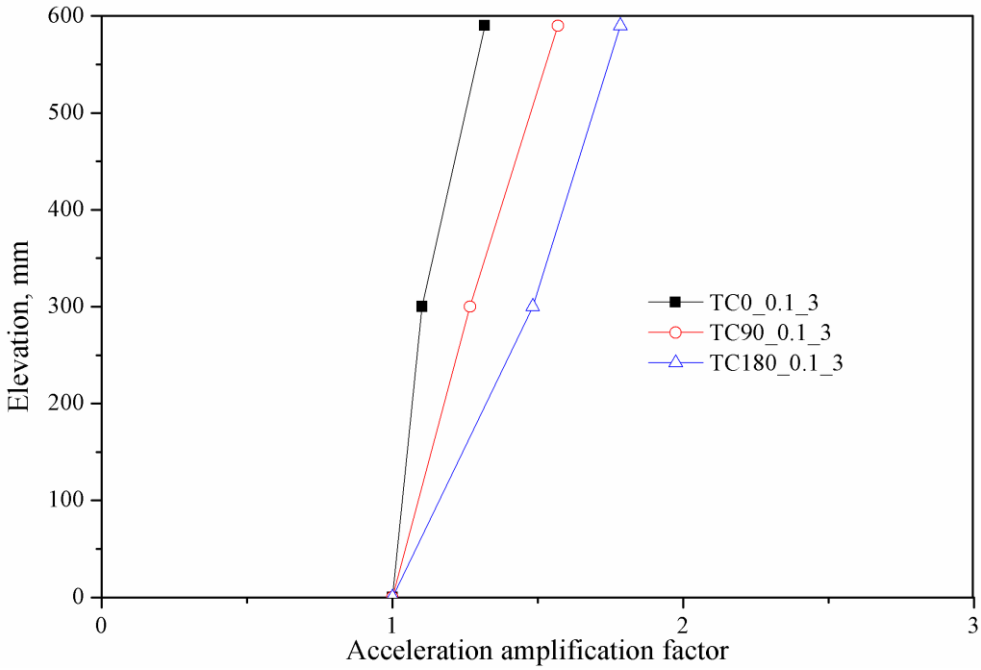

Fig. 5.15 Effect of compressible inclusion on acceleration amplification for 0.1g_3Hz

Fig. 5.16 shows the displacement profiles for dynamic excitation of 0.2*g* acceleration (*a*) at *f* = 3 Hz, revealing the influence of compressible inclusion on the horizontal displacement response of wall. The maximum displacement of 3.22 mm is

observed for TC0_0.2_3 test and the corresponding values for TC90_0.2_3 and TC180_0.2_3 tests are 1.76 mm and 1.11 mm, respectively.

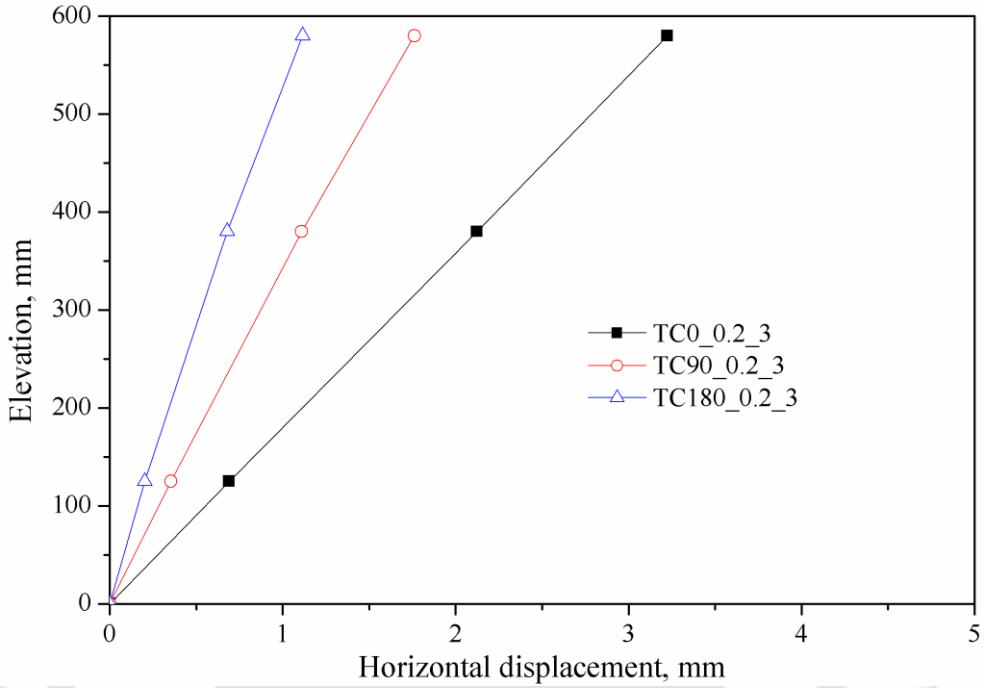

Fig. 5.16 Effect of compressible inclusion on wall displacement for 0.2*g*_3Hz

Fig. 5.17 shows the measured incremental lateral earth pressures along the height of the wall for TC0_0.2_3, TC90_0.2_3 and TC180_0.2_3 tests. It is observed, from the figure, that incremental lateral earth pressures are depicting the decreasing trend with increase in compressible inclusion thickness. Maximum earth pressures are observed for TC0_0.2_3 test and lower earth pressures are observed for TC180_0.2_3 test.

Higher base acceleration (0.3*g*) was applied on model wall at frequency of 3Hz and 5Hz. Fig. 5.19 shows the effect of compressible inclusion on model response in terms of displacement, incremental earth pressure and acceleration amplification factor profiles for 3 Hz. From the Fig. 5.19a, 40% to 60% reduction in top displacement is observed as compared to control cases. From the Fig. 5.19b, there is a nonlinear trend in relative variations of pressures for different model walls; it can be observed that the

pressures are higher at bottom. Further, it can be seen that the earth pressures were significantly affected by the tire chips compressible inclusions.

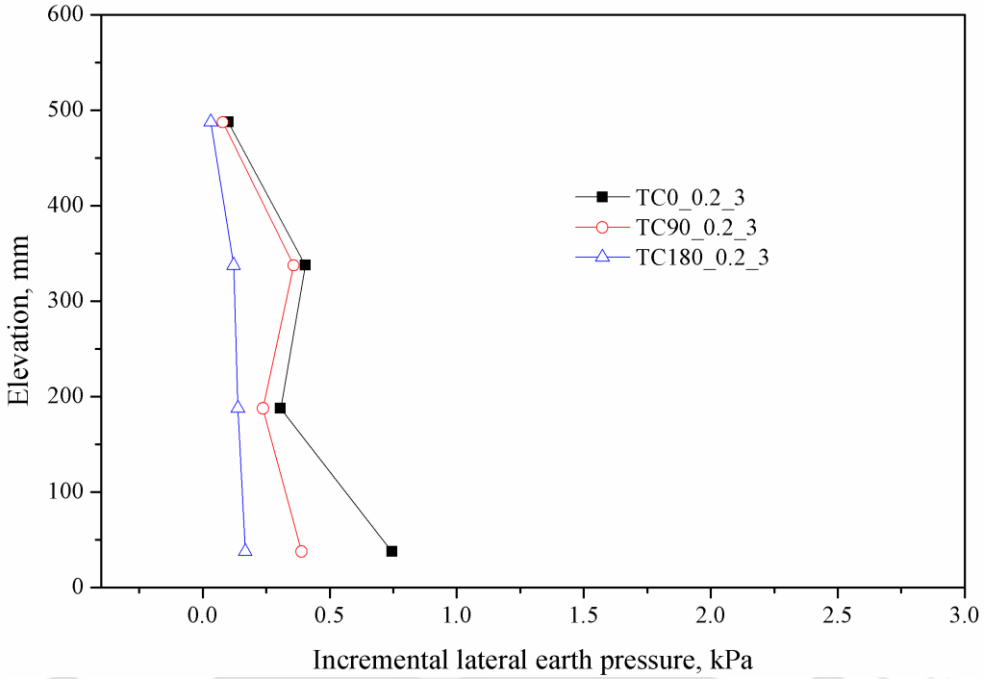

Fig. 5.17 Effect of compressible inclusion on incremental earth pressures for 0.2*g*_3Hz

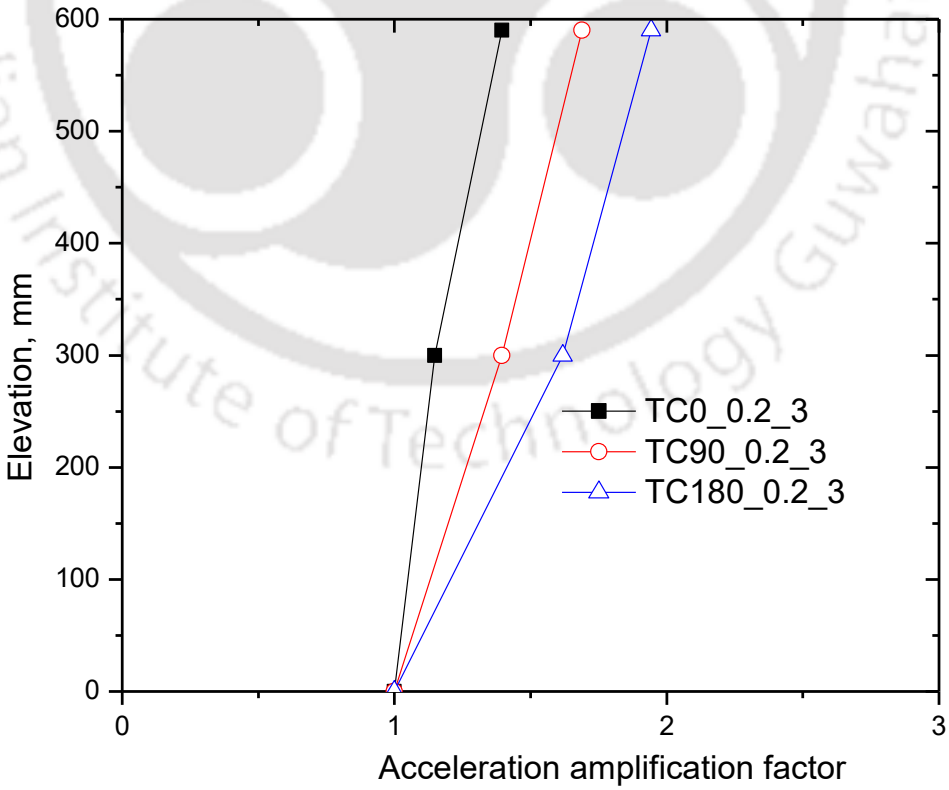

Fig. 5.18 Effect of compressible inclusion on acceleration amplification for 0.2*g*_3Hz

Furthermore, the base acceleration (*a*) of 0.3*g* at 5Hz frequency (*f*) has been applied on different model walls to observe the effect of tire chips as compressible inclusion material. The response of the model wall is shown in Fig. 5.20. Wall top displacements of 3.05, 1.64, and 0.73 mm are seen from the figure, for TC0_0.3_5, TC90_0.3_5, and TC180_0.3_5, respectively. It is revealed that a 76% reduction in top displacements as compared to control case (TC180_0.3_5). Fig. 5.20b shows the incremental earth pressures for the tests TC0_0.3_5, TC90_0.3_5, and TC180_0.3_5. From the laboratory model tests, large reductions in lateral earth pressures were achieved when t/H=0.30 thickness tire chips was used as the vertical compressible inclusion. Fig. 5.19a, Fig. 5.20c, it is observed that the acceleration amplification factors are increased with increasing tire chips layer thickness. Slightly higher acceleration amplifications were observed when compressible inclusion placed in-between the wall and backfill soil.

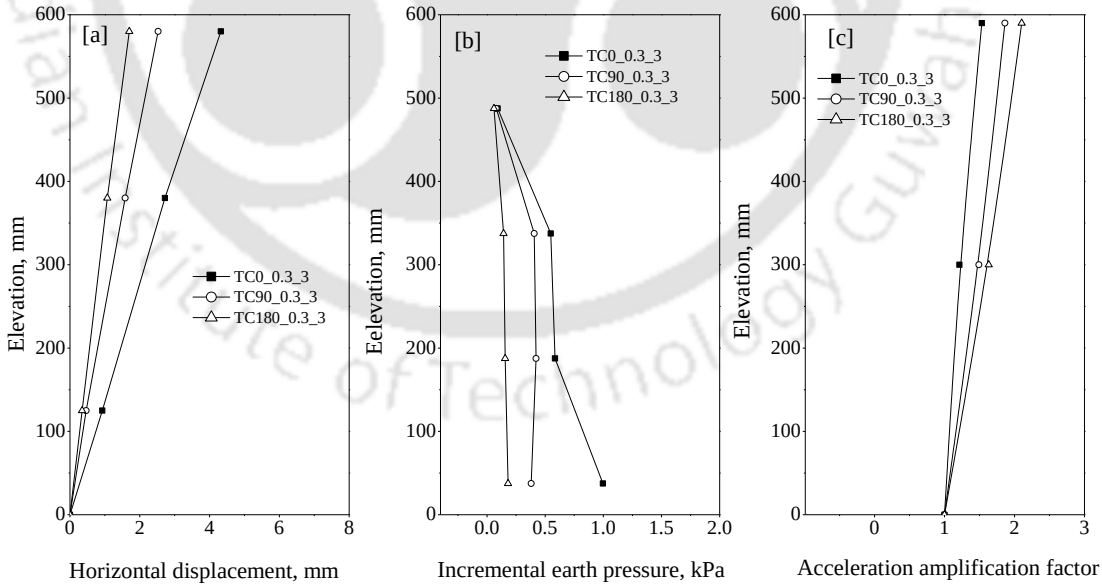

Fig. 5.19 Model wall responses of 0.3g_3Hz dynamic excitation: a) horizontal displacement; b) incremental earth pressure and c) acceleration amplification factor

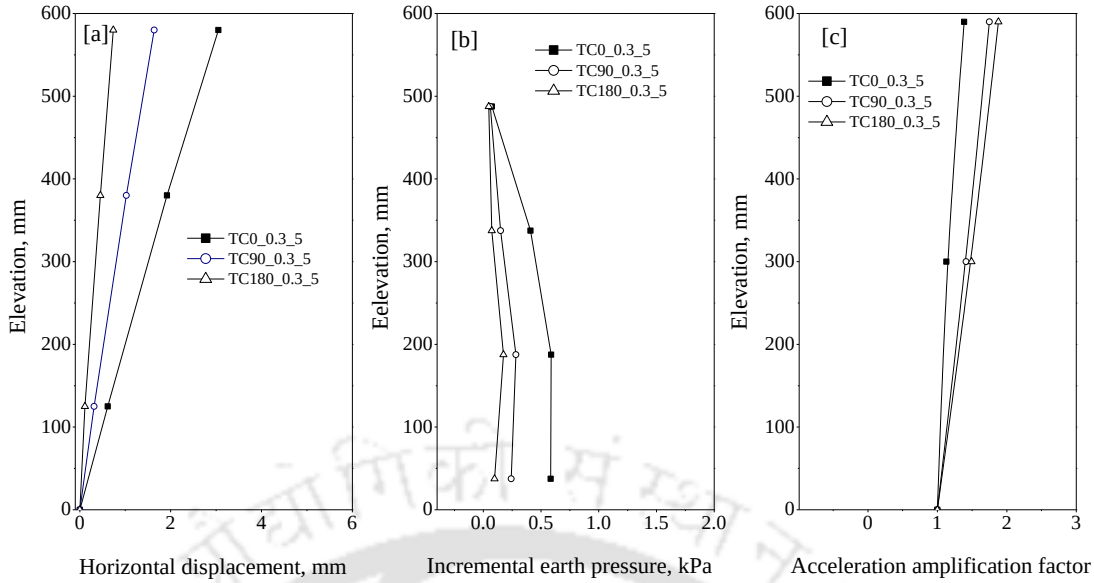

Fig. 5.20 Model wall responses of 0.3g_5Hz dynamic excitation: a) horizontal displacement; b) incremental earth pressure and c) acceleration amplification factor

5.5 MODEL WALL RESPONSE SUBJECTED TO IRREGULAR EARTHQUAKE EXCITATIONS

In this section, physical model tests results for irregular earthquake excitations are discussed. The details about selected EQ records were discussed in Chapter 4. Fig. 5.21 and Fig. 5.22 show the horizontal displacement histories of two compressible thickness at different elevations for SN earthquake excitation. The maximum horizontal displacements values were observed at elevation of 580 mm. Maximum horizontal displacements values are found to be 0.36 mm, 0.27 mm for TC90_SN and TC180_SN, respectively.

Fig. 5.23 and Fig. 5.24 show the incremental lateral earth pressure histories of two compressible thickness at different elevations for NZ earthquake excitation. The maximum incremental earth pressure values were observed at bottom of wall. Maximum incremental earth pressure values are found to be 0.33 kPa, 0.18 kPa for t/H=0.15 and 0.30, respectively.

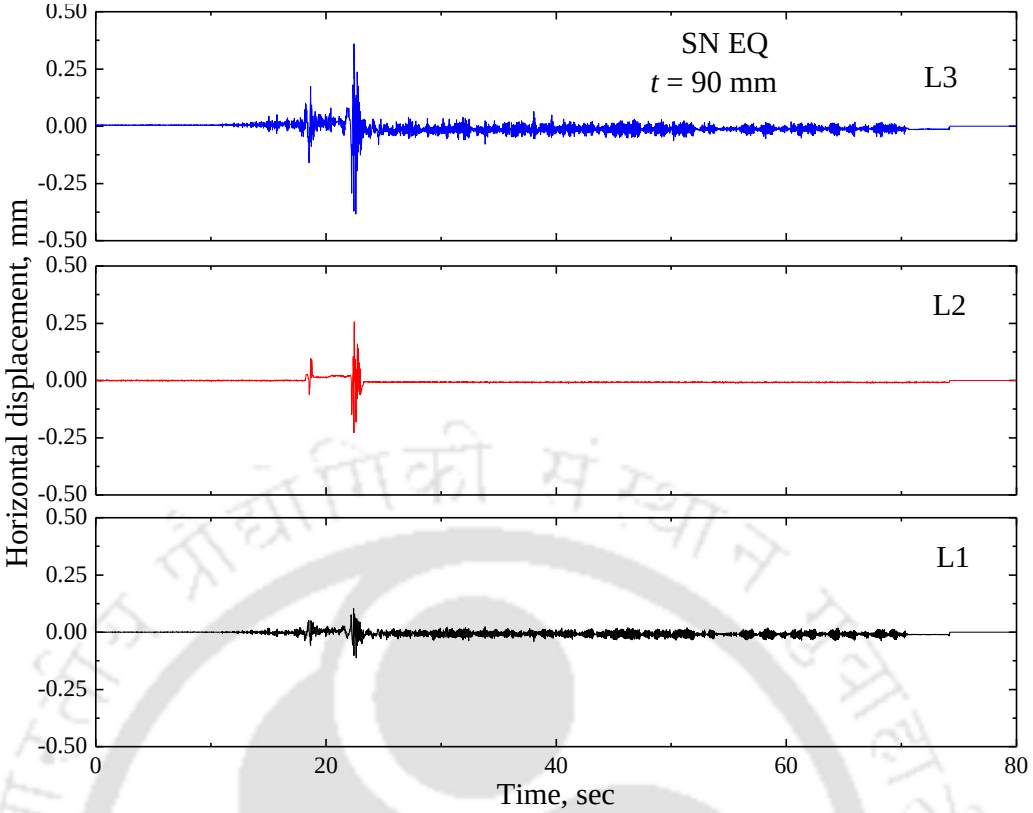

Fig. 5.21 Displacement histories at different elevations for the test TC90_SN EQ

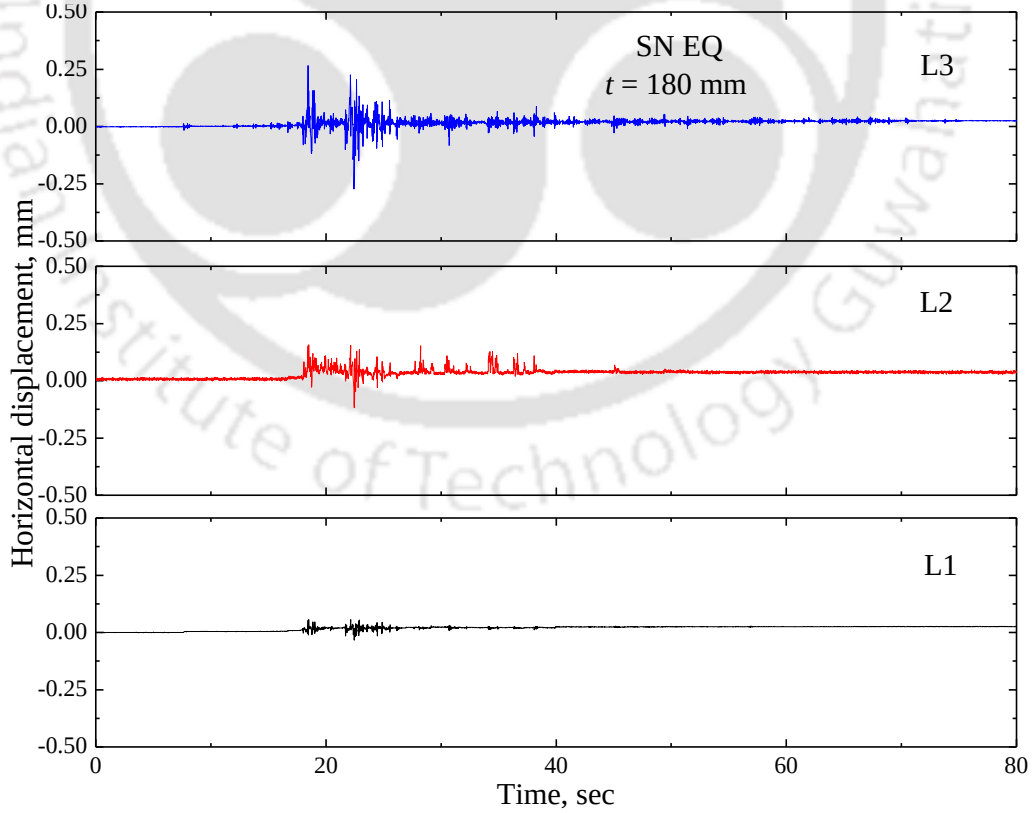

Fig. 5.22 Displacement histories at different elevations for the test TC180_SN EQ

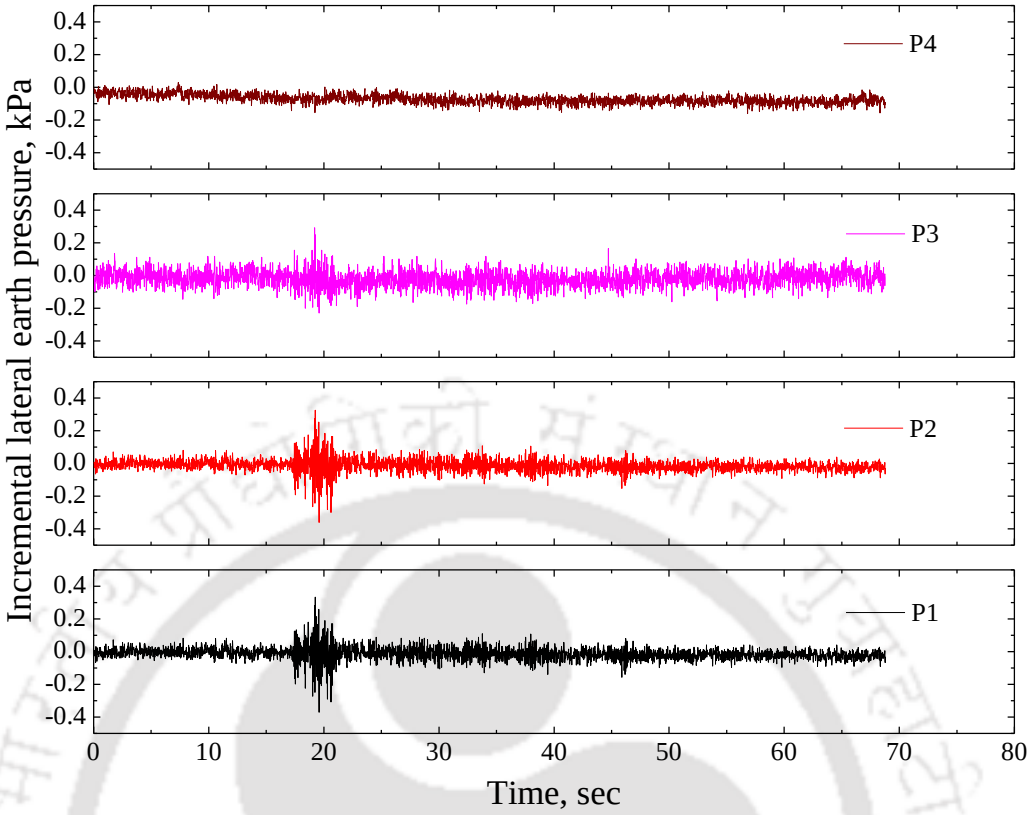

Fig. 5.23 Incremental earth pressure history of TC90_NZ EQ

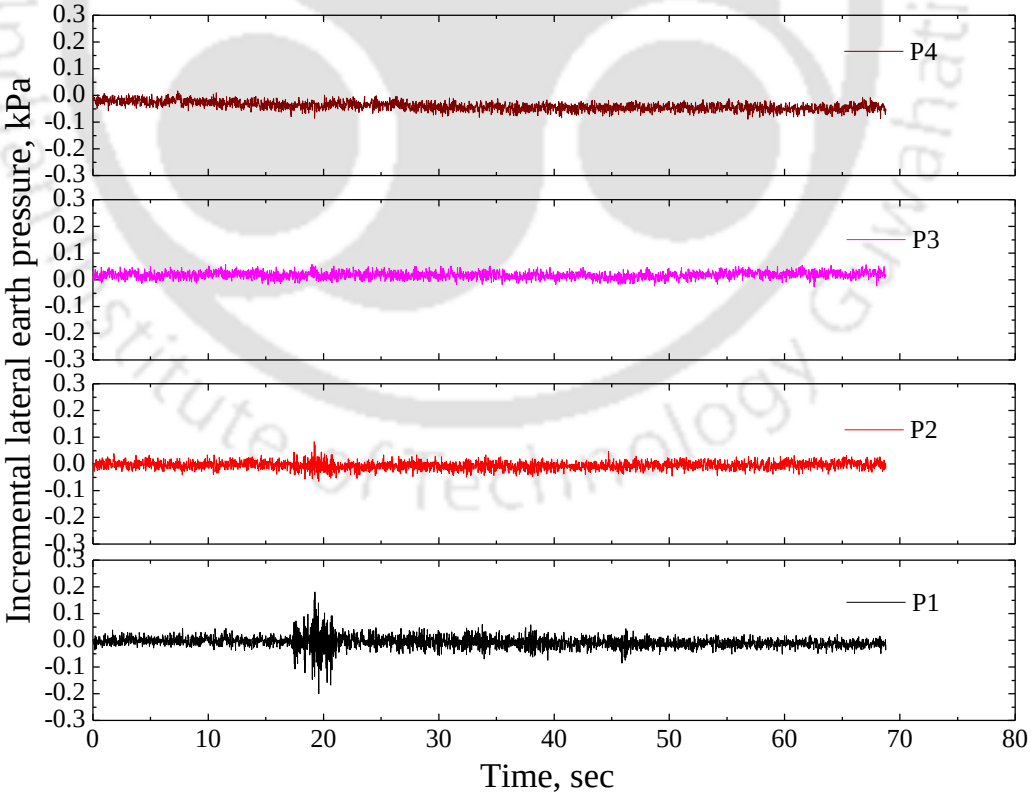

Fig. 5.24 Incremental earth pressure history of TC180_NZ EQ

Model wall responses with different compressible inclusion thickness were compared with that of the controlled case model wall at identical excitation levels. Fig. 5.25 shows the effect of compressible inclusion on model wall displacements along the height of wall for SN EQ excitation. It is observed, from the figure, that the displacements significantly decrease with the increasing compressible inclusion thickness. The maximum displacement of 0·72 mm for the test TC0_SN EQ is reduced to 0·36 mm and 0·27 mm, for the tests TC90_SN EQ and TC180_SN EQ, respectively.

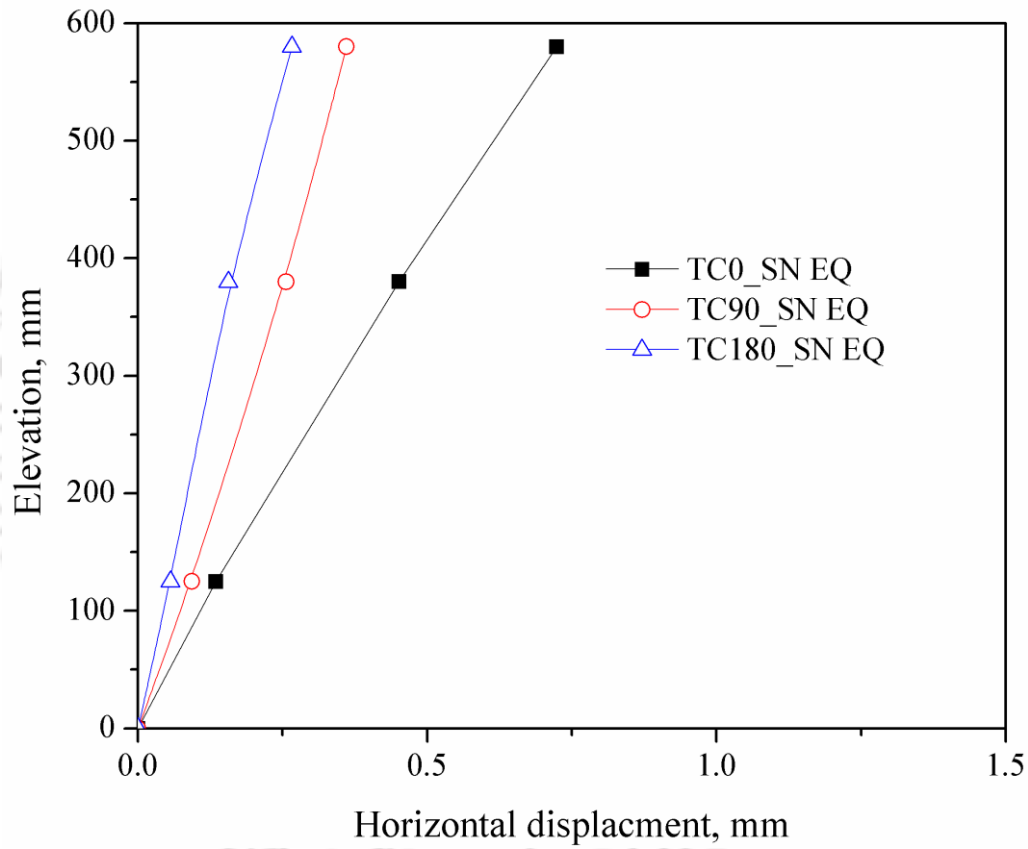

Fig. 5.25 Effect of compressible inclusion on wall displacement for SN EQ

Fig. 5.26 shows the measured incremental lateral earth pressures along the height of the wall for TC0_NZ EQ, TC90_NZ EQ and TC180_NZ EQ tests. It is observed, from the figure, that incremental lateral earth pressures depict a decreasing trend with an increase in compressible inclusion thickness. Maximum earth pressures are observed for the TC0_NZ EQ test and lower earth pressures are observed for the TC180_0·1_3

test. The bottom incremental earth pressure 0·61 kPa is observed for the test TC0_NZ EQ and the corresponding values for the tests TC90_NZ EQ and TC180_NZ EQ are 0·33 and 0·18 kPa, respectively. Fig. 5.27 shows the acceleration amplification along the height of wall for different tests (NZ EQ excitation) which indicates that the acceleration amplification factors are increased on increasing the tire chips compressible inclusion thickness. With the inclusion of compressible tire chips just behind the wall, the sand backfill will tend to move more under cyclic loading, which will result in higher accelerations in the backfill for model wall with thicker compressible inclusions. This type of behavior has been reported by Hazarika et al. (2006).

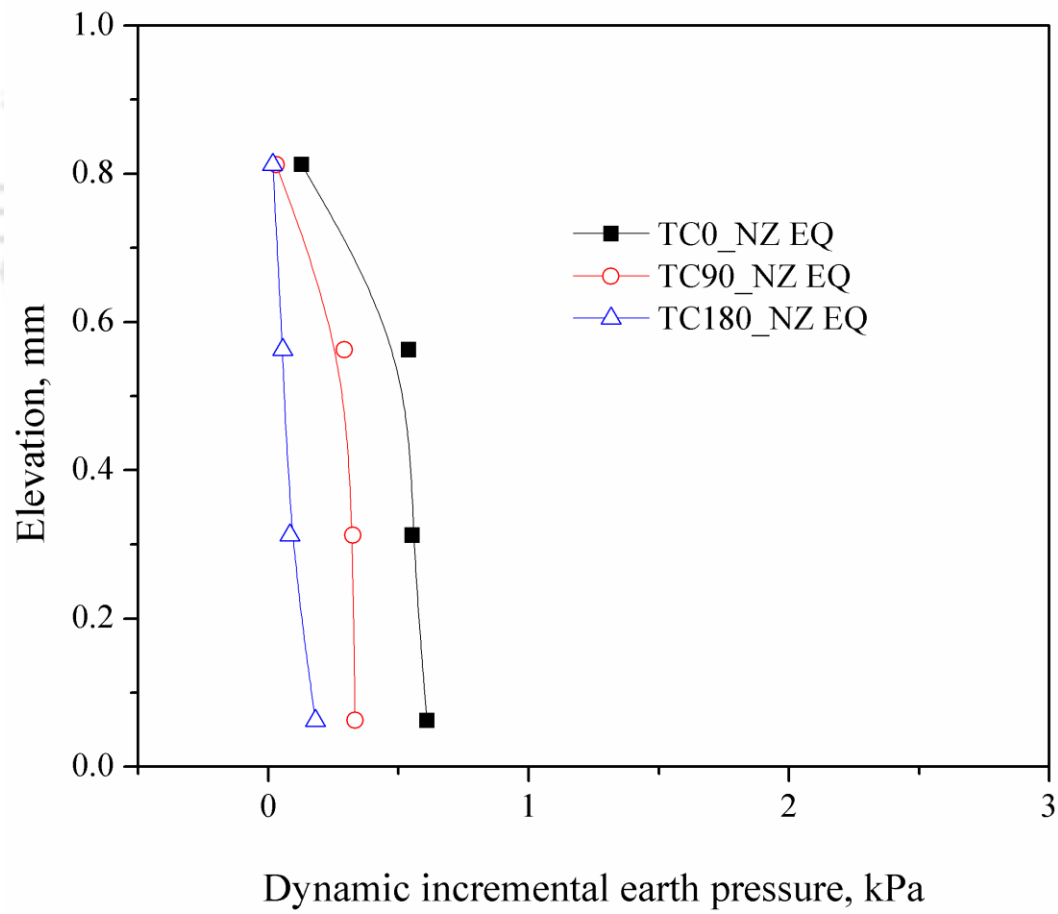

Fig. 5.26 Effect of compressible inclusion on incremental earth pressures for NZ EQ

Further, the results of model wall, in the form of variations of horizontal displacement, acceleration amplification factors and incremental earth pressures along height of the wall after different dynamic excitations are presented in Fig. 5.28 to Fig. 5.31 for different compressible inclusion thickness. The horizontal displacements and incremental earth pressures are decreased by using tire chips as compressible inclusion. For control case, maximum horizontal displacements at the top of wall are ranged within 2.43 mm for Tohoku and 0.72 mm for South Napa earthquake.

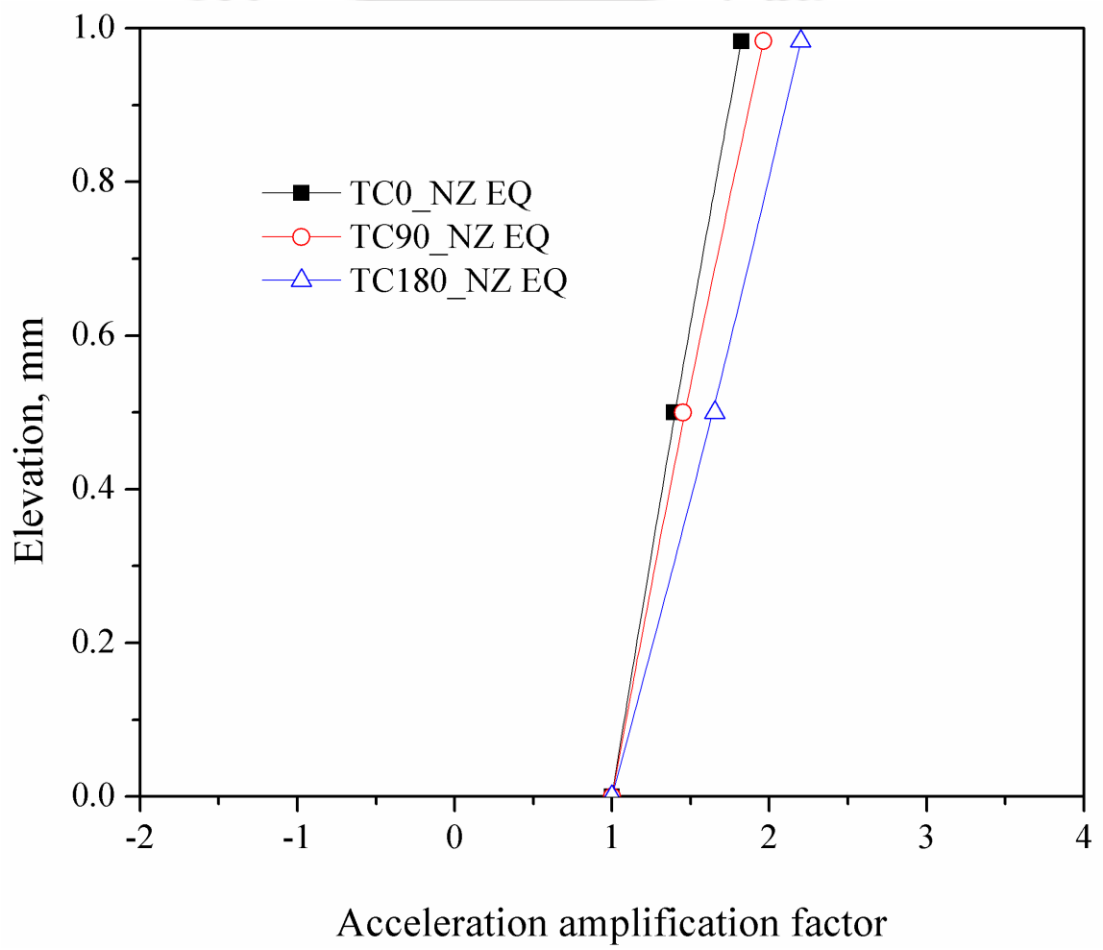

Fig. 5.27 Effect of compressible inclusion on acceleration amplification for NZ EQ

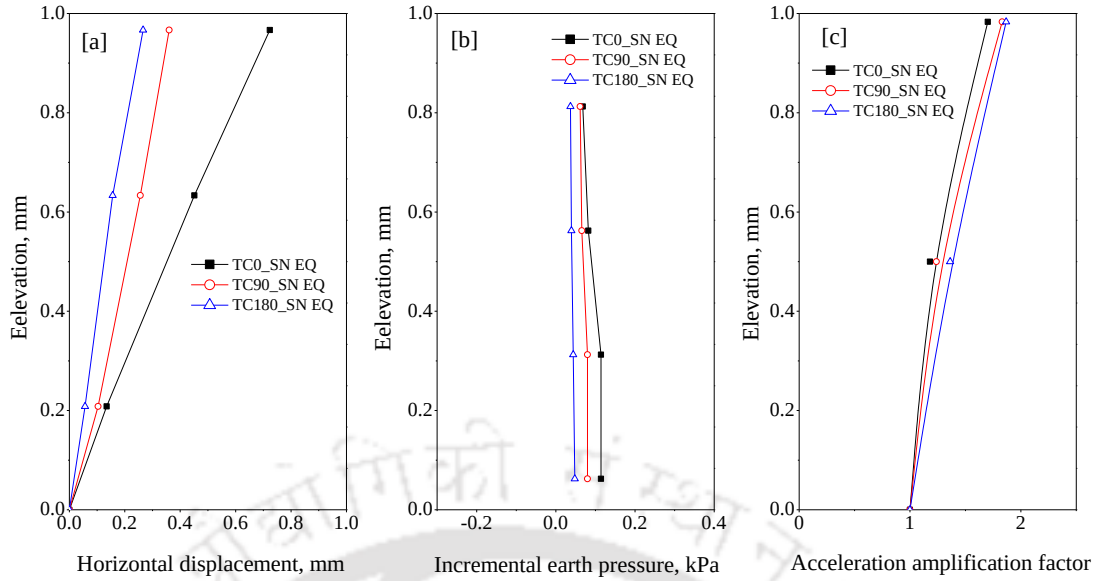

Fig. 5.28 Comparison of model response for SN earthquake: a) Horizontal displacement; b) Incremental earth pressures and c) Acceleration amplification factors

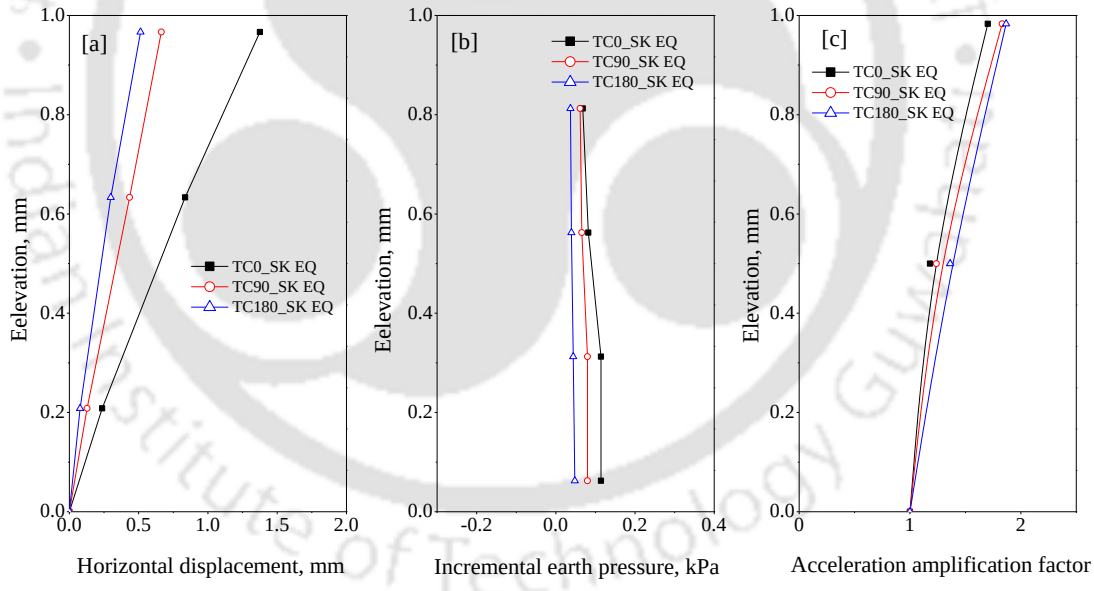

Fig. 5.29 Comparison of model response for SK earthquake: a) Horizontal displacement; b) Incremental earth pressures and c) Acceleration amplification factors

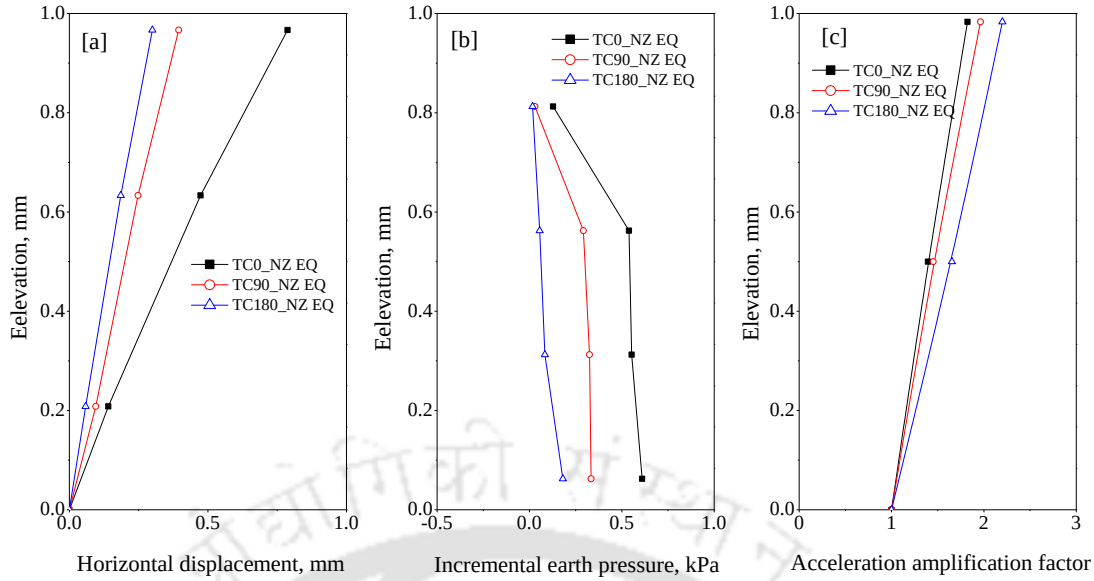

Fig. 5.30 Comparison of model response for NZ earthquake: a) Horizontal displacement; b) Incremental earth pressures and c) Acceleration amplification factors

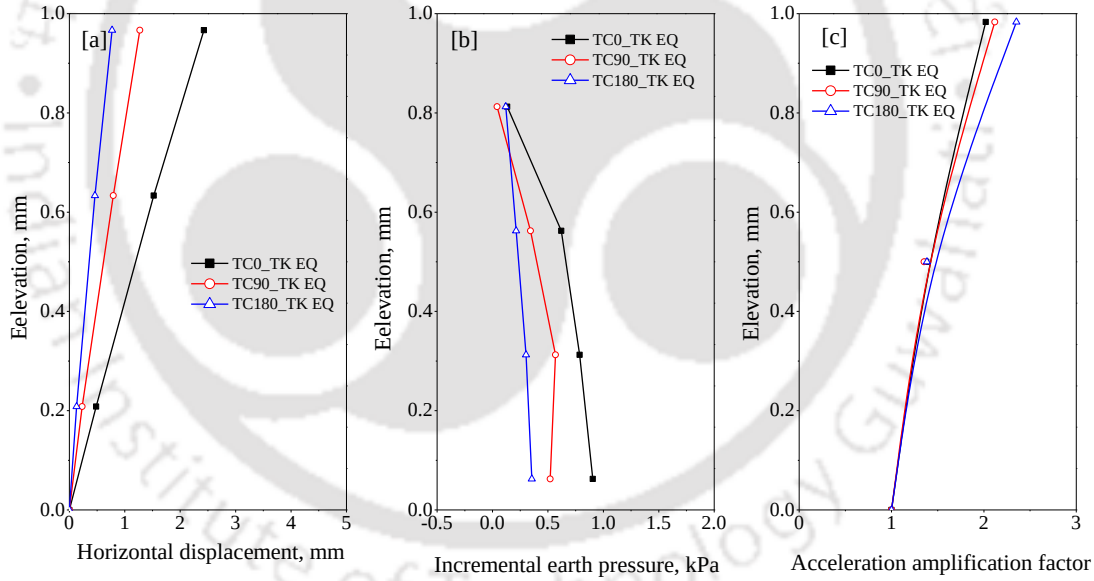

Fig. 5.31 Comparison of model response for TK earthquake: a) Horizontal displacement; b) Incremental earth pressures and c) Acceleration amplification factors

5.6 DISCUSSION OF MAXIMUM VALUES

The results presented above indicate that the tire chips acted well as compressible inclusions in reducing the displacements and lateral earth pressures on the

wall. Among the two different thicknesses considered, the reduction is more in the thicker compressible layer. To quantify the reductions, the measured maximum displacements at top and maximum earth pressures at the bottom of the wall are compared under static and dynamic cases.

Top displacements, earth pressures and their percentage reduction values due to the compressible inclusion are reported in Table 5.4 for static case. From the table, it is concluded that the displacements are reduced up to 25% and incremental earth pressures are reduced up to 60%.

The top displacements, bottom incremental earth pressures with different sinusoidal excitations (at f=3 Hz) for various compressible inclusion thickness shown in Fig. 5.32. Further, the top displacements, bottom incremental earth pressures and their percentage reduction values due to the compressible inclusion are reported in Table 5.5. From these figure and table, it is to be noted that the presence of tire chips inclusion at the wall – soil interface was significantly reduced the earth pressures (70-80% reduction) and wall displacements (60-75% reduction).

Table 5.4 Comparison of maximum displacements, earth pressures and its percentage reduction

Condition	**Top displacement, mm**			**Percentage reduction**	
	***t* = 0 mm**	***t* = 90 mm**	***t* = 180 mm**	***t* = 90 mm**	***t* = 180 mm**
Without surcharge	1.76	1.55	1.43	12.02	18.94
Under 10 kPa	6.03	4.98	4.56	17.34	24.39
Condition	**Earth pressure (elevation of 187 mm), kPa**			**Percentage reduction**	
	***t* = 0 mm**	***t* = 90 mm**	***t* = 180 mm**	***t* = 90 mm**	***t* = 180 mm**
Without surcharge	1.57	1.16	0.57	26.06	63,47
Under 10 kPa	4.8	3.8	2.28	20.83	52.47

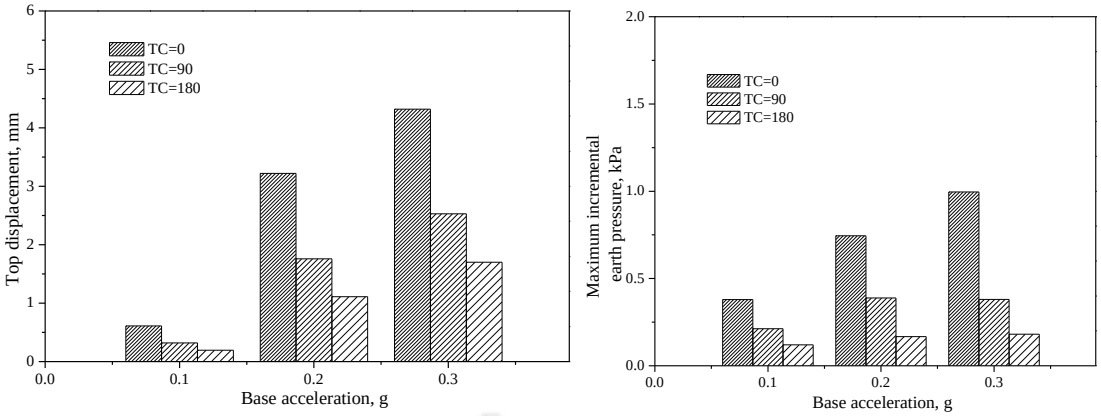

(a) (b)

Fig. 5.32 Effect of compressible inclusion for different base accelerations: (a) top displacements, (b) bottom earth pressures

Further, maximum displacement and maximum incremental earth pressure of the retaining wall models under the four earthquake excitations (SN EQ, SK EQ, NZ EK and TK EQ) are compared in Fig. 5.33.

Table 5.5 Comparison of maximum displacements, earth pressures and its percentage reduction

Input excitation	**Top displacement, mm**			**Percentage reduction**	
	***t* = 0 mm**	***t* = 90 mm**	***t* = 180 mm**	***t* = 90 mm**	***t* = 180 mm**
0.1*g*_3Hz	0.61	0.32	0.195	47.54	68.03
0.2*g*_3Hz	3.22	1.76	1.11	45.34	65.53
0.3*g*_3Hz	4.32	2.53	1.70	41.43	60.65
0.3*g*_5Hz	3.05	1.64	0.73	46.23	76.06
Input excitation	**Bottom incremental earth pressure, kPa**			**Percentage reduction**	
	***t* = 0 mm**	***t* = 90 mm**	***t* = 180 mm**	***t* = 90 mm**	***t* = 180 mm**
0.1*g*_3Hz	0.379	0.211	0.119	44.33	68.60
0.2*g*_3Hz	0.745	0.389	0.167	47.78	77.58
0.3*g*_3Hz	0.996	0.379	0.181	61.95	81.83
0.3*g*_5Hz	0.58	0.24	0.097	58.62	83.27

In addition, maximum displacements and bottom incremental earth pressures with different STC mixtures and its percentage reductions are reported in Table 5.6.

From the table, it is concluded that the displacements are reduced in the range of 60% to 65% and incremental earth pressures are reduced around 70% to 80%.

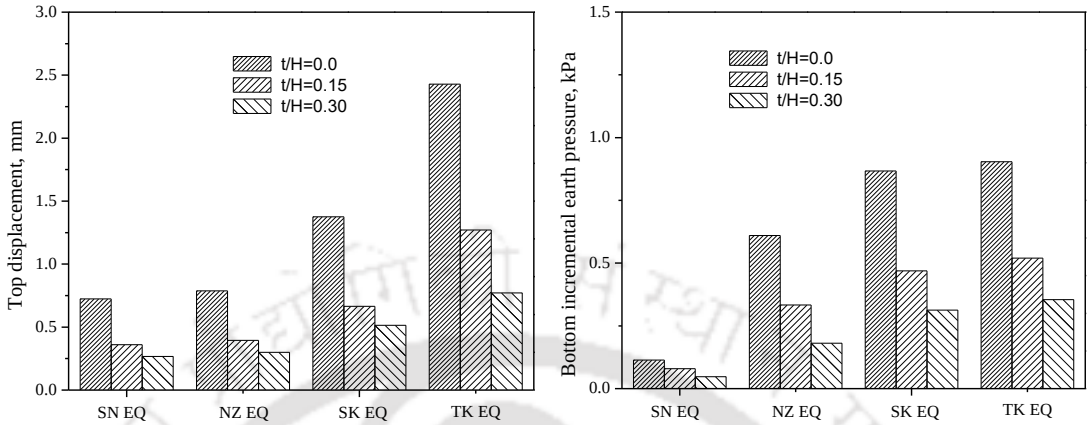

Fig. 5.33 Effect of compressible inclusion for irregular earthquake excitations: (a) top displacements, (b) incremental earth pressures

Table 5.6 Comparison of maximum displacements, earth pressures and its percentage reduction

Input excitation	**Top displacement, mm**			**Percentage reduction**	
	***t* = 0 mm**	***t* = 90 mm**	***t* = 180 mm**	***t* = 90 mm**	***t* = 180 mm**
SN EQ	0.72	0.36	0.27	50.19	63.21
SK EQ	1.37	0.66	0.51	51.72	62.66
NZ EQ	0.79	0.39	0.29	49.92	61.95
TK EQ	2.43	1.27	0.77	47.62	68.25
Input excitation	**Bottom incremental earth pressure, kPa**			**Percentage reduction**	
	***t* = 0 mm**	***t* = 90 mm**	***t* = 180 mm**	***t* = 90 mm**	***t* = 180 mm**
SN EQ	0.379	0.211	0.119	44.33	68.60
SK EQ	0.745	0.389	0.167	47.78	77.58
NZ EQ	0.996	0.379	0.181	61.95	81.83
TK EQ	0.58	0.24	0.097	58.62	83.27

This reduction could be attributed to compressible nature of the tire chips at wall–soil interface, which absorbs the soil movement and brings the soil to the active state so that the earth pressures and displacements are reduced. Similar mechanisms

were also discussed in the case of effectiveness of EPS geofoam as a compressible inclusion (Horvath 1997 and Bathurst et al., 2007). The thickness t/H=0.30, compressible inclusion thickness can be considered as optimum thickness with in the thicknesses considered in the study.

Reduction of the lateral earth pressure and displacement implies a lower design requirement possible, which makes smaller dimensions of the retaining wall with reduced material cost. The additional advantage of providing tire chips as compressible inclusion near the wall facing is getting drainage (Kaushik et al., 2016), which will reduce the pore pressure effects onto the wall.

5.7 SUMMARY

A series of model tests were conducted to examine the performance of retaining walls with scrap tire chips as compressible inclusion, subjected to static and dynamic loading conditions. Results were presented and discussed in terms of incremental earth pressures, horizontal displacements, and acceleration amplifications. The flowing conclusions are drawn from the results presented herein.

- Displacements and lateral earth pressures are low when compressible inclusion was provided behind the wall.
- Displacements and lateral earth pressures are decreased with increasing compressible inclusion thickness.
- The acceleration amplifications increased with the increasing of compressible inclusion.
- Tire chips 180 mm thick is able to minimize the displacements and is found to be efficient in acting as a seismic buffer.

- The maximum horizontal displacement of wall models with compressible inclusions (waste tire chips) is reduced by up to 75%.
- Incremental earth pressures were reduced by up to 80% compared to the control test.

Chapter 6. NUMERICAL SIMULATIONS OF RETAINING WALLS

6.1 INTRODUCTION

This chapter presents numerical simulations of the static and dynamic physical model tests conducted on retaining wall models with different STC mixtures. Numerical models were developed using FLAC^{2D} (Fast Lagrangian Analysis of Continua). Methodology followed in simulating different materials and their properties are discussed. The responses of model, like horizontal displacements, acceleration amplification factors and incremental pressures after dynamic excitation were validated with that of the physical model results. Using the validated numerical model, a full-scale wall model was developed and analyzed for its static and seismic behavior. Behavior of full-scale model wall with different backfill materials (STC mixtures) along with the various parametric studies are presented and discussed.

6.2 OVERVIEW OF FLAC^{2D}

FLAC^{2D} is a two-dimensional explicit finite difference program, based on the Lagrangian calculation scheme, for engineering mechanics computations. Though FLAC^{2D} was originally developed for the use of geotechnical and mining engineers, the program offers a wide range of capabilities to solve complex problems in mechanics (Itasca 2011). Various built-in constitutive models are available in the FLAC^{2D} and can be modified by the user with minimal effort through FISH programming code. FLAC^{2D} also provides some built-in structural elements, which can be used as reinforcement or structural supports, and interface elements as well (Itasca 2011). Interfaces or joints can be defined in a FLAC grid between two or more portions of the grid. These interfaces

are planes within the grid upon which slip and/or separation is allowed that are used to model the effects of joints, faults and frictional interfaces between bodies. Interfaces can connect to structural elements. For example, beam elements may interact with the grid, and may interact with other beam elements via interfaces. Many researchers working on the performance of reinforced soil structures and other geotechnical engineering problems under both static and dynamic conditions used FLAC^{2D} and proved its caliber for the same (e.g. Bathurst and Hatami 1998, Vieira et al. 2006, Hatami and Bathurst 2006, Krishna, 2008, Bhattacharjee and Krishna, 2012, 2015, Krishna and Bhattacharjee, 2016).

The static and dynamic analysis options in FLAC^{2D} permits to study two-dimensional, plane-strain or axi-symmetric problems. The dynamic behavior of model depends upon size of grid, which is governed by the accurate transmission of waves through the model (Itasca 2011). Three aspects that the user should consider when preparing a FLAC model for dynamic analysis are: (1) dynamic loading and boundary conditions; (2) mechanical damping; and (3) wave transmission through the model. The dynamic input can be applied in one of the following ways: (a) an acceleration history; (b) a velocity history; (c) a stress (or pressure) history; or (d) a force history. Material damping can be incorporated in numerical simulation to reproduce the magnitude of energy losses in the natural system subjected to dynamic loading. Rayleigh damping is being commonly used to provide damping that is approximately frequency-independent over a restricted range of frequencies. Alternatively, the local damping can be implemented in FLAC. In this study, local damping is used.

6.3 DEVELOPMENT OF NUMERICAL WALL MODELS

Laboratory tests conducted on retaining wall models of size 800 × 580 mm in plan and 600 mm height, as discussed in Chapter 4, have been simulated numerically

using FLAC^{2D}. The construction sequence adopted in the numerical model is same as that of the physical model tests. The formulation of the numerical models was described in detail in the following subsections.

6.3.1 Numerical Grid

A rigid foundation zone of 875 mm long and 25 mm thick considered at the base of the wall. A grid of 600 mm height and 800 mm long generated to represent the backfill of the model wall. Fig. 6.1 shows the numerical grid considered to simulate the retaining model wall.

6.3.2 Boundary Conditions

The boundary conditions applied to the model represent the actual boundary of the physical model tests. The bottom boundary was completely fixed in vertical direction to represent the rigid boundary. The far end boundary elements are fixed in *x* direction to represent the container boundary. During the construction, the model facing was fixed in horizontal (*x*) direction to represent the temporary support. After the entire model was constructed and the model has been brought to equilibrium, the facing boundaries were released stage by stage, representing the stage wise removal of temporary support.

6.3.3 Materials properties

The properties of the different backfill materials were adopted based on the discussions in the Chapter 3. The sand material was modeled as elasto-plastic Mohr Coulomb material. A small value cohesion of 0.1 kPa has been adopted to prevent computational instability. Similar type of small value of cohesion was also adopted by Hatami and Bathurst (2006) in numerical simulation of reinforced soil walls. Sand tire-chip (STC) mixture materials were also modelled as elasto-plastic Mohr Coulomb

material, assuming as equivalent continuum material with the properties determined from the laboratory tests. The material properties considered for numerical models are shown in Table 6.1.

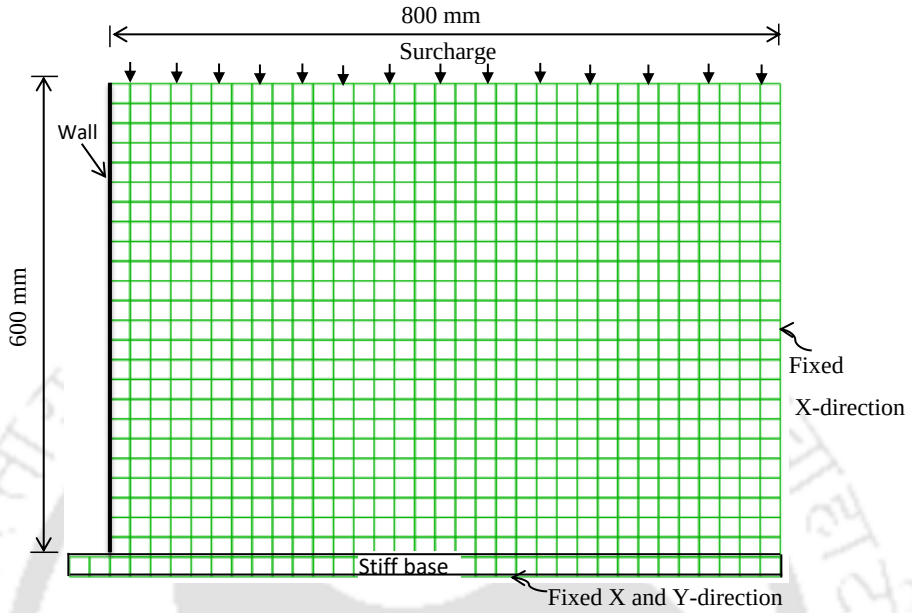

Fig. 6.1 FLAC grid for the model retaining wall

Table 6.1 Material properties used in numerical simulation

STC mixtures	Young's Modulus of backfill, MPa	Unit weight, kN/m^3	Friction angle	Dilation angle
STC0	29.6	15.57	48º	18º
STC30	59.0	13.17	56º	26º
STC40	49.6	12.28	51º	21º

The wall (0.6 m height and 0.58 m width) material was considered as elastic material using beam elements with young's modulus (Steel modulus) of 2×10^{11} Pa. An interface was considered in between backfill soil and wall, which is controlled by relative interface movement, that depend on interface normal stiffness (k_n) and shear stiffness (k_s) values. The normal and shear stiffness values were approximated based on the apparent stiffness (expressed in stress-per-distance units) of a zone in the normal direction obtained from

$$\text{Apparent stiffness} = \max\left[\frac{K+\frac{4}{3}G}{\Delta z_{\min}}\right] \qquad \text{Eq. 6.1}$$

Where K and G are the bulk and shear moduli, respectively, and z_{min} is the smallest width of an adjoining zone in the normal direction.

6.3.4 Selection of grid size

Sensitivity analysis was performed to verify the effect of grid size on wall model behavior. Three different grid sizes 25, 50 and 100 mm were considered for the purpose. Horizontal displacements and lateral earth pressures of the wall after support removal were determined and presented in Fig. 6.2. Maximum horizontal displacement of about 1.75 mm is observed for model with 50 mm size grid while it is about 1.64 mm with 2 % variation for other grid sizes. Horizontal pressure variations are observed to be not so sensitive for the range of grid sizes considered. From these observations, a grid size of 25 mm was considered for numerical simulation of laboratory models.

As numerical distortion of propagating wave in dynamic analysis is a function of modeling conditions, the size of grids was selected in such a way that, it shall be approximately smaller than 1/10 to 1/8 of the wavelength associated with highest frequency component of the seismic wave (Kuhlemeyer and Lysmer 1973). The speed of *p*-wave and *s*-wave propagation through medium were calculated using following relationships

$$C_p = \sqrt{\frac{k+\frac{4G}{3}}{\rho}} \qquad \text{Eq. 6.2}$$

$$C_s = \sqrt{\frac{G}{\rho}} \qquad \text{Eq. 6.3}$$

Where C_p = speed of *p*-wave propagation through medium; C_s = speed of *s*-wave propagation through medium; K = Bulk modulus of medium; G= Shear modulus of medium; ρ = mass density of medium

The maximum frequency (Eq.6.4) that can be modeled accurately for vertically propagating waves is (Kuhlemeyer and Lysmer 1973):

$$f = \frac{C_s}{\lambda} = \frac{\sqrt{G/\rho}}{10\Delta l} \qquad \text{Eq. 6.4}$$

Where f = frequency of vertically propagating waves; λ = wavelength associated with highest frequency component; Δl = largest zone dimension in model.

The maximum frequency that can be propagated accurately in a model of zone size 25 mm was calculated (as per Eq. 6.4) as 34 Hz. As most of the seismic wave energy is concentrated within 15-20 Hz frequency, selection of 25 mm grid size is justified.

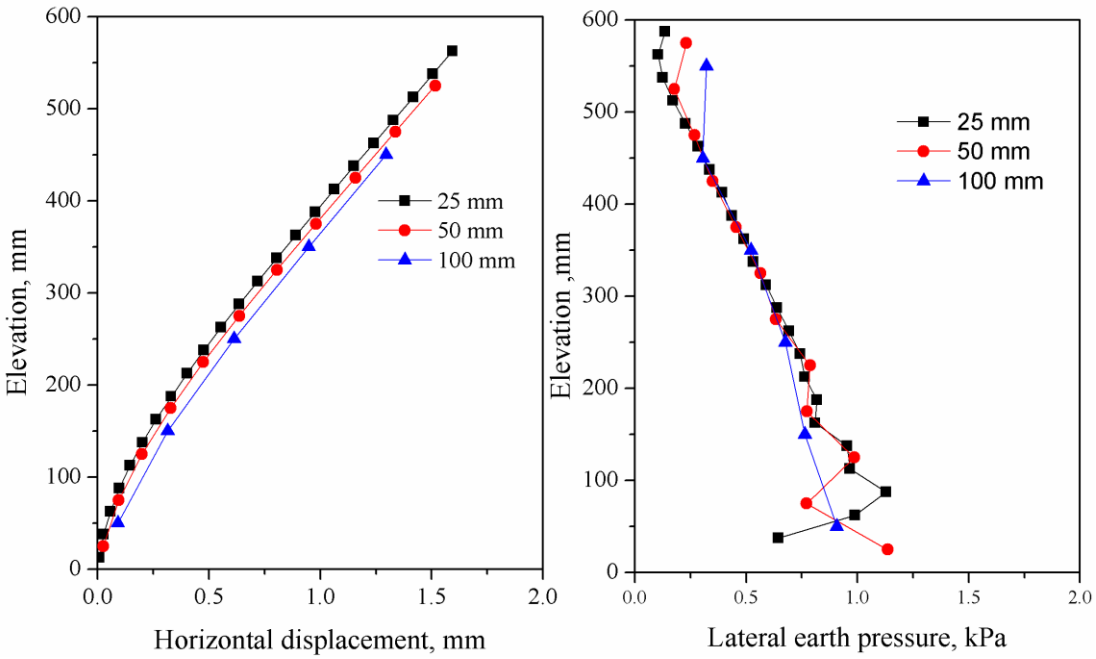

Fig. 6.2 Sensitivity of grid size on model response

6.4 VALIDATION OF NUMERICAL MODELS

Numerical models were validated by comparing with the results of physical model tests that were discussed in Chapter 4. The results are presented in terms of horizontal displacement, lateral earth pressure variation along the height of the wall. For validation of numerical retaining wall, models, under static loading conditions, pure sand (STC0) and different STC mixtures were considered as backfill material. Lateral earth pressures and horizontal displacements of the wall at identical locations of models are presented together for comparison. Fig. 6.3 shows the test results of physical and numerical wall models. Fig. 6.4 shows that the comparison of top displacements with different surcharge pressures for different STC mixtures. The figures demonstrate that the numerical model results are reasonably matching with the physical tests results.

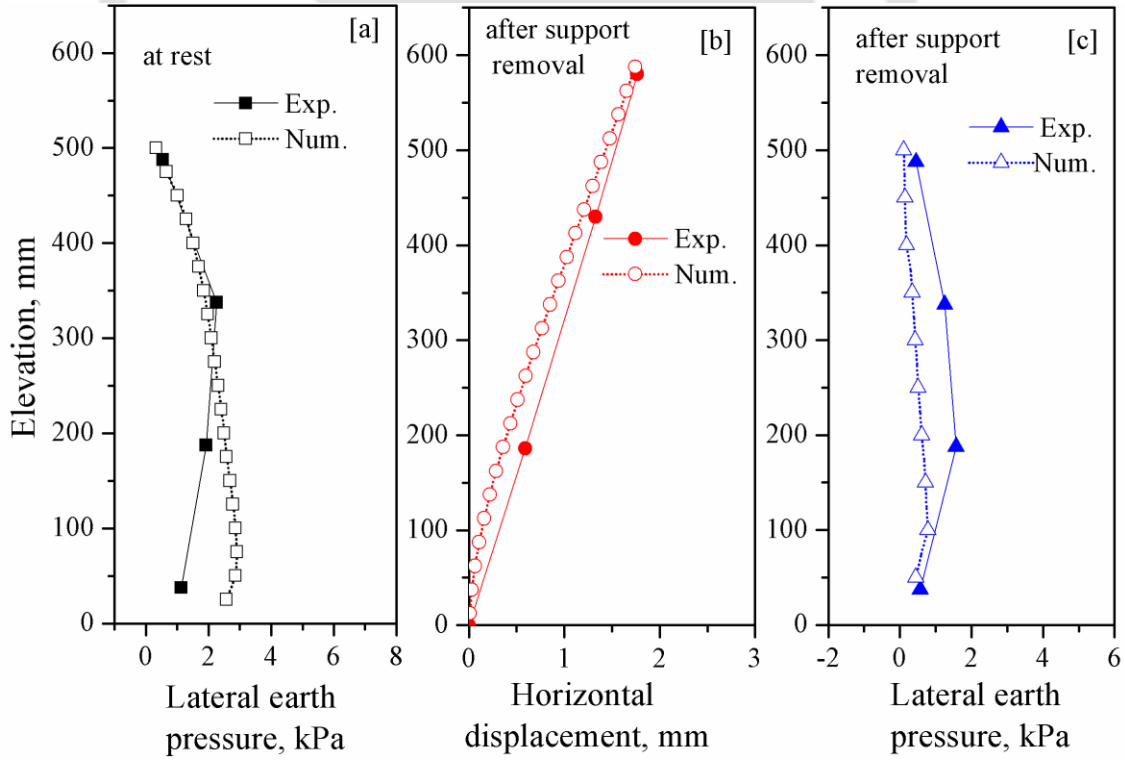

(i)

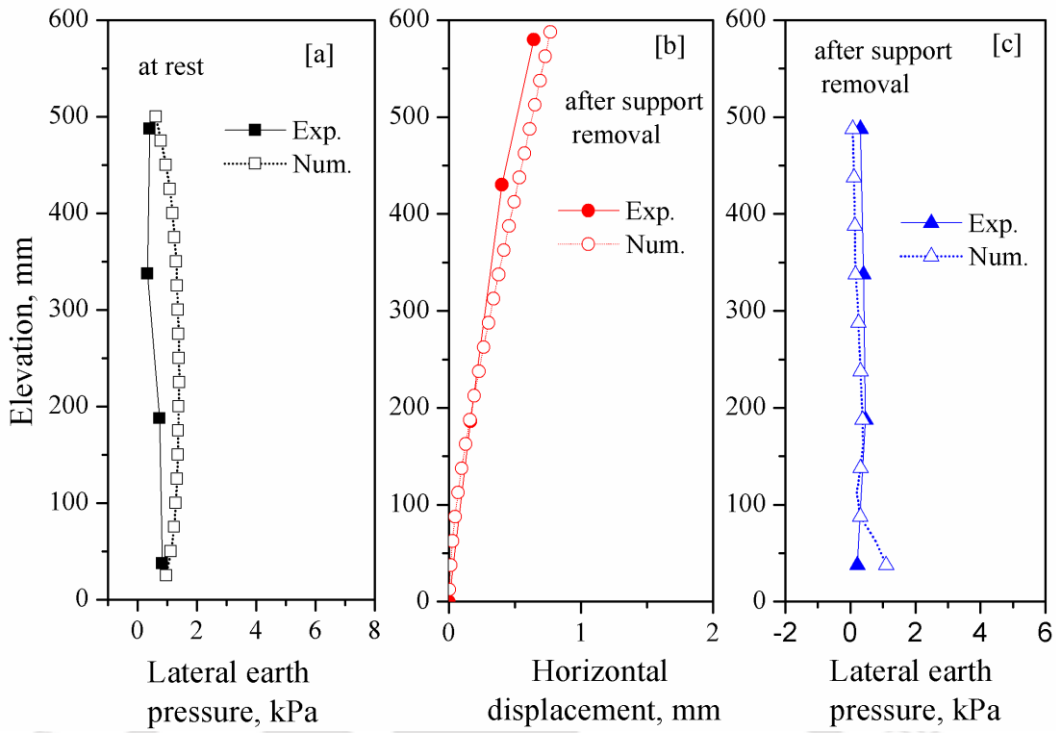

(ii)

Fig. 6.3 Comparison of results from numerical and physical model tests: i) STC0 backfill, ii) STC30 backfill

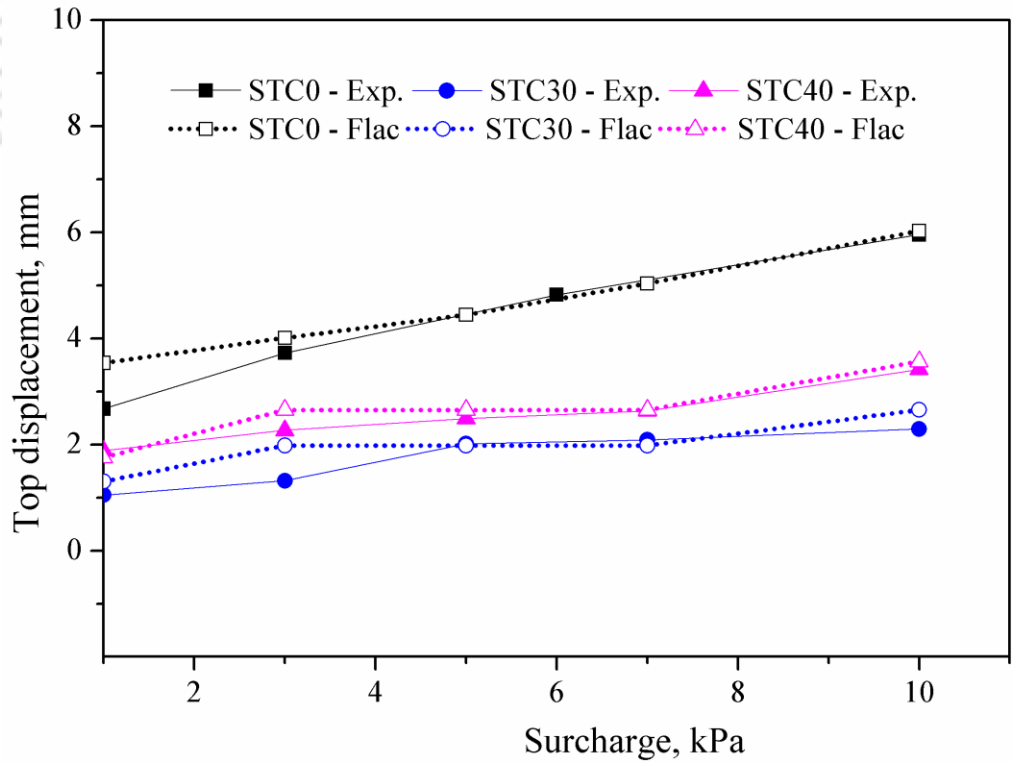

Fig. 6.4 Comparison of top displacement of different test results of numerical and physical models

For validation of the model under dynamic conditions, model walls with pure sand (STC0) and STC30 as backfill materials were considered. Mechanical local damping, a FLAC 2D option was employed in the numerical modelling as a way of allowing for energy loss as a result of internal friction and any slippage along interfaces. Local damping in dynamic problems is useful, as an approximate way to include hysteretic damping and it will absorb most of the energy in waves reflected from distance boundaries (Itasca 2011). Local damping ratio of 10% was adopted for validation and parametric study. Numerical model results are discussed in terms of backfill accelerations, horizontal displacements and incremental lateral earth pressures.

Typical histories of accelerations, horizontal displacements and incremental lateral earth pressures during dynamic loading (a = 0.3g and f = 3 Hz), at different elevations of retaining wall models are shown in Fig. 6.5 to Fig. 6.7. Acceleration, displacement and earth pressure histories obtained from the numerical model are similar to that of physical model tests reported in Chapter 4.

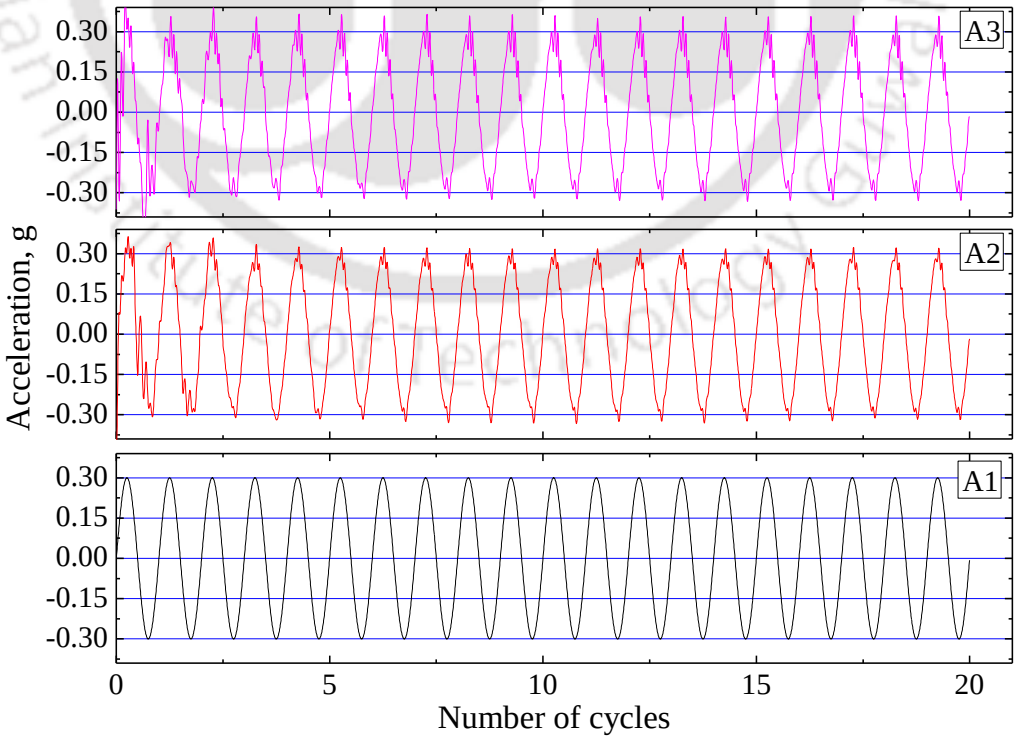

Fig. 6.5 Typical acceleration histories at different elevations (a= 0.3g, f= 3H)

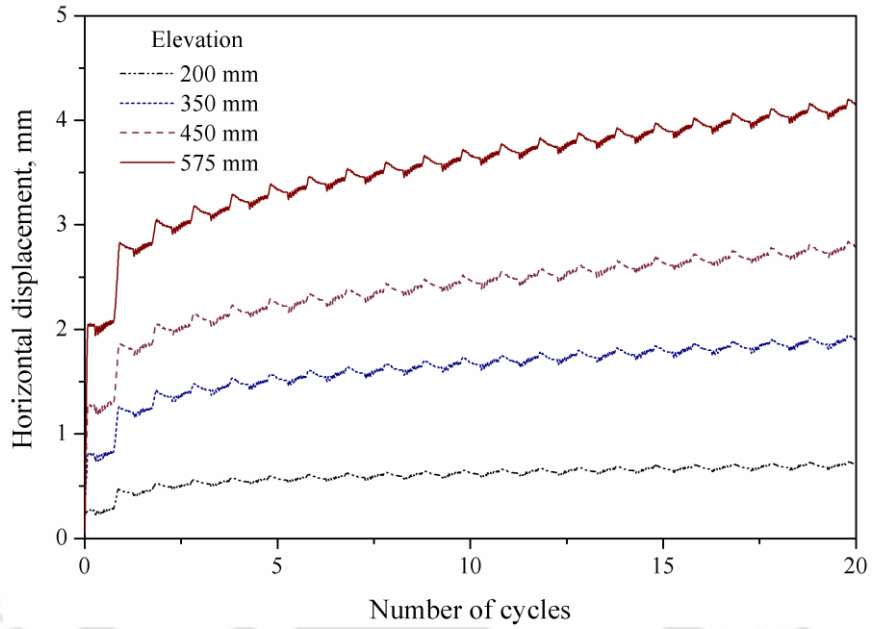

Fig. 6.6 Typical displacement histories in the numerical model at different elevations (a=0.3g, f=3Hz)

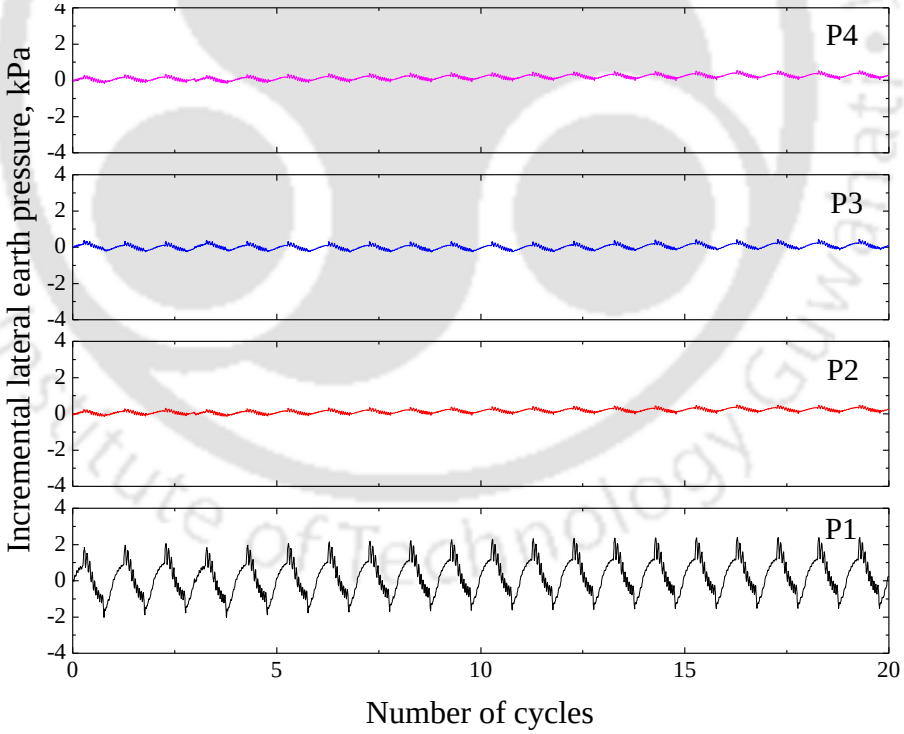

Fig. 6.7 Typical incremental earth pressure histories at different elevations (a=0.3g, f=3Hz)

Fig. 6.8 shows the comparison of responses obtained from physical and numerical models in terms of horizontal displacements, acceleration amplifications and

normalized earth pressures for of STC0 and STC30 backfill walls (a = 0.2g and f= 3 Hz). Fig. 6.9 shows the similar results but for a = 0.3g and f= 3 Hz. The figures show reasonable agreement between the results from physical and numerical models. Further, numerical wall models are well capturing the response of the physical wall models with the variation of backfill materials, surcharge pressures, dynamic base excitations.

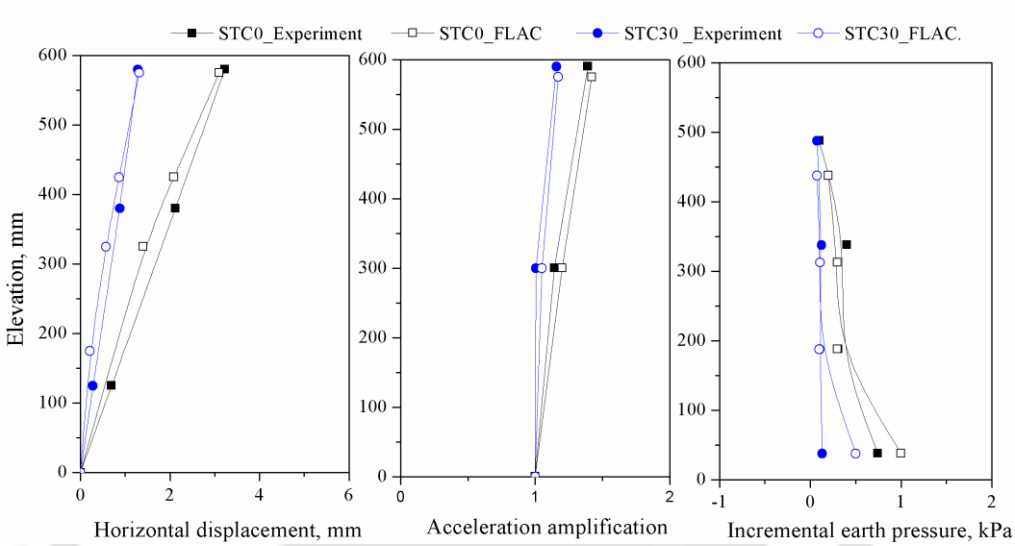

Fig. 6.8 Comparison of results from numerical and physical model tests (a = 0.2g and f= 3 Hz): a) Displacement profiles b) Acceleration amplification and c) Normalized pressure

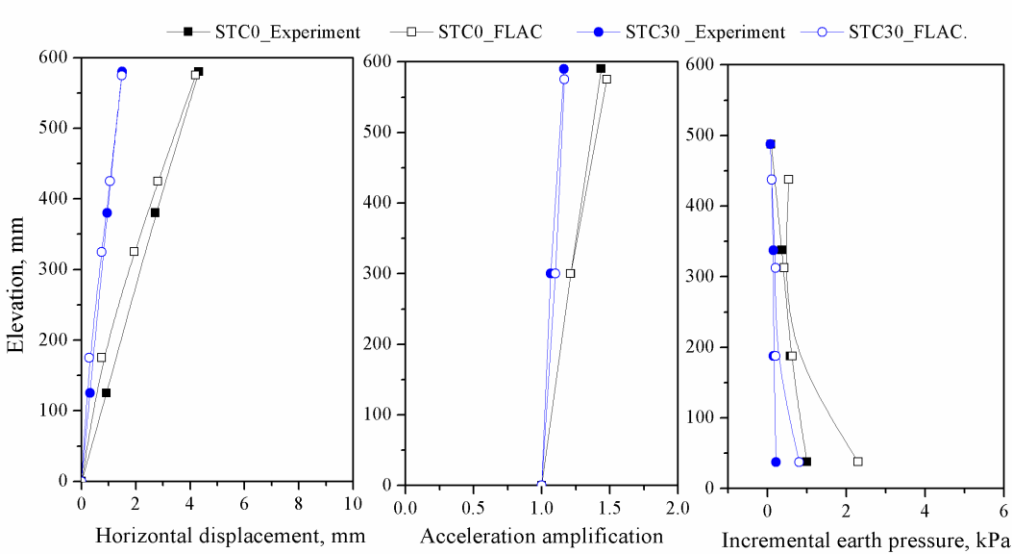

Fig. 6.9 Comparison of results from numerical and physical model tests (a = 0.3g and f= 3 Hz): a) Displacement profiles b) Acceleration amplification and c) Normalized earth pressure

6.5 STATIC RESPONSE OF FULL SCALE RETAINING WALL

Full-scale wall model (Fig. 6.10) of 6 m high (H) and 18 m long with different STC mixtures were studied, using the validated numerical model. The material properties were kept same as that of the laboratory scale numerical models. Retaining wall was modelled as liner elastic using beam elements. Retaining wall responses were discussed in terms of lateral earth pressures, horizontal displacements.

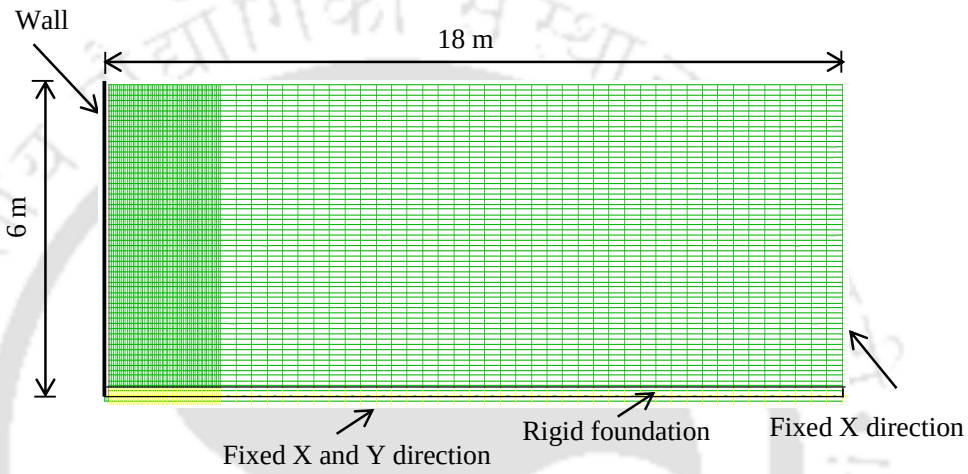

Fig. 6.10 Numerical diagram of full-scale retaining wall model

6.5.1 Effect of STC mixtures

Different types of STC backfills, in terms of tire chips by weight, STC30 (30% tire chips), STC40 (40% tire chips) and STC0 (control case) were considered. The variation of the horizontal displacements and lateral earth pressures along height of the wall are shown in Fig. 6.11 and Fig. 6.12, respectively. The results show that the retaining wall with STC30 backfill exhibits smaller displacements and lateral earth pressures along the wall compared to the STC0 and STC40 backfills.

The variations of the maximum shear forces and the bending moments along the wall are shown in Fig. 6.13 and Fig. 6.14. Maximum values are found at bottom of the retaining wall. The computed results show that, the retaining wall model with

STC30 backfill exhibits a smaller maximum shear force and bending moment along the wall when compared to the STC0 and STC40 backfills.

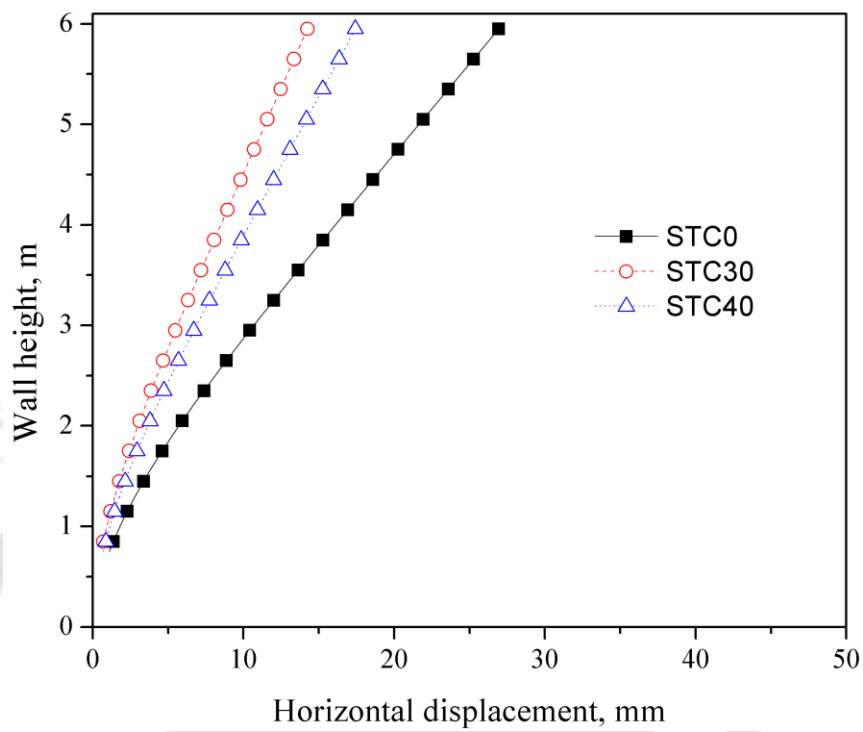

Fig. 6.11 Comparison of horizontal displacements of wall

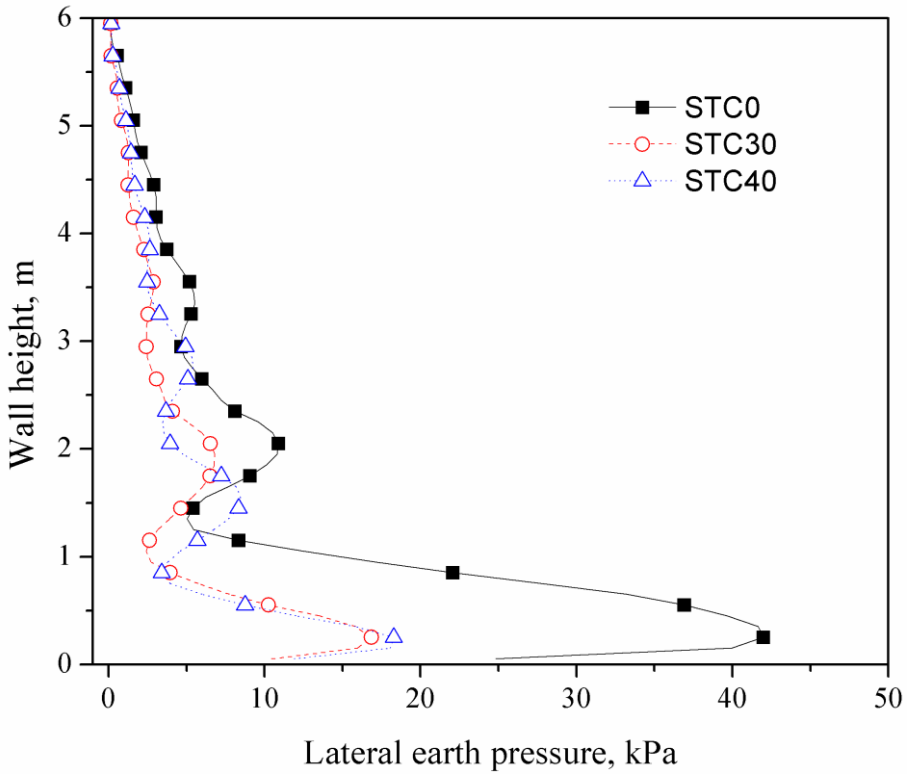

Fig. 6.12 Comparison of lateral earth pressures on wall

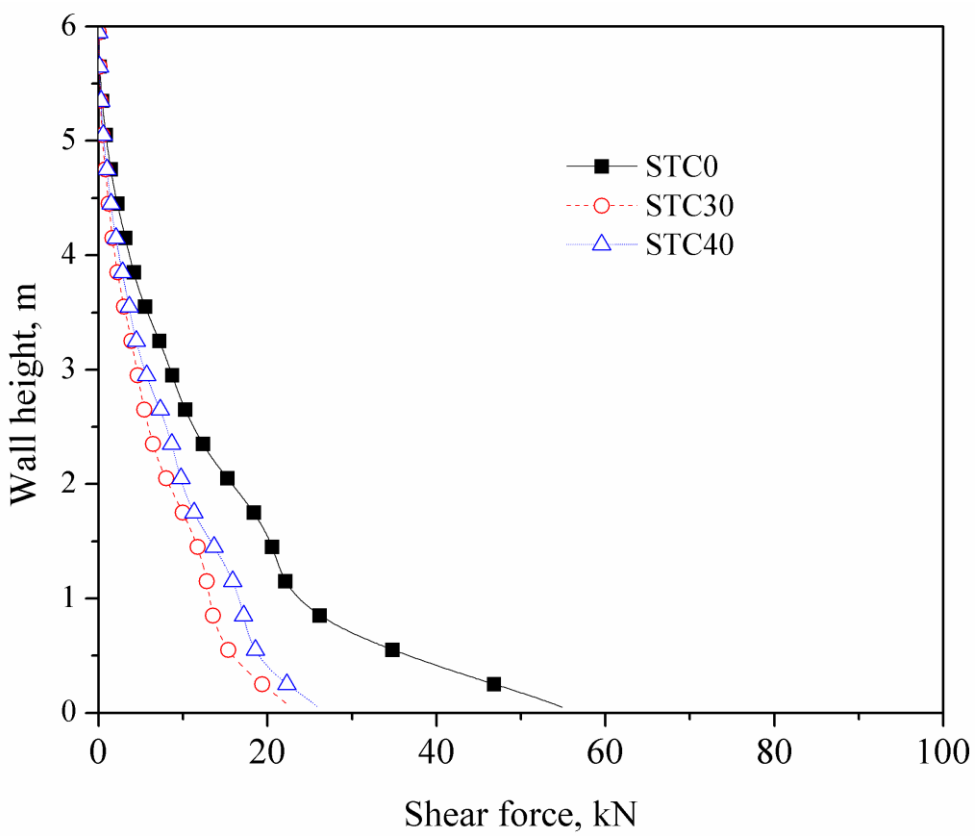

Fig. 6.13 Comparison of shear force of wall

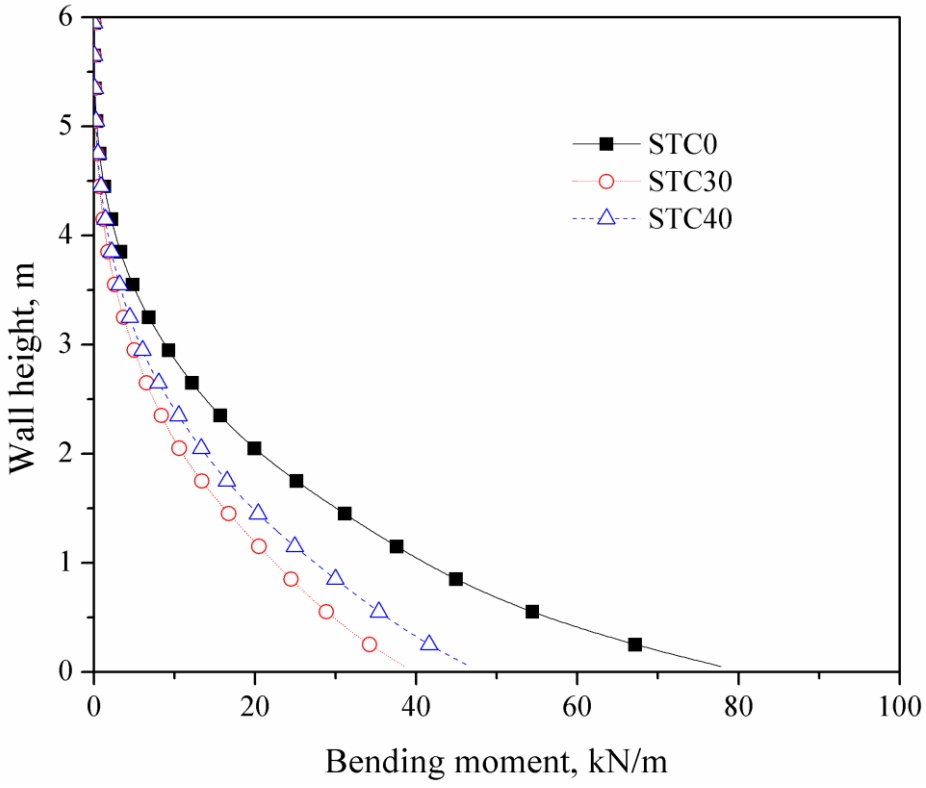

Fig. 6.14 Comparison of bending moment of wall

6.5.2 Effect of surcharge pressure

The full height of retaining wall models with five different surcharge pressures were considered to study the influence of surcharge pressure on displacements, lateral earth pressures, shear and bending moment of wall. The numerical test details are given in Table 6.2.

Table 6.2 Different surcharge pressures applied on model wall

Backfill	Surcharge pressure, kPa
STC0	10, 20, 20, 30, 40 and 50
STC30	

The variation of wall displacements and lateral earth pressures along the height of wall are presented in Fig. 6.15 and Fig. 6.16 for STC0. The figures show that, maximum displacements are observed at top of the wall and maximum lateral earth pressures are observed close to the base of the retaining wall.

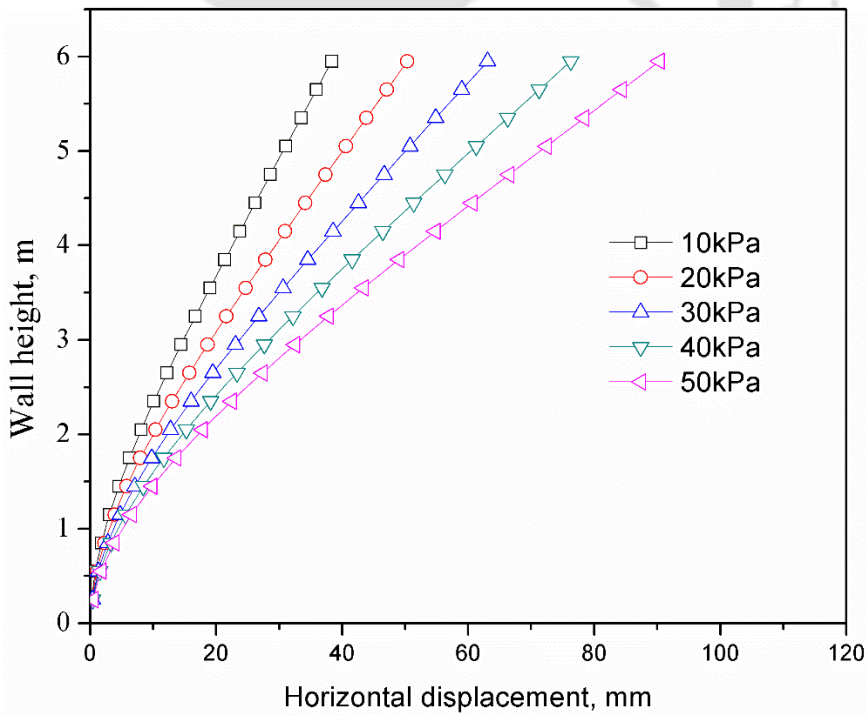

Fig. 6.15 Effect of surcharge pressure on horizontal displacements (STC0)

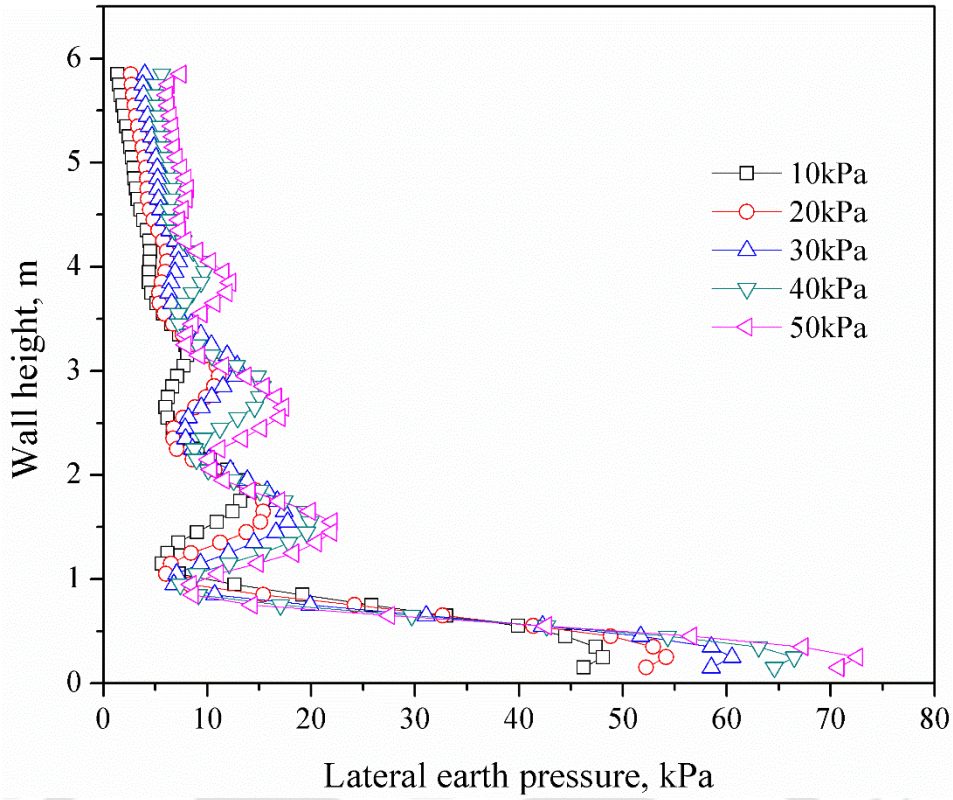

Fig. 6.16 Effect of surcharge pressure on lateral earth pressures (STC0)

By picking, the maximum values of displacements, earth pressures, shear forces and bending moments of wall models for different STC mixtures are shown in Fig. 6.17. Fig. 6.17 (a) shows the top displacements with different surcharge pressures for different STC mixtures. The horizontal displacements for STC0 backfill are 38.35 mm, 50.55 mm, 63.06 mm, 76.29 mm and 90.33 at top of wall near the facing at surcharges of 10 kPa, 20 kPa, 30 kPa, 40 kPa, and 50 kPa, respectively. The corresponding horizontal displacements values for STC30 backfill are 21.61 mm, 29.28 mm, 37.61 mm, 46.38 mm and 54.7 mm. Fig. 6.17(b) shows the maximum earth pressure values with different surcharge pressures for different STC mixtures Fig. 6.17(c) shows the maximum shear force values with different surcharge pressures for different STC mixtures. For STC0 backfill, the shear forces are 62.83 kN, 71.36 kN, 79.55 kN, 88.3 kN and 97.28 kN at bottom of wall for surcharge of 10 kPa, 20 kPa, 30 kPa, 40 kPa, and 50 kPa, respectively. For STC30 backfill, the shear forces are 27.07 kN, 31.98 kN,

36.85 kN, 42 kN and 46.8 kN. Fig. 6.17 (d) shows the maximum bending moment values with different surcharge pressures for different STC mixtures. Further maximum values with different surcharge pressures and its percentage reduction are reported in Table 6.3 and Table 6.4. From the figures and tables, it is concluded that STC30 mixture have lower values for all surcharge pressures in comparison to the control case with STC0.

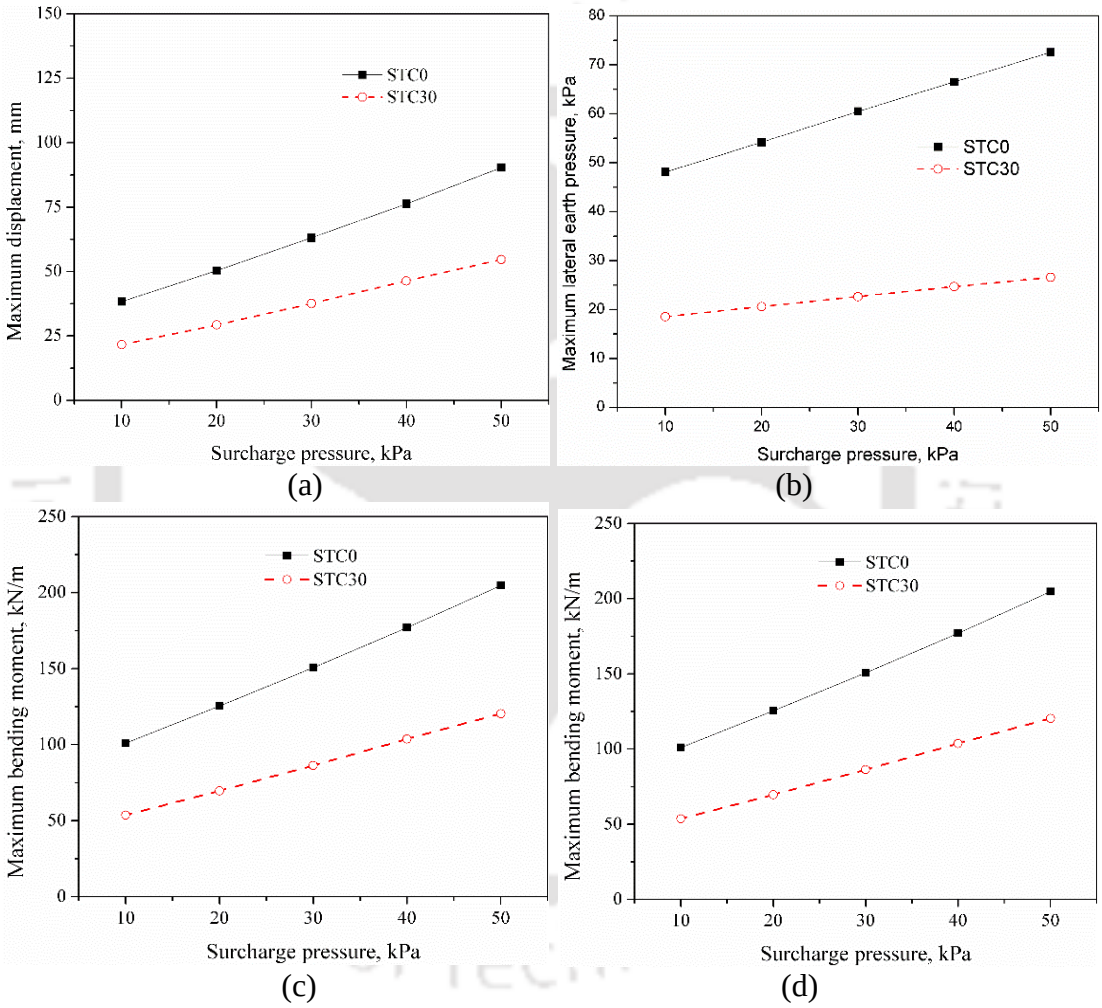

Fig. 6.17 Effect of surcharge pressure on model wall response: a) Top displacements; b) Maximum lateral earth pressures; c) Maximum shear forces; d) Maximum bending moments

Table 6.3 Maximum values of displacements, earth pressures and percentage reduction

Surcharge pressure, kPa	**Maximum displacements, mm**		**Percentage reduction**	**Maximum earth pressures, kPa**		**Percentage reduction**
	STC0	**STC30**		**STC0**	**STC30**	
10	38.35	21.61	43.65	48.08	18.58	61.35
20	50.33	29.28	41.82	54.16	20.61	61.95
30	63.06	37.61	40.36	60.52	22.65	62.57
40	76.29	46.38	39.20	66.5	24.7	62.85
50	90.33	54.7	39.44	72.57	26.57	63.39

Table 6.4 Maximum values of shear forces, bending moments and percentage reduction

Surcharge pressure, kPa	**Maximum shear forces, kN**		**Percentage reduction**	**Maximum bending moments, kN/m**		**Percentage reduction**
	STC0	**STC30**		**STC0**	**STC30**	
10	62.83	27.07	56.91	101	53.69	46.84
20	71.36	31.98	55.18	125.4	69.62	44.48
30	79.55	36.85	53.68	150.7	86.31	42.73
40	88.3	42	52.43	177	103.7	41.41
50	97.28	46.8	51.89	204.7	120.4	41.18

6.5.3 Effect of length of STC mixture zone (b)

The length of STC mixture zone (b) in the backfill is varied to see the sensitivity of STC30 mixture. The full-scale retaining wall with different length of STC30 mixture zone were considered (b/B ratios 0.1, 0.2, 0.3, 0.35, 0.4, 0.5 and 0.6) as shown in Fig. 6.18, where 'B' is total length of backfill.

The variation of the computed top horizontal displacements, bottom lateral earth pressures, bottom shear forces, and bottom bending moments of retaining wall with different b/B ratios are shown in Fig. 6.19. From the figure, maximum model response was found at b/B ratio of 0.0 (i.e. for sand alone case). By increasing b/B STC30 mixture zone, model response is decreased up to b/B of 0.25, after it reaching asymptotic value. It concluded that the optimum b/B ratio is in the range of 0.25 to 0.30.

This implies that even narrow backfill regions also can use STC mixture (STC30) to effectively improving the wall performance.

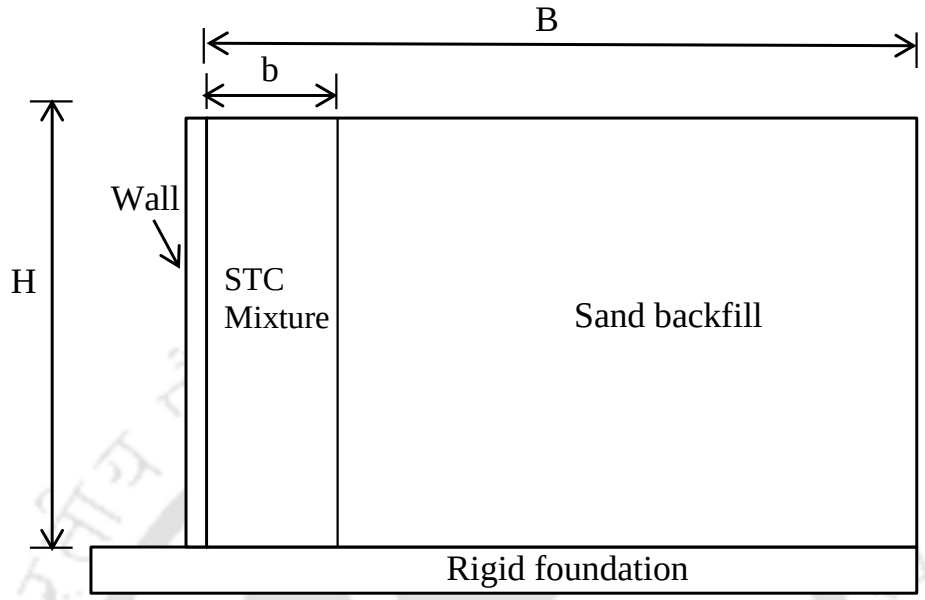

B = Total length of backfill; b = STC length; H = Height of wall

Fig. 6.18 Schematic diagram of sensitivity of the STC30 mixture width

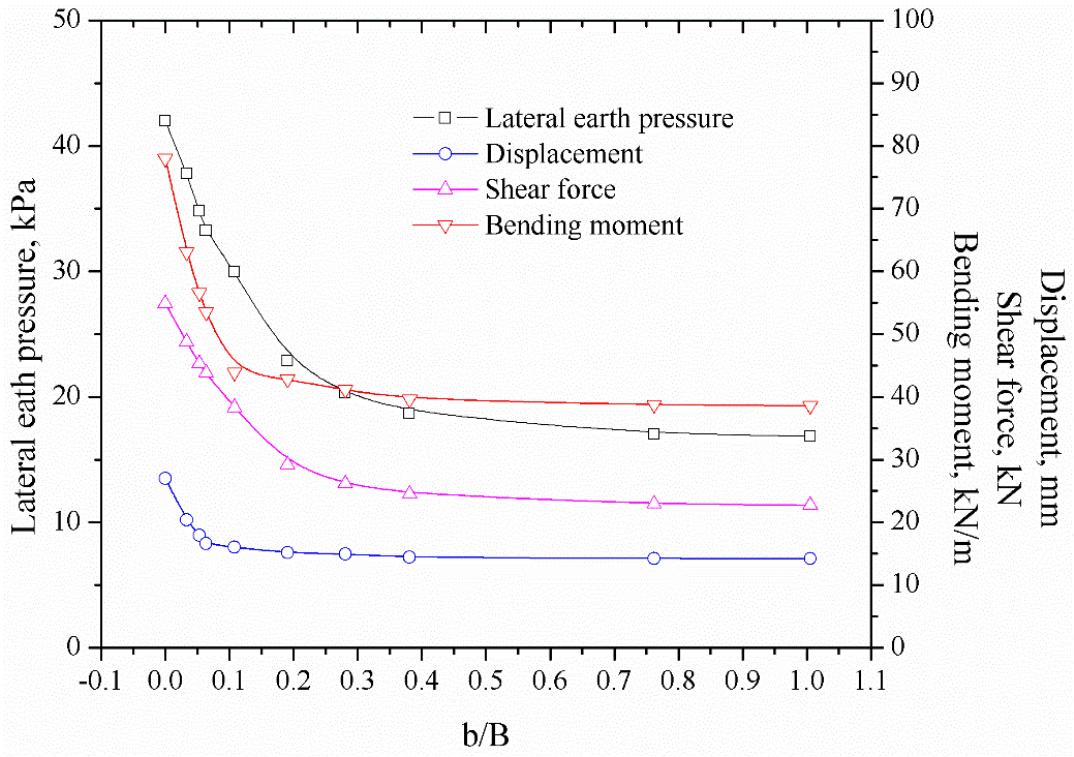

Fig. 6.19 Effect of backfill length of STC30 mixture

6.5.4 Effect of tire chips as compressible inclusion

To study the effect of compressible inclusion, tire chips used as compressible inclusion with different thickness. Thickness of compressible inclusion layer is considered as t/H (t = Thickness of tire chips compressible inclusion, H = Height of wall) and varied from 0.00 to 0.40. Fig. 6.20 shows the schematic diagram of wall. Fig. 6.21 presented the model reposne in terms of horizontal displacements and lateral earth pressures.

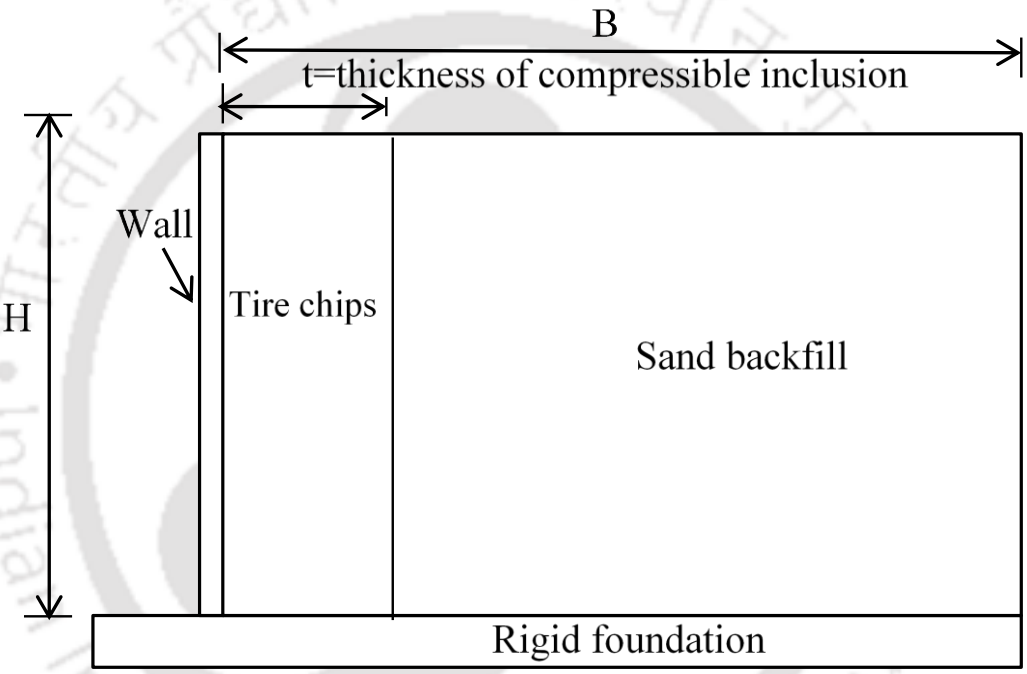

Fig. 6.20 Schematic diagram of model wall with compressible inclusion

Fig. 6.21 shows the effect of compressible inclusion layer thickness on maximum values of displacements and lateral earth pressures. Form the figure it is observed that thickness layer is significantly affecting on model response up to t/H =0.2. When recycled tire chips were used to partially replace the soil backfill, due to the lightweight and compressible nature of the tire chips, the soil thrust on the wall was reduced and thereby the wall displacements were reduced.

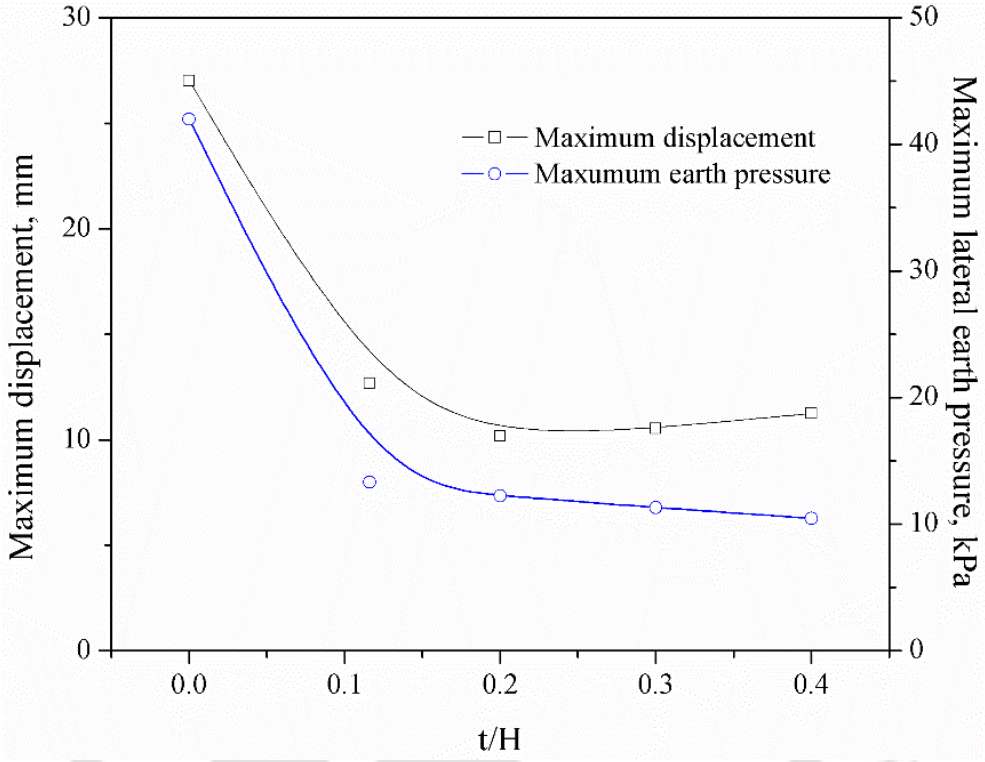

Fig. 6.21 Effect of tire chips as compressible inclusion

6.6 DYNAMIC RESPONSE OF RETAINING WALL

The full-scale retaining wall model was subjected to 20 cycles of sinusoidal dynamic excitation of 0.1*g* acceleration (*a*) at 3 Hz frequency (*f*). Typical variations of displacements with number of cycles of dynamic loading, at different elevations of backfill, are shown in Fig. 6.22. It is observed that the horizontal displacements were increasing nonlinearly with dynamic shaking as observed in the physical model tests.

6.6.1 Effect of frequency (f) of base excitation

Frequency (*f*) of excitation was varied from 3 Hz to 8 Hz at 0.1*g* base acceleration to examine the influence of frequency on the performance of retaining wall model with STC0 backfill. The responses of retaining walls along the elevation in terms of horizontal displacements, lateral earth pressures, shear force and bending moment are shown in Fig. 6.23.

.

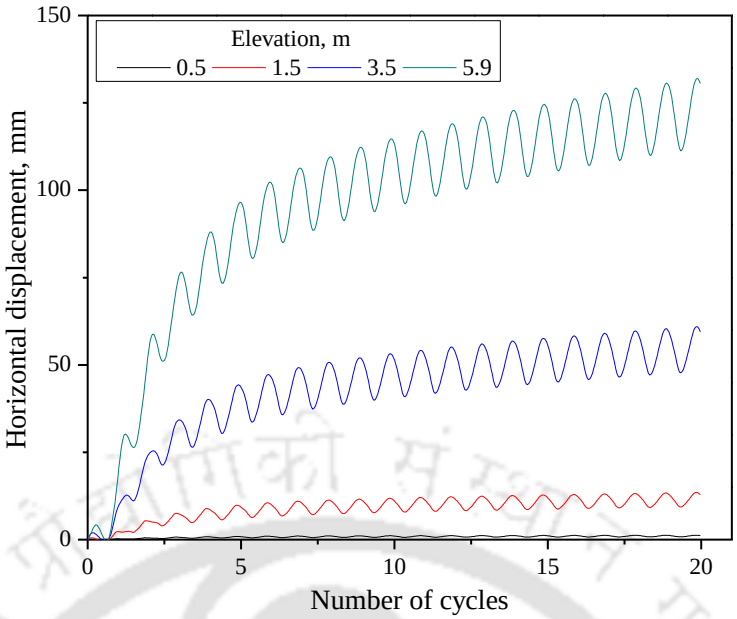

Fig. 6.22 Typical displacement histories at different elevation of wall

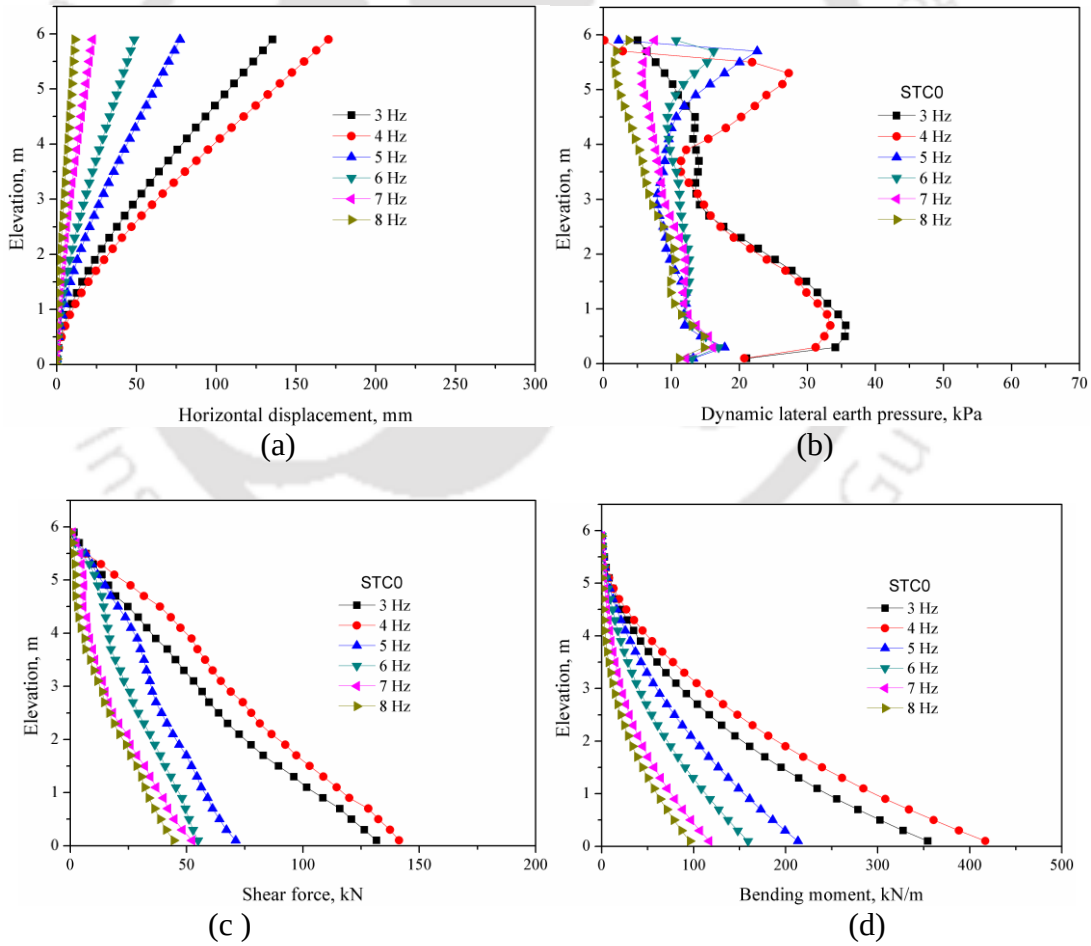

Fig. 6.23 Effect of frequency on wall (a=0.1g, f=3 – 8 Hz) : (a) Horizontal displacements, (b) Lateral earth pressures, (c) Shear forces, (d) Bending moments

Further, maximum displacement values are noted for different frequency of excitations, and shown in Fig. 6.24. The displacements at top of wall are 130 mm, 165 mm, 80, 50, 23 and 11.5 mm for model walls subjected to 3, 4, 5, 6, 7 and 8 Hz respectively. Maximum displacement was found at 4 Hz frequency.

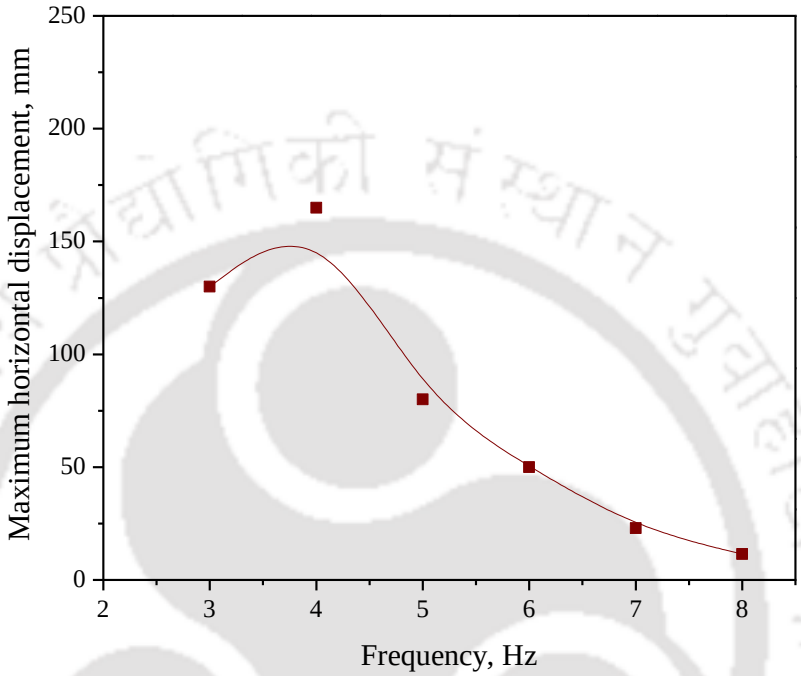

Fig. 6.24 Effect of frequency on maximum horizontal displacements of wall

Fig. 6.25 shows the maximum lateral earth pressures with different frequencies. The maximum incremental earth pressures at bottom of wall are 35.63, 33.36, 17.82, 16.93, 16.08 and 14.79 kPa for model walls subjected to 3, 4, 5, 6, 7 and 8 Hz, respectively. Maximum earth pressure was found at 3 Hz frequency at 0.1g acceleration.

Fig. 6.26 shows the maximum shear force with different frequencies. The shear force at bottom of wall are 131.6 kN, 141.3 kN, 71.11 kN, 54.93 kN, 52.39 kN and 44.43 kPa for model walls subjected to 3 Hz, 4 Hz, 5 Hz, 6 Hz, 7 Hz and 8 Hz respectively. Maximum shear force was found at 4 Hz frequency. Fig. 6.27 shows the maximum bending moment with different frequencies. Maximum bending moment of 416.9 kN/m was found at 4 Hz frequency.

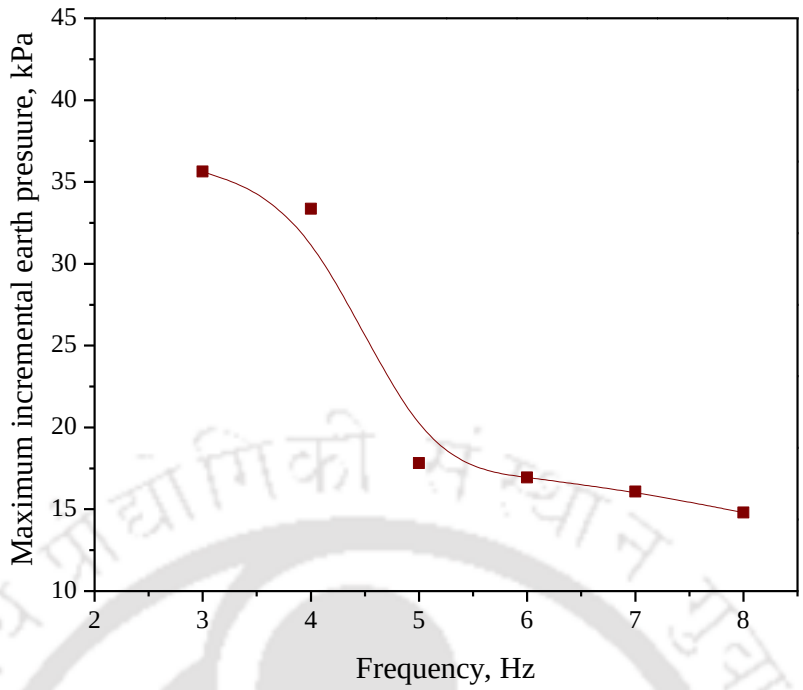

Fig. 6.25 Effect of frequency on lateral earth pressures on wall

The results indicate that frequency of excitation has significant effect on the response of the retaining wall in all the parameters. Among the range of frequencies considered, 4 Hz frequency excitation showed larger response. This may be due to the fundamental frequency of wall model. To confirm this, fundamental frequency (f_{11}) of the wall was calculated using closed-form solutions for two-dimensional problems as per Wu (1994) Equation (Eq.6.1).

$$f_{11} = \sqrt{1 + \frac{H}{B}\left[\frac{1}{2-\upsilon}\right]} \times \frac{1}{4H}\sqrt{\frac{G}{\rho}} \qquad \text{Eq. 6.1}$$

Where, H= height (6.0 m); B = width (5.8 m); G = shear modulus (11380 kPa); ρ = density of soil (1587 kg/m^3) and υ = Poisson's ratio (0.3); all values are corresponding to the sand medium. The fundamental frequency of model wall has been

evaluated as 4.2 Hz. This indicates that frequency of the input motion is close to the fundamental frequency of the wall that resulted in higher wall responses.

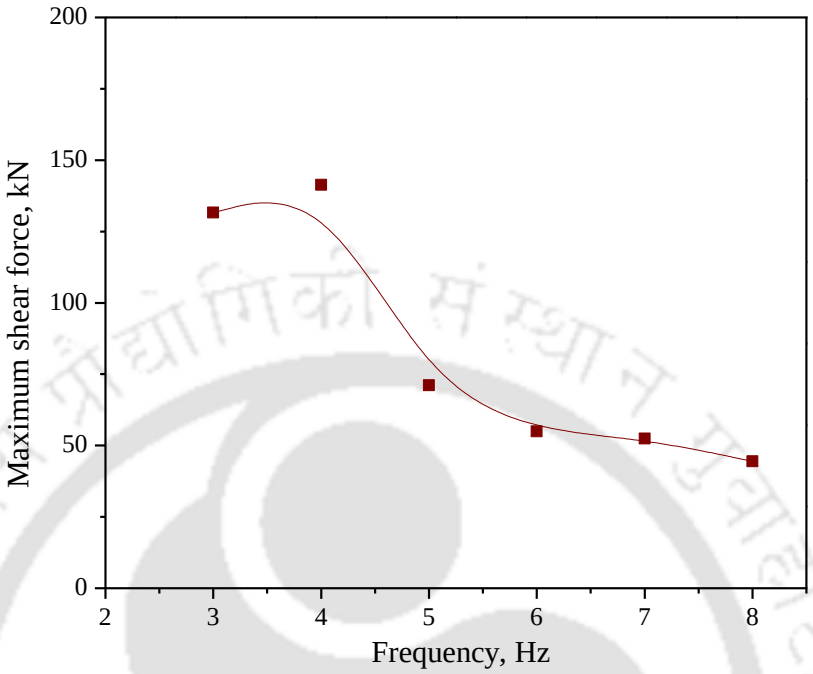

Fig. 6.26 Comparison of shear force with frequency

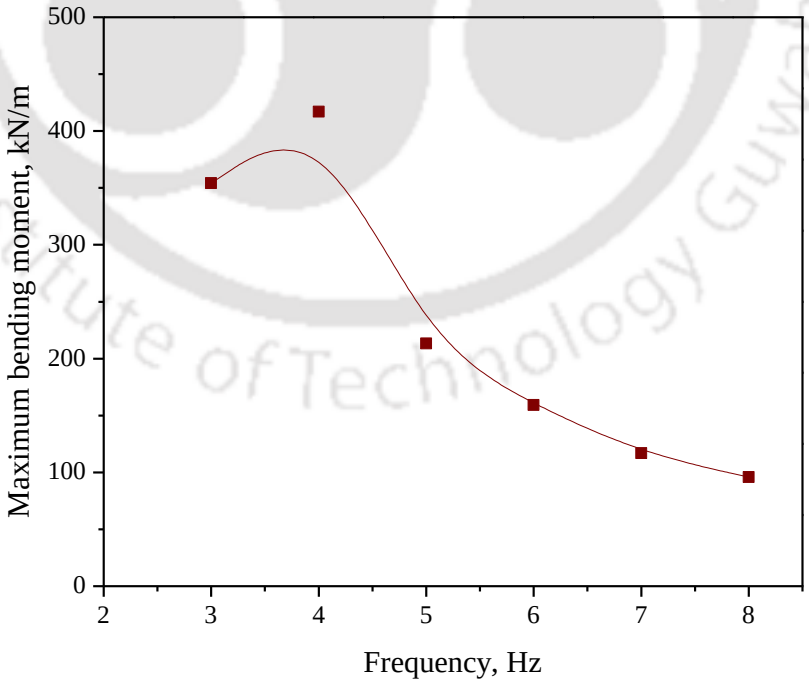

Fig. 6.27 Comparison of bending moment with frequency

6.6.2 Effect of base acceleration (a) of base excitation

The model walls subjected to 20 cycles of dynamic excitation with accelerations of 0.1*g*, 0.2*g*, 0.3*g*, 0.4*g*, 0.5*g* and 0.6*g* at 4 Hz frequency are considered to examine its influence on the performance of retaining walls. As discussed in the previous sections, maximum displacements were found at top and maximum dynamic earth pressures, shear forces and bending moments were found at bottom of the wall. Fig. 6.28 shows maximum displacements and maximum dynamic earth pressures with different base accelerations. The horizontal displacements (STC0 backfill) are 170.3 mm, 317.4 mm, 427.1 mm, 502.4 mm, 558.0 mm and 594.1 mm at top of wall for input accelerations of 0.1*g*, 0.2*g*, 0.3*g*, 0.4*g*, 0.5*g* and 0.6*g*, respectively. The maximum lateral earth pressures (STC0 backfill) are 33.3 kPa, 55.03 kPa, 76.4 kPa, 97.8 kPa, 114.5 kPa and 131.8 kPa at input acceleration of 0.1*g*, 0.2*g*, 0.3*g*, 0.4*g*, 0.5*g* and 0.6*g*, respectively. The lateral earth pressures are increased with increase in input accelerations, due to more inertia force at higher accelerations. Fig. 6.29 shows maximum shear forces and bending moments with different base accelerations. The maximum bending moments (STC0 backfill) are 416.9 kN/m, 732.7 kN/m, 999.9 kN/m, 1211 kN/m , 1370 kN/m and 1481 kN/m at input acceleration of 0.1*g*, 0.2*g*, 0.3*g*, 0.4*g*, 0.5*g* and 0.6*g*, respectively. The bending moments are followed nonlinear trend with increasing base acceleration of excitation. Similar type of trend was found for STC30 mixture backfill case. From this, it is observed that, shear forces on wall are increased with increase in input accelerations, due to more inertia force at higher accelerations.

6.6.3 Effect of STC mixtures

Three different STC mixtures (STC0, STC30 and STC40) were considered to study the effect of STC mixture on dynamic response of full-scale model walls. The variation of the computed horizontal displacements, vertical displacements and lateral

earth pressures (a= 0.1g and f= 4Hz) along the wall are shown in Fig. 6.30 and Fig. 6.31. The computed results show that the retaining wall with STC30 backfill exhibits smaller displacements (horizontal and vertical), lateral earth pressures along the wall than the STC0 and STC40 backfill. The maximum horizontal displacement observed at the top of the wall is about 170.3 mm for STC0 backfill, whereas it is decreased to about 74.75 mm at STC30 backfill. From the Fig. 6.30(b), the maximum vertical displacement observed at the near face of the wall is about 65.22 mm for STC0 backfill, whereas it is decreased to about 30.57 mm at STC30 backfill.

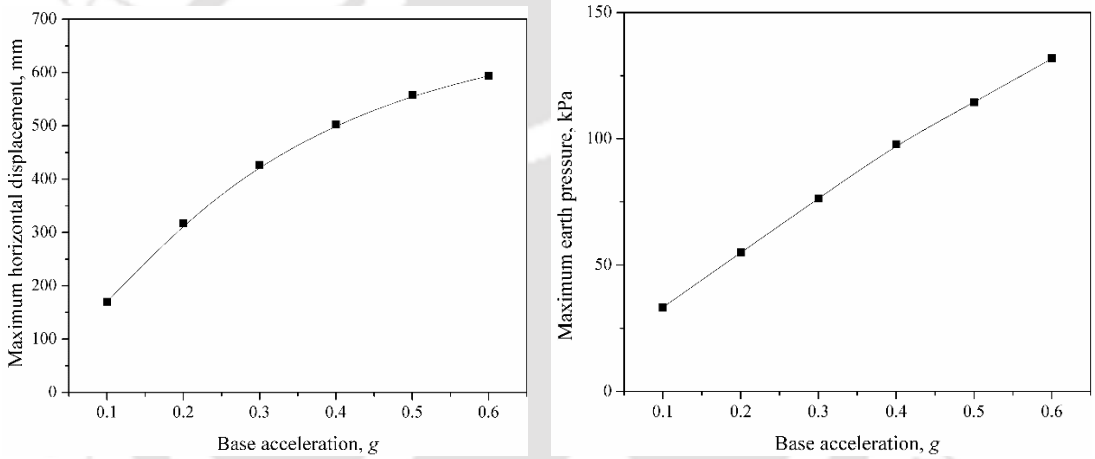

(a) (b)

Fig. 6.28 Effect of base acceleration; (a) Horizontal displacements, (b) Lateral earth pressures on wall

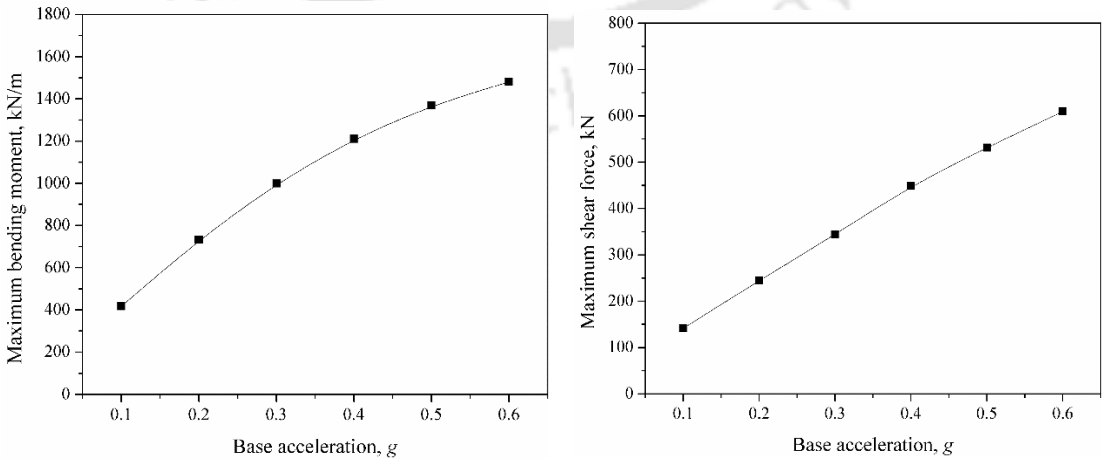

(a) (b)

Fig. 6.29 Effect of base acceleration; (a) Bending moments, (b) Shear forces

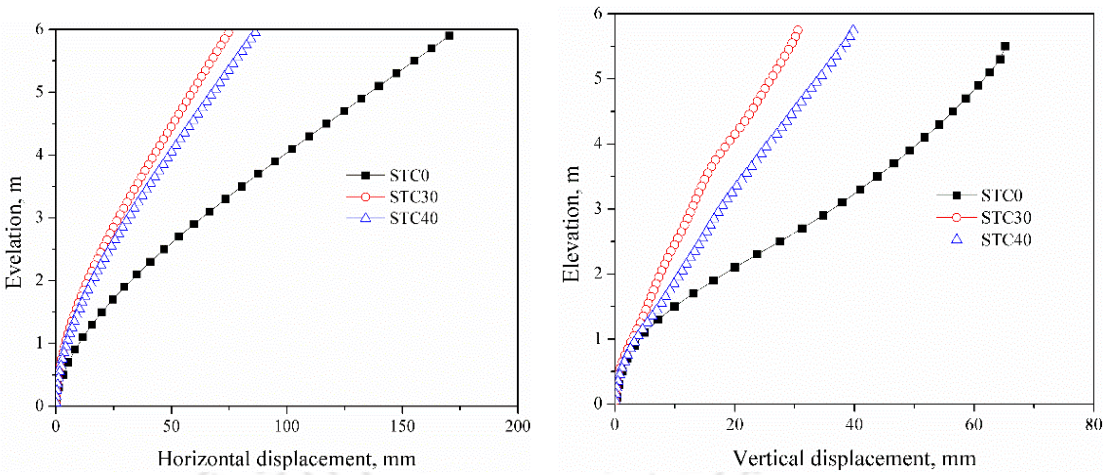

(a) (b)

Fig. 6.30 Comparison of displacements with different STC mixtures (*a*= 0.1g and *f*= 4Hz): (a) horizontal displacement profile, (b) vertical displacement profile

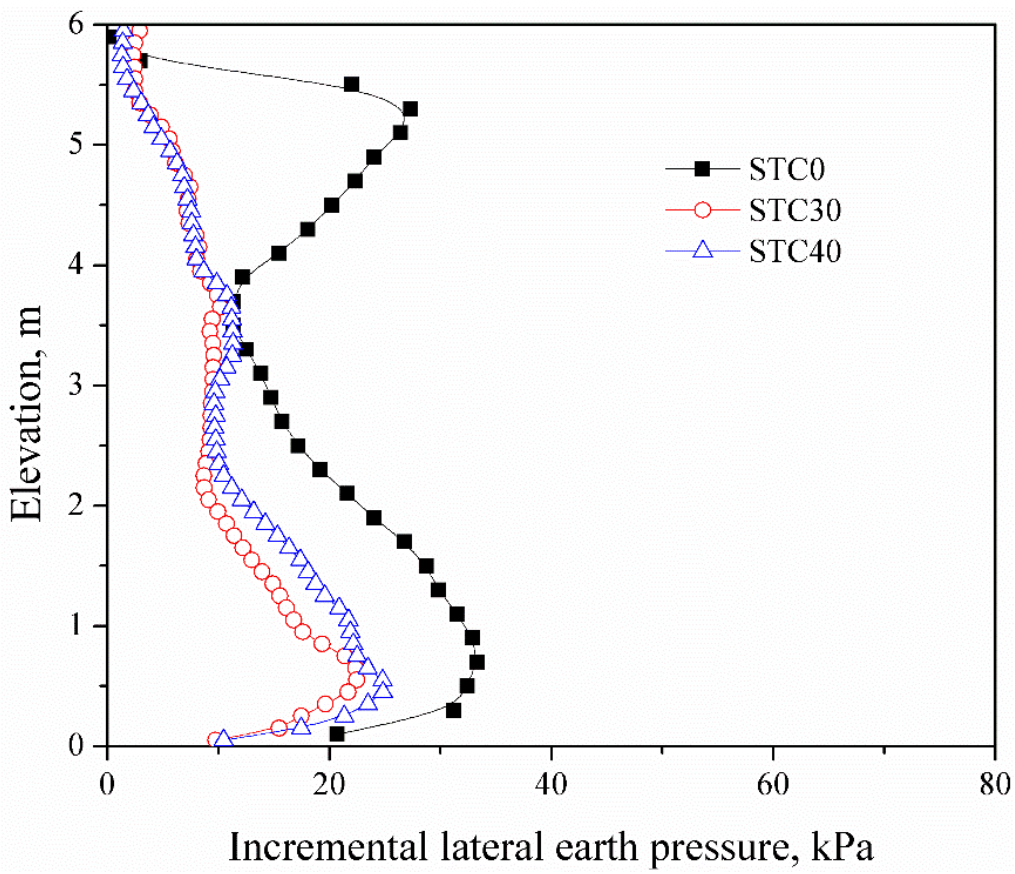

Fig. 6.31 Comparison of lateral earth pressures with STC mixtures (*a*= 0.1g and *f*= 4Hz)

Shear force and bending moment profiles of wall with different STC mixtures are shown in Fig. 6.32 and Fig. 6.33, respectively. Maximum shear force and bending moment are occurred at bottom of the wall and lesser values are observed for STC30

mixture backfill material. The maximum bending moments observed at the bottom of the wall is about 416.9 kN/m for STC0 backfill, whereas it is decreased to about 193.4 kN/m at STC30 backfill. Due to lesser lateral earth pressures, shear force and bending moment values are reduced.

6.6.4 Effect of surcharge pressure

Seven different surcharge pressures (10 kPa, 20 kPa, 30 kPa, 40 kPa, 50 kPa, 70 kPa, and 150 kPa) and two backfills (STC0 and STC30 mixture) were considered at 0.1*g* base acceleration (*a*) and frequency (*f*) of 4 Hz, to study the influence of surcharge pressure on wall response.

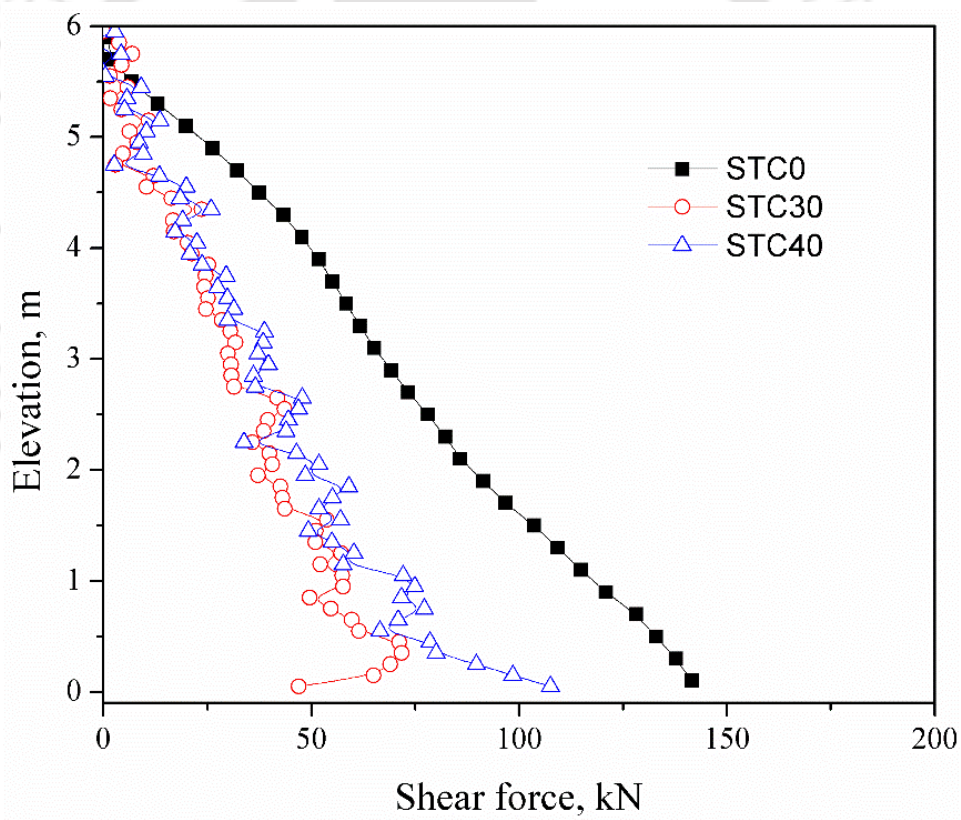

Fig. 6.32 Comparison of shear forces with STC mixtures

Fig. 6.34 shows maximum displacements and maximum dynamic earth pressures with different surcharge pressures. According to Fig. 6.34, increase of surcharge pressure causes a nonlinear increase in horizontal displacements of wall and

dynamic lateral earth pressures. Fig. 6.35 shows maximum shear forces and bending moments with different surcharge pressure. It is observed that higher values were found at higher surcharge pressures. According to Fig. 6.35, increase of surcharge pressure causes a nonlinear increase in shear forces and bending moments.

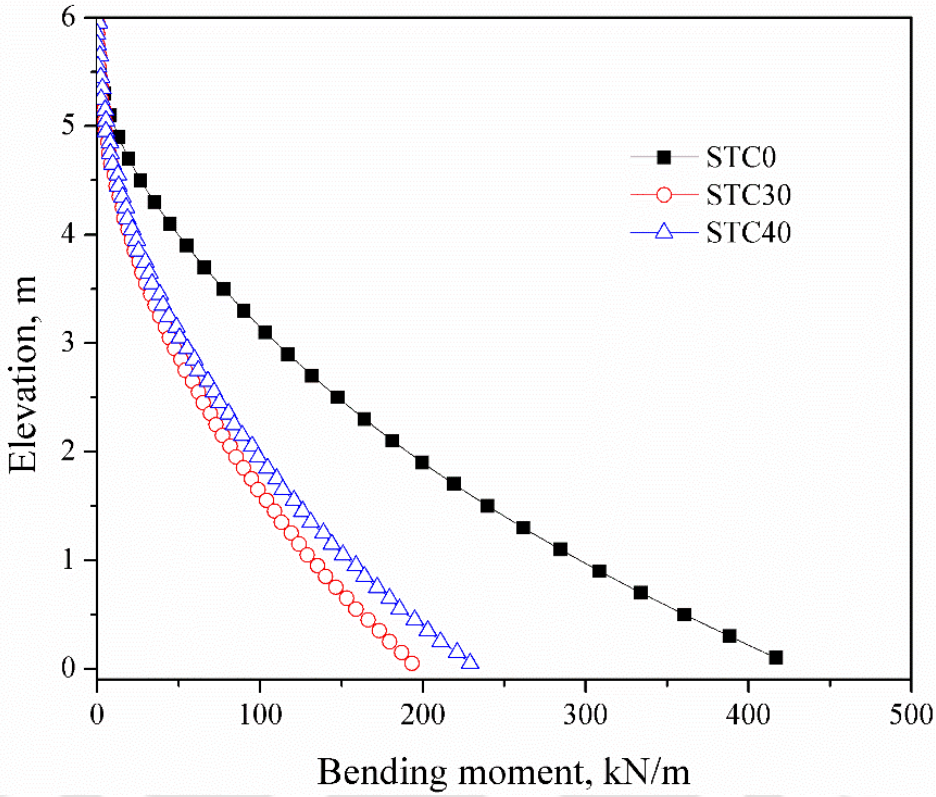

Fig. 6.33 Comparison of bending moments with STC mixtures

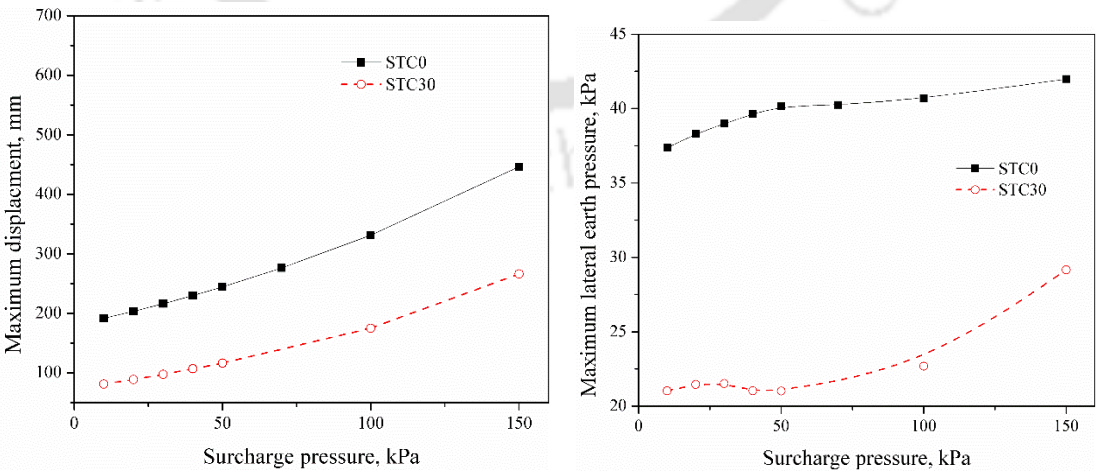

(a) (b)

Fig. 6.34 Effect of surcharge pressure; (a) Horizontal displacements, (b) Lateral earth pressures

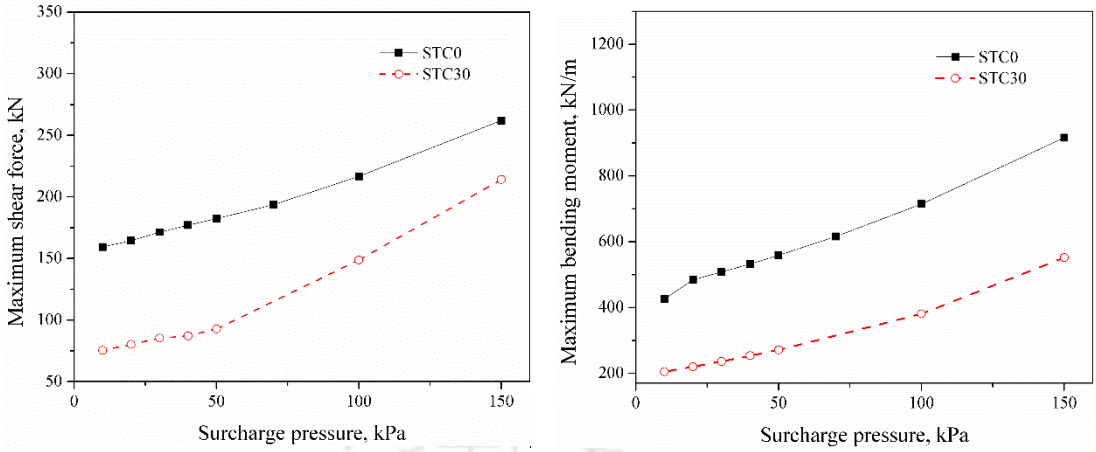

(a) (b)

Fig. 6.35 Effect of surcharge pressure; (a) Shear forces, (b) Bending moments

6.7 NUMERICAL STUDY ON CANTILEVER RETAINING MODEL WALLS

Numerical cantilever retaining wall models have been developed using finite difference programme FLAC^{2D} to simulate the physical model walls reported by Reddy et al. (2014) and Dammala et al. (2015).

6.7.1 Target physical model

Physical model tests on cantilever retaining wall models reported by Reddy et al. (2014) and Dammala et al .(2015) are considered for development of numerical model. The target physical models, tested under static case, were 800 × 580 mm plan area and 600 mm height (H). The wall model (stem and base) was built with 6 hollow aluminum sections of each 100 mm × 50 mm in cross section and 600 mm long. The aluminum sections which were placed one over the other and run through 12 mm diameter steel rods that were bolted at top and bottom panels as shown in Fig. 6.36. The model wall has been placed in a Perspex container box of dimensions of 1200 mm x 600 mm and 1000 mm height providing a backfill width of 800 mm as shown in Fig. 6.37. Thickness of foundation bed and the depth of embedment were maintained as 200

mm, which is 33% of the height of the wall to represent typical field conditions. STC mixtures were prepared by manual mixing to maintain the selected TC percentage levels and are filled only in the backfill with the foundation and embedment having filled with sand. A horizontal frame has been used to arrest the movements of the wall during backfilling. Backfilling was done in six layers of 100 mm depth each by maintaining uniform compaction effort for each layer in such a way that the calculated backfill mass fills the backfill volume. The static loading has been applied up to 10 kPa using concrete cubes on a solid wooden platform on the surface of backfill for uniform distribution of the surcharge load on the backfill. Results obtained through various instrumentations were discussed by Dammala et al. (2015) in terms of wall horizontal displacements and lateral earth pressures. The details about the test configurations with location of various instrumentations are shown in Fig. 6.37.

Fig. 6.36 Typical model wall (Dammala et al. 2015)

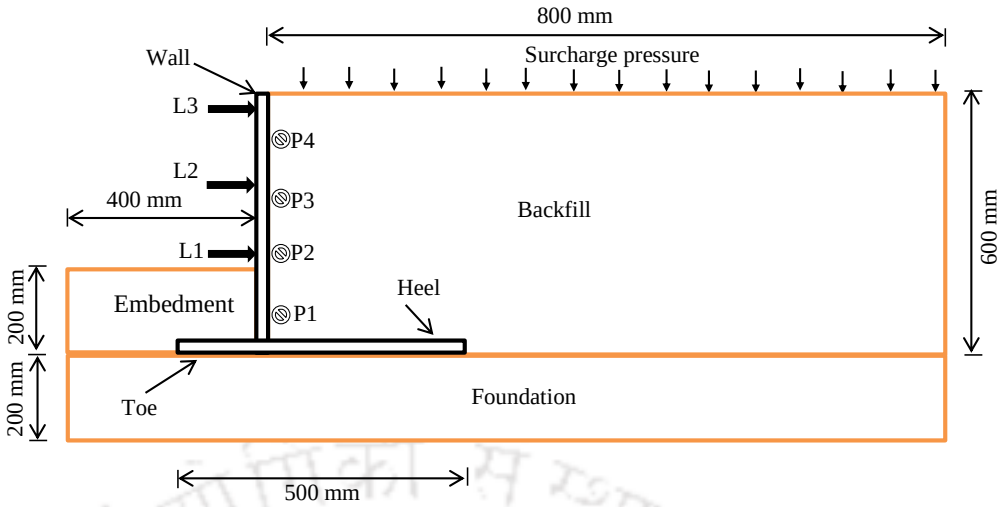

Fig. 6.37 Schematic diagram of cantilever retaining wall model

6.7.2 Development of numerical cantilever retaining wall

The numerical model was developed to simulate the static response of cantilever retaining wall and validated by comparing with the results of physical model tests. The material properties considered in the numerical model are reported in Table 6.1. The stem, toe and heel material were considered as elastic material using beam elements with Young's modulus of 69 MPa and unit weight of 78 kPa.

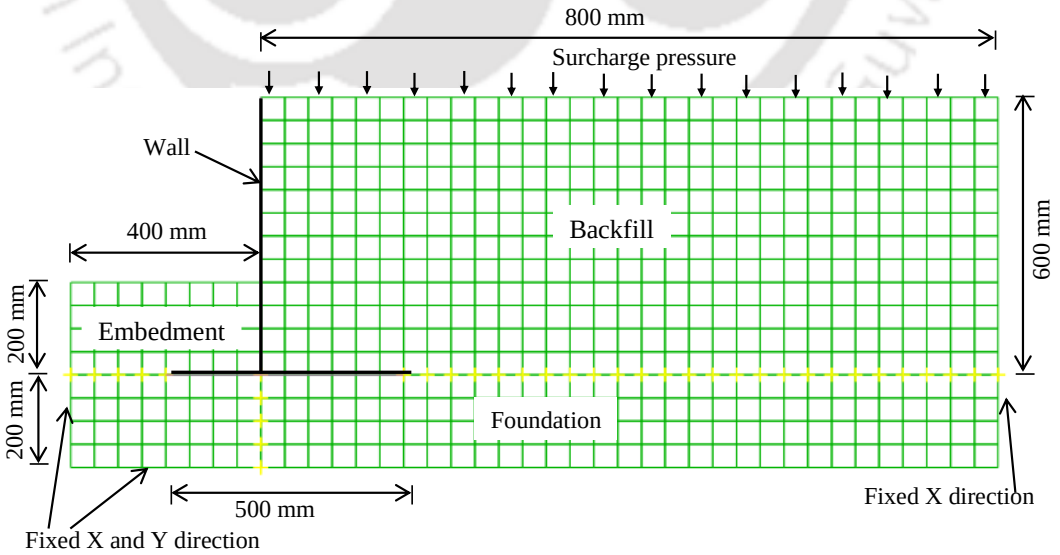

Fig. 6.38 Numerical grid of cantilever retaining wall model

6.7.3 Validation of numerical cantilever retaining wall model

Fig. 6.39 shows the model test results of physical and numerical model wall (STC0 backfill). The figures demonstrate that numerical model results are reasonably acceptable with physical tests results.

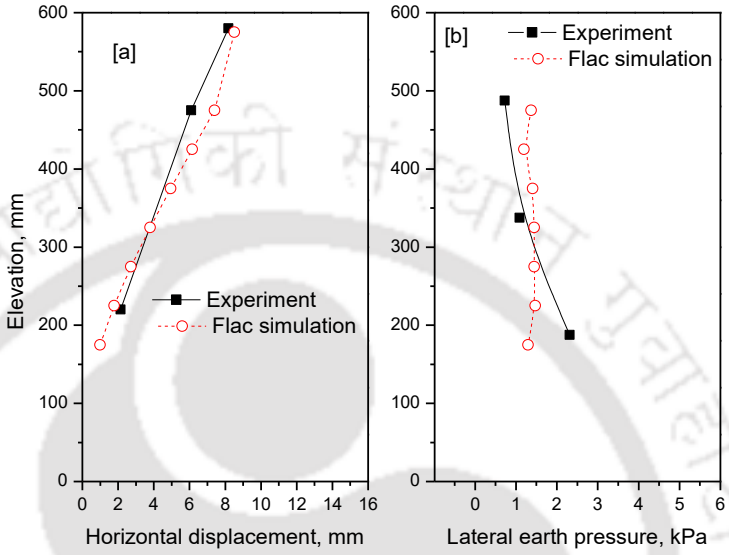

Fig. 6.39 Validation of cantilever retaining wall model

6.8 RESPONSE OF FULL SCALE CANTILEVER WALL MODELS

Static behaviour of a full-scale cantilever retaining wall model of 6 m high (H) and 18 m long (Fig. 6.40) is studied, using the validated numerical model. The model parameters were kept same as that of laboratory model. Retaining wall response measured in terms of lateral earth pressures and horizontal displacements are discussed.

6.8.1 Effect of STC mixtures

Different STC mixtures (STC0, STC30 and STC40) were considered to study the effect of STC mixture as backfill material in cantilever model walls. The variation of the computed horizontal displacement and the lateral earth pressure along the wall are shown in Fig. 6.41 and Fig. 6.42, respectively. The computed results show that the

retaining wall with STC30 backfill exhibits smaller displacements and lateral earth pressures along the wall than the STC0 and STC40 backfill walls.

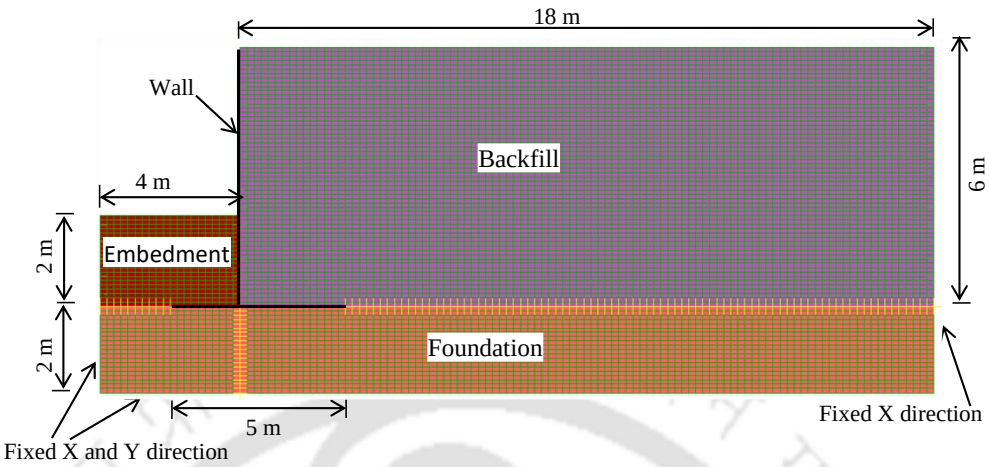

Fig. 6.40 Numerical diagram of full-scale cantilever retaining wall model

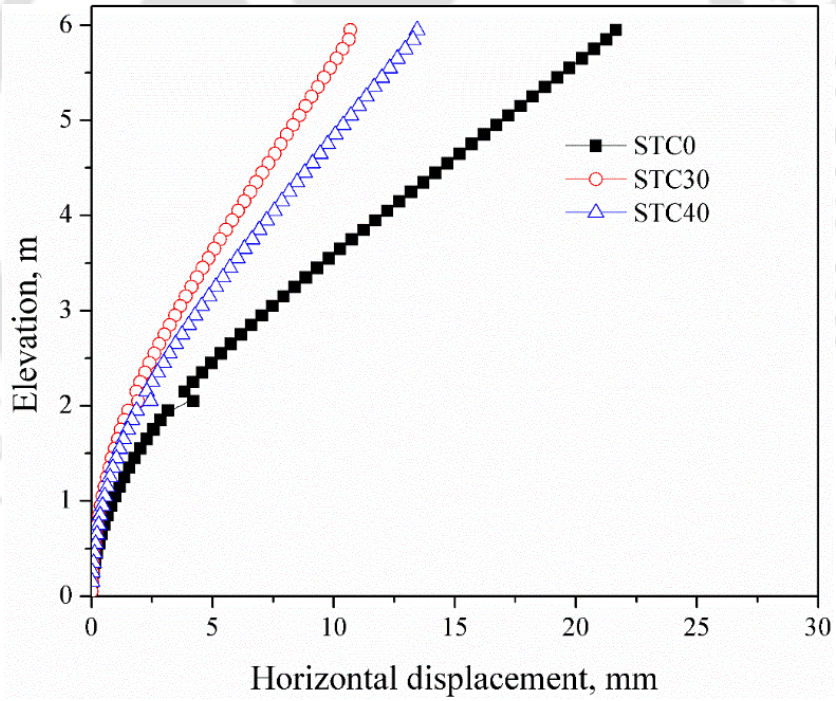

Fig. 6.41 Effect of STC mixture on cantilever wall: Displacement profile

6.8.2 Effect of STC30 zone

Different STC30 zones with, in terms of different slope angles values, 20°, 45°, 60°, 70° , and 80° (as shown in Fig. 6.43) are considered to study the effect of extent of

STC30 mixture zone on the wall behaviour. The response of model wall in terms of horizontal displacements and lateral earth pressures be with different backfill conditions are reported in Table 6.5. From the table it may concluded that, STC30 slope 80 deg is sufficient to control the wall displacements and earth pressures.

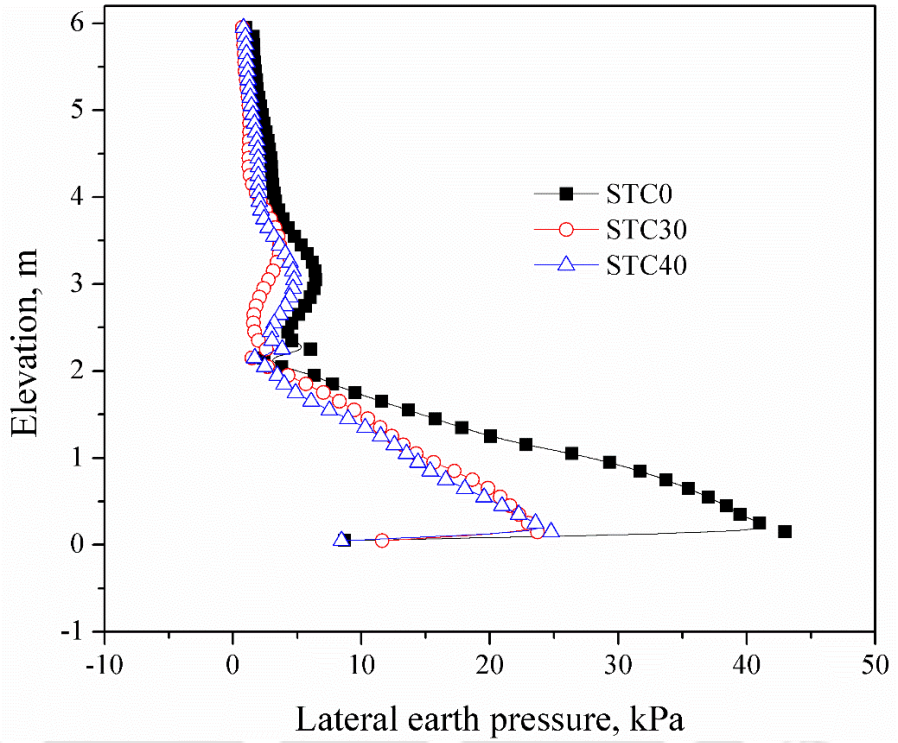

Fig. 6.42 Effect of STC mixture on lateral earth pressure profile of cantilever wall

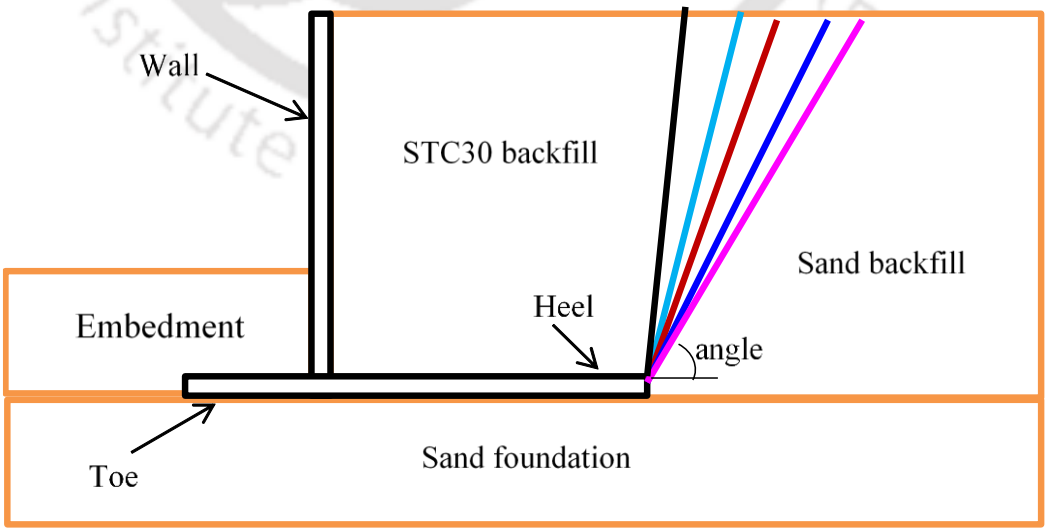

Fig. 6.43 Schematic diagram of sensitivity of the STC30 mixture

Table 6.5 Maximum values of displacements and earth pressures

Backfill (or) Slope from foundation	Horizontal displacement, mm	Lateral earth pressure, kPa
STC0	21.66	42.98
80	11.41	27.66
70	11.3	27.63
60	11.34	27.33
45	11.33	27.06
20	11.12	26.23
STC30	10.69	23.67

6.9 SUMMARY

Numerical models are developed and validated to simulate laboratory model walls. The calibrated numerical models were utilized to develop full-scale numerical models. The flowing conclusion are drawn from the numerical study.

- The developed numerical model for laboratory scale wall is reasonably simulated the static and dynamic responses.
- Full-scale wall response in terms of displacement and earth pressures are significantly changed up to b/B ratio of 0.25. This can be implies that even narrow backfill regions also use of STC30 can be effectively improve the wall performance.
- Retaining wall response was significantly changed when tire chips were used as compressible inclusion (*t*). Model response was decreased up to t/H of 0.2, reached asymptotic value.
- Retaining wall is amplitudes at frequency close to the fundamental frequency of the wall will be amplified by the most.
- Nonlinear behaviour of wall response was observed when increasing base acceleration.

Chapter 7. DESIGN AND COST BENEFIT ANALYSIS OF RETAINING WALLS

7.1 INTRODUCTION

In this chapter, the design and cost benefit analysis of retaining wall systems with STC mixtures as backfill materials are presented. Design of two retaining wall systems with heights of 3 m, 6 m, and 9 m using sand (STC0) and STC30 mixture as backfill materials and their cost implications has been presented for comparison purpose. The details about the material properties, design of retaining walls, and cost benefit analysis discussed in the following sections.

7.2 OPTIMUM MIXING RATIO OF STC MIXTURE

The characterizations of different STC mixtures are presented in Chapter 3. Different STC mixtures (0 to 100% of tire chips by weight) were considered to find the index and engineering properties. Tire chips of 10 × 10 mm size and about 20 mm length, obtained from scraped tires, and locally available poorly graded sand were used. Properties of STC mixtures i.e. void ratio, unit weight and angle of friction value of STC mixtures are shown in Fig. 3.15. From the figure, it can be inferred that the optimum mixing ratio of STC mixture is 30 % where higher friction angle value and lower void ratio are observed. Further, it can also be seen from the figure that at the optimum mixing ratio of the STC mixture, the unit weight was reduced by nearly 20%. These observations show that STC mixtures can effectively work as lightweight material as well as provide better compressibility characteristics (due to lesser void ratio) and high load-carrying behavior (due to high shear strength) for geoengineering applications. The behaviour of retaining wall models backfilled with different STC

mixtures under static and seismic loading conditions were discussed in Chapter 4. The displacement profiles and incremental earth pressures, for the model walls with different backfill materials (STC0 – STC50), indicated that by using STC30 backfill, about 50–60 % reduction in earth pressures and displacements was achieved.

Based on the observed material properties as well as static and dynamic behaviours of retaining wall model with different backfills, STC30 backfill depicted the better performance hence considered to be the optimum mix material. To evaluate the financial benefits in the construction of retaining wall with STC0 (sand) and STC30 mixture as the backfill material were considered. Wall design including the structural designs and cost benefit analyses are presented in the following sections.

7.3 DESIGN OF RETAINING WALLS

The retaining wall systems were designed using two backfill materials (sand and STC30) and compared in terms of dimensions of the wall, backfill volume, backfill material cost, reinforcement, and total cost of retaining wall. Cantilever retaining walls backfilled with sand (STC0) and STC30 mixture have been adopted for evaluating the financial benefits. The design of this wall consists of two parts: (1) the geotechnical design, and (2) the structural design. Cost benefit analysis of both the wall systems has been carried out after arriving final designs of two retaining wall systems. The purpose of cost analysis is to assess the economic feasibility of the proposed retaining wall system with the STC30 mixture as backfill. The properties of STC0 and STC30 are obtained from chapter 3 and reported in Table 7.1. In the design of both the wall systems, the wall friction has been assumed as two-thirds of the friction angle.

Table 7.1 Properties of sand and STC30

Backfill Properties	STC0 (Sand)	STC30
Unit weight (kN/m^3)	15.57	13.17
Angle of internal friction	48°	56°

The retaining wall dimensions have been initially assumed (as per Bowles, 1996) as shown in Fig. 7.1. Stability analyses against sliding and overturning have been done by determining the active earth pressures using the unit weight and friction angle results for the STC0 and STC30 (Table 7.1) along with the Coulomb's method. Once the earth pressures were determined, the trial dimensions provided by Bowles (1996) were used to determine the dimensions of the retaining walls with the STC0 and STC30 backfills that could provide the minimum factor of safeties for overturning, and sliding. This included the minimum factor of safety of 2.0 (IS 14458, 1997). The retaining walls dimensions were changed by trial until they met the minimum factors of safety for overturning, and sliding. The factor of safety against sliding is the ratio of horizontal resisting forces divided by the horizontal driving forces. The factor of safety against overturning is the ratio of the resisting moment and overturning moment. As presented in Table 7.2, the retaining wall dimensions were able to be reduced to lower values when STC30 was considered in the backfill, while still meeting the minimum factors of safety presented in Table 7.3.

When comparing the retaining wall dimensions for different heights, it can be seen in Table 7.2, that the size of the retaining walls decreased as 30 % of tire chips was added to the sand. This is the direct result of the decrease in unit weight and increase in friction angle for STC30 in comparison to STC0 (sand). In the Coulomb Pressure Theory as the unit weight decreased and the friction angle increased, the lateral active earth pressures against the wall decreased. Therefore, the lower earth pressure was observed in the STC30 mixture backfill, resulting in the smallest wall dimensions.

Further, the reduction of earth pressure allowed the reinforced concrete volume to be largely reduced. Both the wall systems with the assumed base widths were found to be safe against both the stability criteria. Once the dimensions of the retaining wall are satisfactory with respect to geotechnical stability, the structural design of stem, toe slab and heel slab have been carried out.

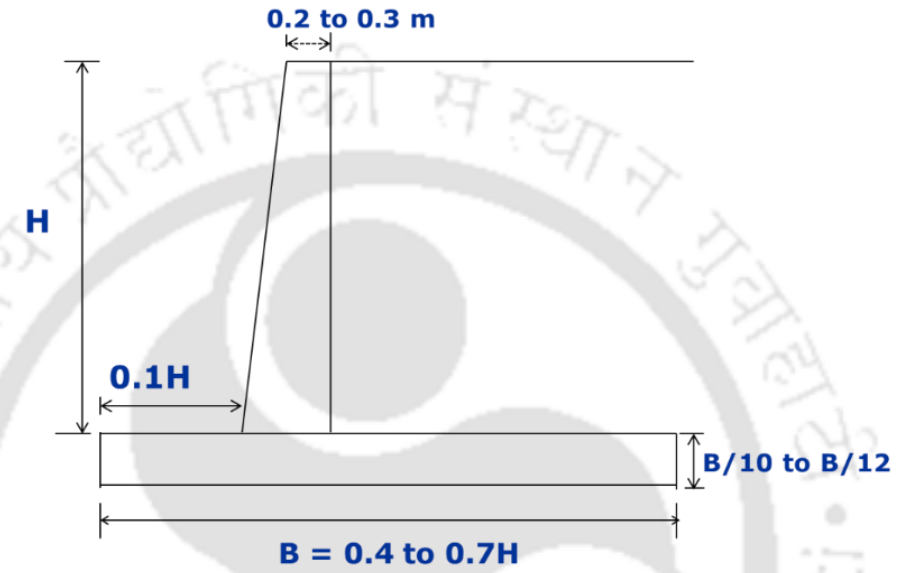

Fig. 7.1 Tentative dimensions of cantilever retaining wall (after Bowles, 1988)

Table 7.2 Final dimensions of retaining walls

Retaining wall parts	3 m		6 m		9 m	
	Sand	STC30	Sand	STC30	Sand	STC30
Stem top width, m	0.2	0.2	0.2	0.2	0.2	0.2
Toe length, m	0.3	0.3	0.6	0.6	0.9	0.9
Heel length, m	0.6	0.3	1.4	1.0	2.0	1.5
Base length, m	1.15	0.9	2.35	1.9	3.5	2.9
Base thickness, m	0.2	0.15	0.4	0.4	0.9	0.65

Table 7.3 Comparison of factors of safety

Height of wall (m)	Sliding factor of safety		Overturning factor of safety	
	Sand	STC30	Sand	STC30
3	2.77	4.12	2.05	2.00
6	2.69	3.97	2.04	2.03
9	2.59	3.92	2.0	2.08

Various related stipulations and clauses of IS 456 (2000) and SP 16 (1980) have been followed while doing the structural design for both the wall systems. M25 grade concrete and Fe500 grade steel have been considered in the structural designs. The retaining wall stem and heel were designed as cantilever members. Shear and moment acting on the wall have been used for flexural analysis of the wall systems. Once the maximum ultimate moment has been determined; the type, spacing, lengths and quantity of required reinforcing bars have been determined. The calculated maximum bending moments and shear forces at stem, toe and heel for sand and STC30 backfill materials are shown in the Fig. 7.2 to Fig. 7.3.

From the Fig. 7.2, it is observed that the maximum bending moments are lower in case of STC30 mixture backfill compared to sand backfill. Maximum bending moments for the stem of STC0 backfill are noted as 14.91, 119.3 and 402.63 kNm for H=3, 6 and 9 m, respectively. For STC30 backfill, maximum bending moments of the stem are noted as 8.57, 68.53 and 231.3 kNm for H=3, 6 and 9 m, respectively. Similarly, maximum bending moments for heel are noted as 6.22, 72.46 and 300.02 kNm for H=3, 6 and 9m, respectively, with STC0 backfill. For STC30 backfill, the corresponding value are 1.39, 31.19 and 119.21 kNm for H=3, 6 and 9 m, respectively.

From the Fig. 7.3, it is observed that the maximum shear forces are lower in case of STC30 mixture backfill compared to sand backfill. Maximum shear forces at the bottom of the walls with STC0 backfill for 6 m height wall is 59.65 KN, which is 34.26 KN with STC30 backfill. It means the retaining wall with STC30 backfill will be more safe than sand alone as backfill material.

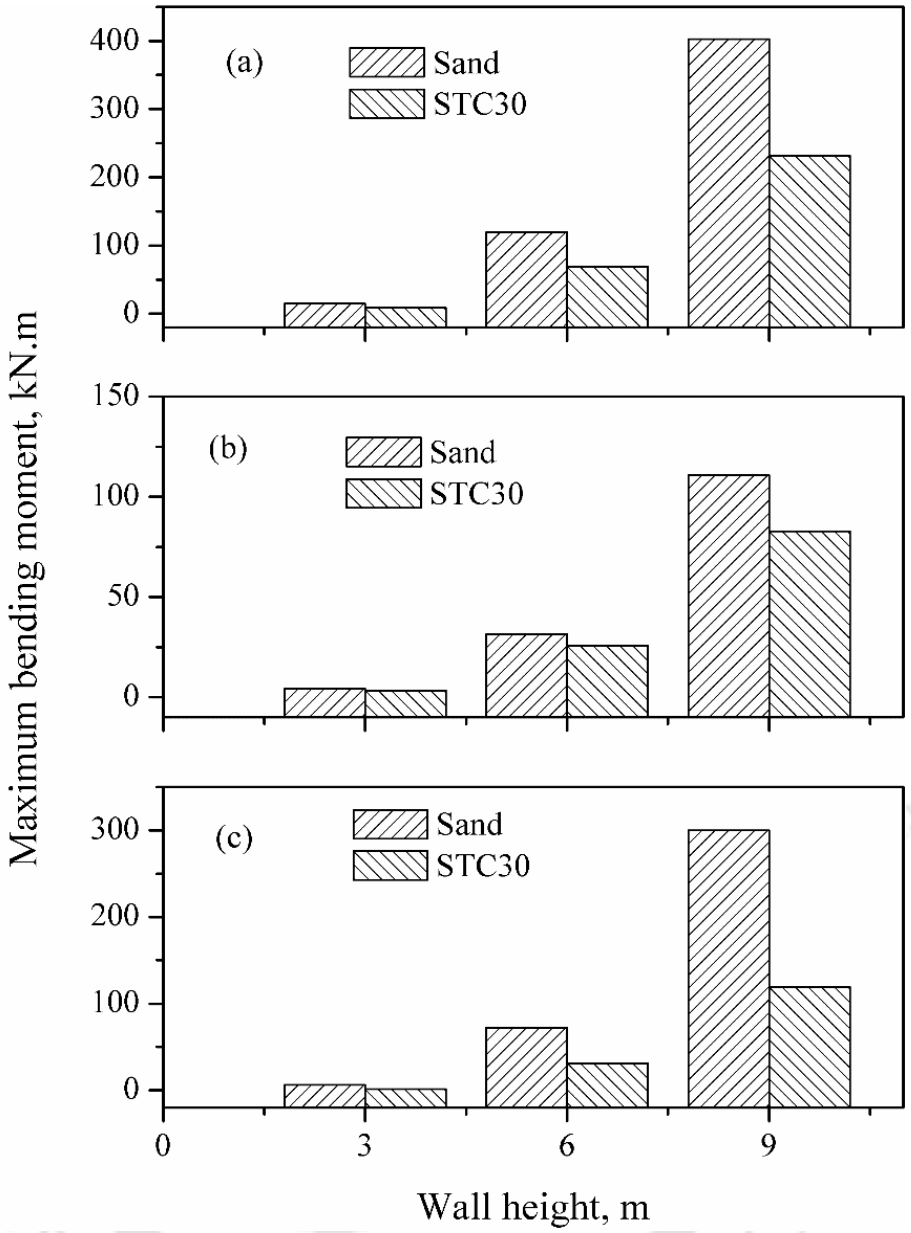

Fig. 7.2 Comparison of maximum bending moments: (a) stem, (b) toe, (c) heel

The percentages of reinforcement for various heights of retaining walls for stem, heel and toe footings with STC0 backfill and STC30 backfill have been reported in Table 7.4. Based on Table 7.4, it is concluded that amount of reinforcement is decreased by using STC30 mixture as backfill material of retaining wall and the difference is clearly shown in higher height of retaining wall.

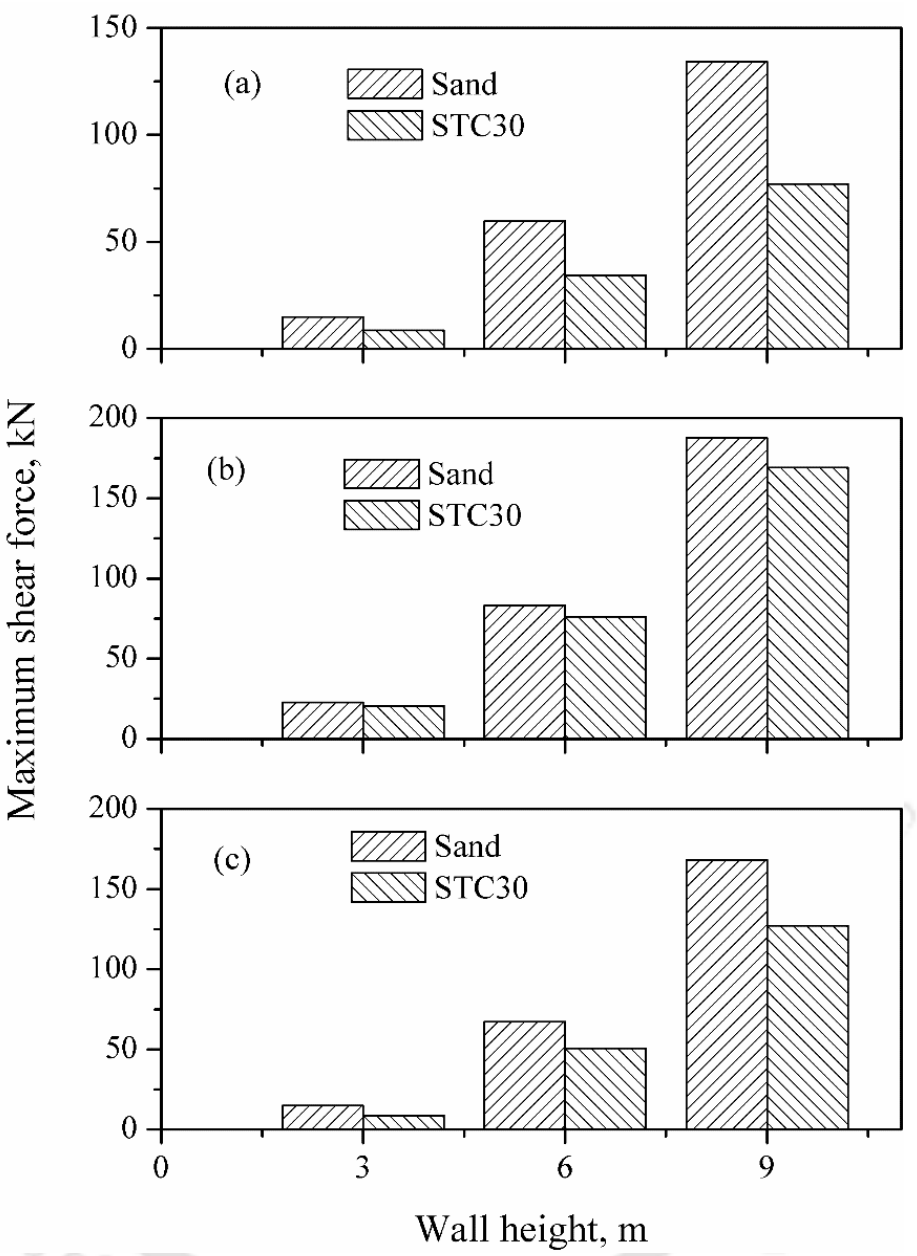

Fig. 7.3 Comparison of maximum shear forces: (a) stem, (b) toe, (c) heel

Table 7.4 Percentage of reinforcement

Height of wall (m)	Percentages of reinforcement					
	Stem		Heel		Toe	
	Sand	STC30	Sand	STC30	Sand	STC30
3	0.07	0.07	0.07	0.07	0.07	0.07
6	0.229	0.167	0.14	0.07	0.07	0.07
9	0.32	0.267	0.08	0.09	0.07	0.07

7.4 COST BENEFIT ANALYSIS

Cost benefit analysis has been performed for retaining wall systems with STC0 (sand alone) and STC30 mixture as backfill materials. The cost estimation is based on the rates of various materials; steel, sand, aggregate, cement, tire chips and others. Based on survey in local market, material costs were adopted as presented in Table 7.5. The cost of recycled tire chips varies from place to place-based availability of scrap tires and local suppliers. Cecich et al. (1996) considered that tire chips cost is less than the sand (sand, $12 and tire chips, $10 per ton). In this study, two cases were considered, one, tire chips cost is double to the sand cost (sand price is Rs.1.5 per kg and tire chips price Rs.3 per kg) considered for cost estimation. Second case, tire chips cost is equal to the sand cost.

For estimating the cost of retaining wall of a specific height, 30 m long wall was considered. Volumes of different materials were calculated as per the designs obtained in the previous section. To quantify the backfill volume, as per Cecich et al. (1996), theoretical volume evaluated from Rankine's wedge (depends on friction angle of the backfill material) was considered. Based on this, for a 30 m long wall, the required volume of backfill of two (sand alone and STC30) retaining wall systems with different heights of wall are shown in Fig. 7.4.

Table 7.5 Materials costs range from local builders

Material	Cost range per kg (Rupees)	Considered this study Cost per kg (Rupees)
Sand	1.0 – 1.5	1.5
Steel	40 – 50	50
Cement	4 – 7	7
Aggregate	1.0 – 1.5	1.5

The estimated backfill cost and total cost are reported in Table 7.6. Based on estimated backfill cost, about 20% to 30% saving and total cost of walls with both the

backfill materials about 20% to 30% saving are seen for the wall with STC30 as backfill. Similar type of saving was also observed in the literature (Cecich et al. 1996 and Livingston and Ravichandran, 2017). This cost saving and utilization of wastes materials show the sustainability of retaining wall systems with the STC30 mixtures backfill. This is to be noted that the amount of savings projected is based on the materials rates adopted in the study. The same may vary place to place depending on availability of various materials.

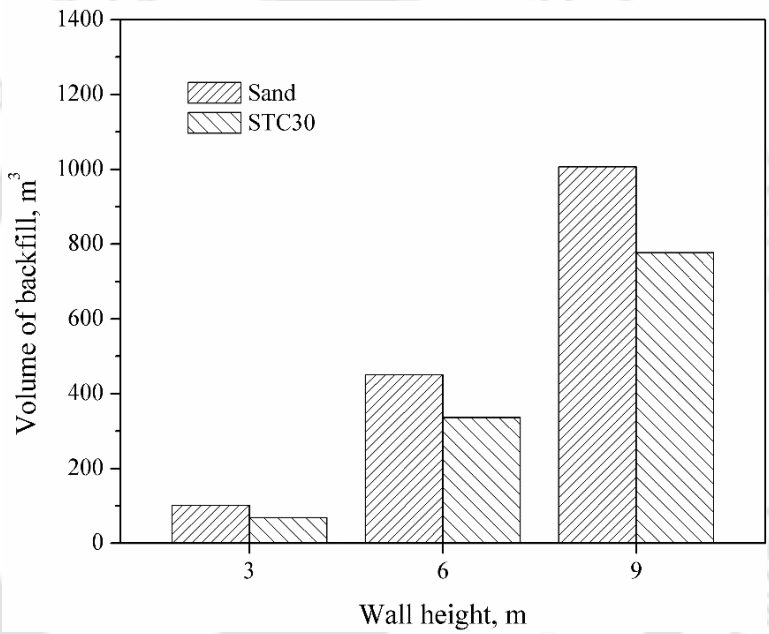

Fig. 7.4 Comparison of backfill volumes for retaining walls

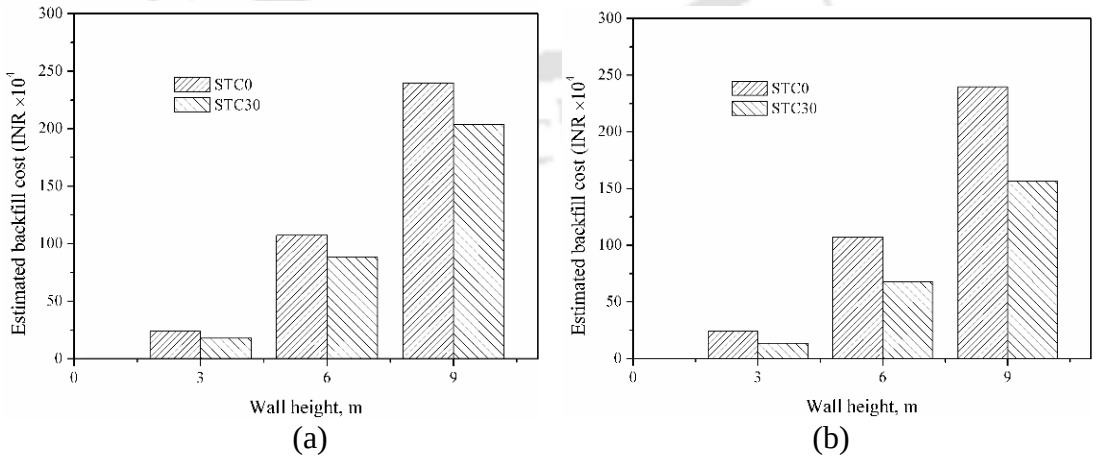

Fig. 7.5 Comparison of estimated backfill material cost for retaining walls; (a) tire chips cost double to sand, (b) tire chips cost equal to sand

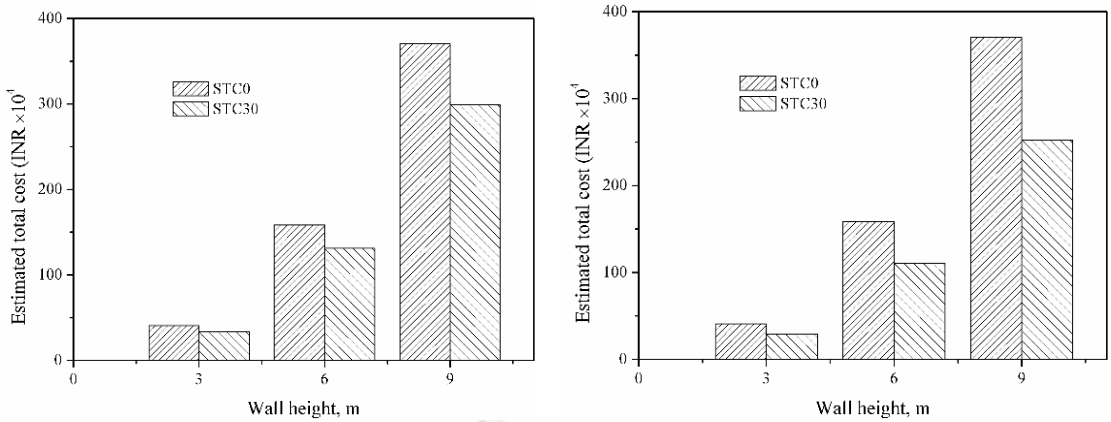

Fig. 7.6 Comparison of total estimated cost for retaining walls; (a) Tire chips cost double to sand, (b) Tire chips cost equal to sand

Table 7.6 Comparison of retaining walls costs (30m long)

Wall height, m	Estimated backfill material cost (Rupees)		% saving	Estimated total cost (Rupees)		% saving
	Sand	STC30		Sand	STC30	
3	241300	178790	25.90	407630	329155	19.25
6	1072360	880145	17.9	1584510	1311820	17.21
9	2396740	2033355	15.16	3703470	2993640	19.17
Sand cost = tire chips cost						
3	241300	137531	43.00	407630	287895	29.37
6	1072360	677034	36.86	1584510	1108710	30.00
9	2396740	1564120	34.74	3703470	2524405	31.84

7.5 Summary

This chapter presented the design and cost benefit analysis retaining wall system with sand and optimum STC mixture as backfill materials. The design of three different retaining walls with heights of 3, 6, and 9 m using sand (STC0) and STC30 mixture as backfill materials and their cost implications has been presented for comparison purpose. By using STC30 properties, the design of retaining walls proven that the dimensions of the retaining wall elements and backfill volumes can be greatly reduced.

From the cost analyses, total cost of retaining wall with STC30 backfill resulted in about 20% to 30% saving, in comparison to total cost of the wall with STC0 backfill.

Based on the study, it can be concluded that using STC30 mixture can be an alternative backfill material, which is not only economically feasible but also environmentally advantageous with the use of scrap-derived geomaterials in retaining wall applications.

Chapter 8. CONCLUDING REMARKS

8.1 SUMMARY OF THE THESIS

The objective of the present study is to ascertaining the engineering properties of sand – tire chips (STC) mixtures, and to study the behaviour of retaining wall models using different STC mixtures as lightweight fill material and tire chips as a compressible inclusion. Index and mechanical properties of different STC mixtures (0–100%) were determined through laboratory investigations and optimum mixing ratio of STC was evaluated. Physical retaining wall models were tested under static and dynamic conditions to investigate their behaviours with different STC mixture backfills. Different parameters varied in model tests are type of backfill, compressible inclusion (*t*), surcharge pressure, and base excitations. Numerical models were developed and validated to simulate the studies on retaining walls using FLAC. Parametric analyses were carried using the developed numerical model for 6 m high prototype scale wall. Further, two retaining wall systems were designed using STC0 and STC30 mixtures and financial benefits were evaluated.

8.2 CONCLUSIONS

The following conclusions were drawn from the present research work.

- Dry unit weight and specific gravity values of STC mixtures were decreased by increasing the percentage of tire chips. When using 30% tire chips by weight, a 20% reduction in dry unit weight was observed, as compare to sand.
- With an increase in TC content, up to 40% of the STC mixture, void ratio was decreased by approximately 50%, which indicates better compressibility behaviour.

- The addition of TC to sand (up to approximately 30–50%) resulted in significantly increased shear strength. For the sand material considered in the study, the friction angles values of STC mixtures were observed as high as 58°. The apparent cohesion intercept of the sand material was also increased from 5 to 25 kPa, with the addition of 40% tire chips by weight.
- The optimum mixing ratio of sand and tire chips, which show better compressibility characteristics (due to lesser void ratio) and high load-carrying behaviour (due to high shear strength), is in the range of 30–40% by weight.
- The model studies with STC mixtures as lightweight backfill material indicated significant improvement in wall behaviour in terms of displacements and lateral earth pressures and accelerations.
- Maximum reduction in displacement is in the order of 65%, for optimum STC mixture (STC30), under both static and dynamic loading condition.
- By using STC30, material dynamic induced pressures were reduced by, up to 80%.
- Tire chips as compressible inclusion, behind the wall showed remarkable advantage in reducing displacements (up to 25% reduction) and lateral earth pressures (up to 60 % reduction), under static loading. The corresponding reductions in dynamic case were, up to 75% and 80%, respectively.
- Within the two thicknesses of TC compressible layer, higher thickness (180 mm) was shown maximum benefit to minimize the displacements and earth pressures.
- The developed numerical model, for retaining wall with different STC mixtures, is able to simulate the behaviour of laboratory models and showed the maximum reductions in displacement and pressures for STC30 backfill.

- Full-scale wall responses, in terms of displacement and earth pressures, were significantly improved with the provision of STC mixture zone behind the wall. The improvement was increased with the increasing the width of zone, but reached asymptotic values at b/B of 0.25. This implies that even narrow backfill regions can also use STC30 material to effectively improving the wall performance.
- From the simulation studies with compressible inclusions, it is concluded that t/H of 0.2 is the optimum value in fixing the thickness of compressible inclusion.
- Retaining wall model showed higher displacement and pressures Reponses at frequency close to the fundamental frequency of the wall.
- Nonlinear behaviour of wall response was observed when increasing base acceleration (beyond 0.4 *g* acceleration).
- Owing to the better compressible behavior and higher, shear strength properties of STC30 material, the designed retaining wall cross-section dimensions and the corresponding reinforcements, for a given height of the wall, were significantly reduced in comparison to that with sand material.
- With the assumed rates of TC, sand, and other materials, using STC30 mixture backfill showed an average saving of 20% to 30% in the total estimated cost of construction.

The results presented in this study conclude that the optimum mixing ratio (30–40%) will effectively work as lightweight material for retaining wall backfill and other applications like, embankments, and foundations. The improved behaviour of retaining wall models is attributed to the lesser unit weight and higher shear strength property of STC materials than that of traditional sand material. This study indicates that the seismic resilience of retaining walls with STC mixtures as back fill materials is

significant. Higher resilience behaviour was observed for model walls with STC30 mixtures. This is equivalent to the volume ratio of 50–60%, which can reduce the demand for huge volume of sand material in any geotechnical application.

STC mixtures prove to be a cost effective lightweight fill material and also reduce the demand for traditional materials with the replacement by recycled scrapped tire chips. Thus, use of tire-derived material in geotechnical applications will create a sustainable future.

Overall, the present research work demonstrate the sustainable aspects of the use of STD geomaterials in retaining wall applications. It is expected that similar advantages with the use of optimum STC mixture can be achieved in various other infrastructure projects. This is to be noted that with increasing use of such materials will also enhance the abundant availability of the materials, which further enhance the financial benefits.

8.3 LIMITATIONS OF THE STUDY

1. Use of tires under the groundwater table or directly in surface water bodies is still not permitted due to concerns regarding potential for groundwater contamination.
2. Only one type of scrap tire-derived geomaterial, which is tire chips of 20mm long 10 × 10 mm square cross sections, was considered. Only one type of dry cohesionless soil (sand) was adopted for the study.
3. In numerical simulations, real sand-tire chip matrix was not considered. Only the representative equivalent properties were adopted. Further, dynamic properties of the materials were not evaluated and utilised in the numerical model.

4. Due to the typical limitations associated with the laboratory scale 1*g* model tests and associated scaling effects, the test results presented here may not be directly extrapolated to get the field wall response. However, the results obtained from this study will help in understanding the relative performance of retaining walls subjected to base shaking with compressible inclusions.

8.4 SCOPE FOR FUTURE RESEARCH

The following are the recommendations for future work:

- Similar type of studies can be conducted using other form and size of STD material and soils.
- Physical model tests can be conducted on mechanically stabilized walls using sand – tire chips mixtures.
- Physical model tests can be conducted on retaining walls resting on deformable foundations
- Numerical model studies can be extended by using more advanced constitutive materials models.
- Numerical models using discrete element method, which consider the sand and TC particles along with their interaction can be adopted for further studies.

REFERENCES

1. AASHTO (2002). *Standard specifications for highway bridges.* (17th Edition 2002), American Association of State Highway and Transportation Officials, Washington, DC, USA.

2. Ahmed, I. (1993). Laboratory study on properties of rubber-soils. Ph.D. thesis, School of Civil Engineering, Purdue University, West Lafayette, Ind.

3. Ahn, S, ll, and Cheng, L. (2014). Tire-derived aggregate for retaining wall backfill under earthquake loading. Construction and Building Materials, 57:105-116.

4. Alqaissi. (2012). Behavior of Strip footings resting on sand mixed with tire-chips. J Eng Dev 16 (4). ISSN 1813–7822.

5. Anbazhagan P., Tsang H.H. and Mamatha M. (2011). Earthquake Hazard Mitigation by Utilizing Waste Tires. Proceeding of International Conference on Recent Innovations in Technology ICRIT 2011, February 2011 RIT Kottayam, Kerala, India, pp 59-64.

6. Anvari, S.M., Shooshpasha, I., Kutanaei, S.S. (2017). Effect of granulated rubber on shear strength of fine-grained sand, Journal of Rock Mechanics and Geotechnical Engineering (2017), doi: 10.1016/j.jrmge.2017.03.008.

7. ASCE. (2011). The role of the civil engineer in sustainable development. ASCE State Government Relations.

8. ASTM D6270 (2012). Standard practice for use of scrap tires in civil engineering applications. American Society for Testing and Materials, West Conshohocken, PA.

9. Attom, M.F. (2006). The use of shredded waste tires to improve the geotechnical engineering properties of sands. Environmental Geology, 49(4), 497-503

10. Ayothiraman, R. and Soumya, S. (2011). Use of shredded tire chips as aggregates in stone column: an experimental study, Proceedings of Indian Geotechnical Conference December 15-17, 2011, Kochi, India, pp.711-714.

11. Ayothiraman, R. and Soumya, S. (2015). Model tests on the use of tire chips as aggregate in stone columns. Proceedings of the Institution of Civil Engineers – Ground Improvement 168(3): 187–193.

12. Balachowski, L. and Gotteland, P. (2007). Characteristics of tire chips-sand mixtures from triaxial tests. Archives of Hydro-Engineering and Environmental Mechanics, 54(1):3–14.

13. Balunaini, U., Yoon, S., Prezzi, M., and Salgado, R., (2009). Tire Shred Backfill in Mechanically Stabilized Earth Wall Applications. FHWA/IN/JTRP-2008/17. Joint Transportation Research Program, Indiana Department of Transportation and Purdue University, West Lafayette, Indiana.

14. Balunaini, U., Mohan, V.K.D, Prezzi, M. and Salgado, R. (2014a). Shear strength of tire chip–sand and tire shred–sand mixtures. Proceedings of the Institution of Civil Engineers - Geotechnical Engineering, 167(6): 585-595.

15. Balunaini, U., Yoon, S., Prezzi, M. and Salgado, R. (2014b). Pullout Response of Uniaxial Geogrid in Tire Shred–Sand Mixtures. Geotech and Geological Engineering, 32(2):505–523.

16. Bandyopadhyay, S. Sengupta, A., and Reddy, G.R. (2015). Performance of sand and shredded rubber tire mixture as a natural base isolator for earthquake protection. Earthquake Engineering and Engineering Vibration, 14 (4): 683-693.

17. Banzibaganye, G. (2014). Investigation into the use of waste tire shreds for reinforcement of sandy soils in South Africa. Master thesis, Univ. of Cape Town, South Africa.

18. Bathurst, R.J., and Hatami, K. (1998). Seismic response analysis of a geosynthetic reinforced soil retaining wall. Geosynthetics International 5(1-2), 127-66.

19. Bathurst, R.J., Zarnani, S. and Gaskin, A. (2007). Shaking table testing of geofoam seismic buffers. Soil Dynamics and Earthquake Engineering 27(4): 324–332.

20. Benda, C. C., (1995). Engineering Properties of Scrap Tires Used in Geotechnical Applications. Report No. 95-1, Vermont Agency of Transportation, Montpelier, VT.

21. Bernal, A., Lovell, C.W, and Salgado, R, (1996). Laboratory Study on the use of Tire Shreds and Rubber-Sand in Backfills and Reinforced Soil Applications, FHWA/IN/JHRP-96/12, Purdue University, West Lafayette, Indiana

22. Bergado, D. T., S.Youwai, and A. Rittirong, (2005). Strength and deformation of flat and cubical rubber tire chip-sand mixtures. Geotechnique, 55(8): 603-606.

23. Bhalla, G., Kumar, A., and Bansal, A. (2010). To study the effect of leachate treated with scrap tire shreds and gravel on soil and groundwater. Current World Environment, 5(1):15-22.

24. Bhattacharjee, A., and Krishna, A.M., (2012) Development of Numerical Model of Wrap Faced Walls Subjected to Seismic Excitation, Geosynthetics International, 19(5): 354-369. DOI: 10.1680/gein.12.00022

25. Bhattacharjee, A., and Krishna, A. M., (2015) Strain Behavior of Backfill Soil in Rigid Faced Reinforced Soil Walls Subjected to Seismic Excitation, International Journal of Geosynthetics and Ground Engineering, DOI: 10.1007/s40891-015-0016-4.

26. Bosscher, J., Edill, T. B., and Kuraoka, S. (1997). Design of highway embankments using tire chips. Journal of Geotechnical and Geoenvironmental Engineering, 123(4): 297–304.

27. Bowles, J. E. (1996). Foundation Analysis and Design. 5th edition. McGraw-Hill International Editions.

28. Bressette, T. (1984). Used tire material as an alternative permeable aggregate. Report No. FHWA/CA/TL-84/07, Office of Transportation Laboratory, California Department of Transportation, Sacramento, CA.

29. Cabalar, A. F. (2011). Direct shear tests on waste tires–sand mixtures. Geotech and Geological Engineering, 29, 411–418.

30. Cecich, V., Gonzales, L., Hoisaeter, A., Williams, J., and Reddy, K. (1996). Use of shredded tires as lightweight backfill material for retaining structures. Waste Management and Research, 14(5): 433-451.

31. Cetina, H., Fenerb, M., and Gunaydin, M. (2006). Geotechnical properties of tire-cohesive clayey soil mixtures as a fill material. Engineering Geology, 88:110- 120.

32. Cosgrove, T.A. (1995). Interface strength between tire chips and geomembrane for use as a drainage layer in a landfill cover. Proceedings of Geosynthetics'95, Industrial Fabrics Association, St. Paul, MN, Vol. 3, pp. 1157-1168.

33. Dammala, P., Reddy, S.B., and Krishna, A.M. (2015). Experimental investigation of applicability of sand -tire chip mixtures as retaining wall backfill. IFCEE, ASCE Geotechnical special publication, pp.1420-1429. DOI:10.1061/9780784479087.128.

34. Dickson, T.H., Dwyer, D.F. and Humphrey, D.N. (2001). Prototype tire shred embankment construction. Transportation Research Record 1755, TRB, National Research Council, Washington DC, pp. 160–167.

35. Edil, T.B. and Bosscher, P.J. (1994). Engineering Properties of Tire Chips and Soil Mixtures. Geotechnical Testing Journal, 17(4): 453-464

36. Eldin, N. N., and Senouci, A. B. (1993). Rubber-tire particles as concrete aggregate. Journal of Material in Civil Engineering, ASCE, 5(4), 478-496.

37. Ertugrul, O. and Trandafir, A. (2011). Reduction of lateral earth forces acting on rigid nonyielding retaining walls by EPS geofoam inclusions. Journal of Materials in Civil Engineering. 23(12): 1711–1718.

38. Feng, Z.Y. and Sutter, K.G. (2000). Dynamic properties of granulated rubber/sand mixtures. Geotechnical Testing Journal, 23(3):338–344.
39. Foose, G.J., Benson, C.H., and Bosscher, P.J. (1996). Sand with shredded waste tires. Geotechnical Testing Journal, 122(9): 760-767

40. Gebhardt, M.A., (1997). Shear strength of shredded tires as applied to the design and construction of shredded tire stream crossings. MS Thesis, Iowa State University.

41. Ghazavi, M. (2004). Shear strength characteristics of sand mixed with granular rubber. Geotech and Geological Engineering, 22(3), 401–416.

42. Ghazavi M. and Sakhi, M.A. (2005). Influence of optimized tire shreds on shear strength parameters of sand. Int. J. Geomech., 5(1), 58–65

43. Ghazavi, M., Ghaffari, J. and Farshadfar, A. (2011). Experimental determination of waste tire chip-sand-geogrid interface parameters using large direct shear tests. Fifth symposium on advances in science and technology.

44. Gotteland, P., Lambert, S., Salot, C., Gras, V. (2007). Investigating the strength characteristics of tire chip–sand mixtures for geo-cellular structure engineering. Proceedings International Workshop on Scrap Tire-Derived Geomaterials, Yokosuka, Japan, pp. 17–40.

45. Graettinger, A.J., Johnson, P.W., Sunkari, P. Duke, M.C. and Effinger, J. (2005). Recycling of plastic bottles for use as a lightweight geotechnical material. Management of Environmental Quality: An International Journal, 16(6):658-669.

46. Hataf and Rahimi (2006). Experimental investigation of bearing capacity of sand reinforced with randomly distributed tire shreds. Construction and Building Materials. 20: 910–916

47. Hatami, K. and Bathurst, R. J. (2006). Numerical model for reinforced soil segmental walls under surcharge loading, Journal of Geotechnical and Geoenvironmental Engineering, 132(6): 673-684.

48. Hazarika, H. and Sugano, T. (2004). Combined use of EPS and tire chips as compressible cushion behind retaining structure – A field Test, Intl.Conf. On geotechnical and geoenvironmental engineering, Mumbai, India, pp.229-234.

49. Hazarika, H., Kohama, E., Suzuki, H. and Sugano, T. (2006). Enhancement of Earthquake Resistance of Structures Using Tyre Chips as Compressible Inclusion. Port and Airport Research Institute, Nagase, Yokosuka, Japan, PARI report no. 045-01.

50. Hazarika, H., and Yasuhara, K. (2007) Scrap Tire-Derived Geo materials-Opportunities, Challenges. Taylor and Francis, UK.

51. Hazarika, H., Kohama, E., and Sugano, T. (2008a). Underwater shake table tests on waterfront structures protected with tire chips cushion. Journal of Geotechnical and Geoenvironmental Engineering, ASCE, 134(12): 1706-1719

52. Hazarika H, Yasuhara K, Karmokar AK and Mitarai Y (2008b) Shaking table test on liquefaction prevention using tire chips and sand mixture, Hazarika & Yasuhara (eds), Taylor & Francis Group, London, ISBN 978-0-415-46070-5,CRC Press, USA, 215-222

53. Hazarika, H., Yasuhara, K., Kikuchi, Y., Karmokar, AK., Mitarai, Y. (2010). Multifaceted potentials of tire-derived three dimensional geosynthetics in geotechnical applications and their evaluation. Geotextile and Geomembrene, 28:303–315

54. Hazarika, H., Okada, H., Hara, T., Ueno, M., Ohsumi, T., Yamanaka, M., Yamazaki, T., Kosaka, N., Minowa, H., and Furuichi, H. (2012a). Case studies of geotechnical damage by the 2011 off the Pacific Coast of Tohoku Earthquake and tsunami in Japan. Proc. of the 15th World Conference on Earthquake Engineering, Lisbon, Portugal, Paper No 4796.

55. Hazarika, H., Kasama, K., Suetsugu, D., Kataoka, S., Yasufuku, N. (2012b). Damage to geotechnical structures in waterfront areas of northern Tohoku due to the March 11, 2011 tsunami disaster. Indian Geotechnical Journal, 43(2):137–152.

56. Hazarika, H. (2013a). Paradigm shift in earthquake induced geohazards mitigation -emergence of nondilatant geomaterials. In: Keynote lecture for the annual conference of Indian Geotechnical Society. CD-ROM, Roorkee.

57. Hazarika, H., Eto, I., Yasufuku, N., Ishikura, R., Fukumoto, Y. (2013b). Fundamental research on tsunami countermeasures for seawalls using low carbon material. In: Proceedings of the 10th national symposium on environmental geotechnology, Tokyo, Japan, pp 351–354.

58. Hazarika, H., Hara, T., Furuichi, H. (2013c). Soil-Structure interaction during earthquake and tsunami – two case studies from the latest disaster in Japan. In: Proceedings of the eighteenth international conference on soil mechanics and geotechnical engineering, Paris, France, pp 131–142.

59. Hazarika, H., Pradhan, K., Hirayu, N., Fukumoto, Y., Yasufuku, N., Ishikura, R. (2014). Protection of seawall against earthquake and tsunami using flexible material. In: Proceedings of the 14th international conference of the International Association for Computer Methods and Advances in Geomechanics (IACMAG), Kyoto, pp 1897–1902

60. Hazarika, H. and Yasuhara, K. (2015). Sustainable and smart materials in Geotechnical constructions. Discovery, 42(195), 233-244.

61. Heimdahl, C., and Druscher, A. (1999). Elastic anisotropy of tire shreds. Journal of Geotechnical and Geoenvironmental Engineering, 125(5): 383–389.

62. Horvath, J.S. (1997). Compressible inclusion function of EPS geofoam. Geotextiles and Geomembranes, 15(1): 77-120.

63. Huggins, E., and Ravichandran, N. (2011). Numerical study on the dynamic behavior of retaining walls backfilled with shredded tires, GeoRisk 2011, ASCE 2011.

64. Humphrey, D.N., Sandford, T.C., Cribbs, M.M., Gharegrat, H., and Manion, W.P. (1992). Tire Chips as Lightweight Backfill for Retaining Walls - Phase I, Dept. of Civil Engineering, University of Maine, Orono, Maine.

65. Humphery, D.N., and Manion, W.P., (1992). Properties of Tire Chips for Lightweight Fill. Proceedings of the Conference on Grouting, Soil Improvement, and Geosynthetics, ASCE, New Orleans, Louisiana, Vol-2, pp. 1344-1355.

66. Humphrey, D.N., Sandford, T.C., Cribbs, M.M. and Manion, W.P. (1993). Shear strength and compressibility of the tire chips for use as retaining wall backfill. Transportation Research Record, 1422: 29–35.

67. Humphrey, D. N. (1996). Investigation of exothermic reaction in tire shred fill located on SR 100 in Ilwaco, Washington. Rep. to the Federal Highway Administration, Washington, DC.

68. Humphrey D, Cosgrove T, Whetten NL, Herbert R (1997)Tire chips reduce lateral earth pressure against the walls of a rigid frame bridge, Seminar on rehabilitation and upgrades in civil and environmental engineering, ASCE. (https://rma.org/sites/default/files/CIV-044-Tire_Chips_Reduced_Lateral_Earth_Pressure_Against_The_Walls_Of_A_Rigid_Frame_Bridge.pdf)

69. Humphrey, D.N., Whetten, N., Weaver, J., Recker, K., and Cosgrove, T.A. (1998). Tire shreds as lightweight fill for embankments and retaining walls, Proceedings of the conference on recycled materials in geotechnical applications, ASCE, 15

70. IS: 2720 (part 3) -1980. Methods of test for soils: Determination of specific gravity for fine, medium and coarse-grained soils. Bureau of Indian Standards, New Delhi.

71. IS: 2720 (part 4) -1985. Methods of test for soils: Grain size analysis. Bureau of Indian Standards, New Delhi.

72. IS: 2720 (Part 14) - 1983. Methods of test for soils: Determination of density index (Relative Density) of cohesionless soils. Bureau of Indian Standards, New Delhi.

73. IS: 14458 (1997). Guidelines for retaining wall for hill area: Part 2 Design of retaining/breast walls. Bureau of Indian Standards, New Delhi.

74. IS: 456 (2000). Code of Practice for Plain and Reinforced Concrete. Bureau of Indian Standards, New Delhi.

75. Kaneda, K., Hazarika, H. and Yamazaki, H. (2008). The numerical simulation of earth pressure reduction using tire chips in backfill. Scrap Tire-Derived Geomaterials – Opportunities and Challenges – Hazarika & Yasuhara (eds). Taylor & Francis Group, London, pp. 245-251.

76. Kaneko, K., Orense, R.P., Hyodo, M. and Yoshimoto, N. (2013a). Seismic response characteristics of saturated sand deposits mixed with tire chips. J. Geotech. Geoenviron. Eng. 139 (4), 633–643.

77. Kaneko, T., Hyodo, M., Nakata, Y., Nyoshi, Hazarika, H. (2013b). Dynamic deformation characteristics and seismic response of tire chip and mixtures with sand. J. Jpn. Soc. Civil Eng., Ser. C (Geo. Eng.) 69 (1), 91–107.

78. Kaushik, M.K., Kumar, A. and Bansal, A. (2016). Drainage performance of different sizes tyre chips used alone and mixed with natural aggregates as leachate drainage layer material. Geotechnical and Geological Engineering 34(1): 167–191.

79. Kumar, A. and Mandal, J.N (2017). Effect of Reinforcement on Multi-Tiered Fly Ash Wall. Procedia Engineering, 189: 446 – 453.

80. Kim, H.K., and Santamarina, J.C. (2008). Sand–rubber mixtures (large rubber chips). Journal of Canadian Geotechnical , 45(10): 1457 -1466.

81. Kim, Y.T., and Kang, H.S. (2013). Effects of Rubber and Bottom Ash Inclusion on Geotechnical Characteristics of Composite Geomaterial, Marine Georesources and Geotechnology, 31(1): 71-85.

82. Krishna, A.M. (2008). Seismic response of geosynthetic reinforced soil wall models using shaking table. PhD Thesis, Department of Civil Engineering, Indian Institute of Science, Bangalore, India.

83. Krishna, A.M. and Bhattacharjee, A. (2016). Behavior of Rigid Faced Reinforced Soil Retaining Walls Subjected to Different Earthquake Ground Motions. ASCE International Journal of Geomechanics, 10.1061/ (ASCE) GM.1943-5622.0000668, 06016007.

84. Kuhlemeyer, R.L., and Lysmer, J. (1973). Finite element method accuracy for wave propagation problems. Journal Soil Mechanics and Foundations, ASCE, Vol. 99, No. SM5, pp. 421-427.

85. Lade, P.V., Liggio, C. D., Jr., and Yamamuro, J. A. (1998). Effects of Non-Plastic Fines on Minimum Maximum Void Ratios of Sand. Geotechnical Testing Journal, TGJODJ, 21(4):336-347.

86. Lawrence, B.K., Chen, L.H., and Humphrey, D.N. (1998). Use of Tire Chip/Soil Mixtures to Limit Frost Heave and Pavement Damage of Paved Roads.

Department of Civil and Environmental Engineering, University of Maine, Orono, Maine.

87. Lazizi, A., Trouzine, H., Asroun, A. and Belabdelouahab, F. (2014). Numerical simulation of tire reinforced sand behind retaining wall under earthquake excitation. Engineering, Technology & Applied Science Research, 4(2): 605-611.
88. Lee, J.H., Salgado, R., Bernal, A., and Lovell, C.W. (1999). Shredded Tires and Rubber-Sand as Lightweight Backfill. Journal of Geotechnical and Geoenvironmental Engineering, ASCE, 125 (2): 132–141.

89. Lee HJ and Roh HS (2006) The use of recycled tire chips to minimize dynamic earth pressure during compaction of backfill. Construction Building Materials, 21(5) :1016-1026

90. Lee, C., Truong, Q. H., Lee, J. S., and Lee, W. (2010).Characteristics of rubber-sand particle mixtures according to size ratio. Journal of Materials Civil Engineering, 22(4), 323–331.

91. Marto, A., Latifi, N., Moradi, R., Oghabi, M., and Zolfeghari, S. Y. (2013). Shear Properties of Sand – Tire Chips Mixtures. EJGE, 325-334.

92. Masad, E., Taha, R., Ho, C. and Papagiannakis, T. (1996). Engineering properties of tire/soil mixtures as a lightweight fill material. Geotechnical Testing Journal, 19:297–304

93. Mashiri, M. S., Sheikh, M. Neaz., Vinod, J. & Tsang, H. (2013). Dynamic properties of sand-tire chip mixtures. In S. Anderson (Eds.), Australian Earthquake Engineering Society Conference, Australian Earthquake Engineering Society. Tasmania, pp. 1-8.

94. Mashiri, M.S., Vinod, J.S., Sheikh, M.N. and Tsang, H. (2015). Shear strength and dilatancy behaviour of sand-tire chip mixtures. Soils and Foundations, 55 (3), 517-528.

95. Mashiri, M. S., Vinod, J. S., and Sheikh, M. N. (2016). Liquefaction Potential and Dynamic Properties of Sand-Tire Chip (STCh) Mixtures, Geotechnical Testing Journal, 39(1),. 69–79, doi: 10.1520/ GTJ20150031. ISSN 0149-6115.

96. Mashiri, M.S., Vinod, J.S., Sheikh, M.N. and Carraro, A. (2017). Shear modulus of sand-tire chip mixtures, Environmental Geotechnics. http://dx.doi.org/10.1680/jenge.16.00016

97. Mondal, B. and Warith, M.A. (2008). Use of shredded tire chips and tire crumbs as packing media in trickling filter systems for landfill leachate treatment. Environmental Technology, 29(8):827-836.

98. Nightingale, D. E. B., and Green, W. P. (1997). An unsolved riddle: tire chips, two roadbeds, and spontaneous reactions. ASTM STP 1275, M.A. Wasemiller and K. B. Hoddinott, eds., Philadelphia, 265–285.

99. Oikonomoun and Mavridou, S. (2008). The Use Of Waste Tire Rubber In Civil Engineering Works.Chapter 9, Sustainability of construction materials Edited by Jamal M. Khatib, CRC

100. Park, J.K., Kim, J.Y. and Edil, T.B. (1996). Mitigation of organic compound movement in landfills by shredded tires. Water Environment Research, 68(1): 4-10.

101. Pando, M., and Garcia, M. (2011). Tire-derived aggregates as a sustainable backfill or inclusion for retaining walls and bridge abutments. Presentation at the sixth Geo3T2 Conf. and Expo, Raleigh, NC.

102. Prasad, D. S. V. and Raju G. V. R. P. (2009). Performance of Waste Tyre Rubber on Model Flexible Pavement, Journal of Engineering and Sciences, Asian Research Publishing Network (ARPN), 4(6): 89-92.

103. Prezzi, M., Duvvuru, M and Kumar, V. (2011). Construction of MSE Wall Using Tire Shred-sand Mixture as Backfill (SPR-3470). JTRP Other Publications and Reports. Paper 3. doi: 10.5703/1288284314675

104. Rao, G.V. and Dutta, R.K. (2006). Compressibility and strength behavior of sand – tire chips mixtures. Geotechnical and Geological Engineering, 24: 711-724.

105. Ravichandran, N., and Huggins, L. (2014). Applicability of shredded tire chips as a lightweight retaining wall backfill in seismic regions. In: Proceedings of geo-congress (GSP 234), ASCE, Atlanta

106. Reddy, K.R and Saichek, R.E. (1998a). Assessment of Damage to geomembrane Liners by Shredded Scrap Tires. Geotechnical Testing Journal, 21(4): 307-316

107. Reddy, K.R. and Saichek, R.E. (1998b). Characterization and performance assessment of shredded scrap tires as leachate drainage material in landfills. Proc. 14th International Conference on Solid Waste Technology and Management, PA

108. Reddy, K.R., and Marella, A. (2001). Properties of different size scrap tire shreds: implications on using as drainage material in landfill cover systems. Seventeenth International Conference on Solid Waste Technology and Management, Philadelphia, PA, USA

109. Reddy, K.R., Marella, A., and Ala, P. (2002). Transmissivity behavior of shredded scrap tire drainage layer in landfill covers system. Proc. 6th International Symposium on Environmental Geotechnology and Global Sustainable Development, Seoul, Korea, 277-285

110. Reddy, K.R., Stark, T.D., and Marella, A. (2008). Clogging potential of tire shred-drainage layer in landfill cover systems. International Journal of Geotechnical Engineering, 2(4), 407-418

111. Reddy, K.R., Stark, T., Marella, A. (2010). Beneficial use of shredded tires as drainage material in cover systems for abandoned landfills. Pract Period Hazard. Toxic Radioact Waste Manag 14(1):47–60

112. Reddy, S.B. and Krishna, AM. (2013). Numerical simulations of earth-retaining structures using EPS geofoam inclusions. Indian Geotechnical Conference, IITRoorkee, India

113. RMA (2016) U.S. Scrap Tire Management Summary. *Rubber manufacturers association.*https://rma.org/sites/default/files/RMA_scraptire_summ_2015.pdf, available from www.rma.org

114. Salgado, R., S. Yoon, and Siddiki, N. Z. (2003). Construction of Tire Shreds Test Embankment. Publication FHWA/IN/JTRP-2002/35. Joint Transportation Research Program, Indiana Department of Transportation and Purdue University, West Lafayette, Indiana, 2003. https://doi.org/10.5703/1288284313165

115. Salgado, R. and Prezzi, M. (2004). Construction of a tire-shreds test embankment. Proceedings of the Institution of Civil Engineers – Engineering Sustainability, 157(2): 65–66

116. Shahin, M.A., Mardesic, T. and Nikra, H. R. (2011). Geotechnical characteristics of bauxite residue sand mixed with crumbed rubber from recycled car tire. Journal of Geoengineering, 6(1): 63-72.

117. Sheikh, M.N., Mashiri. M.S., Vinod. J.S., and Tsang, H.H. (2013). Shear and compressibility behavior of sand-tire crumb mixtures. Journal of Material Civil Engineering, *ASCE***,** 25(10):1366–1374

118. Shrestha, S, Ravichandran, N, Raveendra, M., and Attenhofer, J.A. (2016). Design and analysis of retaining wall backfilled with shredded tire and subjected to earthquake shaking. Soil Dynamics and Earthquake Engineering, 90: 227-239.

119. Singh, B. and Vinot, V. (2011).Influence of waste tire chips on strength characteristics of soils. Journal of Civil Engineering and Architecture, 5(9): 819-827.

120. Soganci, A.S. (2015). Strength characteristics of tire-sand mixtures, Soil Mechanics and Foundation Engineering, 51(6): 306-309

121. SP 16 (1980). Design Aids for Reinforced Concrete to IS 456:1978. Bureau of Indian Standards, New Delhi.

122. Srivastava, A., and Gupta, A. (2014). Model study of load–settlement response of slope prepared with clayey soil mixed with shredded tire waste."Proc., Int. Conf. on Sustainable Civil Infrastructure, ASCE, Reston, VA, 368–375.

123. Srivastava, A., Pandey, S., and Rana, J. (2014). Use of shredded tire waste in improving the geotechnical properties of expansive black cotton soil. Geo mechanics and Geoengineering, 9(4), 303–311.

124. Tandon, V., Velazco, D.A., Nazarian, S., and Picornell, M. (2007). Performance monitoring of embankments containing tire chips: case study. Journal of Performance of Construction Facilities, 21(3): 207–214. doi: 10.1061/ (ASCE) 0887-3828(2007)21:3(207).

125. Tatlisoz, N., Edil, T.B. and Benson, C. (1998). Interaction between reinforcing geosynthetics and soil-tire chip mixtures. Journal of Geotechnical and Geoenvironmental Engineering, 124 (11): 1109–1119

126. Tsai, W.T. (2015). The utilization of scrap tires as an energy source and its environmental benefit analysis in Taiwan. Energy Sources, Part B: Economics, Planning, and Policy, 10(4): 333-339, DOI: 10.1080/15567249.2010.551825

127. Tsang, H.H. (2008). Seismic isolation by rubber-soil mixtures for developing countries. Earthquake Engineering and Structural Dynamics, 37(2): 283-303.

128. Tsang, H.-H., Lo, S. H., Xu, X., Sheikh, M. N. (2012). Seismic isolation for low-to-medium-rise buildings using granulated rubber-soil mixtures: numerical study. Earthquake Engineering and Structural Dynamics, 41(14), 2009–2024. doi:10.1002/eqe.2171.

129. Tweedie, J.J., Humphrey, D.N. and Sandford, T.C. (1998a). Full-scale field trials of tire chips as lightweight retaining wall backfill, at-rest conditions. Transportation Research Record No. 1619, TRB, Washington, D.C., pp. 64-71

130. Tweedie, J.J., Humphrey, D.N. and Sandford, T.C. (1998b). Tire Shreds as Retaining Wall Backfill, Active Conditions. Journal of Geotechnical and Geoenvironmental Engineering, ASCE, 124(11):1061-1070

131. Tweedie JJ, Humphrey DN and Sandford TC (1998c) Tire Chips as Lightweight Backfill for Retaining Walls –Phase 11, A Study for the New England Transportation Consortium, Department of Civil and Environmental Engineering, University of Maine, Orono, Maine. (http://www.uvm.edu/~transctr/pdf/netc/netcr08.pdf)

132. Vieira, C.F.S., Lopes, M.L. and Caldeira, L.M.M.S (2006). Seismic response of a geosynthetic reinforced steep slope using FLAC. Proc. 4th International FLAC Symposium on Numerical Modeling in Geomechanics, MN, USA, Paper No. 05-06

133. Vinod, J. S., Sheikh, N., Mastello, D., Indraratna, B. and Mashiri, M. S. (2015). The direct shear strength of sand-tire shred mixtures. In A. Kulathilaka, K. Senanayake, J. S. M. Fowze, N. Priyankara, P. Rathnaweera, U. Nawagamuwa & N. De Silva (Eds.), Proceedings of the International Conference on

Geotechnical Engineering (ICGEColombo2015) Sri Lankan Geotecnical Society. Sri Lanka, pp. 193-196.

134. Vinot, V. and Singh, B. (2013). Shredded Tire-Sand as fill material for embankment applications. Journal of Environmental Research Development, 7(4A), 1622-1627.

135. Vivas, C. and Calatrava, D. (2016). Application of Soil Reinforced Structures as Urban Transportation System solutions. 2016 Conference of the Transportation Association of Canada Toronto, ON.

136. Warith, M.A., Evgin, E. and Benson, P.A.S. (2004), Suitability of tire chips in landfill leachate collection system. Waste Management, 24(10): 967–979.

137. Wu, W., Benda, C. and Cauley, R. (1997). Triaxial determination of shear strength of tire chips. Journal of Geotechnical and Geoenvironmental Engineering, ASCE, 123(5): 479-482.

138. Xiao, M., Bowmen, J., Graham, M., and Larralde, J. (2012). Comparison of seismic responses of geosynthetically reinforced walls with tire-derived aggregates and granular backfills. Materials in Civil Engineering, *ASCE*, 24: 1368-1377.

139. Xu X. (2009). Earthquake protection of low-to-medium-rise buildings using rubber-soil mixtures. MPhil Thesis, Department of Civil Engineering, the University of Hong Kong, Hong Kong.

140. Yang, S., Lohnes, R.A., and Kjartanson, B.H. (2002). Mechanical properties of shredded tires. Geotechnical Testing Journal, 25(1) **:** 44–52

141. Yoon, S., Zhang, J., Prezzi, M., and Koh, T. (2005). Construction and Performance of a Tire Shred-Sand Demonstration Embankment. Proceedings of the 20th International Conference on Solid Waste Technology and Management, Philadelphia, PA, April, pp. 237 - 246.

142. Yoon, S., Prezzi, M., Siddiki, N. Z. and Kim, B., (2006). Construction of a Test Embankment Using a Sand-Tire Shred Mixture as Fill Material. Waste Management, 26(9):1033-1044.

143. Young, H.M., Sellasie, K., Zeroka, D., Sabris, G. (2003). Physical and chemical properties of recycled tire shreds for use in construction. Journal of Environmental Engineering, ASCE 129(10):921–929.

144. Youwai, S., and Bergado, D. T. (2003). Strength and deformation characteristics of shredded rubber tire–sand mixtures. Canadian Geotechnical Engineering, 40(2), 254–264.

145. Zimmerman, P.S. (1997). Compressibility, hydraulic conductivity, and soil infiltration testing of tire shreds and field-testing of a shredded tire horizontal drain, M.S. Thesis, Iowa State University, Ames, Iowa.

146. Zornberg, J.G., Cabral, A.R. and Viratjandra, C. (2004). Behaviour of tire shred-sand mixtures. Canadian Geotechnical Journal. 41: 227–241.

147. Zornberg, J.G., Costa, Y.D., and Vollenweider, B. (2004b). Performance of prototype embankment built with tire shreds and no granular soil. Transportation Research Record: Journal of the Transportation Research Board, 1874: 70–77. doi: 10.3141/1874-08.

LIST OF PUBLICATIONS

Journals and Special Publications:

1. **Reddy, S.B.,** Krishna, A. M. and Krishna R.R. (2017). "Sustainable utilization of scrap tire-derived geomaterials for geotechnical applications", *Indian Geotechnical Journal*. DOI 10.1007/s40098-017-0273-3
2. **Reddy, S.B.,** and Krishna, A. M. (2017). "Tire Chips as Compressible Inclusions in Earth Retaining Walls", *ICE, Ground improvement*. https://doi.org/10.1680/jgrim.16.00034
3. **Reddy, S.B**., Kumar, D.P. and Krishna, A. M. (2016). "Evaluation of the Optimum Mixing Ratio of a Sand- Tire Chips Mixture for Geoengineering Applications", *ASCE Journal of Materials in Civil Engineering*, Vol. 28, No.2, and DOI: 10.1061/ (ASCE) MT.1943-5533.0001335, 06015007.
4. **Reddy, S.B.,** Krishna, A. M., Dasaka, S.M. (2016). "Seismic resilience of retaining walls backfilled with sand–tire chips mixtures", *Japanese Geotechnical Society Special Publication*, Vol. 3, No. 2, pp. 20-23.
5. **Reddy, S.B.,** and Krishna, A. M. (2015). "Recycled Tire chips Mixed with Sand as Lightweight Backfill Material in Retaining wall Applications: An Experimental investigation", *International Journal of Geosynthetics and Ground Engineering*, Vol. 1, No. 4. DOI 10.1007/s40891-015-0036-0.
6. Dammala, P. K., **Reddy, S. B.,** and Adapa, M. K. (2015). "Experimental investigation of applicability of sand tire chip mixtures as retaining wall backfill", *ASCE Geotechnical Special Publication* – 256, Proceedings of IFCEE, San Antonio, Texas, USA, pp. 1420-1429.

Under review/preparation:

7. **Reddy, S.B.,** and Krishna, A. M. (-). "Sand - Scrap Tire Chip Mixtures for Improving the Dynamic Behaviour of Retaining Walls", *Geomechanics and Engineering* (Under review).

Book Chapters:

1. **Reddy, S.B**., and Krishna, A.M. (2017). "Sand –tire chips mixtures for sustainable Geo-engineering applications". Sustainability issues in civil engineering, Springer Special Issue. (http://www.springer.com/us/book/9789811019289#aboutBook).
2. **Reddy, S.B**., Krishna, A.M., and Arun Ch. B. (2017). "Feasibility Study of Retaining Walls Backfilled with Sand -Tire Chips Mixtures". Developments in Geotechnical Engineering, Geoenvironmental Practices and Sustainability 978-981-10-4076-4, 436443_1.
3. **Reddy, S.B.,** and Krishna, A.M. (2017). "Mitigation of dynamic loading effects on retaining walls using recycled tire chips". Springer Special Issue. (Provisionally selected).

Conferences:

1. **Reddy, S.B.** and Krishna, A. M. (2018) "Numerical studies of retaining walls with scrap-tire derived geomaterials" *ASCE Geotechnical Special Publication, Proceedings of IFCEE 2018*, Florida USA. (Abstract accepted)
2. **Reddy, S.B.** and Krishna, A. M. (2018) "Physical model studies on the seismic response of retaining walls with sand-tire chips mixtures" *GeoChina 2018*. (Accepted)
3. **Reddy, S.B**. and Krishna, A. M. (2017) "Sustainability approach for retaining walls using sand -tire chips mixtures" *Indian Geotechnical Conference (IGC-2017)*, IIT Guwahati, India. (Accepted)

4. **Reddy, S.B**. and Krishna, A. M. (2016) "Mitigation of dynamic loading effects on retaining walls using recycled tire chips" *Indian Geotechnical Conference (IGC-2016)*, IIT Madras, India.
5. **Reddy, S.B.**, Krishna, A.M. and Bosakia, A. (2016). "Feasibility Study of Sand–Tire Chips Mixtures as Backfill Material in Retaining Walls". *Indo-US workshop, Geo-Chicago Conference in USA* on 19th August 2016.
6. **Reddy, S.B**., Kumar, D.P. and Krishna, A. M. (2014). "Evaluation of sand - tire chip mixture properties for sustainable geotechnical applications", *Proceedings of International Conference on Sustainable Civil Infrastructure, ASCE India*, Hyderabad, India, 17-18 October 2014, pp. 417-426.
7. **Reddy, S.B.**, Kumar, D.P. and Krishna, A. M. (2014). "Behaviour of Cantilever Retaining Wall Models with Sand-Tire Chip Mixtures", *Proceedings of Golden Jubilee Conference of the IGS Bangalore Chapter, Geo-Innovations*, 30-31 October 2014, Bangalore, India, 30-31 October 2014, Paper No: GD4, 8p.
8. Kumar, D.P., **Reddy, S.B**. and Krishna, A. M. (2014) "Evaluation of Optimum Mix of Sand-Tire Chip Mixtures For Geotechnical Applications" *Indian Geotechnical Conference (IGC-2014), Kakinada*, India, 18-20 December 2014, pp. 723-728.
9. Krishna, A.M., Bhattacharjee, A., and **Reddy, S.B.** (2014). "Numerical Modeling of Geosystems: Reinforced Soil Retaining Structures", Sub-Theme lecture presented in *Indian Geotechnical Conference 2014*, 18-20 December 2014, Kakinada, India. PP. 2625-2636.
10. **Reddy, S.B.** and Krishna, A. M. (2013). "Numerical simulations of earth-retaining structures using EPS geofoam inclusions", *Proceedings of Indian*

Geotechnical Conference 2013, Roorkee, India, 22-24 December 2013, CD-ROM..

11. **Reddy, S.B.** and Krishna, A. M. (2013) "Numerical study on geofoam applications in retaining structures" Proc. *4th Indian Young Geotechnical Engineers Conference*, 17-18, May 2013, Chennai, pp. 103-106.
12. **Reddy, S.B.** and Krishna, A. M. (2012) "Measures to reduce the earth pressure on retaining structures", *Indian Geotechnical Conference,* Delhi, India,13-15, Vol. 2, pp. 727- 730